

MOTORCYCLE STEERING BEHAVIOUR

Christopher Graeme Giles

Submitted in accordance with the requirements for  
the degree of Doctor of Philosophy

The University of Leeds  
Department of Mechanical Engineering

April 1985

ABSTRACT

The thinking behind the choice of a data recording method that will be used to gather information on the frequency responses of motorcycles is discussed. The design and development of a microcomputer based data acquisition system (including transducers and signal conditioning circuitry) is described, along with the test and data processing strategies to be used.

A new theoretical model is developed which includes a frame flexibility that allows the rear wheel of the motorcycle to yaw and camber about an inclined axis. The effects of changes in axis position and stiffness are investigated, and stability results are presented for the straight-running condition.

The measurement of this stiffness (and that relating to a flexibility involving the front frame) for a large motorcycle, by both static and dynamic methods, is described. The nature of the flexibility involving the front wheel assembly is examined, and conclusions are drawn regarding the validity of theoretical models and the use of appropriate stiffness measurement methods.

Theoretical frequency responses of a motorcycle to steering torque inputs are calculated for the straight-running condition. An attempt is made to interpret the responses by studying the effects on them of various motorcycle parameter alterations, and comparing these with the changes in handling performance as predicted by riders' experiences with real machines. The common notion that there exists a trade-off between stability and responsiveness is examined.

Two new theoretical models, each representing a motorcycle towing a type of trailer, are developed and the stability results are presented. The effects of trailer parameter variations are described and recommendations relating to the design and use of the combinations are made.

A description is given of the design and development of a microcomputer controlled, modal motion simulator, which employs stepper motors driving a scale model motorcycle. The simulation strategy and software are discussed and improvements are suggested.

## CONTENTS

	Page
<u>ABSTRACT</u>	i
<u>CONTENTS</u>	ii
<u>LIST OF FIGURES</u>	v
<u>LIST OF TABLES</u>	vi
ACKNOWLEDGEMENTS	vii
1. <u>INTRODUCTION</u>	1
1.1. THE MOTORCYCLE PROBLEM	2
1.2. THESIS OBJECTIVES AND STRUCTURE	5
2. <u>DEVELOPMENT OF A MEASURING SYSTEM TO DETERMINE THE FREQUENCY RESPONSES OF MOTORCYCLES TO STEERING CONTROL INPUTS</u>	7
2.1. INTRODUCTION	8
2.2. MEASURANDS	8
2.3. MEASUREMENT SYSTEM REQUIREMENTS	9
2.4. DATA RECORDING OPTIONS AVAILABLE	10
2.5. DESIGN OF A MICROCOMPUTER BASED DATA ACQUISITION SYSTEM	12
2.5.1. Transducers and Conditioning	12
2.5.2. Amplification and Filtering	17
2.5.3. Data Acquisition Module	19
2.5.4. Microcomputer and Interfacing	19
2.5.5. Power Supplies	23
2.5.6. Electromagnetic Interference Shielding	24
2.6. TESTING AND DATA PROCESSING STRATEGIES	24
2.7. BENCH TESTING OF THE SYSTEM	27
3. <u>THE INFLUENCE OF REAR WHEEL ASSEMBLY FLEXIBILITY ON MOTORCYCLE STABILITY</u>	28
3.1. INTRODUCTION	29
3.2. THE MODEL	30
3.3. THE EQUATIONS OF MOTION	32
3.4. RESULTS	34
3.5. DISCUSSION	34
3.6. CONCLUSIONS	40

	Page
4. <u>STATIC AND DYNAMIC FRAME STIFFNESS AND DEFLECTION</u>	
<u>MODE MEASUREMENTS</u>	41
4.1. INTRODUCTION	42
4.2. STATIC STIFFNESS MEASUREMENTS	42
4.2.1. Method	42
4.2.2. Results	45
4.3. DYNAMIC MEASUREMENTS	48
4.3.1. Method	48
4.3.2. Results	52
4.4. DISCUSSION	53
4.4.1. Front Frame	53
4.4.2. Rear Frame	56
4.5. CONCLUSIONS	58
5. <u>THE FREQUENCY RESPONSES OF MOTORCYCLES TO</u>	
<u>STEERING TORQUE INPUTS</u>	59
5.1. INTRODUCTION	60
5.2. METHOD	62
5.3. RESULTS	62
5.4. DISCUSSION	86
5.5. CONCLUSIONS	91
6. <u>THE STRAIGHT LINE STABILITY CHARACTERISTICS</u>	
<u>OF MOTORCYCLE AND TRAILER COMBINATIONS</u>	92
6.1. INTRODUCTION	93
6.2. THE MODELS	94
6.3. THE EQUATIONS OF MOTION	94
6.3.1. Equations for the Twin Wheel Trailer	96
6.3.2. Equations for the Single Wheel Trailer	97
6.4. RESULTS	98
6.5. DISCUSSION	98
6.5.1. The Twin Wheel Trailer	98
6.5.2. The Single Wheel Trailer	109
6.6. CONCLUSIONS	123

	Page
7. <u>DESIGN OF A MODAL MOTION SIMULATOR</u>	124
7.1. INTRODUCTION	125
7.2. METHOD OF OPERATION	125
7.3. DERIVATION OF THE ACTUATOR MOTIONS	126
7.4. DEVELOPMENT OF THE SIMULATION MODEL	128
7.5. LIMITATIONS AND POSSIBLE REFINEMENTS	132
8. <u>CONCLUSIONS</u>	135
<u>NOMENCLATURE</u>	138
<u>REFERENCES</u>	141
<u>APPENDIX 1 DATUM PARAMETER VALUES</u>	143
<u>APPENDIX 2 DERIVATION OF THE EQUATIONS OF MOTION</u>	146
A2.1. THE REAR WHEEL YAW/CAMBER MODEL	147
A2.2. THE TWIN WHEEL TRAILER MODEL	162
A2.3. THE SINGLE WHEEL TRAILER MODEL	168

LIST OF FIGURES

	Page	
2.1	Data acquisition system	13
2.2	Angular position, rate gyro, acceleration and wheel speed transducers	14
2.3	Torque transducer and strain signal conditioning unit	14
2.4	Block diagram of strain signal conditioning unit	16
2.5	Block diagram of signal conditioning circuitry	18
2.6	Block diagram of data acquisition module	20
2.7	Flow diagram for data collection program	22
2.8	Nascom microcomputer, power supplies, signal conditioning, monitor and cassette recorder	25
3.1	Model dimensions	31
3.2-4	Oscillatory mode eigenvalues for changes in various rear wheel assembly parameters	35-37
3.5-7	Eigenvectors for various oscillatory modes	38
4.1	Measuring apparatus used for the static tests on the rear wheel	44
4.2	Motorcycle layout for static measurements	45
4.3	Front wheel deflection results	46
4.4	Rear wheel deflection results	47
4.5	Shaker connected to front wheel for dynamic tests	50
4.6	Experimental and matched theoretical frequency responses for the front wheel assembly	53
4.7	Experimental frequency responses for the rear wheel assembly	54
4.8	Oscillatory mode eigenvalues for static and dynamic stiffness data	57
5.1	Selected frequency response gains for the datum case	64-65
5.2	Selected frequency response gains for various speeds, datum case	66-67
5.3-11	Selected frequency response gains for various parameter changes	68-85
6.1	Dimensions of trailer	95

	Page	
6.2	Oscillatory mode eigenvalues for changes in trailer size, twin wheel trailer	99
6.3	Capsize mode results corresponding to Fig.6.2	100
6.4-6	Various eigenvectors for the datum case, twin wheel trailer	101
6.7-11	Oscillatory mode eigenvalues for various parameter changes, twin wheel trailer	103-107
6.12	Double drawbar configuration	110
6.13	Oscillatory mode eigenvalues for datum case and modified twin wheel trailer	111
6.14	Oscillatory mode eigenvalues for changes in trailer size, single wheel trailer	112
6.15-18	Various eigenvectors for the datum case, single wheel trailer	113
6.19-24	Oscillatory mode eigenvalues for various parameter changes, single wheel trailer	115-116 &118-121
6.25	Oscillatory mode eigenvalues for datum case and modified single wheel trailer	122
7.1	Model restraints and actuator attachment points	127
7.2	Actuator driver circuit	129
7.3	Nascom microcomputer and modal motion simulator	133
A2.1	Rear wheel yaw/camber model dimensions	147
A2.2	Axis system definitions	148
A2.3	Relationship between fixed and moving axes	150
A2.4	Steered and cambered unit vector	155
A2.5	Rear tyre forces and velocities	157
A2.6	View of trailer from above	162
A2.7	Trailer tyre velocities	166
A2.8	Definition of axis system 8	168

LIST OF TABLES

	Page	
4.1	Statically measured frame parameters	48
4.2	Dynamically measured frame parameters	52

ACKNOWLEDGEMENTS

I would like to express my gratitude to my supervisor, Robin Sharp, for his tireless help and encouragement throughout the last three years. Thanks also to Stuart Allen for his help with all matters electronic, and to the other academic and technical staff who have assisted me in my various endeavours.

To my parents

CHAPTER 1

INTRODUCTION

A brief review of previous work on motorcycle steering behaviour is given with particular reference to that most relevant to this thesis. The overall objectives of the research programme are outlined and the main subject matter of each chapter is indicated.

### 1.1. THE MOTORCYCLE PROBLEM

Over the last fifteen years there has been a steadily increasing interest in studying the dynamic properties of motorcycles. This interest is prompted by concern for the safety of riders and the desire for optimum handling performance under both road and racing conditions, as well as commercial considerations. The motorcycle rider is particularly vulnerable to serious injury in an accident, and one body of research has concentrated on improving the crash-worthiness of the machine. Other researchers have set about improving the dynamics of the motorcycle so as to decrease the chances of an accident occurring, by examining the stability and controllability properties. The latter is intrinsically harder to study theoretically than the former, because of the need for a realistic rider control model. The complicated nature of the control task and the multitude of largely arbitrary assumptions required has restricted progress in this field. Hence, research in this area has concentrated on experimental assessment of the accident avoidance capabilities of the motorcycle/rider combination, as carried out by Weir and Zellner (1979) and Rice (1978). Such work has succeeded in providing an enhanced understanding of both the control problem and rider behaviour, but practical design recommendations have been less forthcoming.

The largest body of previous research has been concerned with the theoretical modelling of motorcycle dynamics so as to arrive at an accurate prediction of the real life stability properties. It is generally thought that free control (e.g. hands off) is more important than fixed control (e.g. steer displacement) because the latter has been shown to be an undesirable, if not dangerous, control strategy as far as the motorcycle is concerned, Sharp (1971). With automobiles, there exists a simple relationship between the steady state responses and the stability characteristics, driver opinion being strongly related to such responses. This is not the case with motorcycles, however, and thus the fixed control results are of comparatively little interest.

Most theoretical work has concentrated on the straight-running behaviour, mainly because rigorous analysis of the cornering case is an extremely lengthy and error prone procedure. It is desirable that suspension freedoms are included in such an analysis because of

the strong coupling of in-plane and out-of-plane motions. Also, the resultant equations are non-linear and have to be linearised for each chosen steady cornering condition. The gross behaviour is predicted by evaluating the equilibrium values of the equation coefficients and then calculating the small perturbation characteristics using these coefficients. An additional problem involves the fact that the tyre loads are time variant and the representation of this requires further complication of the tyre model. The cornering behaviour is not studied in this thesis and the reader is referred to the work of Koenen (1983) for a detailed account of this subject.

In real life, the motorcycle is known to exhibit two oscillatory instabilities during straight running. The weave mode is lightly damped at high speeds and involves mainly rolling, yawing and steering motions. A similar oscillation is particularly common during cornering, and is thought to be strongly influenced by suspension properties. Roland (1973) and Weir and Zellner (1979) have obtained experimental recordings of the weave mode and it is also represented in the results of Verma (1978) and Aoki (1979). From a very early stage, theoretical models such as that of Sharp (1971) have succeeded in simulating this mode, which is unstable at very low speeds (below about 8 m/s), but has a low characteristic frequency so that the rider is able to maintain control fairly easily. The frequency increases with increasing forward speed and the mode becomes well damped at medium speeds. At high speeds, the weave mode approaches the stability boundary again and has a frequency of around 3 Hz.

The other oscillatory mode is commonly called the medium speed wobble and is dominated by steering motions. It has been recorded experimentally by Eaton (1973), Roe and Thorpe (1976) and Weir and Zellner (1979) and is again represented in the results of Verma (1978) and Aoki (1979). Its frequency of around 8 Hz is known to be relatively independent of speed and the worst speed range is usually about 15 to 20 m/s. However, the early theoretical results were less successful in representing this mode accurately, indicating that the wobble mode was well damped in this speed range and only unstable at very high speeds. This instability was thought to be the "speedman's wobble" as described in early work by Pearsall

(1922) and Wilson-Jones (1951), but the aforementioned experimental work in the 1970s threw doubt upon this conclusion because of the apparent mis-match of speeds. As a result, a considerable amount of work was done to refine the tyre model, which was thought to be the source of error. However, the insensitivity of the theoretical results to many of the more esoteric features of the advanced tyre models, led to a shift in emphasis towards the modelling of frame flexibilities. The models of Sharp and Alstead (1980) and Spierings (1981) succeeded in accurately predicting the course of the wobble mode with speed, due to the inclusion of a torsional flexibility at the steering head whereby the front frame can rotate relative to the rear frame about an axis perpendicular to the steer axis. The stability characteristics have been shown to be critically dependent upon the parameters relating to this flexibility. Hence, this feature has now been incorporated into several other models, including that of Koenen (1983) who has succeeded in identifying other significant oscillatory modes, arising during steady cornering, that closely resemble the known behaviour of real motorcycles, such as front wheel "patter". It is now thought that "speedman's wobble" was more likely to have been a weave oscillation, in view of the fact that a complete description of it is not available.

In addition to the two oscillatory modes, there is evidence in the theoretical results of a static, capsize mode. This may be stable at all speeds up to the top speed of the machine, or marginally divergent for high speeds. It consists mainly of rolling motions at low speed, although these decrease in magnitude at higher speeds. The obvious roll instability of the motorcycle when stationary is represented in the theoretical results by the weave mode eigenvalue splitting into two, positive, real roots at below walking pace.

The frequency of occurrences of oscillatory instabilities in real life is illustrated by the results of a questionnaire sent to 1000 Swedish riders with machines larger than 240 cc, Brorsson (1983). Of those who replied, 45 per cent reported being involved in at least one weaving or wobbling incident during 1982, and serious incidents happened to 8 per cent of respondents. What appears likely to have been high speed weaving was experienced by 28 per cent of riders at a mean speed of around 40 m/s. Clearly,

investigations aimed at yielding more stable designs of motorcycles have a large role to play in the improvement of rider safety, although this is not to deny that most motorcycle accidents involve a large element of human error.

## 1.2. THESIS OBJECTIVES AND STRUCTURE

This thesis doesn't contain an extensive literature review, and I would refer the reader to the work of Sharp (1982) and (1984b) and Alstead (1982), for a more detailed and wide ranging account of the subject. Any previous work that is strongly related to the content of this thesis is briefly reviewed in the introduction to each chapter.

As I have already said, the theoretical model of Sharp and Alstead (1980) succeeded in accurately representing the main characteristics of the behaviour of motorcycles when running straight ahead. However, so far there has been no detailed comparison of the theoretical and experimental responses of a chosen machine in order to further validate the model. The main objective of my work has been to facilitate this comparison by developing a data acquisition system. The thinking behind the choice of the data recording method, the system itself, and the testing and data processing strategies to be used are described in Chapter 2.

After the discovery that the inclusion of steering head flexibility in the theoretical model strongly affected the stability results, it was felt desirable to extend the model to include one further flexibility which is commonly considered by motorcyclists to be very important. The development of this new model and the corresponding free vibration results are contained in Chapter 3.

Once it had been found that certain structural flexibilities are important features of theoretical models, it became clear that such models require the insertion of valid frame data if accurate predictions of behavioural properties are to be made. Chapter 4 relates the measurement of frame stiffnesses for the front and rear wheel assemblies by static and dynamic methods, the aims being to examine the real life nature of the flexibilities and to obtain appropriate data.

As mentioned earlier, the control aspect of the motorcycle problem is still something of a "black art". Little attempt has been made to relate experimental measurements or theoretical predictions of handling performance to riders' subjective opinions. Indeed, it is presently difficult to define exactly what good performance is in any coherent way. Nevertheless, riders do show strong preferences for certain design features, partially dependent upon the intended usage of the motorcycle, and the design process is clearly influenced by certain unwritten rules. In Chapter 5, I have attempted to shed further light on the interaction of design and performance, with particular reference to the effects of various parameters on the responsiveness of motorcycles.

Since the theory has successfully described the straight-running behaviour of conventional motorcycles on their own, it is now possible to apply with confidence the same techniques to other, non-standard design configurations. Chapter 6 describes the development of the theory to cover motorcycles towing trailers, and the straight line stability results are presented along with the effects of trailer parameter variations.

Because the modal motions of motorcycles involve several variables, it is often difficult to imagine what a particular mode shape looks like on a real machine. The design and development of a portable modal motion simulator aimed at alleviating this difficulty is dealt with in Chapter 7.

Chapter 8 contains a discussion of the conclusions from Chapters 2-7 with reference to the objectives presented here.

CHAPTER 2

DEVELOPMENT OF A MEASURING SYSTEM TO DETERMINE THE FREQUENCY  
RESPONSES OF MOTORCYCLES TO STEERING CONTROL INPUTS

This chapter describes the thinking behind the choice of the data recording method, and goes on to outline the design and development of a microcomputer based data acquisition system, including transducers, signal conditioning and computer peripherals. The test and data processing strategies are also discussed.

## 2.1. INTRODUCTION

In order to validate and improve some of the theoretical modelling details, there arises a need for a data acquisition system that will enable information about rider inputs and motorcycle responses to be measured over the frequency range of interest. For reasons that will be outlined later, we decided that the most informative and convenient test procedure consists of riding the motorcycle in a straight line at constant speed, whilst providing steering torque inputs at varying frequencies by means of rider steer effort. The data thus collected may then be analysed to provide frequency responses for direct comparison with theoretically predicted responses. The frequency range of interest for this comparison extends from zero to a little beyond the natural frequency of the wobble mode of oscillation, say 12 Hz, but, on account of an interest in another oscillation which occurs during heavy braking and which may have a higher frequency, the measuring system has been designed round the notion that good data up to 19 Hz will be obtainable.

## 2.2. MEASURANDS

The conventional wisdom of motorcycle handling is that the main rider control input is the handlebar torque. The rider lean angle and his upper body lean torque can also be regarded as control inputs, but in the experiments planned, the rider lean angle will initially be regarded as a response, and the test rider's aim will be to minimise body lean as a control input. In future, information may be gathered on how the rider's body behaves when oscillations occur, and some experiments may be directed at learning more about how the rider acts as a controller. This will at least entail the measurement of rider upper body lean angle.

Other responses of importance are steer angle, roll angle, yaw velocity and lateral acceleration. Later experiments may involve measurement of structural strains in key positions indicated by the theory. This will reveal the extent to which frame flexing influences the responses.

The forward speed of the motorcycle affects the behaviour strongly and must also be measured to allow comparison between

predictions and measurements in respect of the other variables.

### 2.3. MEASUREMENT SYSTEM REQUIREMENTS

Because of the low weight of motorcycles and restricted available space, the measuring system must be compact and light enough not to appreciably affect the dynamic characteristics of the machine. Motorcycles in general, and especially the type we intend testing, are subject to appreciable levels of vibration, which realistic isolation strategies will only partially attenuate, and the system must work reliably under such conditions. It must be sufficiently rugged to withstand the knocks which are an inevitable consequence of experimental work in the field. A further environmental requirement concerns the electromagnetic radiation coming from the motorcycle's electrical system. The data measurement system must be unsusceptible to, or amenable to protection from, this potentially disruptive interference so as to prevent corruption of the data or system malfunctions.

The size and weight restriction has implications for the power supply. Batteries are the most convenient power source and use could possibly be made of the motorcycle's charging system, so it is clear that the system must work off a d.c. supply, most conveniently 12V, and have low power consumption.

Cost, not only in terms of purchase price, but also in terms of time required for system development and testing, is of course a large factor in the evaluation process. To this end it is also desirable that the system makes maximum use of proprietary subsystems.

The investigation of motorcycle dynamics involves a continuous evolution of the theory to include further parameters of interest and it is important that the measuring system should be adaptable. For example, investigation of the cornering behaviour is likely to require measurement of front and rear suspension movements, but in the foreseeable future, measurement of eight parameters at the same time should suffice. For subsequent data processing by digital computer, in order to arrive at the required frequency response functions, the data should be stored in a recoverable form, and the recorder storage capacity should be sufficient for the results of at

least one complete test run.

#### 2.4. DATA RECORDING OPTIONS AVAILABLE

Although the decision about the method of data recording had already been taken when I started on the project, I feel it will be useful to outline the various options that were available with regard to the above criteria. Since the method was decided upon some years ago, rapid changes in data recording technology may have altered the relative merits of the various systems and anyone embarking on a similar programme should take note of these changes.

##### (a) Ultra-violet light recorder

This method would appear to satisfy the requirements relating to cost, weight, size and power consumption and has adequate frequency response. However, the data collected would yield information about time histories only and no data processing to yield frequency responses would be possible, making the data difficult to interpret.

##### (b) Tape recording - AM or FM

Amplitude modulation has the disadvantage of very poor low frequency performance. Frequency modulation requires expensive modulation/demodulation electronics and very accurate tape speed control. This makes FM recorders costly, heavy and bulky, and they are likely to be relatively fragile also. Further, even if 75% of the equipment cost were associated with the FM tape recording system, it would still be the weakest link in the measurement chain as far as signal to noise ratio is concerned. Information storage capacity and frequency response capability far exceed current requirements.

##### (c) Pulse code or pulse width modulated tape recording

These methods overcome the need for an expensive tape speed control system but require more expensive electronics compared with (b). The information density is somewhat lower, but would still be more than adequate, and the dynamic range would normally be a substantial improvement over that available from an FM system.

(d) Telemetry

Data transmission by radio from the motorcycle to a stationary base is technically feasible without implying high expenditure, and removes the need for a recording facility on the bike. However, it would imply the existence of a stationary recording station near to the test area to which many of the previous considerations would apply. Further, it would imply the manning of the recording station and the requirement for a communication and coordination system between the test rider and the person at the base. With the adoption of this stratagem, only test areas near to which a suitable ground station could be set up would be satisfactory.

(e) Umbilical connection between motorcycle and pursuit vehicle

This allows information transmission by cable rather than by radio link, but poses such safety problems as to severely limit the test speeds obtainable. The requirements for a test car with a recording system on board, double manning, and communication and coordination systems are also obvious, and this approach is clearly far from optimum.

(f) Digital cassette recorder

This type of recorder tends to be fairly bulky, delicate, very expensive, and does not provide the complete solution to the measurement problem since it would require the addition of signal conditioning, multiplexing and analogue to digital conversion electronics to gather data. It would also be overendowed with respect to frequency response and storage capacity.

(g) Microcomputer/cassette recorder

The incoming data may be multiplexed, digitised and stored in the microcomputer's memory. Then the data may be dumped onto an ordinary cassette tape so that the next trial can be performed. For data analysis the memory can be reloaded from cassette, and the data transferred to a large computer. The advantages of this method include small size, low power consumption, relative cheapness, good resolution and frequency characteristics. Disadvantages are that the fast access memory is limited, requiring frequent data transfer to tape, and development of the system may be time consuming due to

the learning time involved. Faults in the digital logic or errors in the required programs may also be difficult to identify, and screening from electromagnetic interference is clearly necessary.

Despite these disadvantages, it was judged that the microcomputer system appeared to be the most effective solution then available, and the rest of the chapter describes development of the data acquisition system and the test and data processing strategies involved.

## 2.5. DESIGN OF A MICROCOMPUTER BASED DATA ACQUISITION SYSTEM

A block diagram of the data acquisition system can be seen in Fig.2.1.

### 2.5.1. Transducers and conditioning

The following transducer types have been selected (see Fig.2.2). The main considerations affecting each choice are outlined.

#### (i) Forward speed (10-60 m/s)

A magnetic/inductive pickup is mounted on one front fork leg and outputs a pulse every time the head of a bolt glued to the wheel rim passes it. This pulse sequence is passed to an amplifier and filter. The resulting waveform has a fundamental frequency equal to the wheel rotation frequency, in which the phase information is preserved. This is viewed as an important consideration since it is suspected that some steering vibrations are significantly forced by front wheel or tyre imperfections, as theoretically investigated by Sharp and Alstead (1983).

#### (ii) Steer torque ( $\pm 20$ Nm)

The torque transducer (Fig.2.3) consists of an upper assembly attached to the handlebars and a lower assembly attached to the steering head yoke. The two assemblies can rotate relative to each other about an axis parallel to the steer axis, by means of a pair of adjustable taper roller bearings held in the cylinder of the lower assembly. Force is transmitted from one assembly to the other

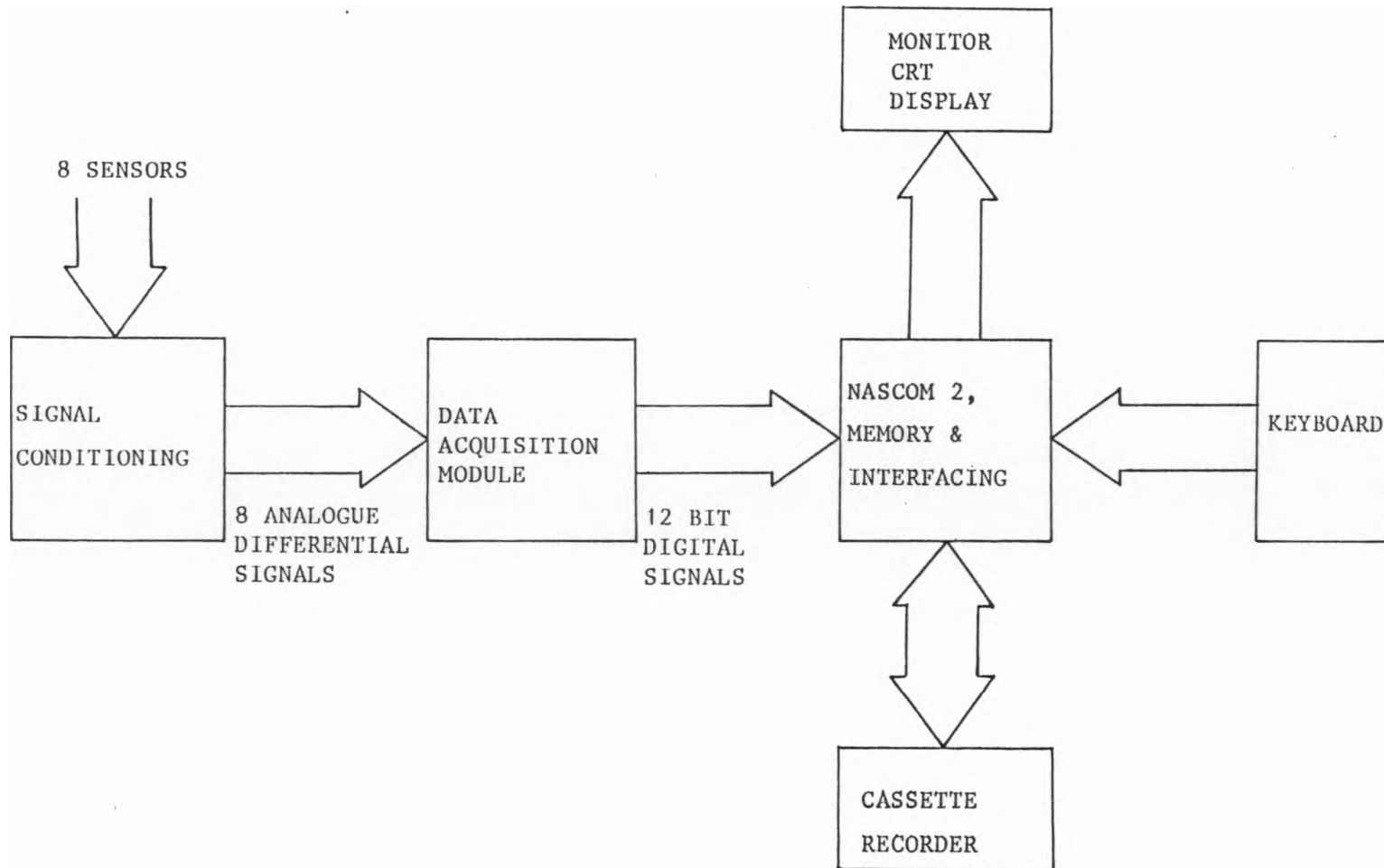


Figure 2.1

Data acquisition system



Figure 2.2  
Angular position, rate gyro, acceleration and wheel speed transducers (left to right).

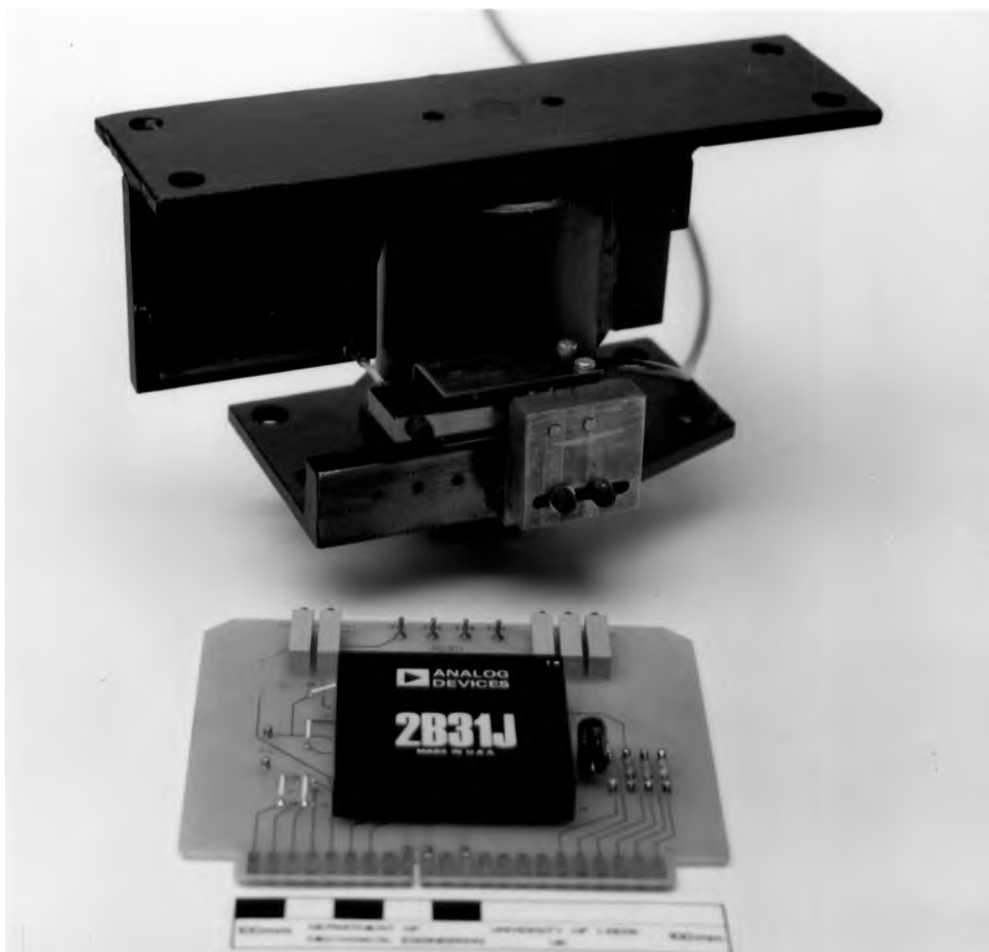


Figure 2.3  
Torque transducer and strain signal conditioning unit.

through a proprietary strain gauge type force transducer of range  $\pm 250$  N. The restraint provided by the bearings means that the transducer is minimally sensitive to any bending or axial loads applied to the handlebars, but will respond to torque inputs with a minimum of friction loss. Mechanical stops are provided that limit the relative rotation of the two assemblies in order to prevent the transducer from being overloaded.

The signal conditioning is carried out by a single proprietary unit (seen in front of the torque transducer in Fig.2.3) which converts a d.c. supply into an adjustable, regulated d.c. bridge excitation voltage, and provides variable output gain and offset and a 60 dB/Decade, adjustable cut-off, low pass filter (Fig.2.4). The output varies between 0 to  $\pm 5$ V, the conditioner input voltage being  $\pm 15$ V d.c. and the power consumption less than 0.5W. The signal conditioning, along with a shunt resistor calibration facility, is mounted above the headlamp, near to the transducer so as to minimise contamination of the low level signals from the strain gauge bridge.

(iii) Steer angle ( $\pm 20$  degrees)

This is measured using a d.c./d.c. angular position transducer working on the variable differential transformer principle. The transducer is mounted on the rear frame of the motorcycle, just underneath the steering head, and the shaft is driven via a toothed rubber belt and pulleys from the bottom of the steering yoke. Resolution is infinite and the required supply voltage is 10V, which is derived from a 15V supply by means of a simple voltage regulator. The maximum output is in the region of 1V, and the power consumption approximately 0.5W.

(iv) Rider lean angle ( $\pm 30$  degrees)

We envisage that this will be measured using the same type of transducer as in (iii). A hinged rod will join a point somewhere in the middle of the rider's shoulderblades to the input shaft of the transducer, which will be situated behind the rider at the level of the base of his trunk, with its axis horizontal. Precautions will be taken to ensure that the device cannot injure the rider in the event of an accident.

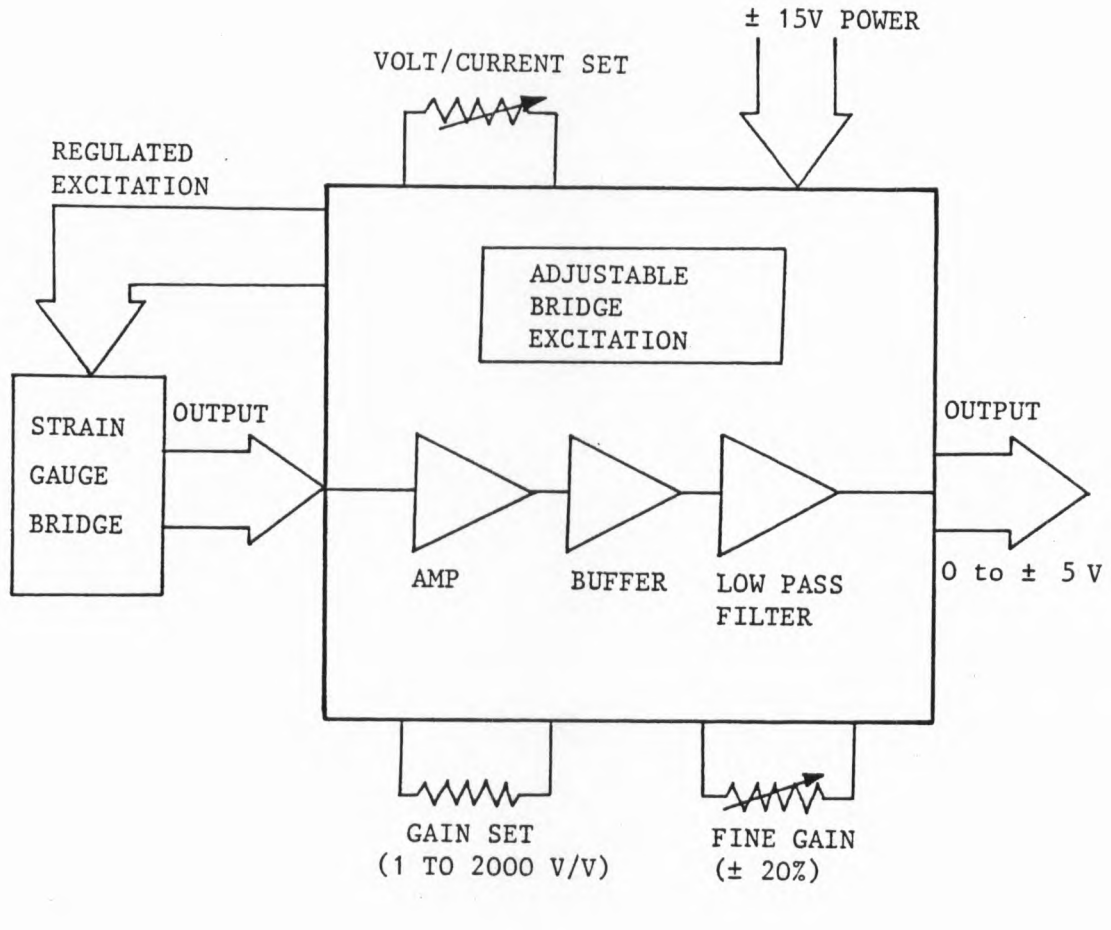


Figure 2.4

Block diagram of strain signal conditioning unit.

(v) Roll and yaw rates ( $\pm 40$  deg/sec)

A dual axis rate transducer, consisting of a spinning, mercury filled sphere in which are located two pairs of piezo-electric paddles, is employed. This is a proprietary unit and it contains the necessary demodulation electronics so that again it is a d.c./d.c. device. Supply voltages of  $\pm 15V$  are required with power consumption less than 2W. Maximum measurable turn rates are 60 deg/sec in respect of each axis, and corresponding outputs are then 2.4V.

(vi) Lateral acceleration ( $\pm 0.5g$ )

A d.c. supplied servo accelerometer, requiring  $\pm 15V$ , is mounted with its sensitive axis perpendicular to the plane of symmetry of the motorcycle. Since the output is partly due to

rolling and yawing motions, the theoretical calculation of the relevant frequency response has been adjusted so as to give results for the lateral acceleration of the point on the motorcycle at which the accelerometer is mounted. This enables easy comparison between theoretical and experimental results. The accelerometer has a flat frequency response down to d.c., very low cross axis sensitivity, and gives 5V output for a 10g acceleration. Maximum power consumption is 0.3W.

(vii) Frame flexing

The stiffness of the motorcycle frame around the steering head is known to influence significantly the stability properties, but at present we are unsure exactly which strain measurements will give meaningful results. Further experimental investigations in the laboratory and refinements of the theoretical model will hopefully show us the best measurement strategy. In the meantime it is likely that the experimental study will involve strain gauging the frame to measure the amount of flexing occurring during the tests, and the signal conditioning will be carried out using the same type of unit as for the steer torque transducer. Provision has been made for the signal conditioning card to be housed in the same box as that for the steer torque transducer.

2.5.2. Amplification and filtering

A block diagram of the amplification and filtering circuitry can be seen in Fig.2.5.

The output signals from the transducers require amplification before being fed to the analogue to digital converter (ADC), so that the maximum voltage occurring on each channel will be of roughly the same magnitude, ensuring maximum utilisation of the ADC's resolution. The amplification electronics were designed and built in the engineering department to suit our specific application.

A calibration facility is included whereby each transducer output line can have a suitable known voltage applied to it before the signal conditioning stage. Hence any changes in the system such as gain drift downline of the calibration stage can be accounted for in the data processing.

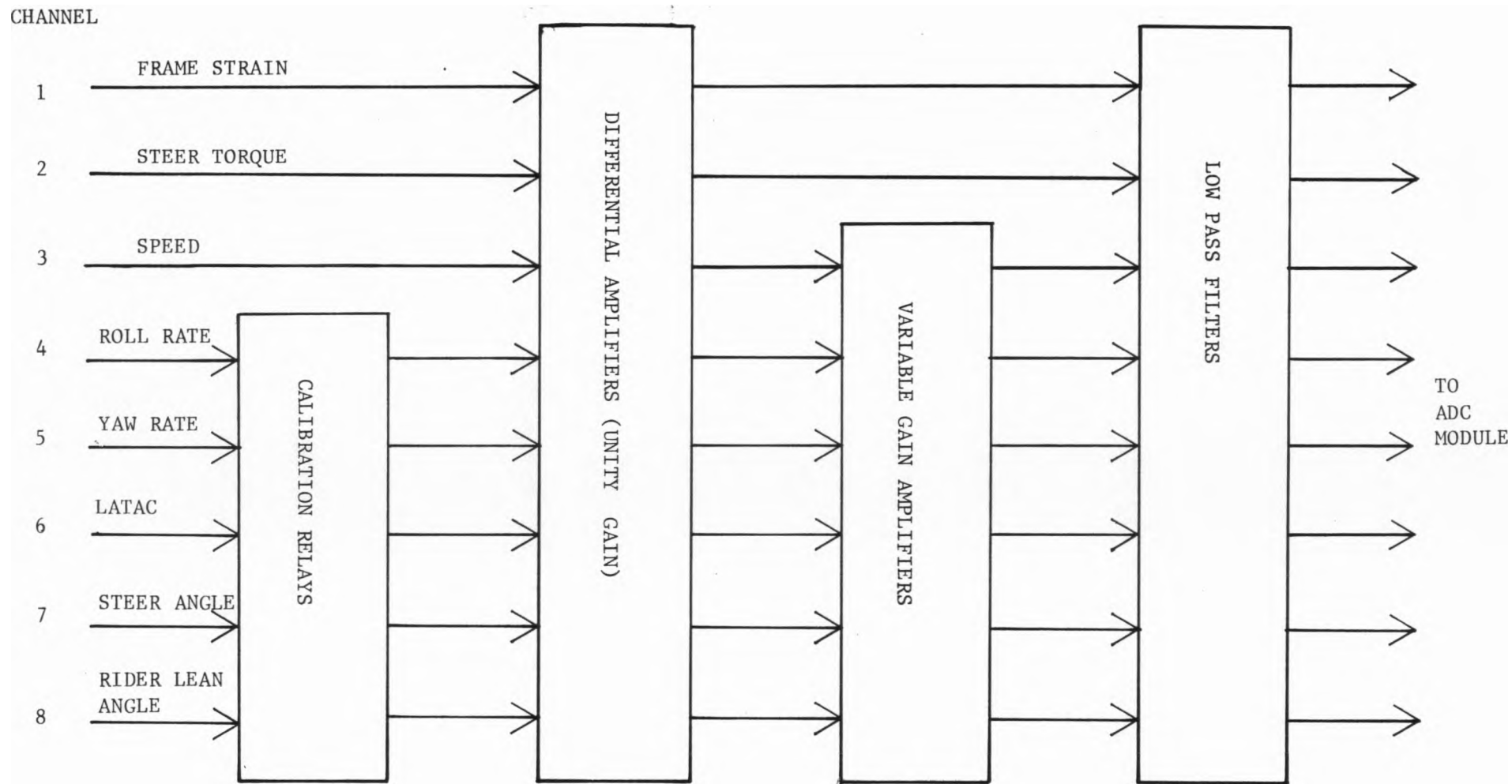


Figure 2.5  
Block diagram of signal conditioning circuitry.

The second section of the signal conditioning circuit consists of unity gain differential amplifiers, aimed at rejecting common mode signals occurring on both of a channel's inputs, such as might result from electromagnetic pickup on the leads from the transducer. High precision resistors and low noise operational amplifiers have been used to achieve a high common mode rejection ratio.

The third section employs variable gain amplifiers to set the desired signal level (except for the strain gauge type transducers, whose signals will have already been amplified).

The low pass filters, which form the last section of the signal conditioning, are proprietary items, selected to eliminate aliasing problems by attenuating signals outside the frequency range of interest. They are sixth order Butterworth type filters, with a cut-off frequency of 19 Hz.

#### 2.5.3. Data acquisition module

After signal conditioning, the signals are fed to the data acquisition module for conversion to digital form. This self-contained unit comprises a 16 channel multiplexer, differential amplifier, sample and hold circuit, a 12 bit, high speed analogue to digital converter and all of the programming, timing and control circuitry needed to perform the data acquisition function (Fig.2.6). It will accept up to 16 single or 8 differential analogue inputs, can be set up to operate on any of 8 input voltage ranges, and has gain and offset adjustment facilities.

The multiplexer output channel selection is controlled by 4 address lines so that the microcomputer can select which channel is sampled.

The 12 bit digital output gives a resolution of 0.024 per cent of the full scale voltage range selected, and the maximum digitization rate is far in excess of the system requirements.

#### 2.5.4. Microcomputer and interfacing

The microcomputer chosen is a Nascom 2, incorporating the Z80 microprocessor which can address up to 64K (where K=1024) memory locations. The Nascom 2 board comes complete with cassette,

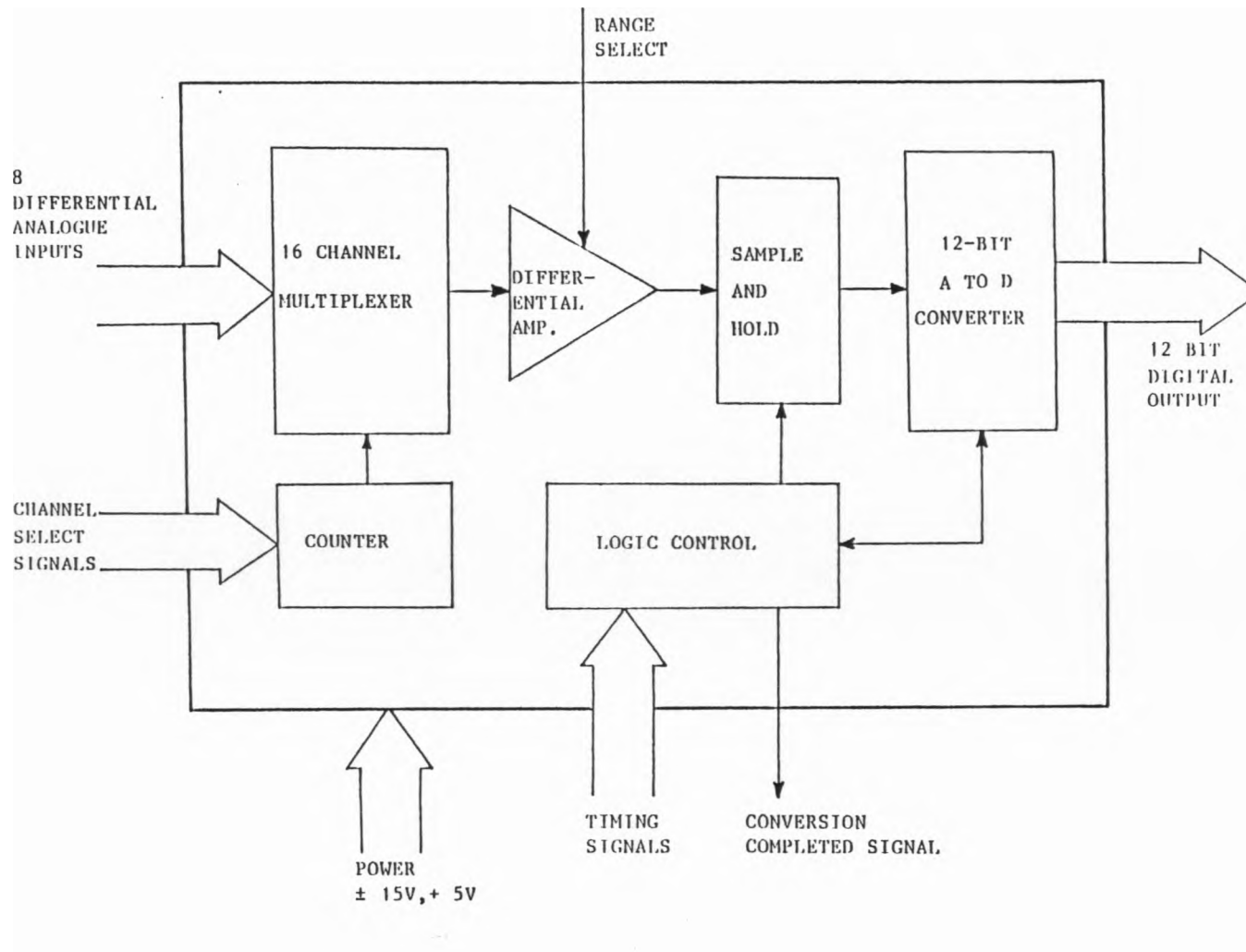


Figure 2.6

Block diagram of data acquisition module.

parallel port, serial port, and TV/monitor interfaces.

Since each computer memory location can hold an eight bit word, or byte, and the data acquisition module provides a 12 bit word, then the interfacing procedure can store each sample as two bytes of memory. This can be accomplished as follows: the 8 most significant bits (MSB's) are stored in an 8 bit buffer and the 4 least significant bits (LSB's) are stored in another buffer with the spare 4 bits as trailing zeros. When the computer receives a signal telling it that the conversion of one sample is completed, it lets the 8 MSB's onto the data bus and stores them in a free memory location. It then lets the 4 LSB's onto the data bus and stores them in the next memory location. It then tells the data acquisition module to perform the next conversion. Alternatively, to optimise the use of the limited fast access memory, two successive 12 bit samples can be packed into 3 bytes. This entails filling a microprocessor register containing the 4 LSB's of the first sample with the 4 LSB's of the next sample, replacing the trailing zeros, and the result is stored in memory after the two lots of 8 MSB's. This is easily accomplished in an assembly language program. This strategy results in a one quarter reduction in the memory space occupied by a given number of samples, and consequently allows longer test durations or more tests before the memory becomes full. The cost is a slight increase in the complexity of the data acquisition and processing programs, since the data has to be "unpacked" again once it is transferred to the mainframe computer. This is not a major problem and I decided to adopt the latter method of data storage.

When all eight channels have been sampled once, a delay is initiated in the computer until it is time to sample the channels again. The length of the delay is decided by the required sampling rate, and is controlled by the frequency of a crystal oscillator circuit which produces a square wave input to a buffered port. The processor polls the input port until it sees a falling edge, which initiates conversion.

The other routines in the data collection program control the taking of calibration data, the illumination of a panel of light emitting diodes (LED's) which tell the rider what the micro is doing, and the monitoring of the data collection, according to the flow diagram in Fig.2.7.

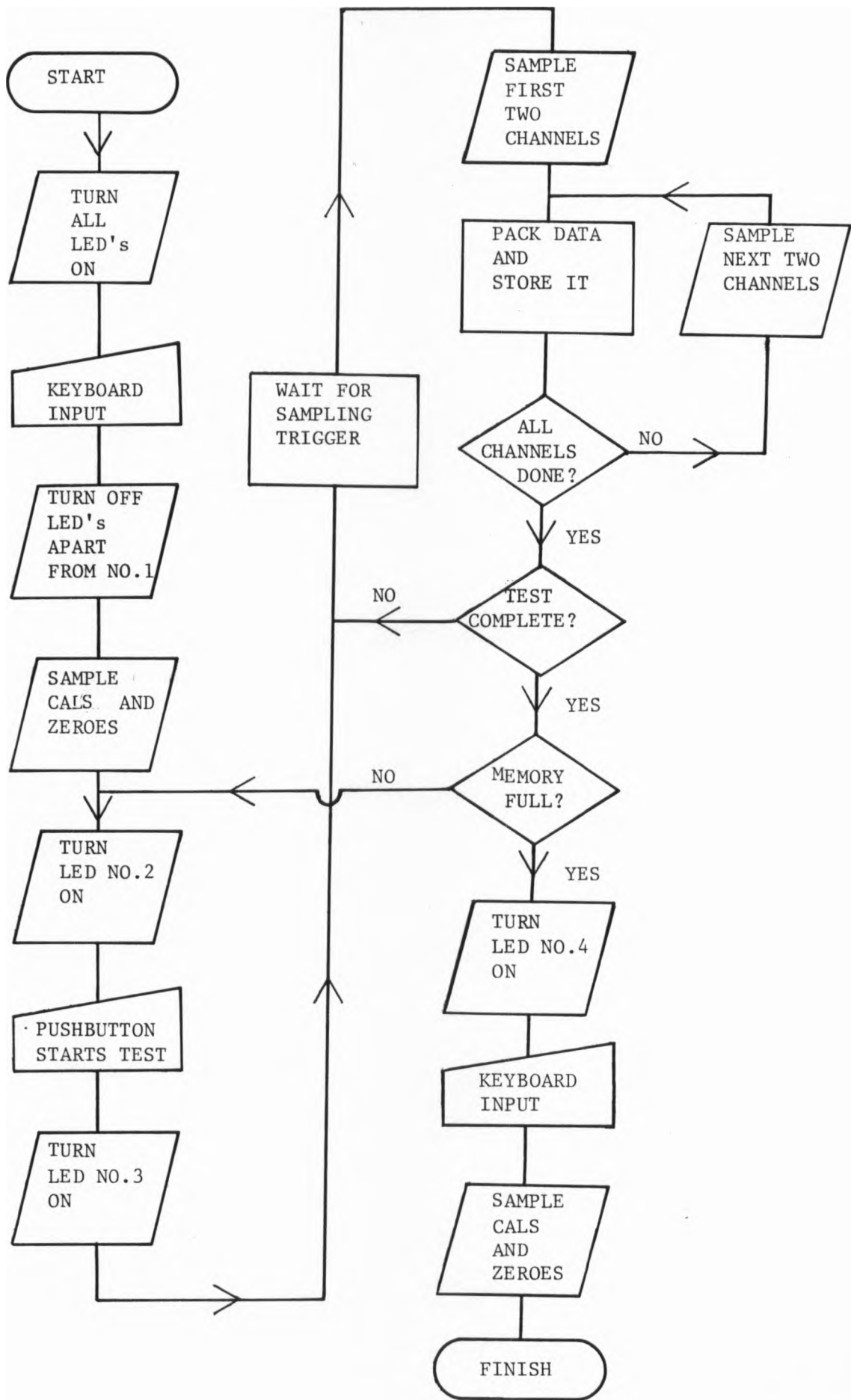


Figure 2.7

Flow diagram for data collection program.

The software required to implement these procedures is written in assembly language, and once fully developed will be burnt into an EPROM which retains the program when all power to the micro is switched off. Data obtained from the tests is loaded into static random access memory.

The frequency range of interest (0 to 19 Hz), together with the analogue anti-aliasing filters which could conveniently be purchased, dictated the need for a sampling frequency of around 100 Hz. Test durations of around 20 seconds are planned for reasons which are yet to be discussed. With the 8 signal channels, 16K data samples per test are implied, which, in turn, implies the need for 24K bytes of fast access memory, since  $1\frac{1}{2}$  bytes are needed for each data sample. This is well within the microcomputer's capacity, and we should be able to perform two tests before it becomes necessary to empty the memory onto cassette.

The Nascom operating system includes a standard routine for writing data from memory to cassette and vice versa, the data transmission rate being 1200 baud.

Data transmission from the microcomputer to a mainframe computer is relatively straightforward. The binary data bytes are transmitted, via the serial port of the Nascom, to the input device of the mainframe so that they are read into a data file. After the data has been "unpacked", the transducer outputs relating to the samples may then be derived from the recordings of the calibration signals and the known equivalences.

#### 2.5.5. Power Supplies

The microcomputer requires voltages of +12V and  $\pm 5$ V which are readily obtainable from a commercially available d.c./d.c. converter, powered by the motorcycle battery, and giving a regulated output with low noise.

The angular rate transducer, strain gauge supply and conditioning units, ADC unit and other signal conditioning equipment require  $\pm 15$ V, also obtained from d.c./d.c. converters powered by a 12V battery.

The cassette recorder and a monitor unit which will be employed at the test site for system checking, run off their own internal batteries or can be powered by the 12V battery on the motorcycle.

While choosing the d.c./d.c. converter units, some care was taken to ensure that their maximum power outputs comfortably exceed the total power requirements of the above mentioned equipment.

#### 2.5.6. Electromagnetic interference shielding

In order to protect the data acquisition system from electromagnetic interference, it is desirable to encase the computer and signal conditioning in a nearly continuous metal case. All the openings in the case, such as those for connectors, must be kept as small as possible. The case will be mounted on the rear of the motorcycle, and have a hinged lid to enable access to the computer keyboard and conditioning electronics when the motorcycle is stationary. Gaps around the edges of the hinged lid will be sealed with conductive, highly compressible gasket.

Since the wires leading to and from the case are likely to act as aerials, they will be screened with aluminium foil, and twisted pairs of wires will be used wherever possible to minimise magnetic field pickup. At the entrance to the case, ferrite beads will be strung over the wires, which will provide substantial noise attenuation over the range of 1 MHz to 500 MHz by presenting a series inductance and resistance to the signal, impedance being a function of frequency.

Figure 2.8 is a photograph of the microcomputer, power supply and signal conditioning boxes, the portable monitor and the cassette recorder.

#### 2.6. TESTING AND DATA PROCESSING STRATEGIES

We decided to use a swept frequency steer torque input as the test method for the following reasons:

- (i) The test can be performed on a relatively narrow road without any need for a specially generated mechanical input, the rider providing the required input torque.



Figure 2.8

Nascom microcomputer, power supplies, signal conditioning, monitor and cassette recorder.

- (ii) Similar methods applied to automobiles have been shown to be capable of discriminating between different types of car, and results are largely driver independent, according to Verma (1981).
- (iii) The results can be processed easily to give information on the frequency response properties of the motorcycle for direct comparison with theoretical responses.
- (iv) Similar methods have been used with success in a previous experimental study of motorcycle handling by Aoki (1979).

The data processing entails a computer program taking the data from each test run and converting the input and each output signal into a Fourier series equivalent by means of the Fast Fourier Transform algorithm. Thus for each Fourier frequency component there will be an associated signal amplitude and phase. Linear systems (as the motorcycle is assumed to be for small perturbations about a steady running condition) have output at a certain frequency entirely dependent on input at that frequency, and comparison of input and output gives the frequency response at that frequency. When this is repeated for all frequencies of interest, one can obtain plots of gain and phase versus frequency for each output related to the input. Theoretically calculated motorcycle frequency responses of this form can be seen in Chapter 5.

This method of data processing requires, for best accuracy, that the data is periodic in the analysis window (i.e. it represents one full cycle of a repeating signal). This means that it is desirable that the test signals start and end at zero. It is also desirable that the input signal contains approximately uniform signal strength through the frequency range of interest. These requirements have implications for the test procedure:

The test should start with the motorcycle moving in a straight line at constant speed with all inputs and outputs as near zero as is practicable. The rider should apply approximately sinusoidal steer torque inputs, first slowly and then with increasing frequency up to the maximum he can manage. The input should then be terminated and the responses allowed to die away so that at the end of data gathering the motorcycle is quiescent. This strategy will

allow the use of a uniform windowing function during the data processing, which gives the most accurate Fourier transform of a periodic signal.

The tests should be performed several times at each speed so that the results can be averaged. Averaging over several tests allows the calculation of coherence functions which will indicate the reliability and repeatability of the data.

We have developed a data processing program which takes the data for several tests at a certain motorcycle speed, and computes the required information on frequency responses and coherence functions.

#### 2.7. BENCH TESTING OF THE SYSTEM

Before the data acquisition system was fitted to the motorcycle, we wanted to check that it and the data processing programs were working properly. Thus we simulated various transducer inputs in the laboratory and digitised them. The samples were transferred to the mainframe computer and processed to yield frequency responses. These were compared with the known frequency components and phase relationships of the inputs and good agreement was obtained.

CHAPTER 3

THE INFLUENCE OF REAR WHEEL ASSEMBLY FLEXIBILITY ON MOTORCYCLE  
STABILITY

The development of a new theoretical model involving a freedom for the rear wheel assembly to yaw and camber about an inclined axis, is described. Parameter variations concerning the new flexibility are studied in an attempt to reveal the influence of rear swinging arm stiffness on straight line stability.

### 3.1. INTRODUCTION

For many years it has been part of the folklore of motorcycling that lack of rigidity in the rear swinging arm is one of the major causes of poor handling. High stiffness in this area is often claimed to be a panacea, and "box section" swinging arms are a popular aftermarket accessory. In fact, from having read many motorcycling publications, I have gained the impression that the major motorcycle manufacturers would have some difficulty selling a "sports" machine (the performance of which is oriented towards superlative handling and speed), if it had the conventional type of swinging arm.

Various theoretical studies of straight line stability aimed at explaining this obsession have been undertaken, starting with Sharp (1974). He included a torsional flexibility of the swinging arm whereby the rear wheel can camber relative to the rear frame about a horizontal, longitudinal axis passing through the centre of the wheel. The effects on the wobble and capsize modes were negligible. Although very low stiffnesses, such as could be representative of clearances caused by worn swinging arm bearings, were found to adversely affect the weave stability at medium and high speeds, normal stiffness values were found to be adequate. Any increase in stiffness above that normally obtaining had very marginal effects, and Sharp concluded that it would be adequate to assume infinite torsional rigidity of the rear swinging arm for modelling purposes. Flexibilities for both front and rear wheels were included in a model by Verma (1978), who measured the relevant static stiffnesses and deflection mode shapes associated with lateral forces at the tyre/road contact points. However, the inclusion of these flexibilities didn't lead to any better agreement between experiment and theory than had been found for a rigid framed model, and thus his results are inconclusive. Kane (1978) developed a much simplified model incorporating a bending flexibility of the rear frame about a vertical axis. However, his model doesn't allow any roll freedom, assumes a vertical rake angle for the steering axis and neglects tyre slip. These simplifications are so severe as to make the theoretical results incomparable with real life stability characteristics. Various flexibilities of the rear frame have been modelled by Johansen (1982), including torsional and lateral bending

freedoms for the rear wheel assembly. He concludes that torsional flexibility of the kind modelled by Sharp has a substantial effect on stability, decreasing stiffness leading to more wobble damping, but a slightly deteriorated weave mode. Increasing the bending stiffness was shown to stabilise some modes, and have little effect on others. His results, however, show the wobble mode to be minimally damped at high speed, rather than at medium speed as found by many other theoretical studies, and this must cast doubt on the overall validity of Johansen's findings. Unfortunately it isn't possible to check his analysis because a full account of it isn't available.

The lack of any consistent and clear message about the role of rear swinging arm flexibility, allied to the discovery of the importance of frame flexibility at the steering head by Sharp and Alstead (1980) and Spierings (1981), resulted in the modelling of the new degree of freedom of the rear wheel assembly that is explained here.

### 3.2. THE MODEL

The model is a development of that used by Sharp and Alstead (1980) which already incorporates a freedom for the front frame to rotate relative to the rear frame about an axis perpendicular to the steer axis. The single extra degree of freedom introduced here allows the rear wheel assembly to yaw and camber relative to the rear frame about an inclined axis, the orientation and position of which is described by  $\epsilon_1$  and  $a_4$  (Fig.3.1). It is clear that this freedom may be used to investigate the separate effects of both yaw and camber of the rear wheel by choosing  $\epsilon_1$  and  $a_4$  appropriately. The relevant stiffness and axis position has been measured on a large motorcycle, as described in Chapter 4.

The tyre model employed is the parabolic approximation of the taut string model developed by Pacejka (1971) and (1972). It has been extensively described by Sharp and Alstead (1980) and Alstead (1982), and I will not go into any details here.

The model involves the following set of assumptions:

(a). The motorcycle consists of two longitudinally symmetric frames joined by a hinge at the steering head, and the rider is rigidly attached to the rear frame.



### 3.3. THE EQUATIONS OF MOTION

These were obtained using the energy method of Lagrange, and a detailed description of their derivation appears in Appendix 2. The six equations are as follows:

$$(M_f + M_r + M_b)(\dot{v} + Ur) + (M_fk - M_b b_2)\dot{r} + (M_f j + M_r h + M_b b_1)\ddot{\phi} + M_f f \ddot{\gamma} + M_f e \ddot{\delta} - M_b a_2 \ddot{\lambda} = Y_f + Y_r + X_f(\cos \epsilon \delta - \sin \epsilon \gamma) + X_r \cos \epsilon_1 \lambda \quad (3.1)$$

$$(M_fk - M_b b_2)(\dot{v} + Ur) + (M_f k^2 + I_{rz} + I_{fx} \sin^2 \epsilon + I_{fz} \cos^2 \epsilon + M_b b_2^2 + I_{rwx} \sin^2 \epsilon_1 + I_{rwx} \cos^2 \epsilon_1 + 2I_{rwxz} \sin \epsilon_1 \cos \epsilon_1)\dot{r} + \{M_f jk - I_{rxz} + (I_{fz} - I_{fx}) \sin \epsilon \cos \epsilon - M_b b_1 b_2 + (I_{rwx} - I_{rwx}) \sin \epsilon_1 \cos \epsilon_1 + I_{rwxz} (\sin^2 \epsilon_1 - \cos^2 \epsilon_1)\} \ddot{\phi} + (M_f fk - I_{fx} \sin \epsilon) \ddot{\gamma} + (M_f ek + I_{fz} \cos \epsilon) \ddot{\delta} + (M_b a_2 b_2 + I_{rwx} \cos \epsilon_1 + I_{rwxz} \sin \epsilon_1) \ddot{\lambda} = \{i_{fy}/R_f + (i_{ry} + i_{rwy})/R_r\} U \dot{\phi} + D_c h_{cp} U^2 \phi + (i_{fy} \cos \epsilon / R_f) U \dot{\gamma} + (i_{fy} \sin \epsilon / R_f) U \dot{\delta} + (t + \ell \cos \epsilon) X_f \delta + (i_{rwy} \sin \epsilon_1 / R_r) U \dot{\lambda} + (a_4 - b \cos \epsilon_1) X_r \lambda + (s_1 - \ell \sin \epsilon) X_f \gamma + \ell Y_f - b Y_r + M_{zf} + M_{zr} \quad (3.2)$$

$$(M_f j + M_r h + M_b b_1)(\dot{v} + Ur) + \{M_f jk - I_{rxz} + (I_{fz} - I_{fx}) \sin \epsilon \cos \epsilon - M_b b_1 b_2 + (I_{rwx} - I_{rwx}) \sin \epsilon_1 \cos \epsilon_1 + I_{rwxz} (\sin^2 \epsilon_1 - \cos^2 \epsilon_1)\} \dot{r} + (M_r h^2 + M_f j^2 + M_b b_1^2 + I_{fx} \cos^2 \epsilon + I_{fz} \sin^2 \epsilon + I_{rx} + I_{rwx} \cos^2 \epsilon_1 + I_{rwx} \sin^2 \epsilon_1 - 2I_{rwxz} \sin \epsilon_1 \cos \epsilon_1) \ddot{\phi} + (I_{fx} \cos \epsilon + M_f f j) \ddot{\gamma} + (M_f e j + I_{fz} \sin \epsilon) \ddot{\delta} + (I_{rwx} \sin \epsilon_1 - I_{rwxz} \cos \epsilon_1 - M_b a_2 b_1) \ddot{\lambda} = - \{(i_{ry} + i_{rwy})/R_r + i_{fy}/R_f\} Ur + (M_f j + M_r h + M_b b_1) g \phi + (i_{fy} \sin \epsilon / R_f) U \dot{\gamma} + (M_f fg - Z_f s_1) \gamma - (i_{fy} \cos \epsilon / R_f) U \dot{\delta} + (M_f eg - Z_f t) \delta - (i_{rwy} \cos \epsilon_1 / R_r) U \dot{\lambda} - (M_b a_2 g + Z_r a_4) \phi + M_{xf} + M_{xr} \quad (3.3)$$

$$\begin{aligned}
 & M_f f (\dot{v} + Ur) + (M_f f k - I_{fx} \sin \epsilon) \dot{r} + (M_f f j + I_{fx} \cos \epsilon) \ddot{\phi} \\
 & + (M_f f^2 + I_{fx}) \ddot{\gamma} + M_f e f \ddot{\delta} = - (i_{fy} \cos \epsilon / R_f) Ur - (i_{fy} \sin \epsilon / R_f) U \dot{\phi} \\
 & + (M_f f g - Z_f s_1) \phi - D_f \dot{\gamma} + (M_f f g \cos \epsilon - S_f - Z_f \cos \epsilon s_1) \gamma - (i_{fy} / R_f) U \dot{\delta} \\
 & + (M_f e g - Z_f t - X_f s_1) \cos \epsilon \delta - X_f t \sin \epsilon \delta - s_1 Y_f - \sin \epsilon M_{zf} \\
 & + \cos \epsilon M_{xf} \tag{3.4}
 \end{aligned}$$

$$\begin{aligned}
 & M_f e (\dot{v} + Ur) + (M_f e k + I_{fz} \cos \epsilon) \dot{r} + (M_f e j + I_{fz} \sin \epsilon) \ddot{\phi} + M_f e f \ddot{\gamma} \\
 & + (M_f e^2 + I_{fz}) \ddot{\delta} = - (i_{fy} \sin \epsilon / R_f) Ur + (i_{fy} \cos \epsilon / R_f) U \dot{\phi} \\
 & + (M_f e g - Z_f t) \phi + (i_{fy} / R_f) U \dot{\gamma} + (M_f e g - Z_f t) \cos \epsilon \gamma - D_s \dot{\delta} \\
 & + (M_f e g - Z_f t) \sin \epsilon \delta - t Y_f + \cos \epsilon M_{zf} + \sin \epsilon M_{xf} \tag{3.5}
 \end{aligned}$$

$$\begin{aligned}
 & - M_b a_2 (\dot{v} + Ur) + (M_b a_2 b_2 + I_{rwz} \cos \epsilon_1 + I_{rwxz} \sin \epsilon_1) \dot{r} + (I_{rwz} \sin \epsilon_1 \\
 & - I_{rwxz} \cos \epsilon_1 - M_b a_2 b_1) \ddot{\phi} + (I_{rwz} + M_b a_2^2) \ddot{\lambda} = - (i_{rwy} \sin \epsilon_1 / R_r) Ur \\
 & + (i_{rwy} \cos \epsilon_1 / R_r) U \dot{\phi} - (M_b a_2 g + Z_r a_4) \phi - D_r \dot{\lambda} - (S_r + M_b a_2 g \sin \epsilon_1 \\
 & + Z_r a_4 \sin \epsilon_1) \lambda - a_4 Y_r + \cos \epsilon_1 M_{zr} + \sin \epsilon_1 M_{xr} \tag{3.6}
 \end{aligned}$$

The tyre model equations and the relevant parameter values are as given by Sharp (1984b).

The equations are linearised for small perturbations from a straight running condition by eliminating motion variable terms of second or higher order, because they are negligibly small. The equations have constant coefficients, and may be reduced to first order by introducing another four equations of the form  $\Gamma - \dot{\gamma} = 0$ , allowing terms like  $\ddot{\gamma}$  and  $\ddot{\lambda}$  to be replaced by  $\dot{\Gamma}$  and  $\dot{\Lambda}$  respectively. This results in a total of fourteen first order equations, including those for the tyre forces and moments.

These equations are easily solved using standard computer routines to give eigenvalues and eigenvectors for the free vibration

behaviour of the motorcycle, as explained by Sharp (1982).

### 3.4. RESULTS

Results in the form of eigenvalues are given in Figs.3.2, 3 and 4, covering the speed range 5 to 55 m/s in 5 m/s increments, the plot symbol size increasing by 20% for each speed increment. The datum parameter values can be seen in Appendix 1. Only the effects on stability of rear wheel assembly parameters are illustrated, since studies of the influences of other parameters have been documented by Sharp (1984b) and Koenen (1983).

Results for the capsize mode have not been presented because the eigenvalues follow the same course with speed as presented by Sharp and Alstead (1980) for model C, without the rear wheel assembly flexibility, and are negligibly affected by the parameter variations studied here.

Selected eigenvectors for the least damped oscillatory modes are given in Figs.3.5, 6 and 7.

### 3.5. DISCUSSION

The datum results show the wobble mode to be least damped at around 15 m/s with a characteristic frequency of around 8 Hz, in agreement both with previous theoretical findings and with the known stability properties of real motorcycles. The corresponding eigenvectors for this speed are plotted in Fig.3.5, and it can be seen that the rear frame deflection is dominated by the other motion variables. These results are in general agreement with mode shapes measured experimentally by Verma (1978), in terms of amplitude and phase relationships between  $r$ ,  $\dot{\phi}$  and  $\dot{\delta}$ .

The weave mode eigenvalues also follow their expected course with forward speed, the mode being unstable at very low speeds, then becoming highly damped at medium speed, but only marginally stable at the top speed of the motorcycle. The characteristic frequency of the oscillation rises throughout the speed range to reach about 3 Hz at high speed. Eigenvectors for the high speed weave can be seen in Fig.3.6. Again, the rear wheel assembly flexion is small compared with the other motion variables, whose relationships are similar to

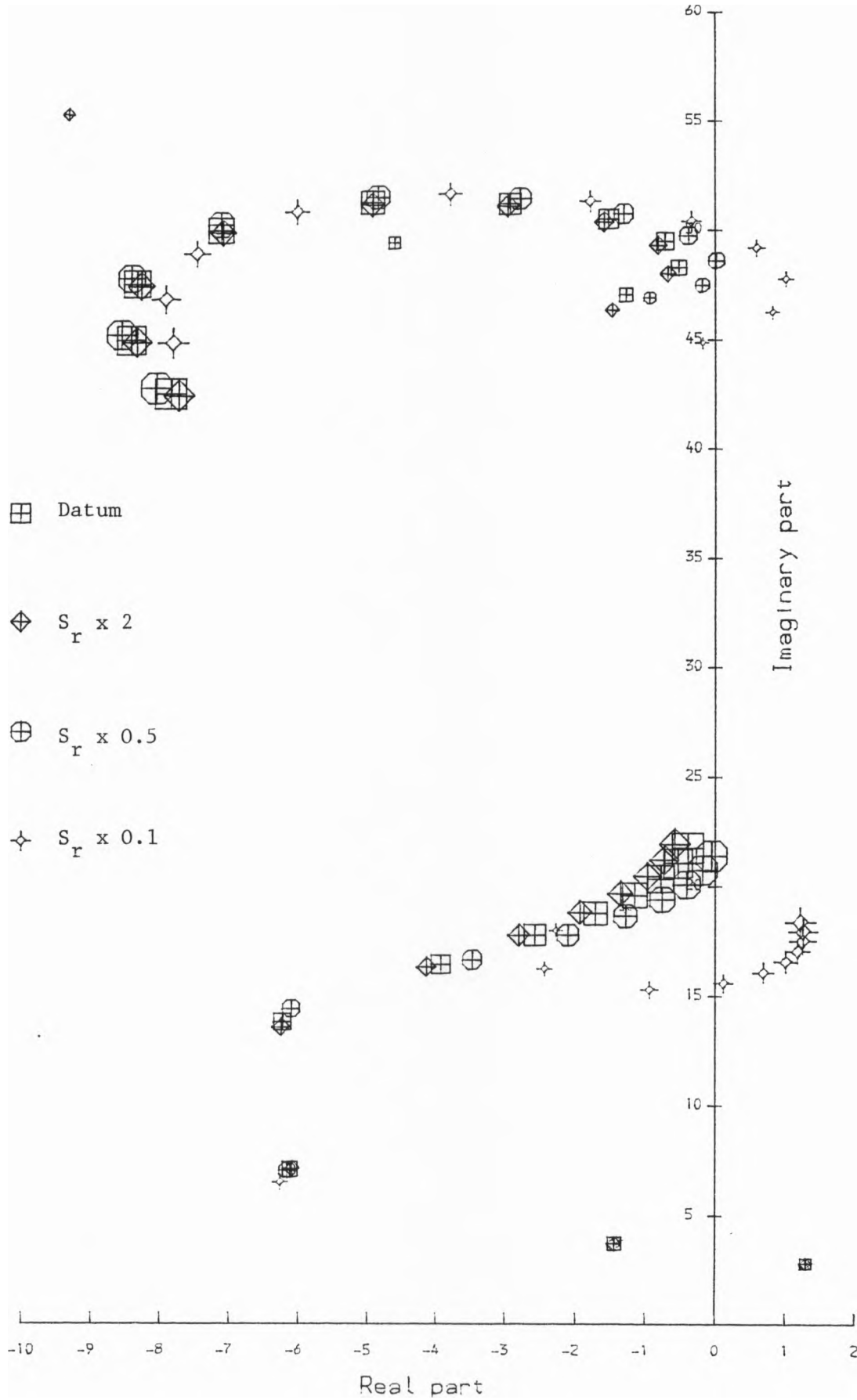


Figure 3.2

Oscillatory mode eigenvalues for changes in rear wheel assembly stiffness.

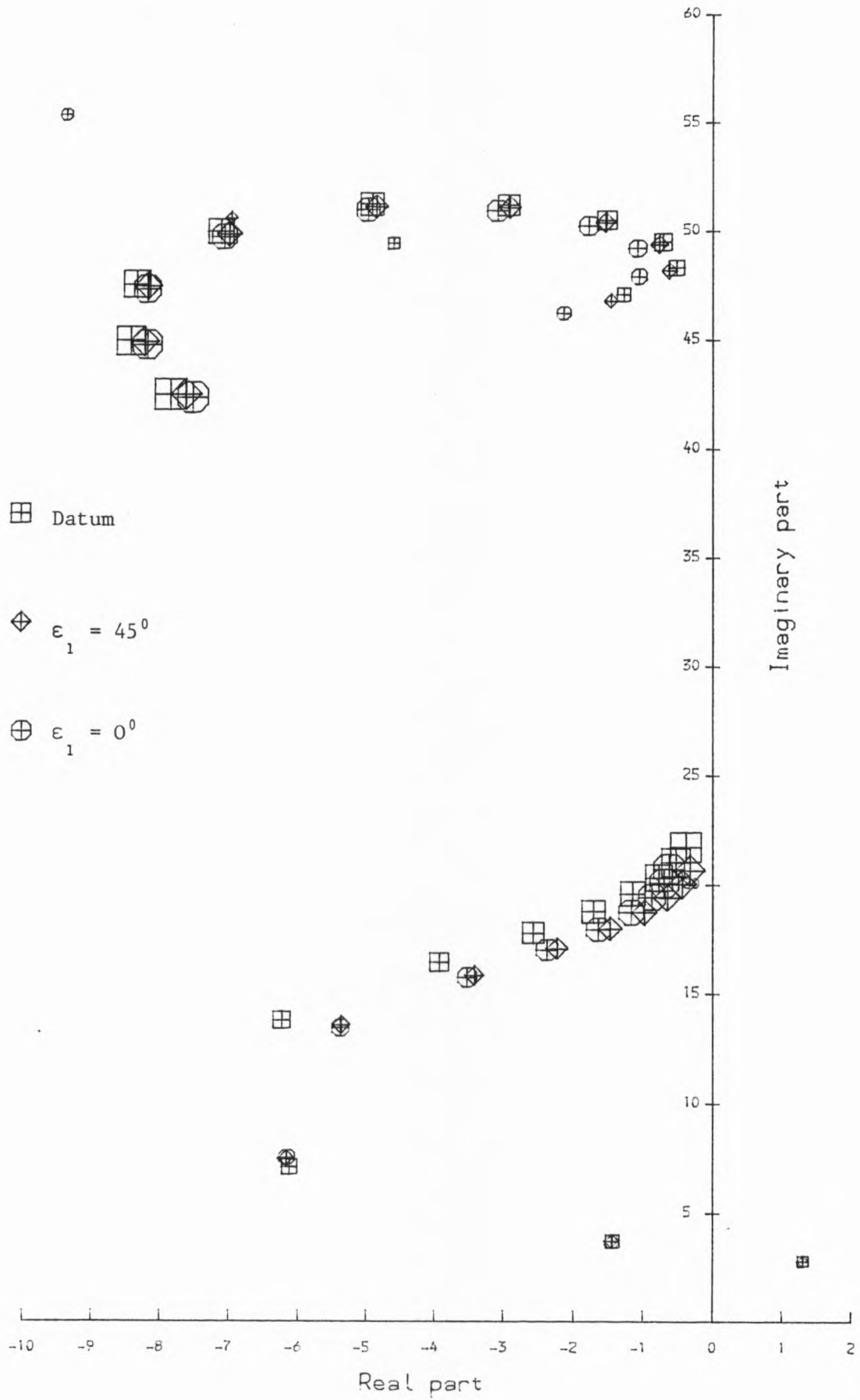


Figure 3.3

Oscillatory mode eigenvalues for changes in rear twist axis inclination angle.

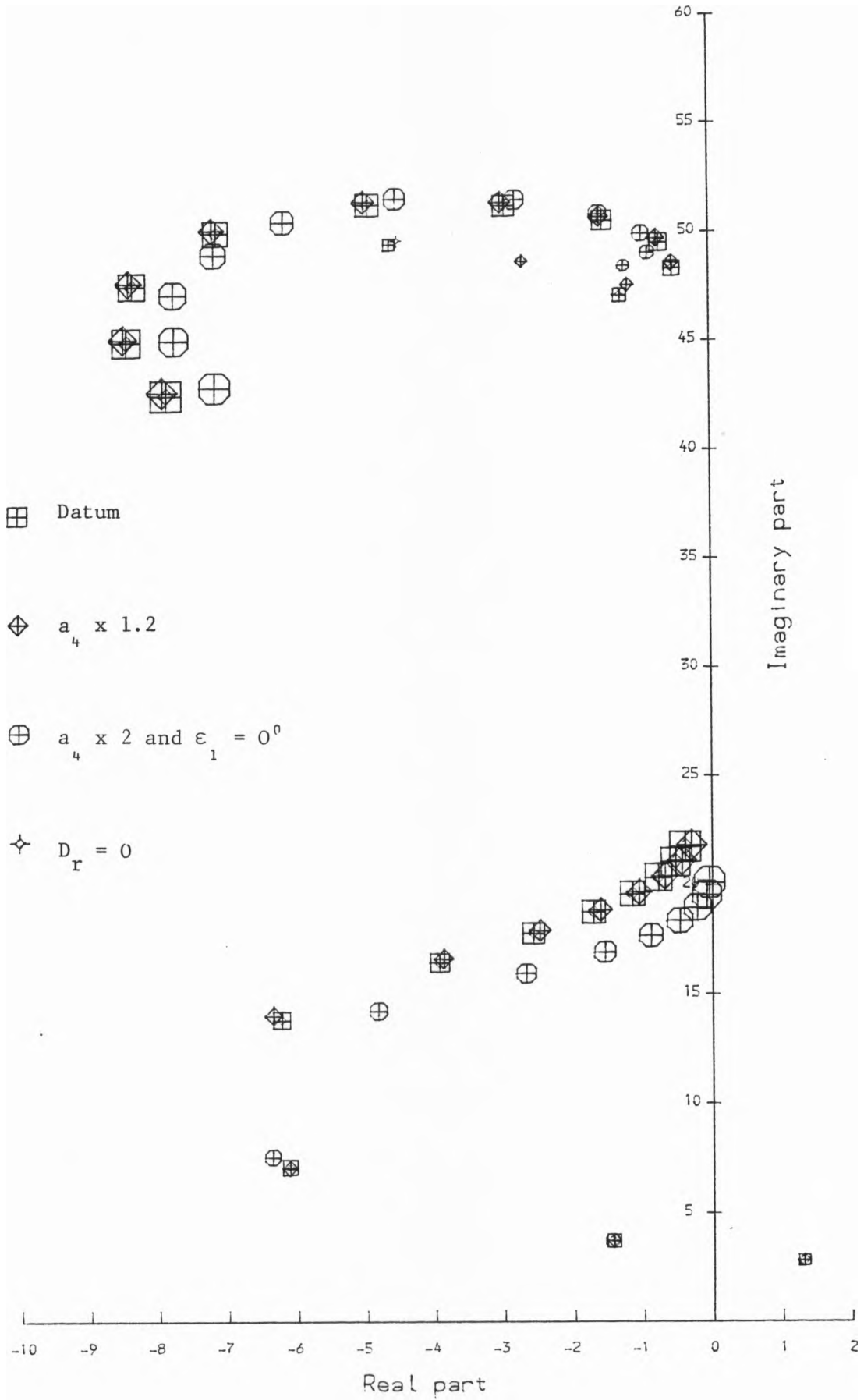


Figure 3.4

Oscillatory mode eigenvalues for changes in rear twist axis position and structural damping.



Figure 3.5

Wobble mode eigenvectors, 15m/s, datum case.

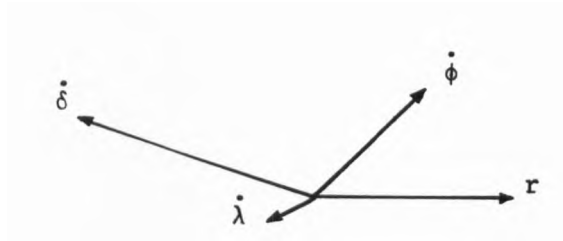


Figure 3.6

Weave mode eigenvectors, 55m/s, datum case.

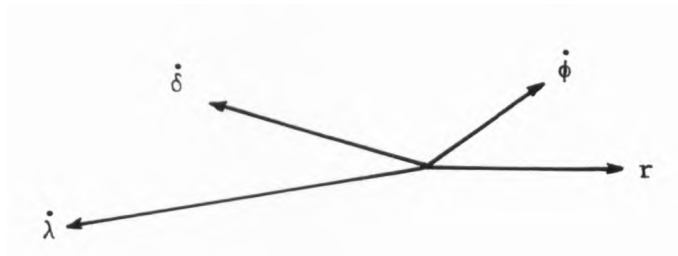


Figure 3.7

Weave mode eigenvectors, 55m/s, very low rear wheel assembly stiffness.

those found experimentally by Roland (1973) and Aoki (1979).

Fig.3.2 shows the effects of altering the rear wheel assembly stiffness, the datum value being that measured on a large motorcycle as described in Chapter 4. Doubling the stiffness has a marginally beneficial effect on the wobble mode eigenvalue at the least damped speed, and also slightly improves the weave mode damping at high speed. Reducing the stiffness to one half of the datum value has a small detrimental effect on both modes, the wobble mode reaching the stability boundary at 15 m/s.

A dramatic decrease in stiffness, to one tenth of that normally obtaining, can be seen to cause appreciable instability at both medium and high speeds. The course of the lower frequency oscillation eigenvalues with speed is dramatically changed from that of the 'normal' weave mode. There are three oscillatory modes of significance at low speed. One of them is the wobble mode and another follows the normal course of the weave mode up to 15 m/s (in fact, the relevant plot symbols lie directly over those of the weave mode), after which it becomes heavily damped. The third starts off being moderately damped at low and medium speeds, and the corresponding eigenvectors bear little resemblance to those characteristic of a weave oscillation. Then, as speed increases further, the damping reduces sharply until at high speed the mode is unstable and its eigenvectors resemble those of a weave mode (Fig.3.7), although the eigenvector associated with the rear wheel flexibility is much larger than in Fig.3.6, as one would expect. Although this amount of flexibility is unlikely to be present in a modern motorcycle, the results illustrate the probable effects of worn swinging arm or wheel bearings, and agree with my own and others' experiences with real motorcycles in this respect.

The effects of altering the orientation of the rear wheel assembly twist axis can be seen in Fig.3.3. This parameter variation was made in order to investigate whether or not the eigenvalues would be more affected by a flexibility that produced rear wheel steering rather than camber angle. This was expected to be the case because the magnitude of motorcycle tyre side forces is more strongly affected by side slip angle than by camber angle, in the ratio of approximately 8:1. It can be seen that making the twist axis vertical causes an increase in wobble mode damping at medium

speed, and a small increase in the high speed weave damping when compared with the datum results. However, the effects are much smaller than was expected.

Varying the position of the twist axis has little effect on either oscillatory mode, Fig.3.4. Increasing  $a_4$  by 20% slightly reduces weave mode damping at high speed, and moving the axis to a vertical orientation approximately 1m in front of the wheel spindle further destabilises the weave mode, while increasing the wobble mode damping at the most critical speed. This axis position corresponds approximately to that found at resonance during the dynamic stiffness measurements on the rear wheel assembly, as explained in Chapter 4. Moving the axis forward seems to have negated the small beneficial effect on the weave mode of making the twist axis vertical that was seen in Fig.3.3.

Eliminating the structural damping coefficient,  $D_r$ , from the calculations had negligible effect on the eigenvalues, Fig.3.4.

### 3.6. CONCLUSIONS

I conclude that this development of the theoretical model has not succeeded in fully explaining motorcyclists' obsession with rear swinging arm rigidity. It is clear, however, that an increase in rear wheel assembly stiffness has no detrimental effects on the straight line stability properties, and the small gains at high speed may be worthwhile obtaining for sports or racing motorcycles. Clearances in the swinging arm and/or wheel bearings are likely to cause a major deterioration in stability, but the stiffness levels typically found on large motorcycles in good condition are likely to be adequate.

CHAPTER 4

STATIC AND DYNAMIC FRAME STIFFNESS AND DEFLECTION MODE

MEASUREMENTS

A comparison between two different methods of determining the stiffness of a motorcycle frame is made. The first employs conventional, static loading of the frame with deflections and mode shape measured by dial gauges. The second entails dynamic loading of the frame by means of a sinusoidally driven shaker with deflections obtained by means of an accelerometer, electronic data processing then yielding frequency response information. Conclusions are drawn about the implications for accurate modelling of motorcycle frame flexibilities, and about the measurement procedures that can be used to obtain data relating to these flexibilities.

#### 4.1. INTRODUCTION

If there is to be a comparison between theoretical predictions and experimental measurements of stability, to examine the validity of the theoretical models developed, then accurate data on the relevant flexibilities must be obtained. Previous studies, outlined in Chapter 3, have involved examination of the static stiffnesses of motorcycle frames, and the flexibilities have been modelled by associating with each one a single extra degree of freedom involving connections between lumped masses. In reality, of course, the masses and stiffnesses are distributed, but this is much more difficult to represent mathematically. It is questionable whether these approximations are sufficient to give an accurate representation of the true behaviour of the motorcycle under dynamic conditions. At the wobble mode frequency of approximately 8-10 Hz the motorcycle tyres will be exerting oscillatory side forces of that frequency to the front and rear frames. Should the natural frequencies of the front or rear frames lie near to the excitation frequency, structural representations deriving from the resonant mode properties, rather than the static properties, may well yield better models for the study of steering behaviour.

This investigation was aimed at comparing the static and dynamic characteristics of the frame of a large conventional, road going motorcycle and thence finding the most accurate way of representing it mathematically without inconvenient complication of the model.

The study of rear frame properties undertaken was prompted by the motorcycle manufacturers' obsession with rear swinging arm rigidity, and the consequent development of a new model involving a freedom of the rear wheel assembly to yaw and camber about an inclined axis, as detailed in Chapter 3.

#### 4.2. STATIC STIFFNESS MEASUREMENTS

##### 4.2.1. Method

When considering the contribution that frame stiffnesses make to motorcycle stability, I would argue that the function of the frame is to connect the tyre forces with the inertia forces related

to the accelerations of the large central masses (i.e. engine, gear-box and rider). Thus, when considering which strategy to adopt for the stiffness measurements, we decided that anchoring the main mass to a baseplate and deflecting the frame by means of load applied near the tyre contact patches, would give the most realistic simulation of the actual role of the frame. It proved most convenient to anchor the frame by means of the engine mountings.

The practical difficulties envisaged in applying loads via the tyre contact patches were thought to outweigh the slight loss of realism that other methods involved, and I decided to apply the loads to the wheel rim as near to the tyre contact area as was possible. The load was applied using a clamp on the wheel rim connected to weights via a low friction rope and pulley arrangement. Deflections of the wheel rim were measured using dial gauges which were also anchored to the baseplate, Fig.4.1.

Sharp and Alstead (1980) showed that, for the front frame, a flexibility involving rotation of the front fork and wheel assembly about an axis perpendicular to the steer axis had a pronounced effect on motorcycle stability. Hence, I loaded the wheel rim laterally at one point and measured the deflected shape to ascertain the required axis position and thence the stiffness. To ensure that bending of the wheel rim did not lead to a false picture of the mode shape, deflection measurements were taken with the dial gauges in various positions.

It was evident from inspection that the most likely mode of deflection would involve a rotation as previously described, and consequently only two dial gauges were needed to define the mode shape, axis position and torsional stiffness. To prevent the applied load inducing rotation about the steer axis, the rim clamp was placed on the axis line, and also the forks were held with a bracing bar at the bottom yoke. A third dial gauge was used to check that no such rotation occurred, Fig.4.2.

Finding the inclined axis of rotation of the rear wheel and frame assembly required three dial gauges placed against the wheel rim so as to form the corners of a right-angled triangular plane, with the lower two gauges parallel with a line connecting the wheel/road contact points (Fig.4.2). The wheel was loaded laterally

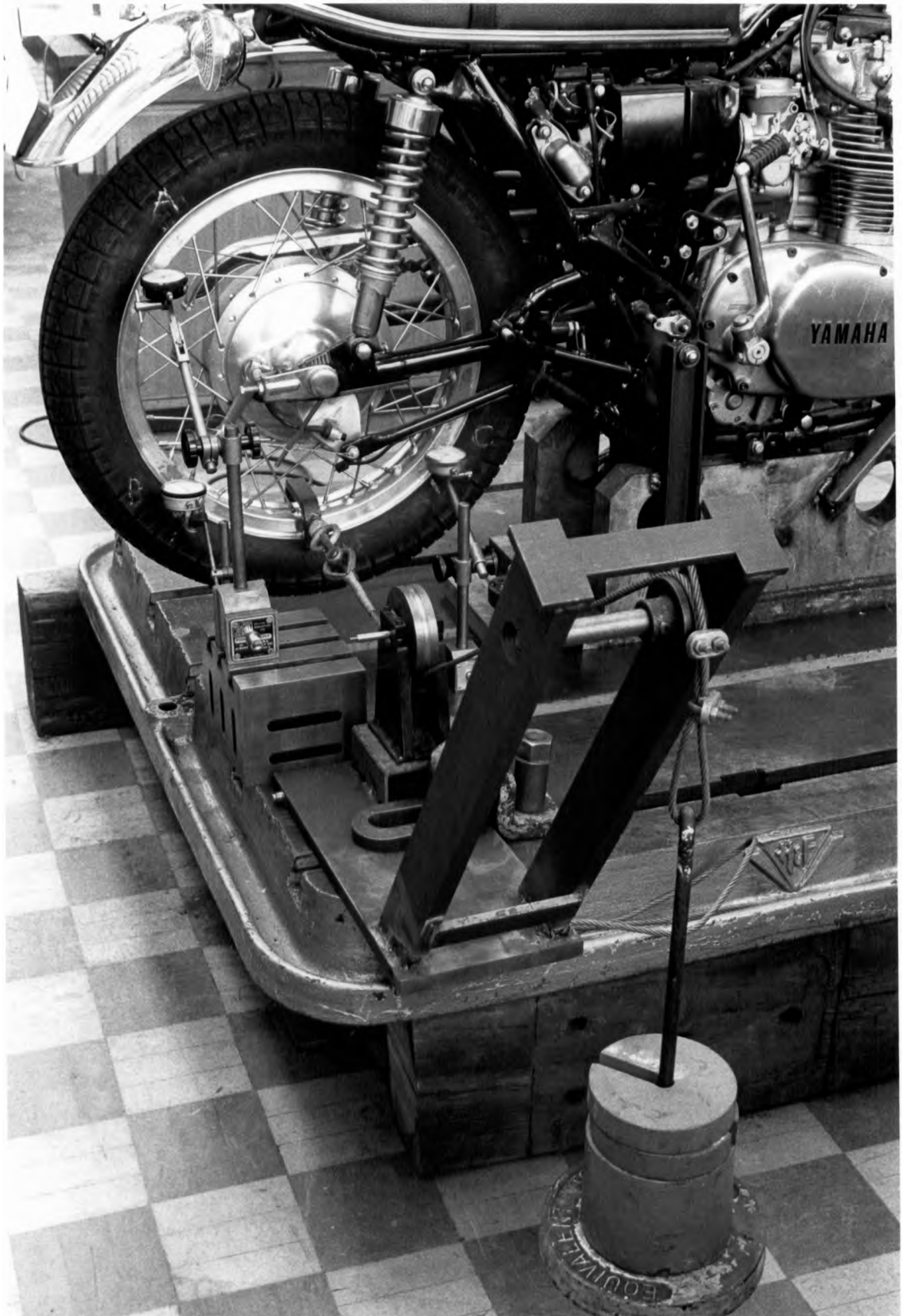


Figure 4.1

Measuring apparatus used for the static tests on the rear wheel.

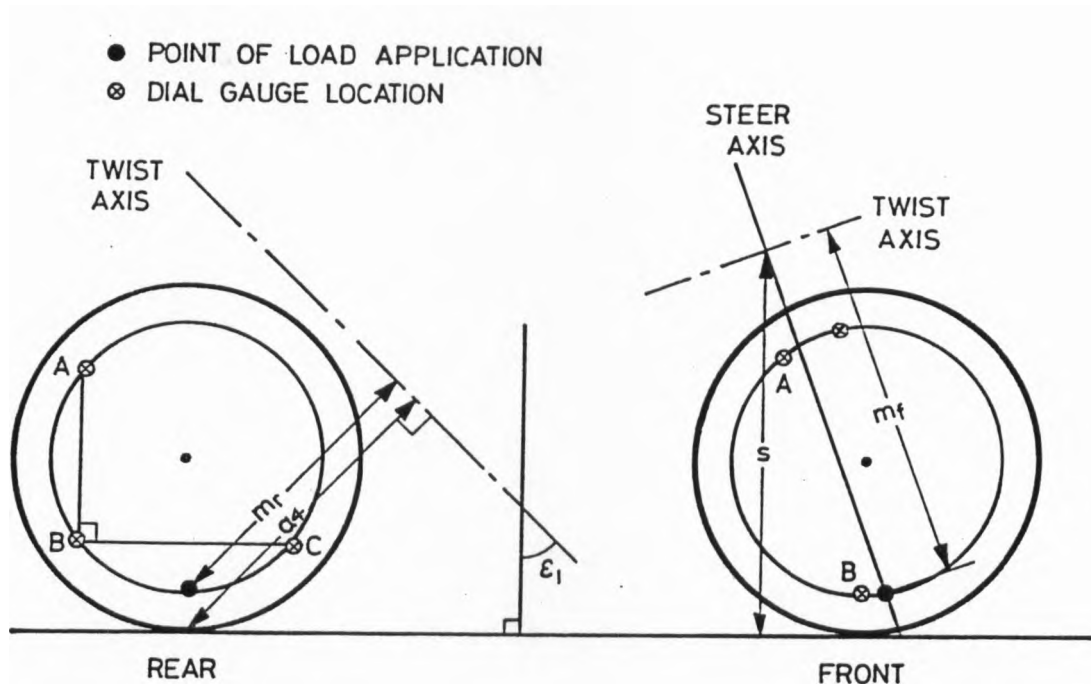


Figure 4.2

Motorcycle layout for static measurements.

as for the front, and simple geometry was used to calculate the orientation and position of the inclined axis and thence the torsional stiffness about the axis. This method differs from a previous study by Verma (1978) since it takes into account the contribution to stiffness from the spring/damper units and the upper rear frame. The measurements were taken with the dial gauges in various positions as for the front wheel rim.

#### 4.2.2. Results

The results for the front and rear frames are presented as graphs of dial gauge indication against load, calculated rotation about the relevant axes against load, Figs.4.3 and 4.4, and are shown in Table 4.1 as calculated torsional stiffnesses along with the data required to define the positions and orientations of the axes.

It can be seen from the graphs that the measurements were within the linear ranges of the frame stiffnesses and that the data points (not all of which are marked, for clarity) fall very close to the straight lines fitted by the method of least squares. Also, the

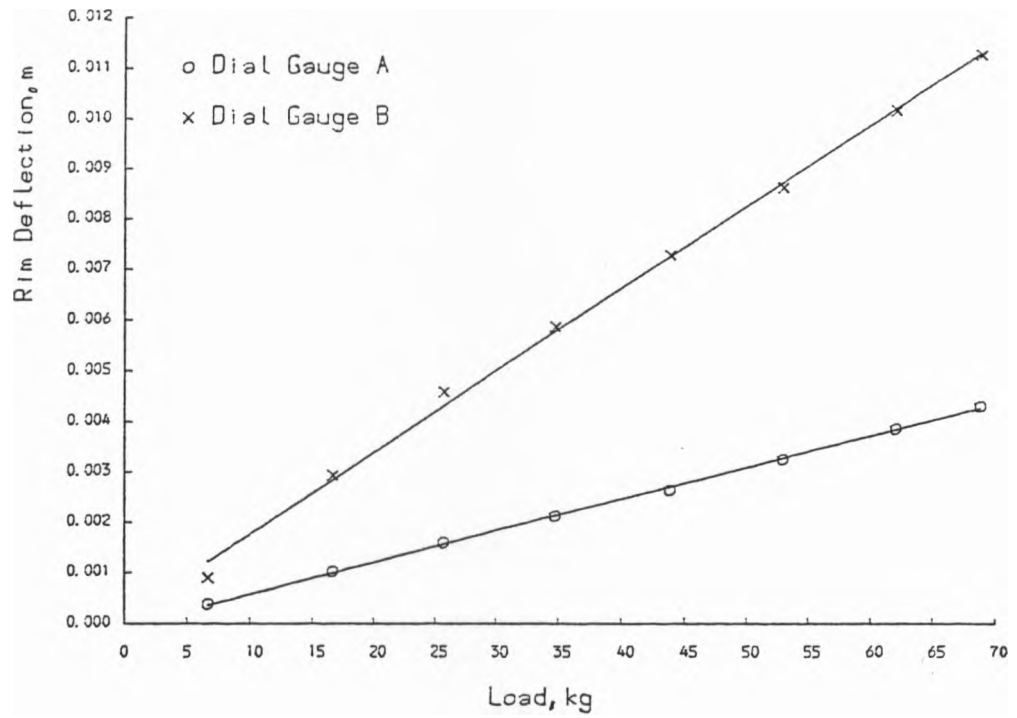


Figure 4.3(a)

Front wheel rim deflection versus load.

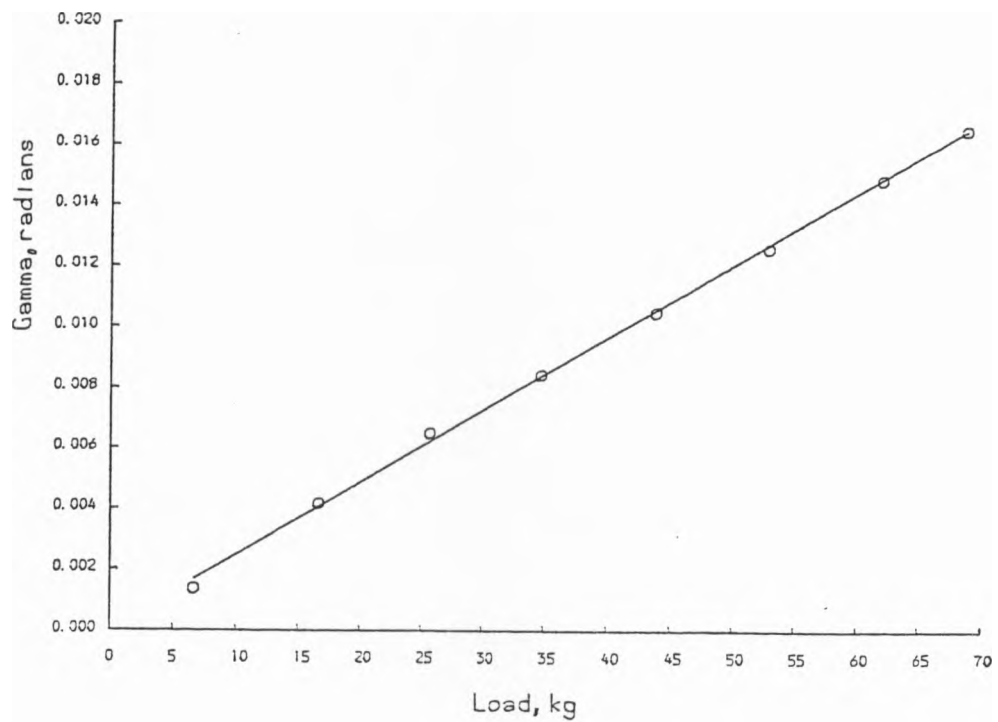


Figure 4.3(b)

Front wheel assembly rotation versus load.

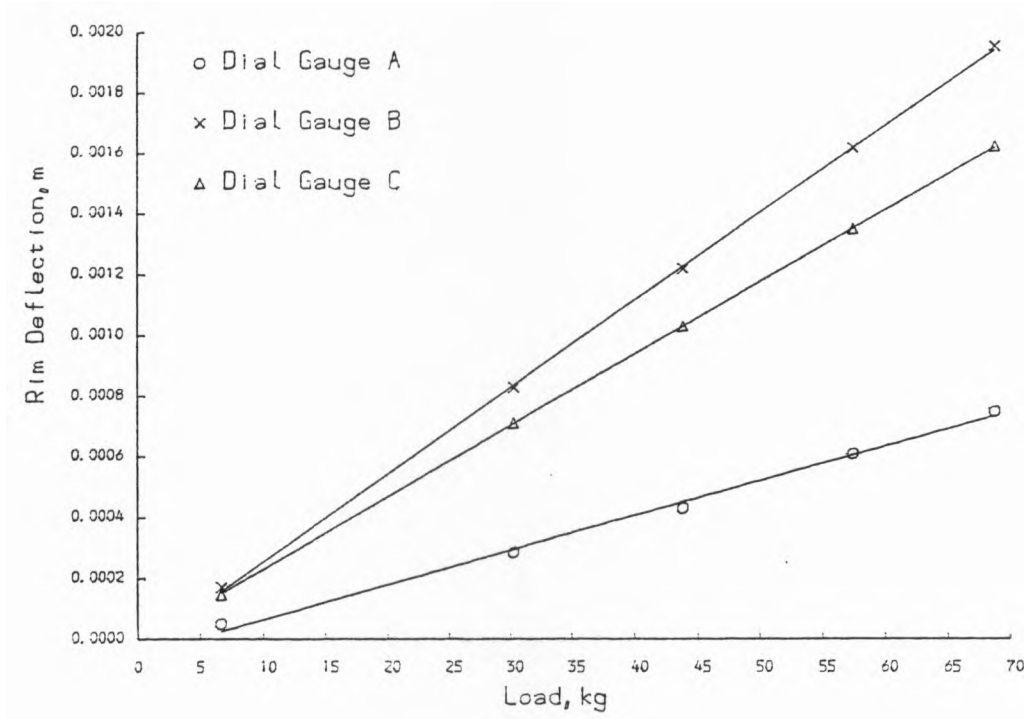


Figure 4.4(a)

Rear wheel rim deflection versus load.

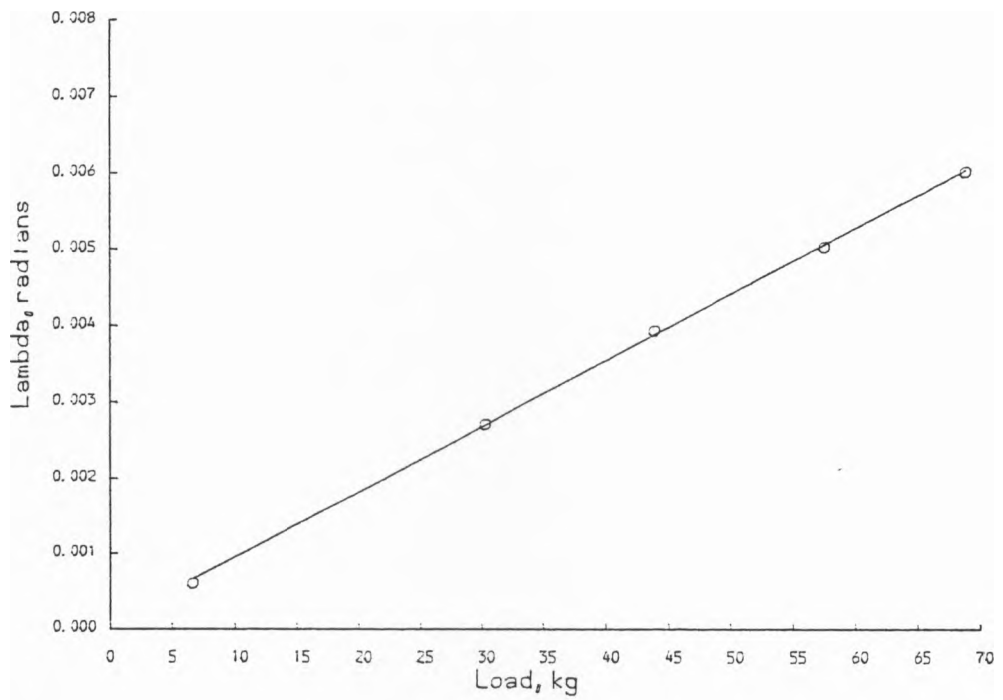


Figure 4.4(b)

Rear wheel assembly rotation versus load.

FRONT FRAME	C, kNm/rad.	$m_f$ , m	s, m	
	28.2	0.69	0.71	
REAR FRAME	C, kNm/rad.	$m_r$ , m	$a_4$ , m	$e_1$ , degrees
	46.0	0.410	0.525	82.0

Table 4.1 Statically measured frame parameters.

lines have very little zero offset, indicating that mechanical clearances (such as would be caused by worn bearings) are small.

Movement of the dial gauges to different positions showed that no localised wheel rim deflection occurred, and the results proved repeatable to within 2 per cent. The third dial gauge used on the front wheel rim showed that no rotation about the steering axis took place.

#### 4.3. DYNAMIC MEASUREMENTS

##### 4.3.1. Method

For all the dynamic tests, the same method of anchoring the machine was used as for the static tests.

A relatively simple way of ascertaining the resonant frequencies of the front and rear frames was to hit the sidewall of the relevant tyre with a hammer, with a force transducer on its face, and monitor the resultant vibration with an accelerometer. The signals from the two transducers were amplified and passed to a dual channel spectrum analyser which is capable of Fourier transforming the signals to give the frequency response function (amplitude and phase) and coherence levels. I took care to use the uniform windowing function on the spectrum analyser so as to ensure that the momentary force input was adequately sampled, as well as the more prolonged acceleration output. The sampling period was adjusted so that the response had died away at the end of data capture. The

resonant frequency can be obtained from the peak in the transfer function, and the damping as a proportion of critical from the phase information, or from the half power points. The advantages of this method are its simplicity and the fact that the system is unaltered from that studied in the static tests. The disadvantages are that some of the input energy is absorbed and distributed by tyre deflection, it is difficult to obtain information on the mode of deflection shape and it is not possible to concentrate the input power in narrow frequency bands to examine behaviour at specific frequencies.

To overcome these disadvantages I used a shaker to apply forces to the wheel rim, at the same points as those used in the static tests, and with the same clamping arrangement. Since the addition of the weight of the clamp, shaker diaphragm and the force transducer connected between the two altered the system being studied, there was clearly a compromise to be reached between using a shaker big enough to produce sufficient deflection (and acceleration output) and one small enough not to appreciably affect the system's characteristics. The shaker was suspended from above so as to support its weight but allow it to move along the horizontal axis of the force input, Fig.4.5. The shaker was driven by a sine wave generator capable of generating a wide range of frequencies and having a variable amplitude control. Thus the input power could be concentrated at the frequencies of interest. The data processing was achieved in the same way as for the hammer test previously described, except that the Hanning windowing function was used, since it was otherwise impossible to ensure that the data was periodic during the analysis window, and the use of the uniform window would have given erroneous results.

This method enabled easy identification of the mode shape at the frequencies of interest. The input power could be concentrated at the relevant frequency with a constant desired amplitude, and movement of the accelerometer around the wheel rim yielded the mode shape via the relative acceleration outputs, acceleration amplitude being related to displacement amplitude (for sinusoidal responses) by the relationship,

$$\text{Acceleration amplitude} = \omega^2 \times \text{Displacement amplitude}$$

where  $\omega = 2\pi f$

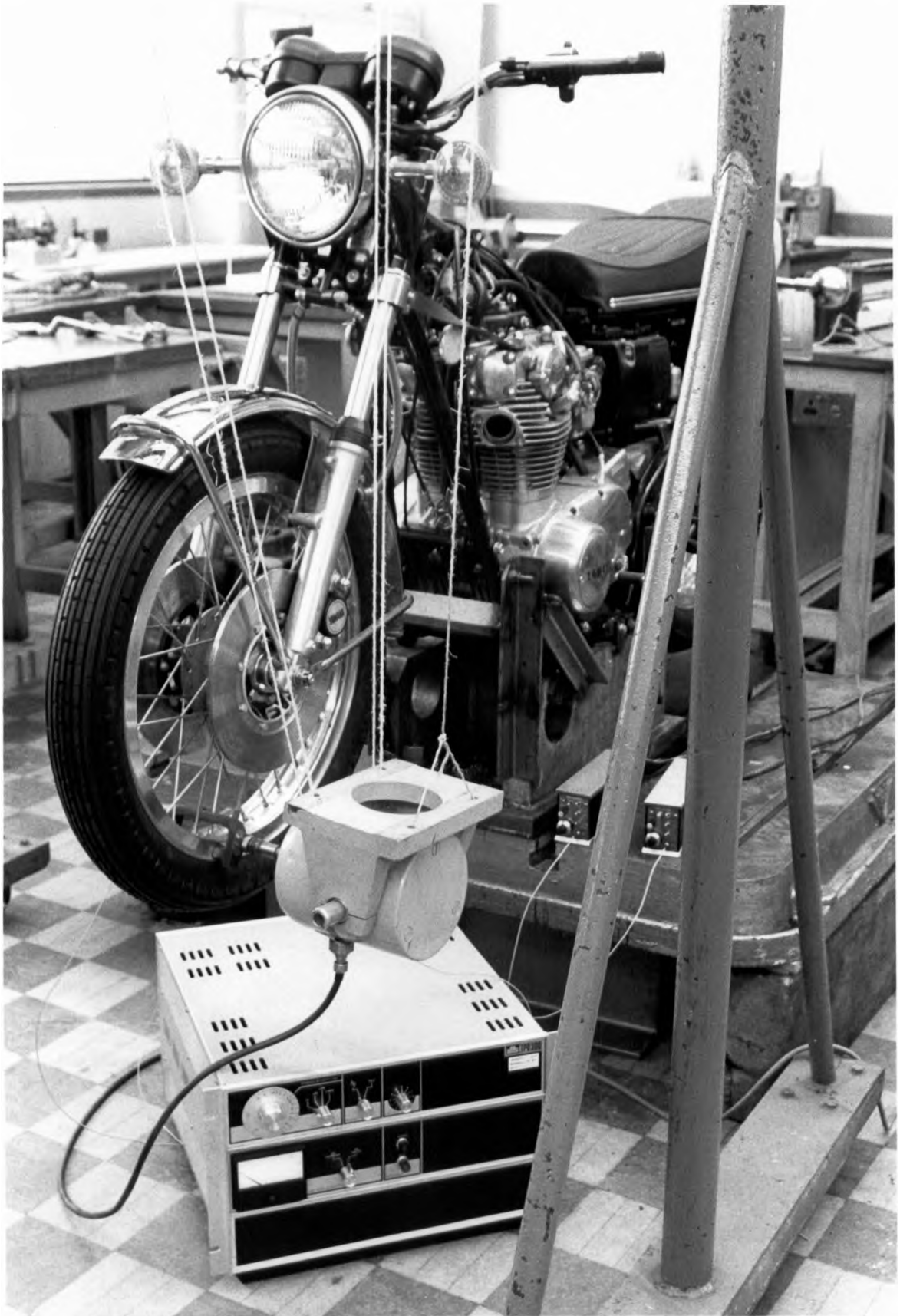


Figure 4.5

Shaker connected to front wheel for dynamic tests.

The stiffness at the frequency of interest was obtained by mounting the accelerometer on the clamp and measuring the transfer function gain at that frequency. When the relevant transducer sensitivities and signal amplification factors were noted, it was then simple to calculate the linear stiffness. Extrapolation of the rim displacement readings (using the same methods as were used for the static tests) then gave the locations of the axes of rotation and moment arm lengths. These were then used to transform the linear stiffnesses to torsional ones via the relationship:

$$\text{Torsional stiffness} = m^2 \times \text{Linear stiffness at clamp.}$$

However, the stiffness thus calculated includes the effect of the inertia of the system, which may be appreciable if excitation is near the resonant frequency, and since the objective was to compare the results yielded by static and dynamic tests, it was desirable to find the indicated static stiffness (i.e. with the inertial effect removed).

This can be obtained using the formula (from the theory of forced vibration for single degree of freedom systems):

$$\text{Measured torsional stiffness} = C\sqrt{((1-r^2)^2 + (2\zeta r)^2)}$$

where  $r = \frac{f}{f_n}$

The damping as a proportion of critical,  $\zeta$ , is calculable by two methods, both entailing excitation of the system over a range of frequencies either side of resonance. One method involves measuring the gain at resonance and finding the frequencies either side of resonance at which:

$$\text{Gain} = \frac{1}{\sqrt{2}} \times \text{Gain at resonance}$$

These are called the half power points,  $f_1$  and  $f_2$  say, and the damping is given by:

$$\zeta = \frac{(r_2 - r_1)}{2} \quad (\text{for } \zeta < 0.1)$$

where  $r_1 = \frac{f_1}{f_n}$  and  $r_2 = \frac{f_2}{f_n}$

The other method entails finding the gradient of the relative phase characteristic at resonance. Then:

$$\left[ \frac{d\phi}{dr} \right]_{r=1} = \frac{1}{\zeta}$$

and the gradient is easily obtained from the phase response plot on the spectrum analyser. Knowing  $\zeta$ , the indicated static stiffness,  $C$ , can be calculated.

It is evident that if  $C$  and  $\zeta$  are found by calculation from the response around resonance, the theoretical response of a matched single degree of freedom system can be calculated for any frequency, and a curve of gain against frequency can be drawn for comparison with that obtained directly by measurement. A similar thing can be done for the phase response. These comparisons indicate whether or not it is valid to treat the motorcycle problem as a single degree of freedom, lumped mass system.

#### 4.3.2. Results

Frequency responses for the shaker test showing gain and phase information for the front and rear frames can be seen in Figs.4.6 and 4.7. The calculated stiffness for the front wheel is given in Table 4.2 along with the axis location parameters. Indicated static stiffness values for the rear wheel assembly were not calculated for reasons that will be explained in the next section.

	$f_n$ , Hz	$C$ , kNm/rad.	$m_f$ ,m	$s$ ,m	$\zeta$
FRONT FRAME	12.0	80.0	1.0*	0.99*	0.036
REAR FRAME	24.0				

\*Obtained at resonance

Table 4.2 Dynamically measured frame parameters.

The hammer test indicated resonant frequencies of approximately 12 Hz for the front, and approximately 24 Hz for the rear wheel assemblies. Coherence values for this test were consistently in the region of 0.9 at resonance, and those for the shaker tests were

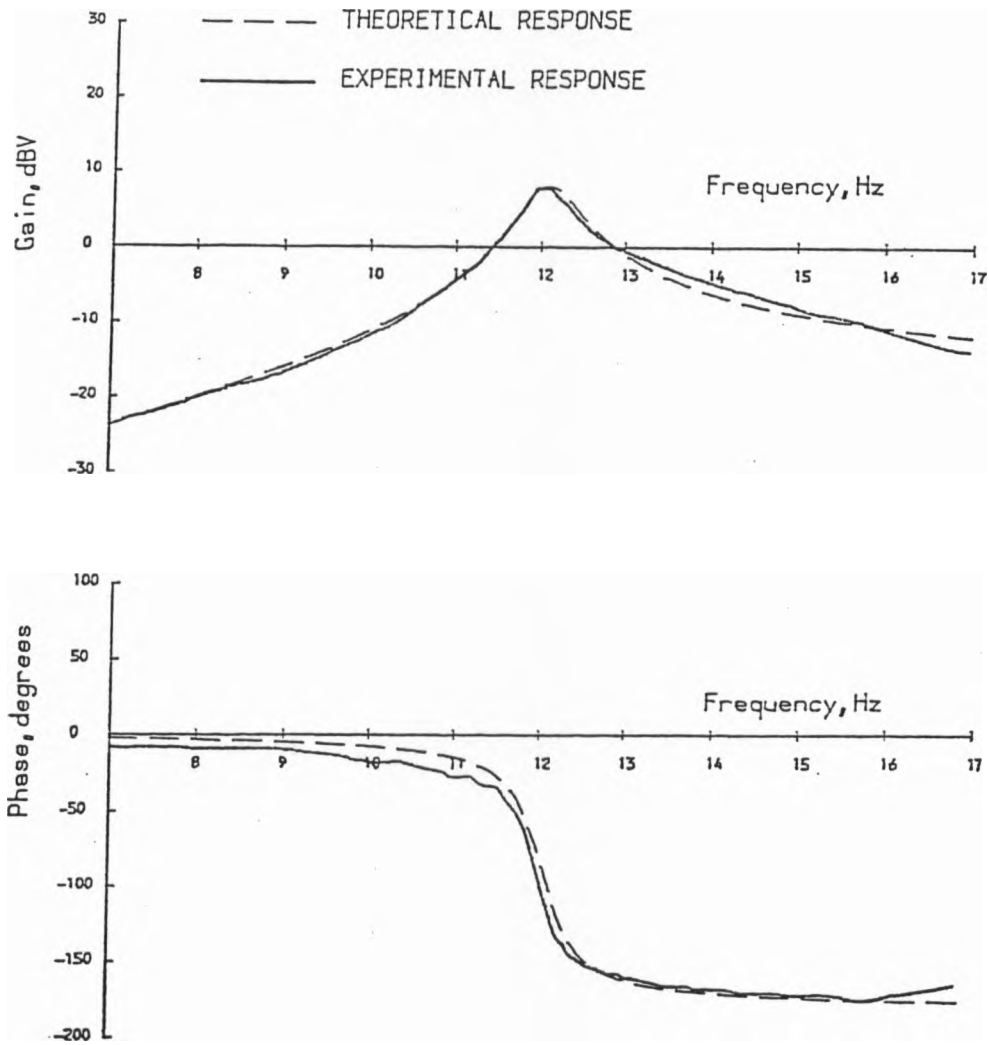


Figure 4.6

Experimental and matched theoretical frequency responses for the front wheel assembly.

close to 1.0.

#### 4.4. DISCUSSION

##### 4.4.1. Front Frame

There is a large difference between the values obtained by static and dynamic methods, not only in the stiffness values but also in the locations of the twist axis. The static results indicate an axis below the steering head, and a comparatively low stiffness. However, the dynamic results yield a higher axis, just slightly above the centre of the steering head and a higher

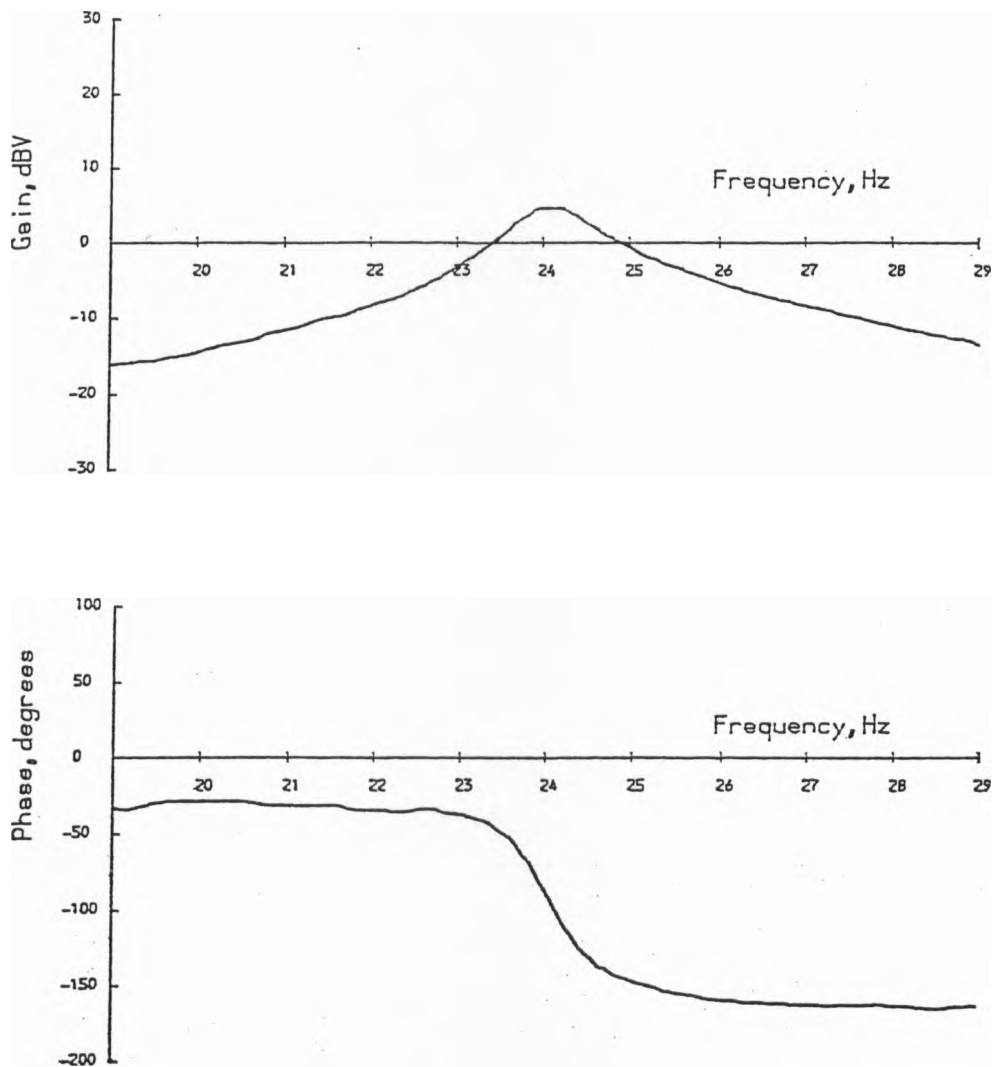


Figure 4.7

Experimental frequency responses for the rear wheel assembly.

stiffness. In fact, the dynamic measurements yield values close to the optimum indicated by Sharp and Alstead (1980) (although the axis is slightly higher in this case), at which a satisfactory compromise is reached between wobble and weave mode damping throughout the speed range.

The close agreement between the response characteristics obtained by the hammer tests and the shaker tests appear to indicate that the changes to the systems entailed in the latter had little effect on the behaviour of the frames.

The comparison of the measured responses with those obtained from single degree of freedom theory, Fig.4.6, shows that the front

frame is behaving similarly to a single degree of freedom system down to frequencies below the wobble mode frequency, and thus it would appear that the lumped mass assumption is adequate.

The best explanation for the large discrepancy appears to be the difference in the mode shape and the consequent change in the moment arm length. I saw that the static load induced a compression of the fork leg on the side at which the load was applied, bending of the other leg, and a slight twisting of the steering head. The dynamic loads did not produce compression of either fork leg, and the frame tubes leading to the steering head appeared to be undergoing appreciable deflection so that the steering head could twist about an axis perpendicular to the steer axis.

We think that the reason for this difference is that at resonance the force being applied by the shaker at the wheel rim is small. The main effective force input is coming from the inertia of the system, since at resonance, inertial effects and stiffness effects are equal and opposite. This is equivalent to applying a lateral force at the mass centre of the front frame, appreciably higher than the point of application of the static force. It is not surprising, therefore, if one considers that the frame has a translational stiffness also, that the mode of deflection differs substantially between the static and dynamic tests. The implication of this is that the dynamically measured moment arm cannot be used to calculate the equivalent static torsional stiffness, as presented in Table 4.2.

Also, the real machine's frame stiffness properties at the steering head can be realistically represented by a combination of a torsional flexibility, as above, and a translational, lateral flexibility. The thinking behind the use of just a torsional flexibility was based upon the notion that the two flexibilities could be combined by moving the twist axis to a suitable height, e.g. the nodal point found by the static stiffness measurements. Subsequent theoretical work by Sharp (1984) has indicated that the torsional and lateral deflections of the front frame are unlikely to be in phase or anti-phase during a wobble mode oscillation, in respect of which the frame flexibility properties are most important. Thus the required nodal point shifts up and down during the cycle of oscillation. Clearly this means that the two flexibilities cannot be

combined as above so as to represent the frame's dynamic behaviour adequately. Future work on the theoretical model will involve adding a lateral flexibility at the steering head, and experimental work will be carried out to determine the relevant stiffnesses by static force application.

Sharp intends to undertake an experimental examination of motorcycle stability in the near future (as explained in Chapter 2) and those results will give further information about which is the best modelling strategy to adopt.

To illustrate the importance of accurate representation of the flexibilities, the static and dynamic stiffness values yielded by this investigation have each been inserted in Sharp and Alstead's model C (1980) (which allows rotation of the steering head about an axis perpendicular to the steer axis) and a plot of the resultant eigenvalues can be seen in Fig.4.8. The effect on the weave mode is small, the static data giving rather less damping at very high speed. The effect on the wobble mode is large however, and the static data indicates an instability in the 5 - 25 m/s speed range, with rapidly increasing damping above 30 m/s. The dynamic data indicates that the wobble mode is stable throughout the speed range, but rather less highly damped than the static data indicates at high speed.

#### 4.4.2. Rear Frame

The static stiffness measurements indicate that the rear wheel assembly was rotating about an almost horizontal axis running through the upper part of the wheel. This rather unexpected axis location differs from that used in the previous theoretical investigation of rear wheel flexibility by Sharp (1974), in that it consists of wheel camber about an appreciably higher axis.

Both the hammer and shaker tests show the resonant frequency of the rear wheel assembly to be around 24 Hz, well removed from the wobble mode frequency. This indicates that the static stiffness should give an adequate representation of the real life situation.

However, it is interesting to note that at frequencies near the resonant frequency, the mode of deformation of the rear wheel

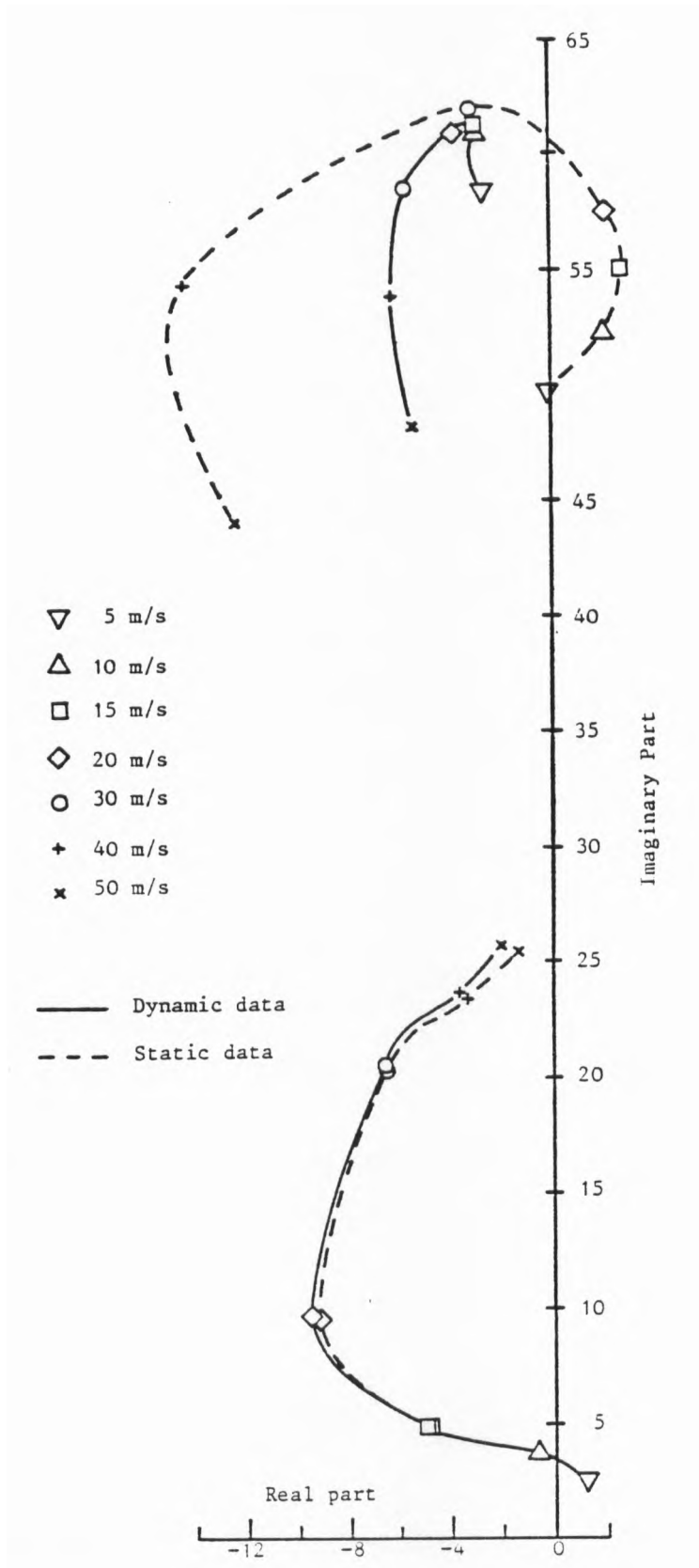


Figure 4.8

Oscillatory mode eigenvalues for static and dynamic stiffness data.

assembly had changed significantly to rotation about an almost vertical axis located approximately 1m forward of the wheel centre. This is likely to be due to inertial effects as explained for the front frame.

#### 4.5. CONCLUSIONS

The assumption that the frame flexibilities of conventional motorcycles can be modelled as consisting of lumped masses, appears to be adequate as far as representation of frequency response is concerned.

A comparison of static and dynamic stiffness measurements has shown a large discrepancy between the results, both in terms of stiffness values and indicated mode shapes. This has been explained by the considerable inertial forces affecting measurements made in the region of resonance, and by the existence of a significant translational flexibility, and I conclude that dynamically arrived at stiffness properties are likely to be misleading. These differences have been shown to have a large effect on the theoretically predicted wobble mode behaviour. Consequently, a re-examination of the problem has shown up a deficiency in the modelling details for the flexibility at the steering head. A new model is being developed and further stiffness measurements are being made.

It is expected that a future comparison of theoretical and experimental stability analyses will indicate the most true to life modelling strategy.

CHAPTER 5

THE FREQUENCY RESPONSES OF MOTORCYCLES TO STEERING TORQUE

INPUTS

Frequency responses to steering torque inputs are calculated for the straight running case. Parameter changes are made in order to compare the theoretical effects on the responsiveness of a motorcycle, with those predicted by experience. The relationship between stability and responsiveness is also discussed.

### 5.1. INTRODUCTION

During about twelve years of motorcycling, some of them spent competing in road racing, I have noticed that the motorcycling fraternity has firmly held beliefs about which design features are likely to affect strongly the responsiveness of a motorcycle and in what way. What exactly they mean by responsiveness is hard to pin down, but for the purposes of this chapter I will interpret it as being a measure of the physical effort required to bring about a desired manoeuvre, e.g. avoidance of an obstacle. Experiments by Rice (1978) and by Weir and Zellner (1979) have identified the use of two main control inputs during various manoeuvres, steer torque and rider upper body lean. There is a degree of uncertainty about the relative importance and efficacy of the two inputs, different riders using different amounts of each. A photographic study by N.P.S.R.I. (1976) concluded that body lean appears to be an activity which accompanies the lean of the motorcycle, rather than producing it. Difficulty has been encountered in modelling the rider upper body freedom accurately, because of the human body's dissimilarity from a linear spring and damper, as it is represented by Koenen (1983). Other experimental studies by Eaton (1973) and Verma (1978) have inhibited upper body lean relative to the motorcycle by means of a bracing frame, and yet the control task was still easy using steer torque alone. I don't think that it would be similarly easy to perform rapid manoeuvres without using the handlebars, however. For these reasons I regard steer torque as being the primary control input, and will not consider responses to rider upper body movements.

Changes in responsiveness due to design modifications are obviously more likely to be represented in the forced vibration behaviour (i.e. the frequency responses) than in the free vibration behaviour (i.e. the eigenvalues and eigenvectors). The latter has been extensively studied in order to identify the effects on stability of various parameter changes, but the former has received far less attention, despite having the advantage that frequency responses constitute a full representation of the dynamic properties of a linear system, whereas stability results do not. Also, experimental studies (such as those described in Chapter 2) will generally yield frequency responses rather than eigenvalues and eigenvectors,

so they are more useful for the purposes of validating the theory by comparison of the theoretical and experimental behaviour of selected machines.

Sharp and Alstead (1983) have studied the theoretical effects of various wheel and tyre imperfections on the frequency responses of a large motorcycle, and Aoki (1979) has measured the frequency responses of various machines during straight and curved running. Aoki's results for the pulse response test have been found to agree fairly closely with theoretically predicted eigenvectors, in respect of the phase relationships between the motion variables at the appropriate modal frequencies, Sharp (1982).

There are problems in interpreting the frequency responses, however, which may have discouraged more extensive treatment. Firstly, one can generate an enormous volume of results, with graphs of the gain and phase relationships of several variables over a selected frequency range, for many different speeds. Faced with such a vast amount of potential information for just one machine configuration, the prospect of wading through the results for multifarious parameter changes becomes daunting. Secondly, it is difficult to establish exactly what responses are indicative of good dynamic properties. Sharp and Alstead (1983) argued that the most desirable type of responses will involve minimal changes in gain and phase throughout the frequency range of control inputs, since these will prove easiest for the rider to learn and utilise. Since their results indicate that steering torque inputs, of appropriate frequencies at certain forward speeds, will strongly excite the weave and wobble mode oscillations, it clearly follows that flat frequency responses are very desirable because they would tend to indicate the absence of any easily excited oscillatory modes. Sharp and Alstead also indicate that the study of stability properties may need to be supplemented by the calculation of frequency responses, since design changes that have desirable effects on the significant eigenvalues may have response disadvantages. This potential conflict between stability and responsiveness is a strong theme of motorcycling folklore, and most motorcyclists appear to think that long wheelbase machines, for example, whilst being very stable, tend to have sluggish handling properties. These sorts of parameter effects will form the core of this investigation.

Unfortunately, the results presented here are strictly only indicative of the straight running behaviour of the motorcycle, and much of the received wisdom about real life parameter effects has probably been deduced from the cornering behaviour, such as entering a turn or negotiating a chicane. Nevertheless, I think that it is useful to enter into some guarded speculation, since the main events involved in initiating a turn, for example, occur whilst the machine is still within the linear region of the model.

### 5.2. METHOD

The model is the one developed in Chapter 3, and the same assumptions apply here. The method of obtaining the frequency response information has been fully described by Sharp and Alstead (1983). The input is considered to be a sinusoidal steer torque applied by the rider between the the rear frame and the front fork assembly, contributing a single term to the forcing vector, representing the amplitude of the torque.

Care was taken to ensure that results were computed only for speeds at which both oscillatory modes were stable.

### 5.3. RESULTS

The datum parameter values are listed in Appendix 1, and are the same as those used in Chapters 3 and 6.

I have chosen to present results for the frequency response function gains only. The phases are of comparatively little interest, and showed their expected form, i.e. rapid changes in phase angle corresponding to peaks in the gains at the weave and wobble mode frequencies. The phase relationships between the main motion variables at these frequencies agree well with the relevant eigenvectors yielded by the free vibration results.

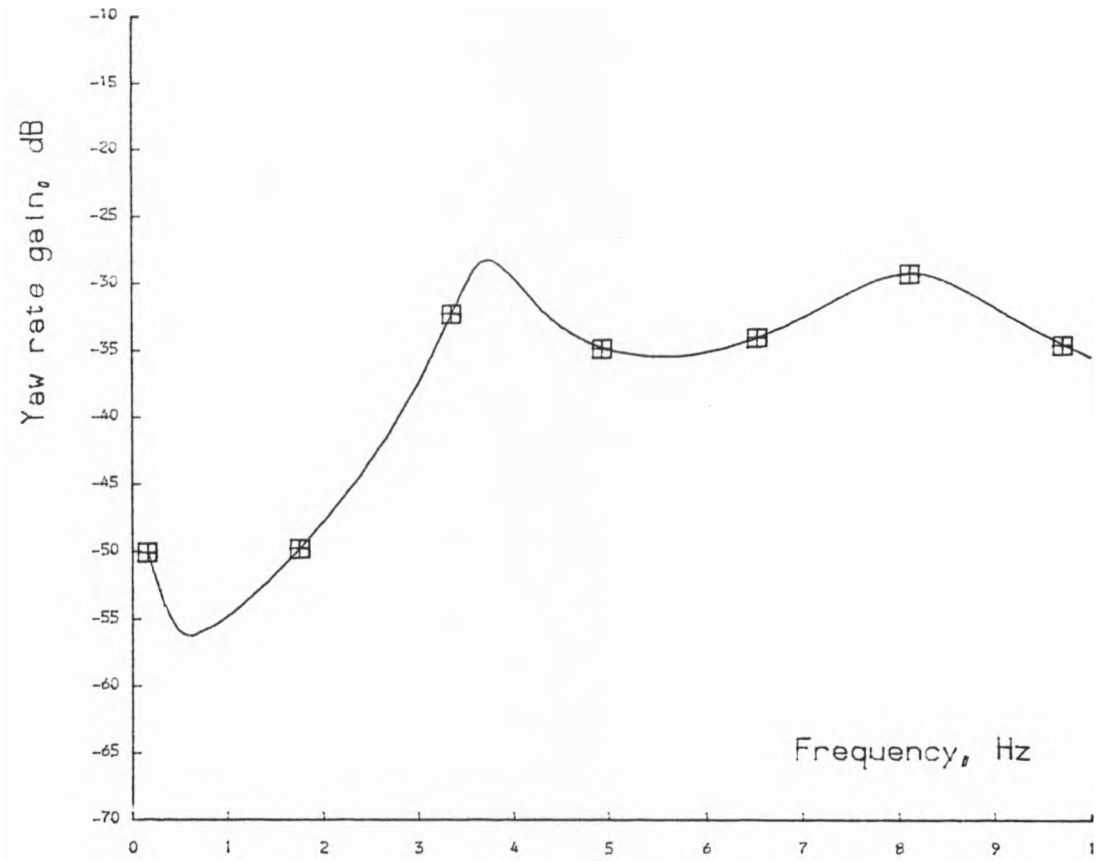
The frequency range extends from near d.c. to 10 Hz, covering the natural frequencies of both significant oscillatory modes. When considering sinusoidal steer inputs, I estimate that a rider would have difficulty producing significantly more than 2 Hz. However, the input power spectrum measured during the pulse response test (involving a brief, nominally triangular steer torque) by Aoki

(1979) showed significant power from 0.2 to 6 Hz. I would argue that rider steer torque inputs during rapid manoeuvres (especially under racing conditions) are likely to have similar power spectra. Hence, I will regard the frequency range from d.c. to 6 Hz as being of the most interest for the purposes of this discussion.

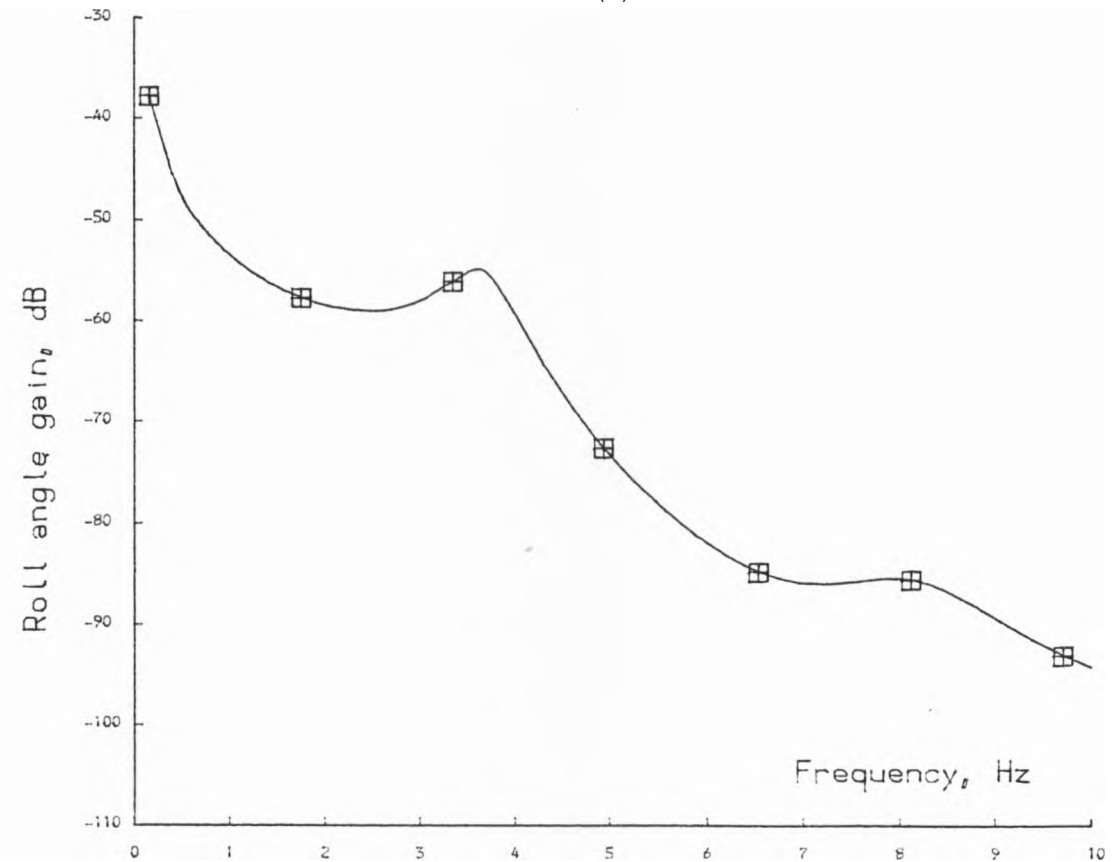
Results are presented for yaw rate, roll angle, steer angle and lateral acceleration (latac) gains in dB, as shown in Figure 5.1, (a) to (d) respectively. I regard these particular variables as being of the most interest because I consider the primary requirement to carry out a turn to be the development of yaw rate and latac, steer angle and roll angle being the means of achieving this. A most interesting discussion of this topic was presented by Wilson-Jones(1951), who concluded that to initiate a left hand turn, it is desirable to momentarily turn the steering to the right until the required rolling motion takes place, when the rider can steer into the turn. I think that this turn initiation mechanism primarily concerns the development of side force from the front tyre due to the steer induced slip angle. Rice (1978) found that experienced riders tended to use a lot more of this reverse torque than less skilled riders and were more successful at obstacle avoidance as a result. Evidently it will be easier to generate the required slip angle if the steer angle/steer torque gain is high rather than low, over the appropriate frequency range, and I will use this as one indication of responsiveness.

The rapid development of a large roll angle will enable maximum utilisation of the camber thrust of the tyres to help provide the required latac and yaw rate, and hence I regard the roll angle gain as an important response.

All of the results, with the exception of Fig.5.2, are presented for a single speed only, 40 m/s, because of the aforementioned excess of data. I chose this speed because it is high enough to be in the range where responsiveness is felt to be most crucial (particularly by racing motorcyclists), yet is sufficiently removed from the critical speeds of the weave and wobble modes.



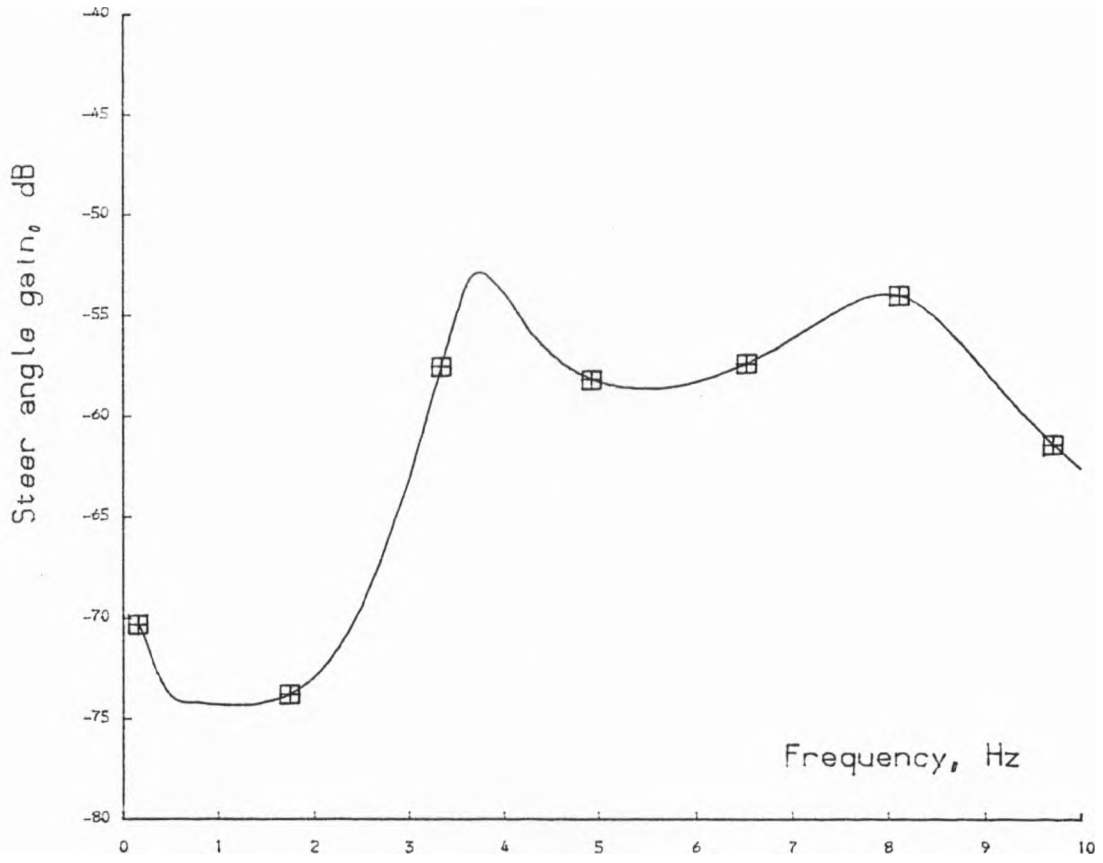
(a)



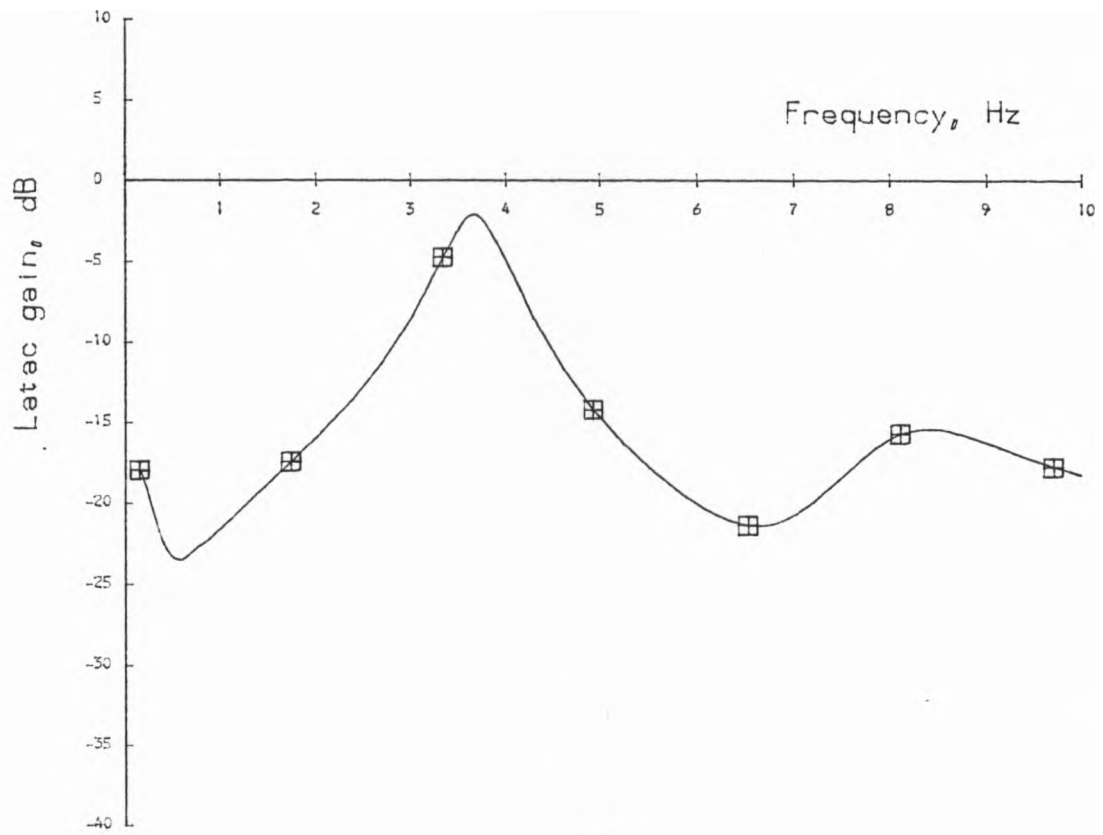
(b)

Figure 5.1

Selected frequency response gains for the datum case.

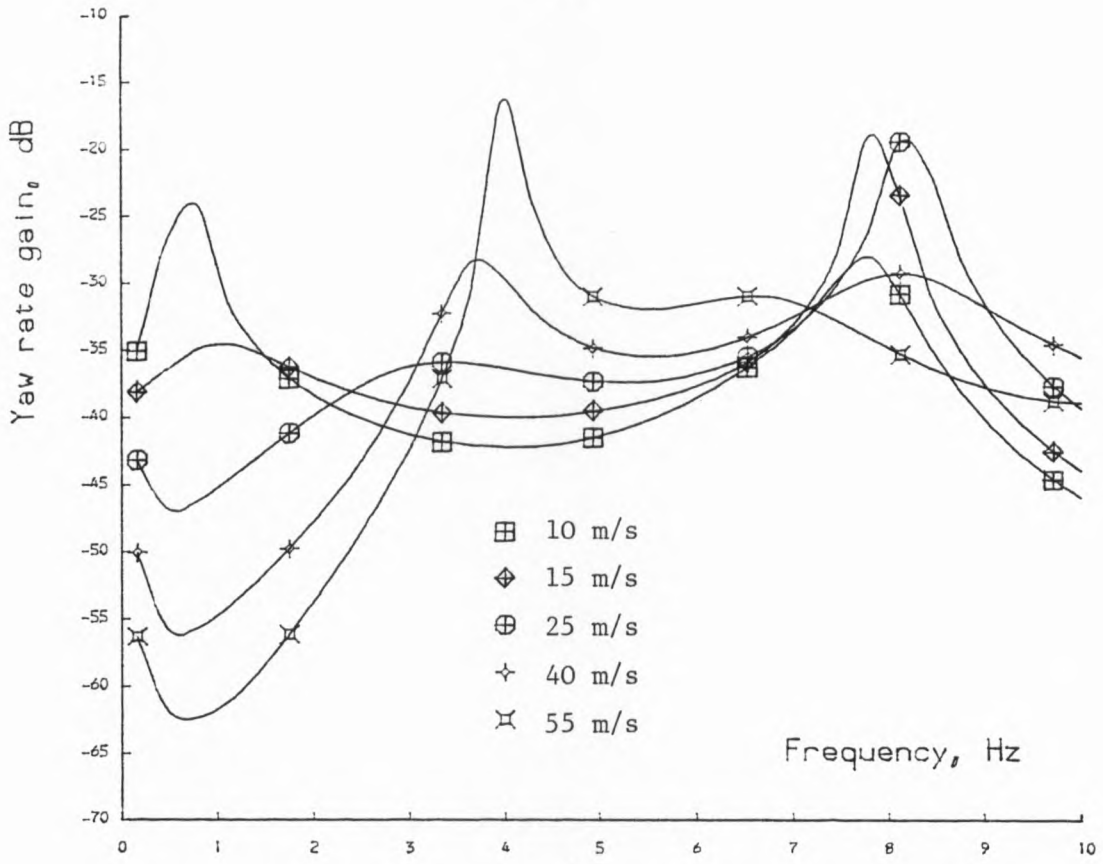


(c)

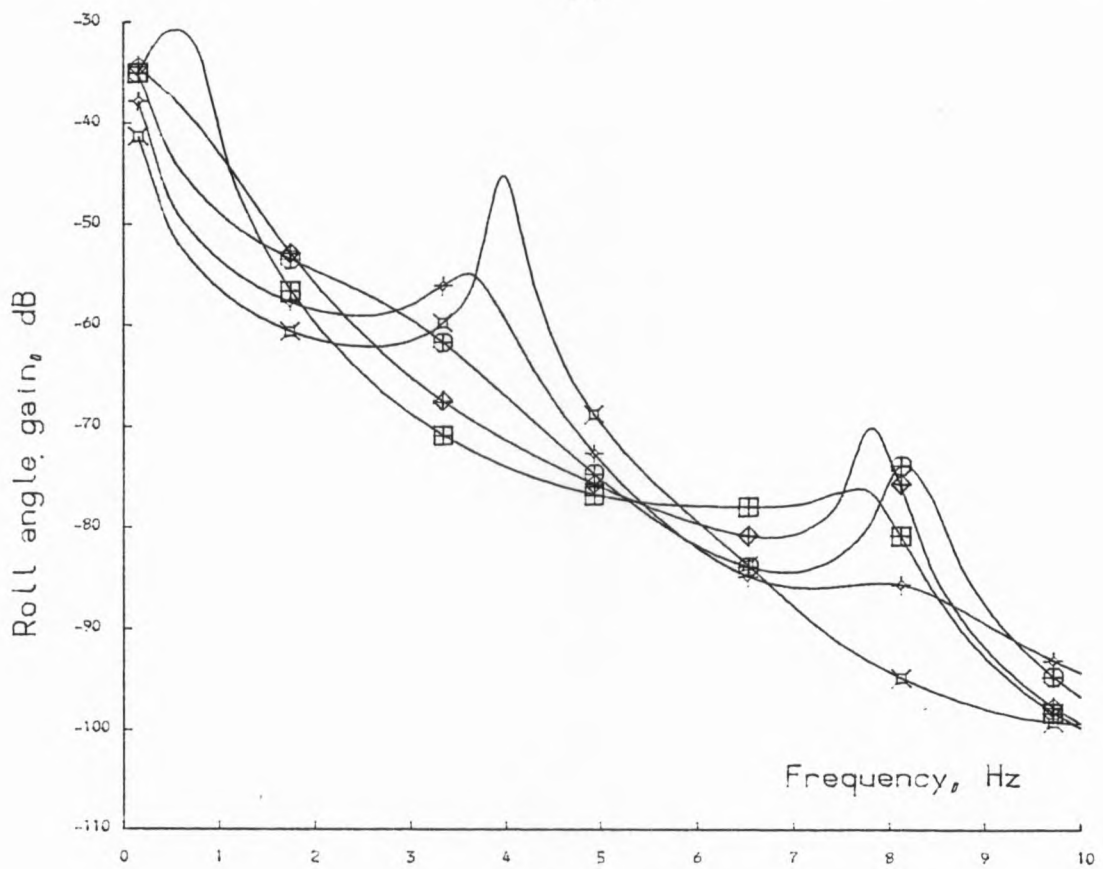


(d)

Figure 5.1 (cont.)



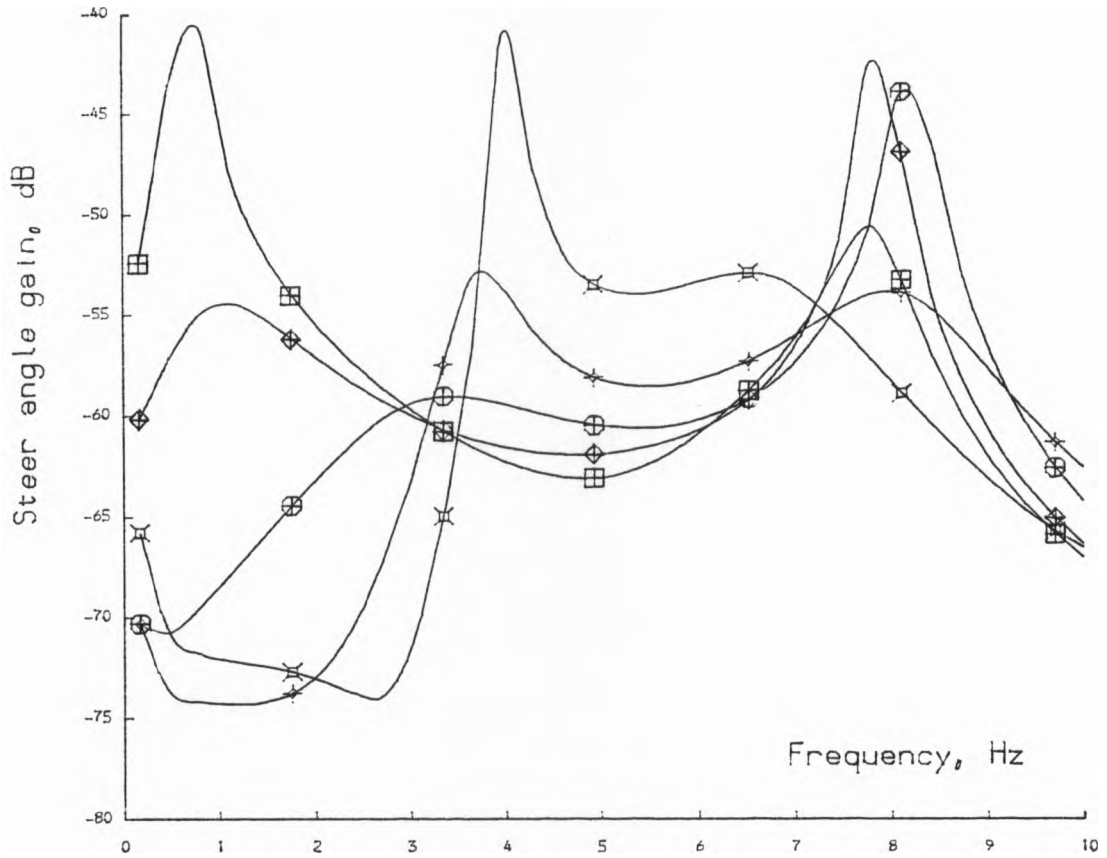
(a)



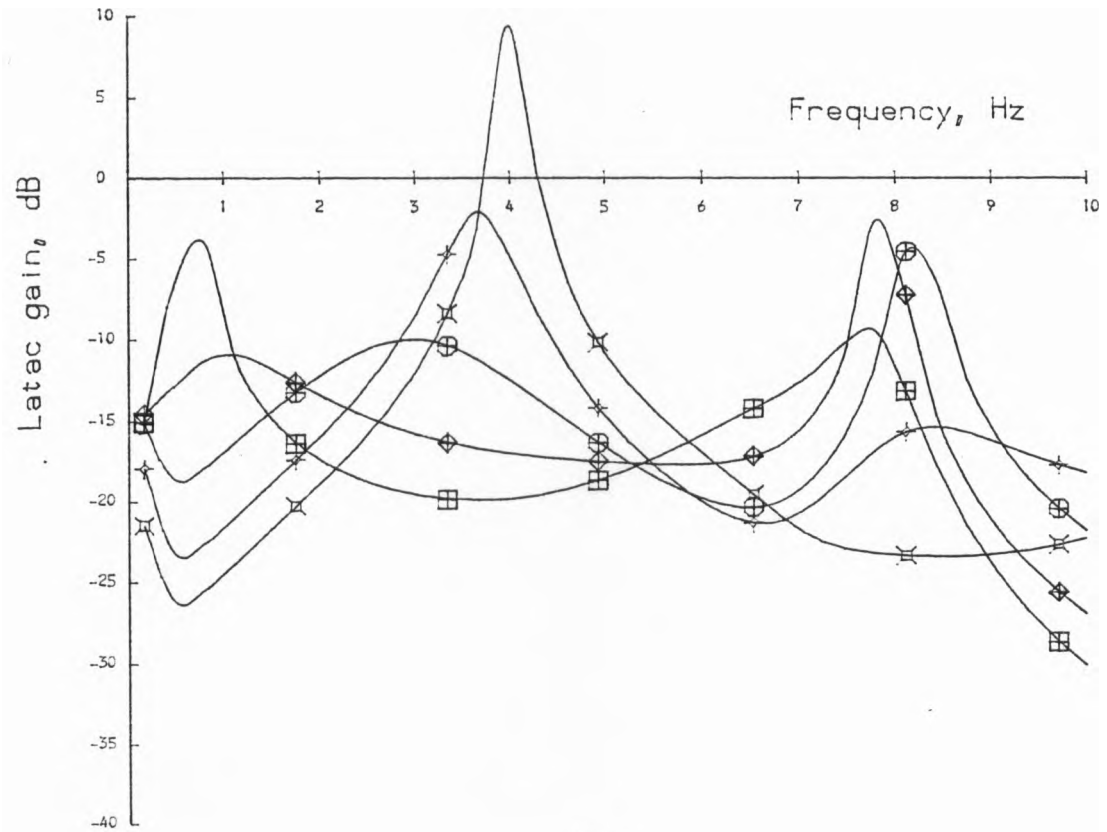
(b)

Figure 5.2

Selected frequency response gains for various speeds, datum case.

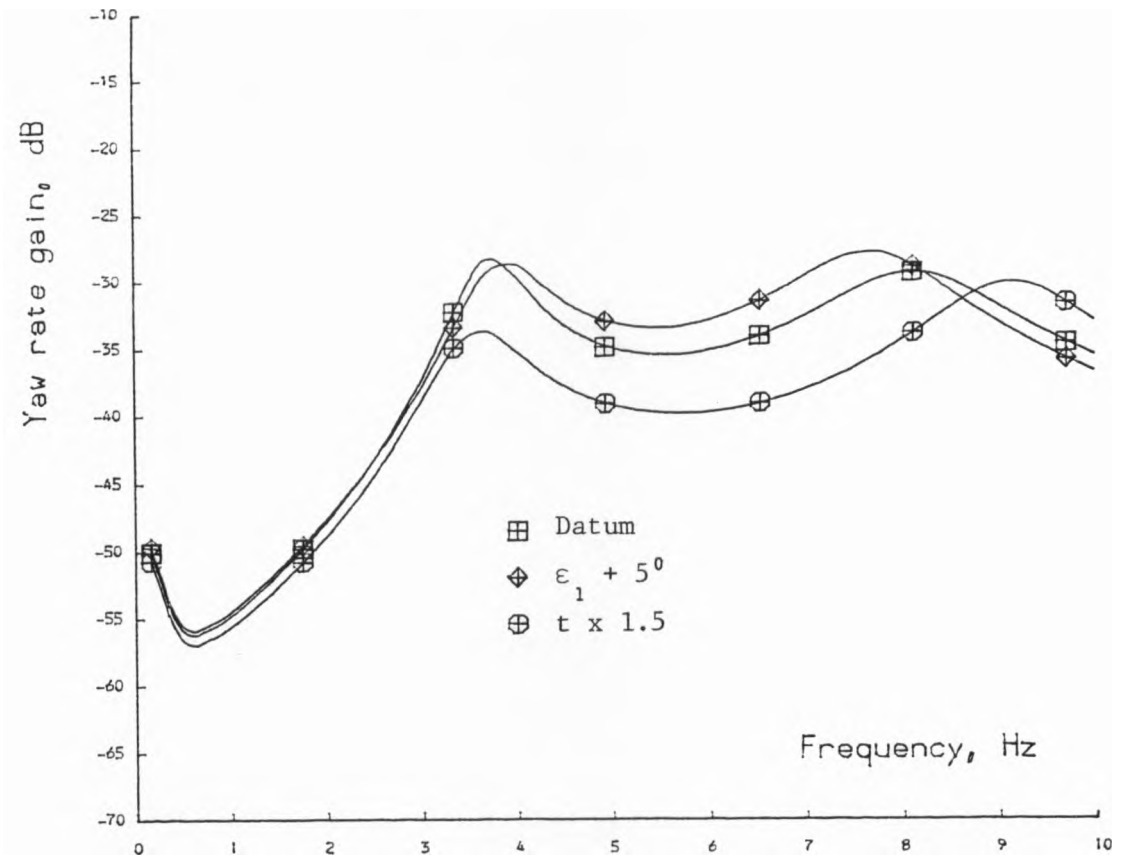


(c)

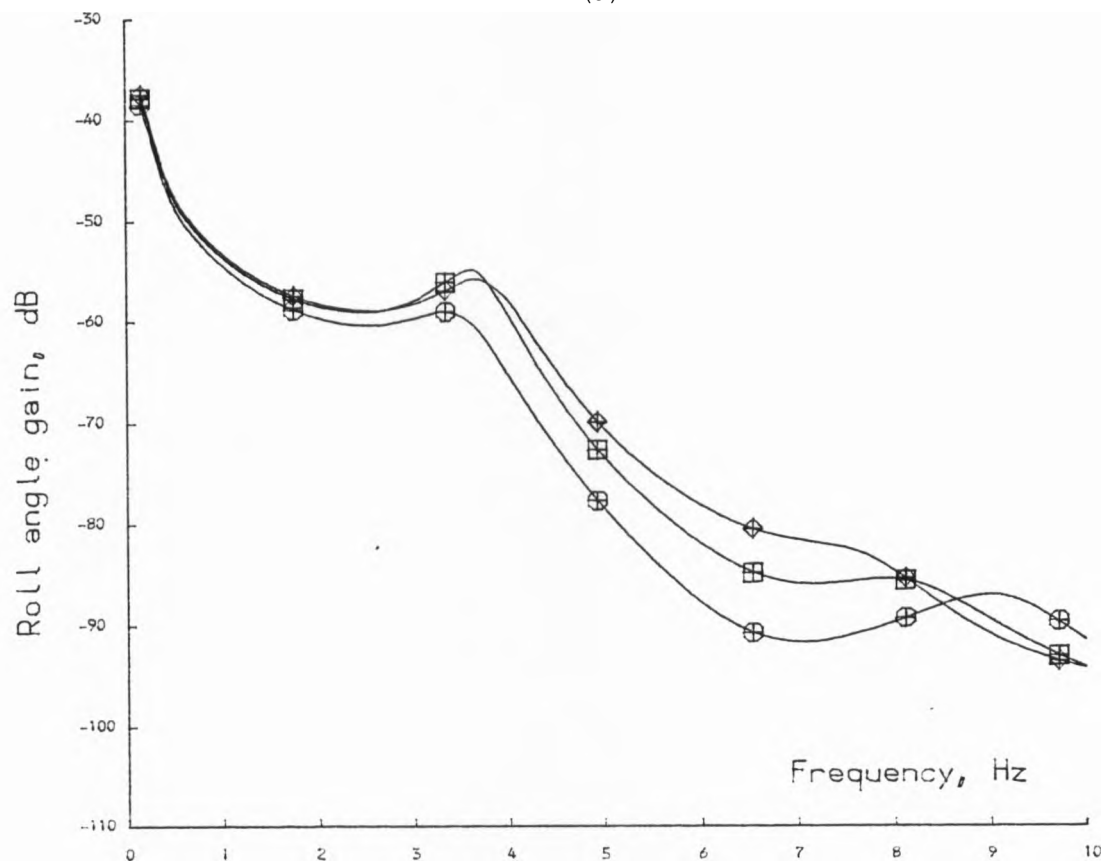


(d)

Figure 5.2 (cont.)



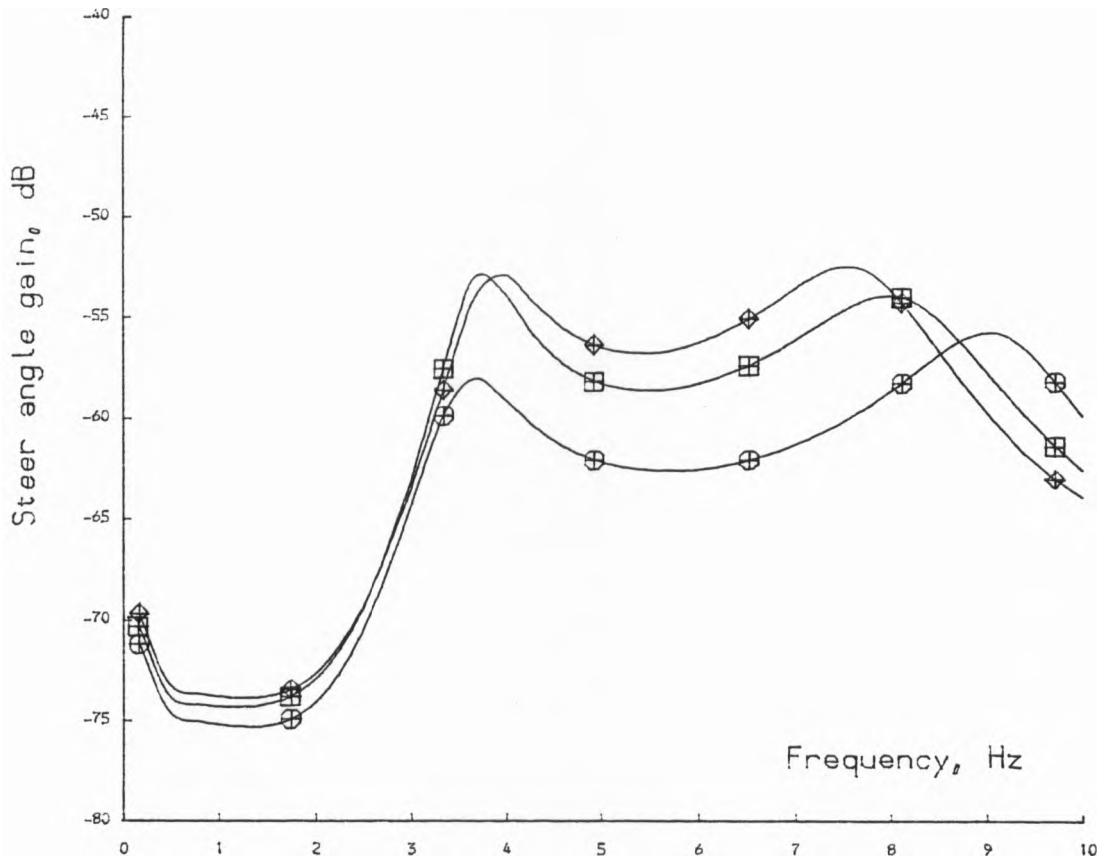
(a)



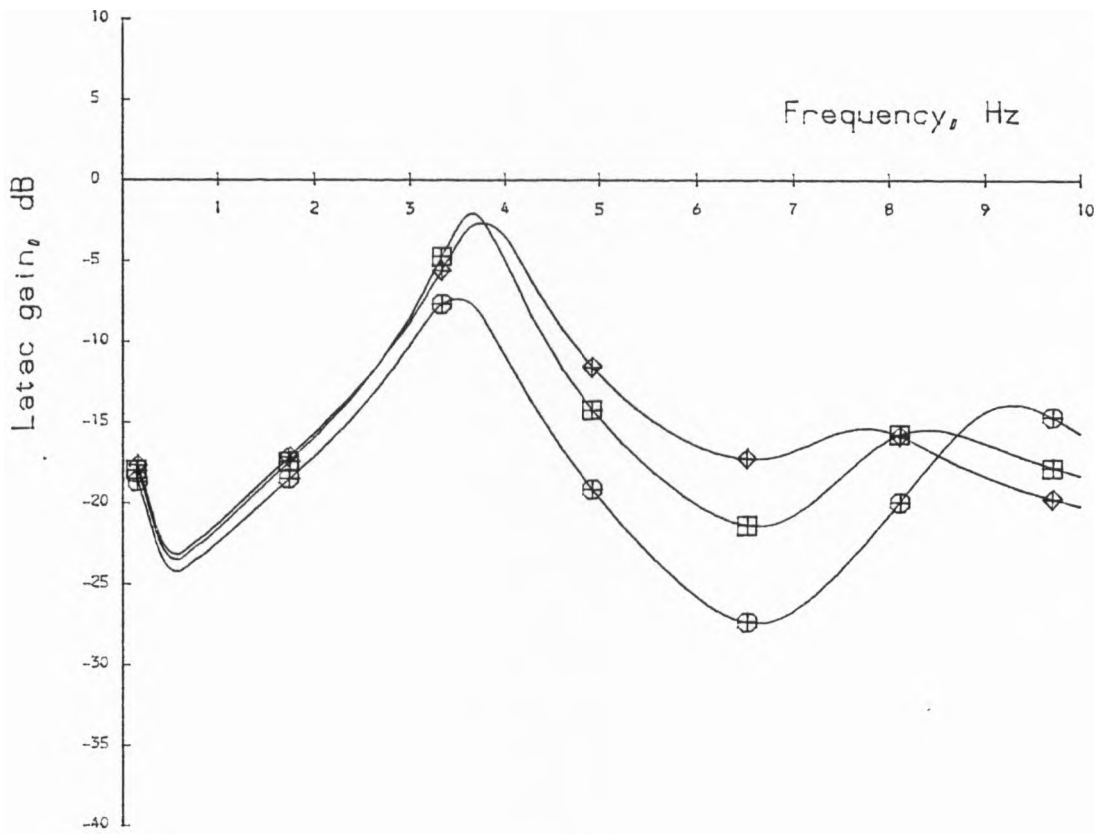
(b)

Figure 5.3

Selected frequency response gains for changes in steering geometry.

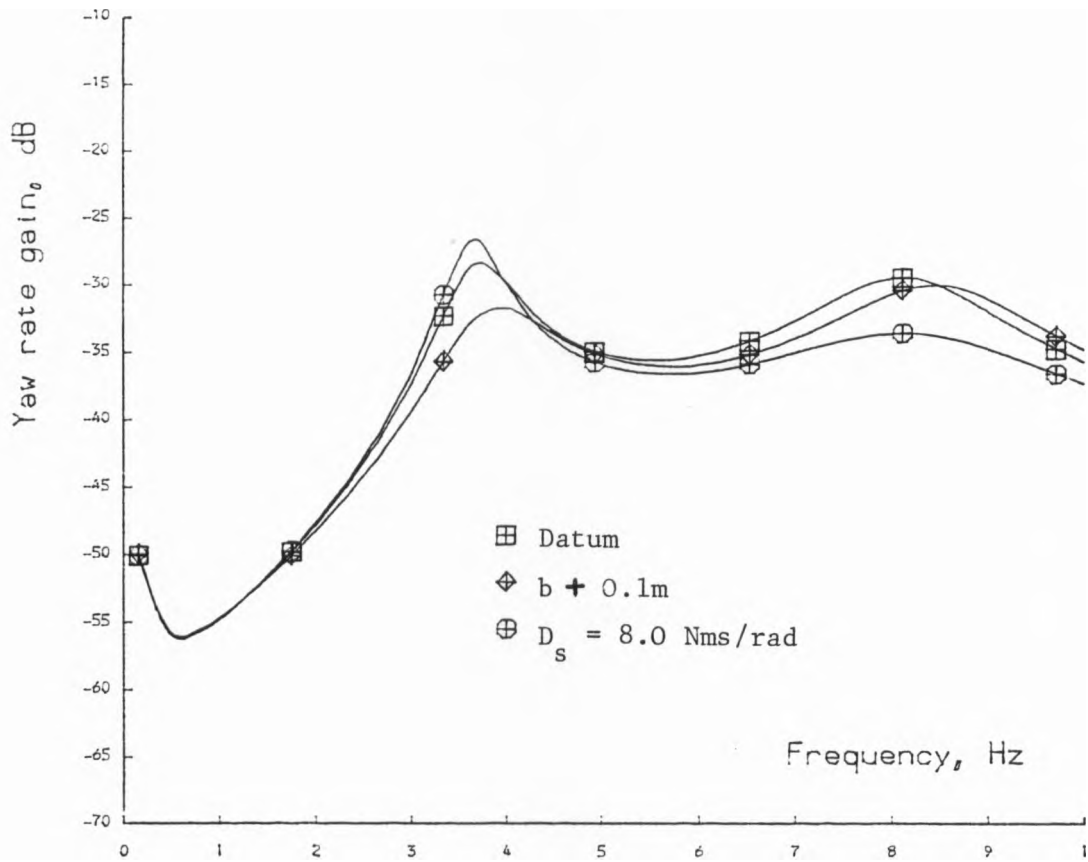


(c)

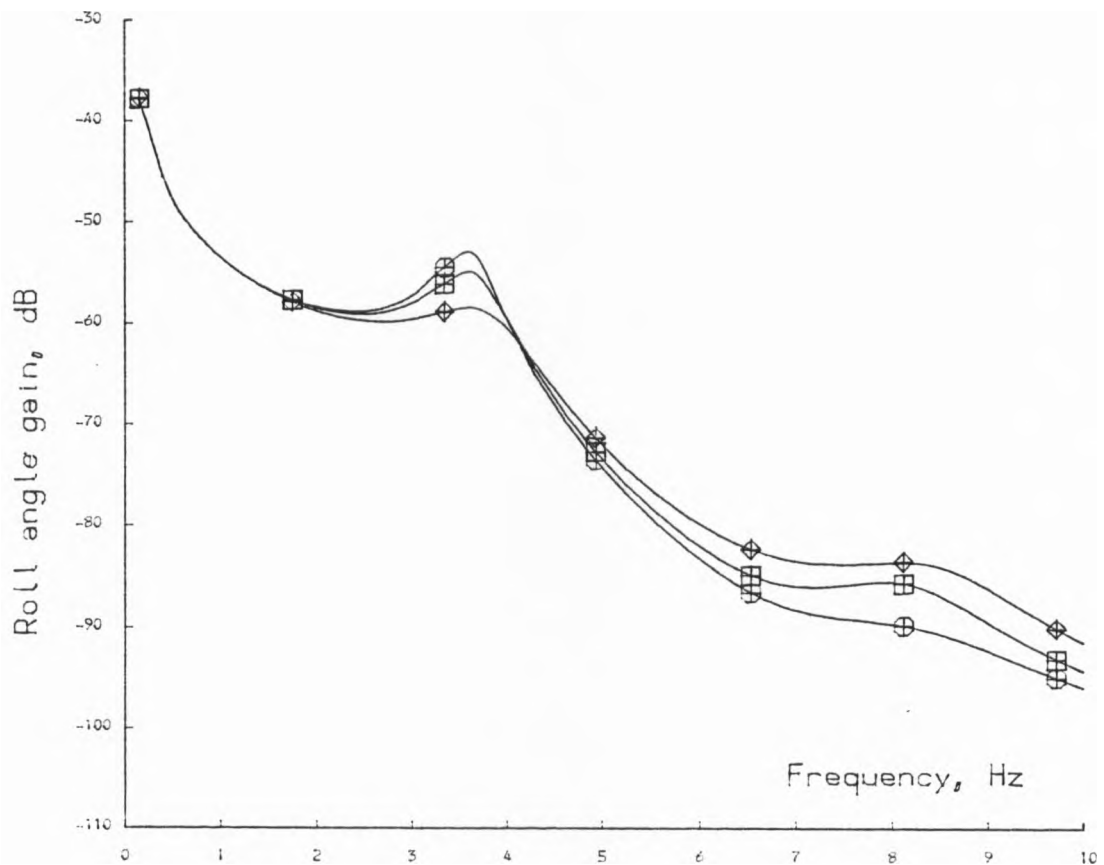


(d)

Figure 5.3 (cont.)

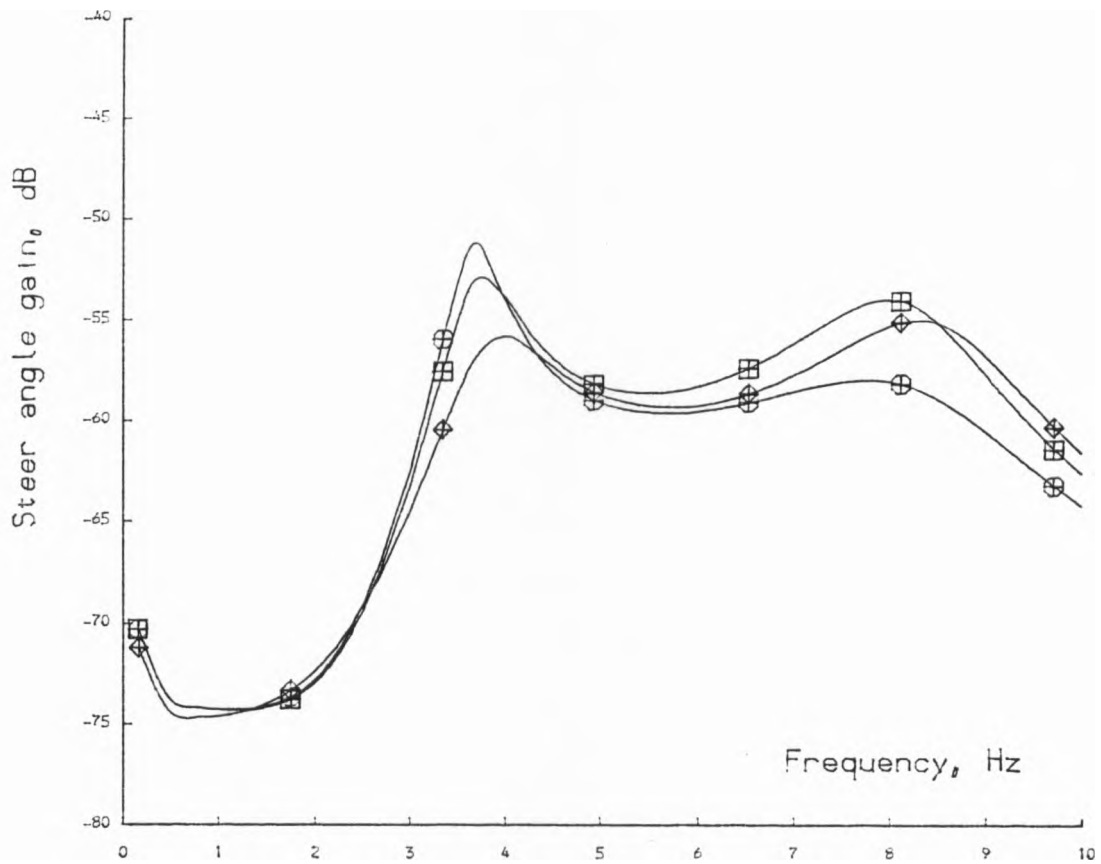


(a)

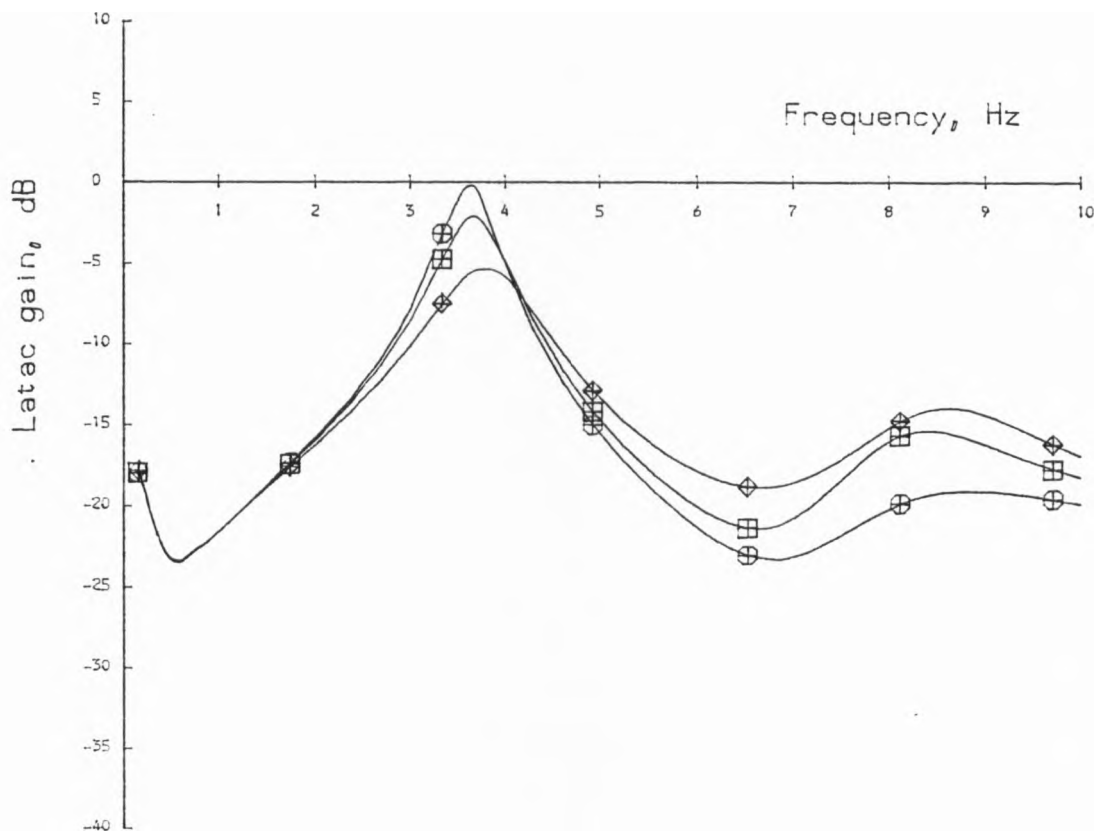


(b)

Figure 5.4  
Selected frequency response gains for changes in wheelbase and steer damping.

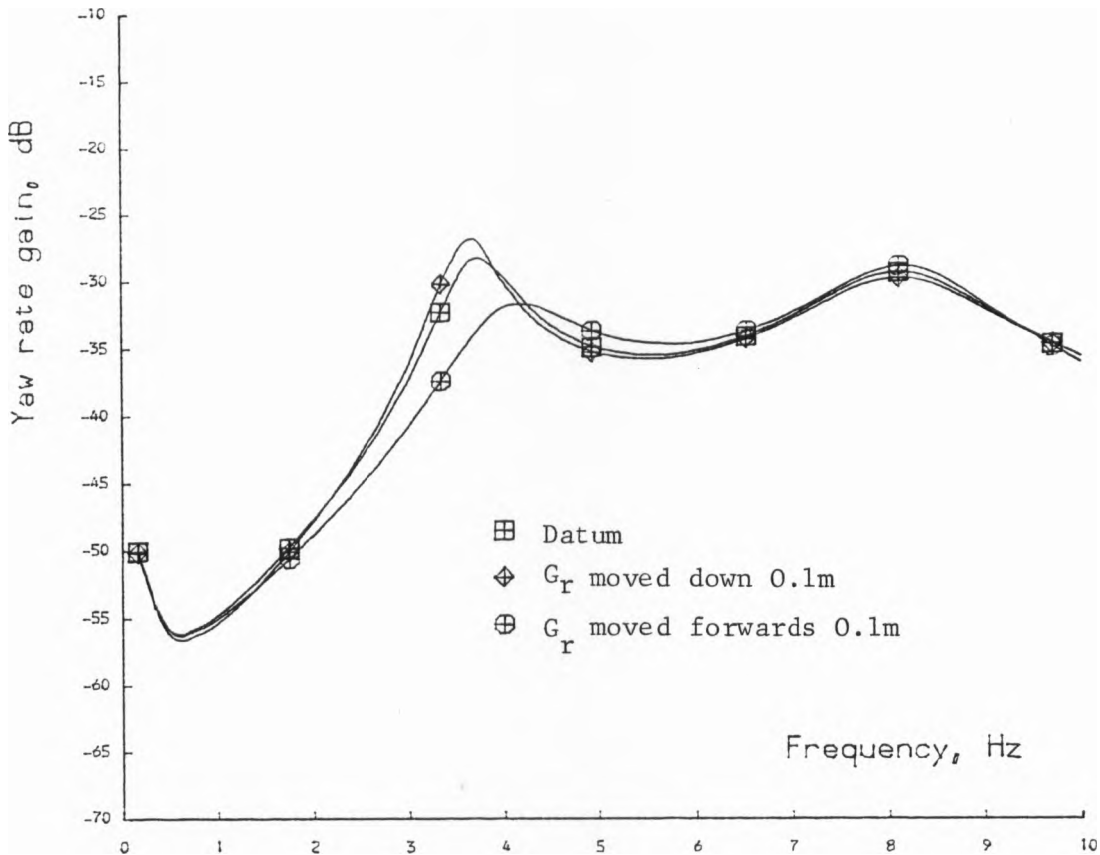


(c)

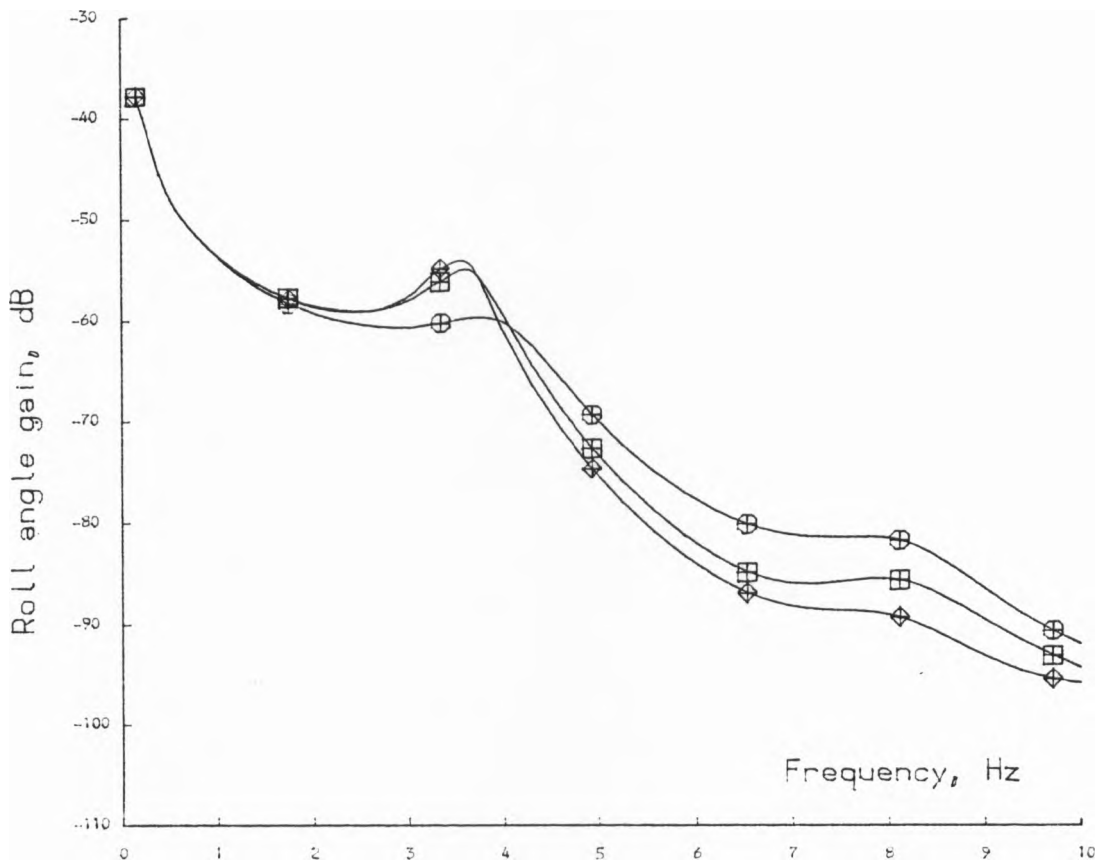


(d)

Figure 5.4 (cont.)



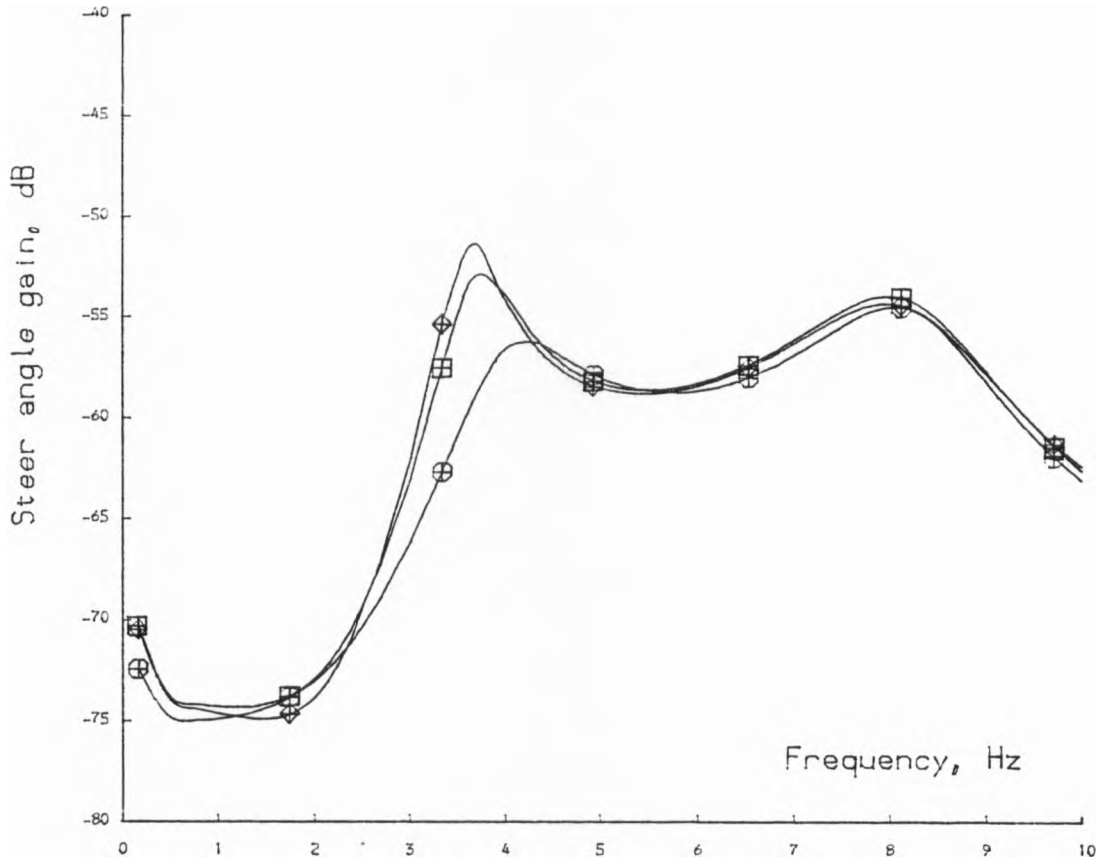
(a)



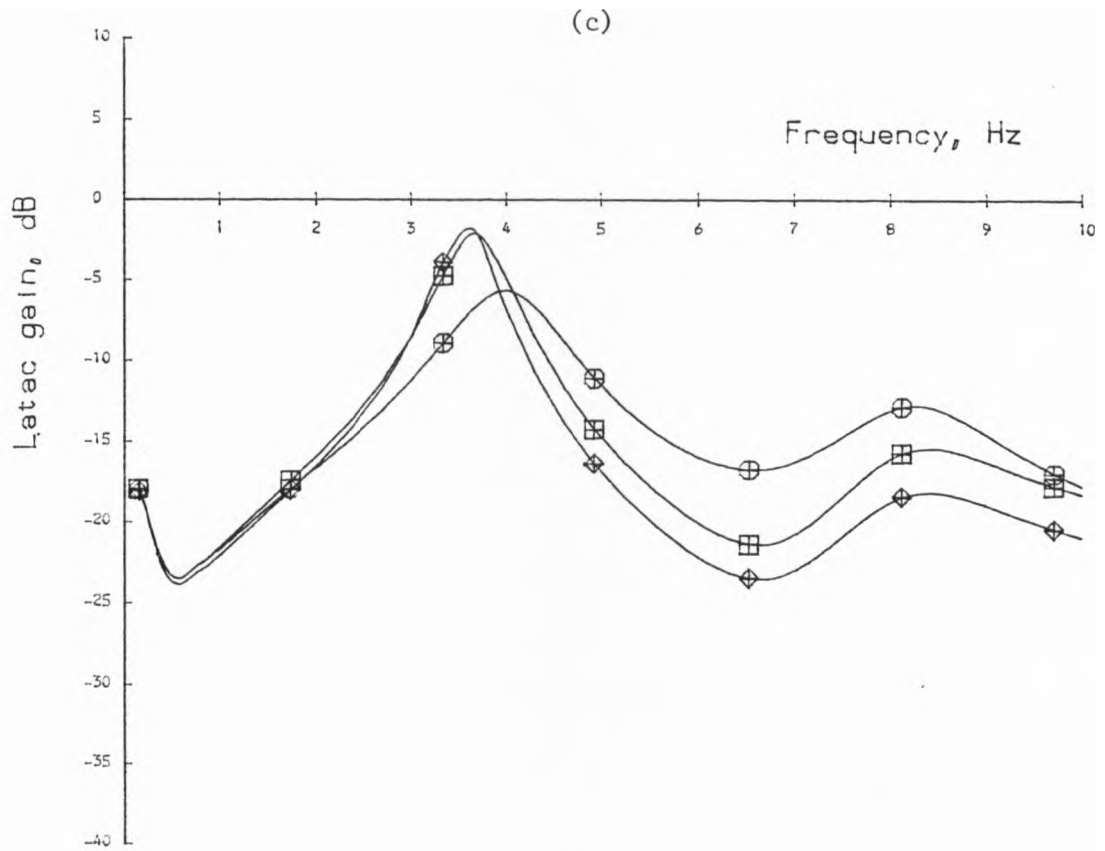
(b)

Figure 5.5

Selected frequency response gains for changes in the position of the rear frame c.g.

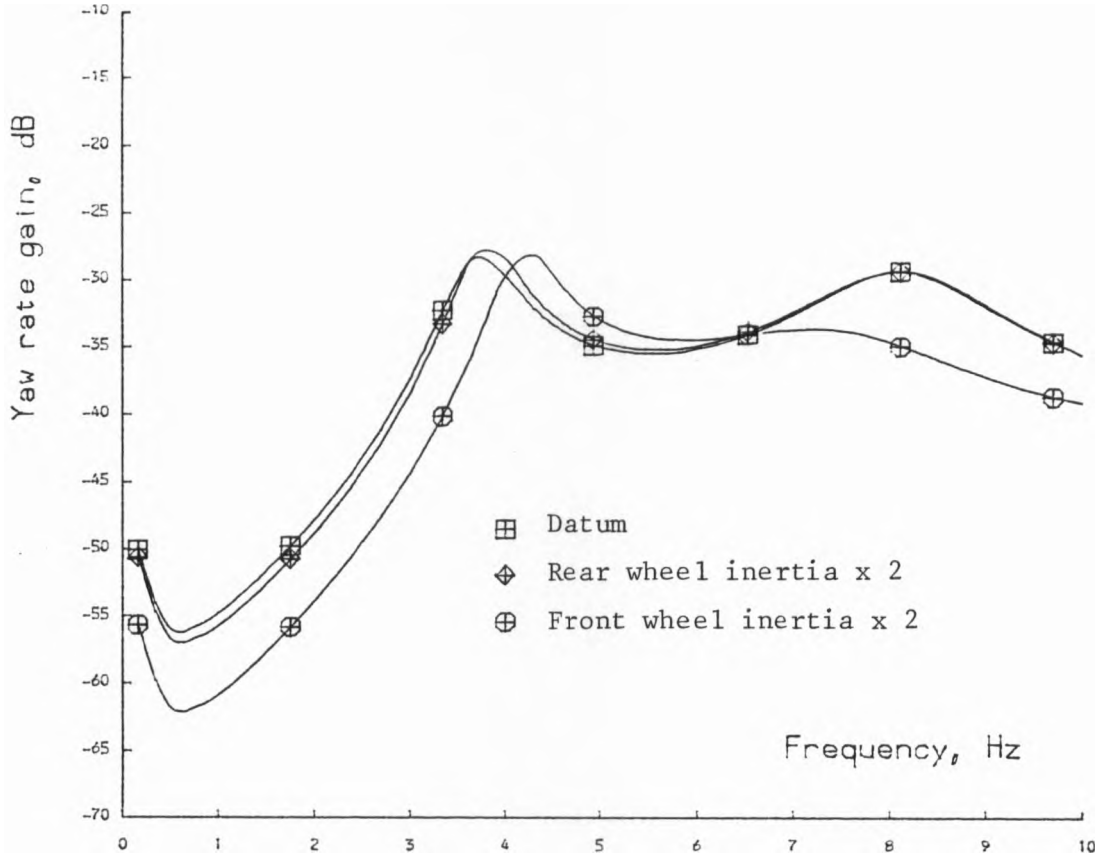


(c)

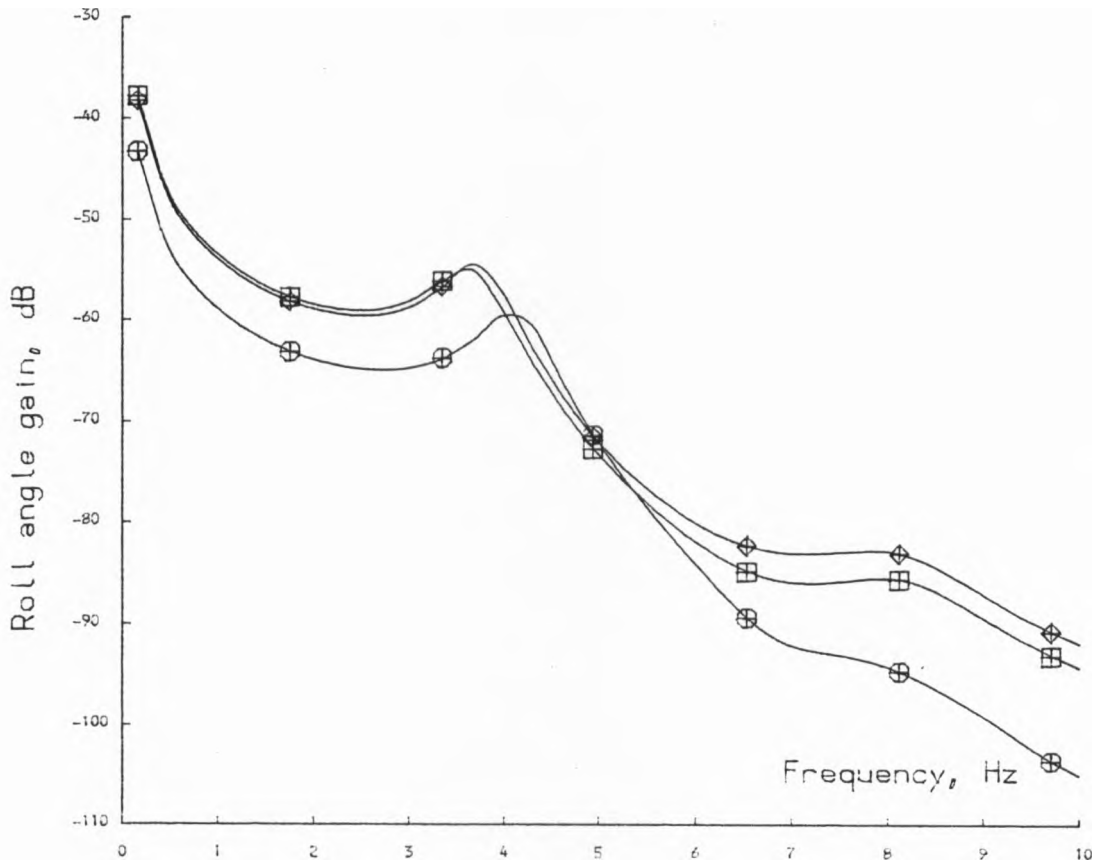


(d)

Figure 5.5 (cont.)



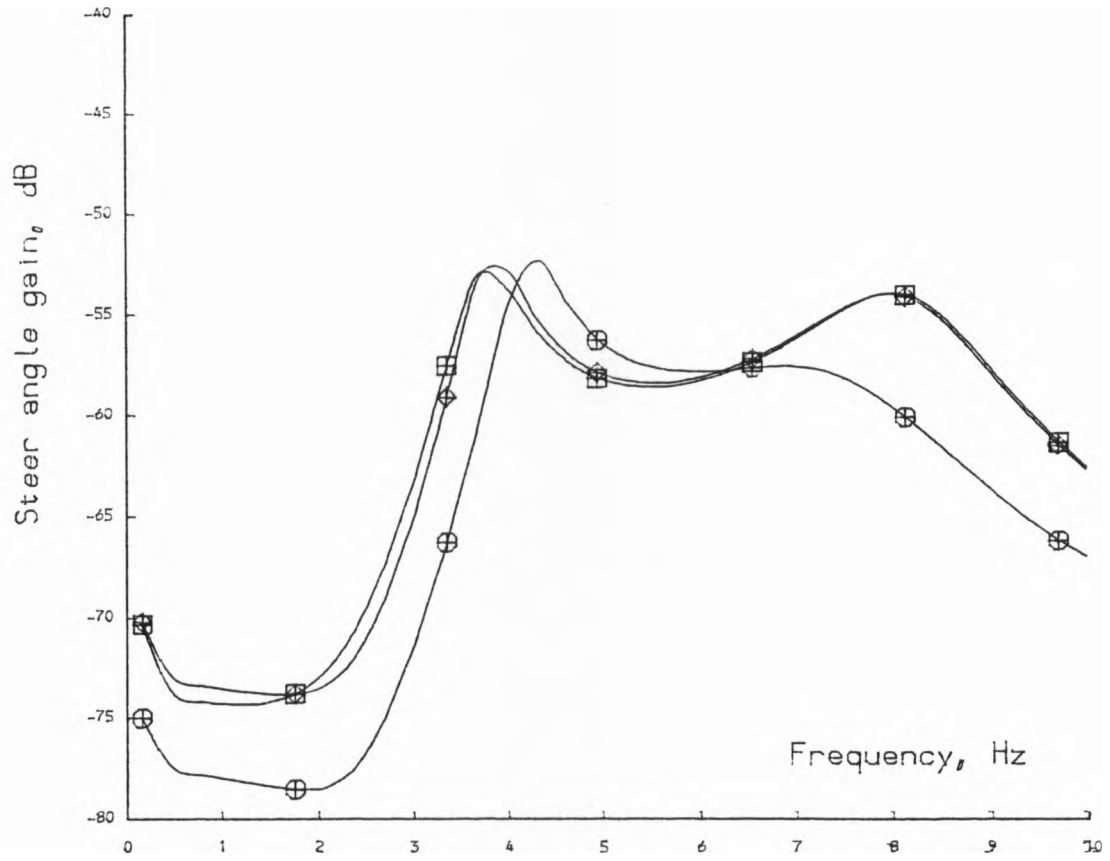
(a)



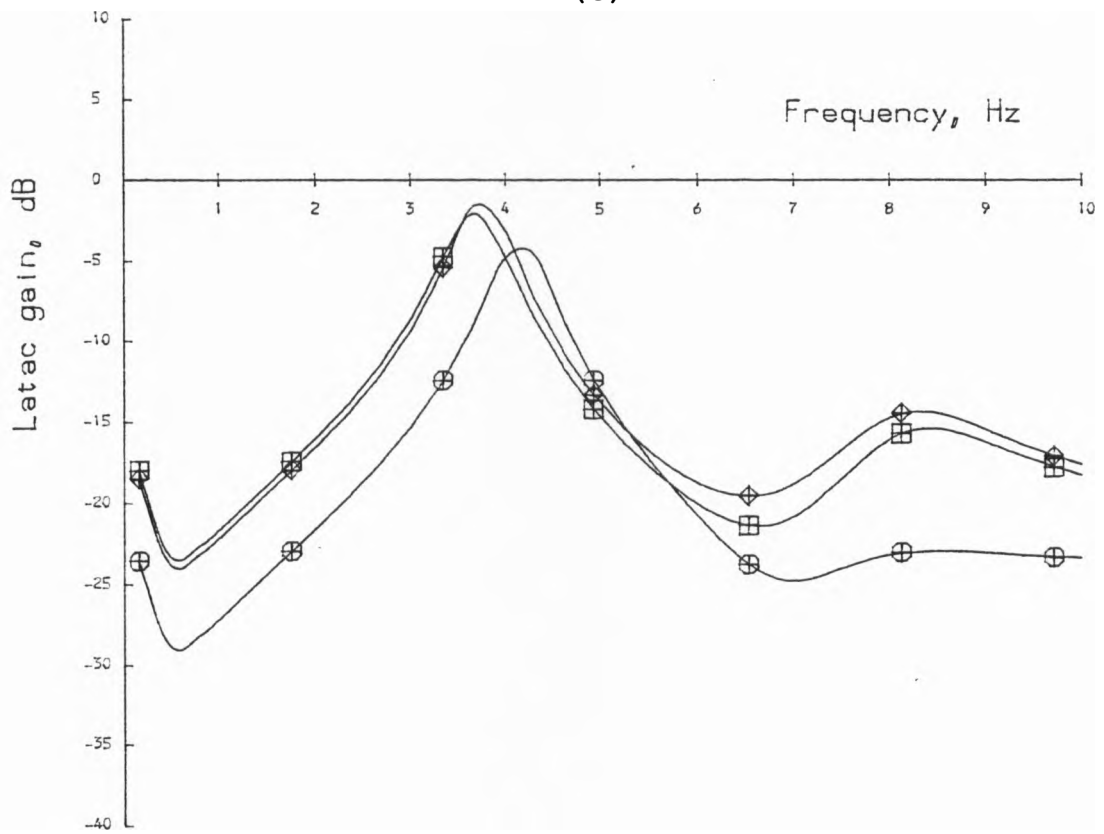
(b)

Figure 5.6

Selected frequency response gains for changes in wheel inertias.

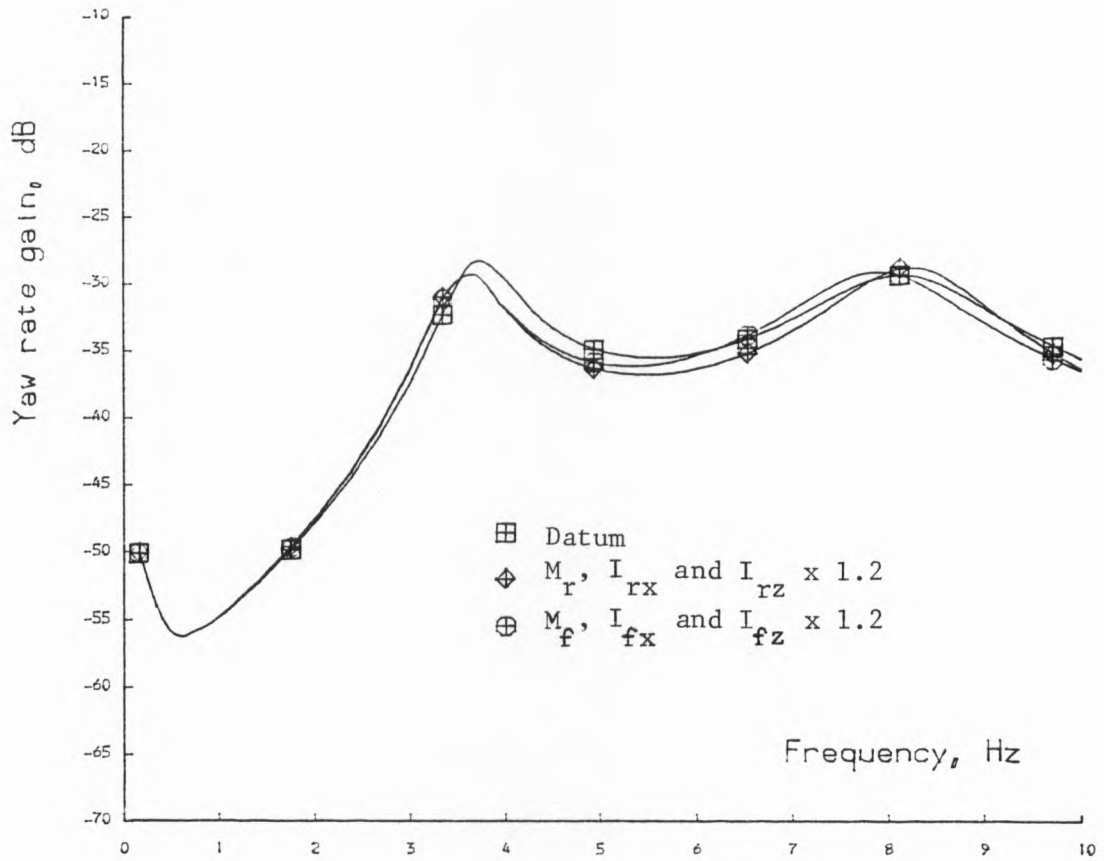


(c)

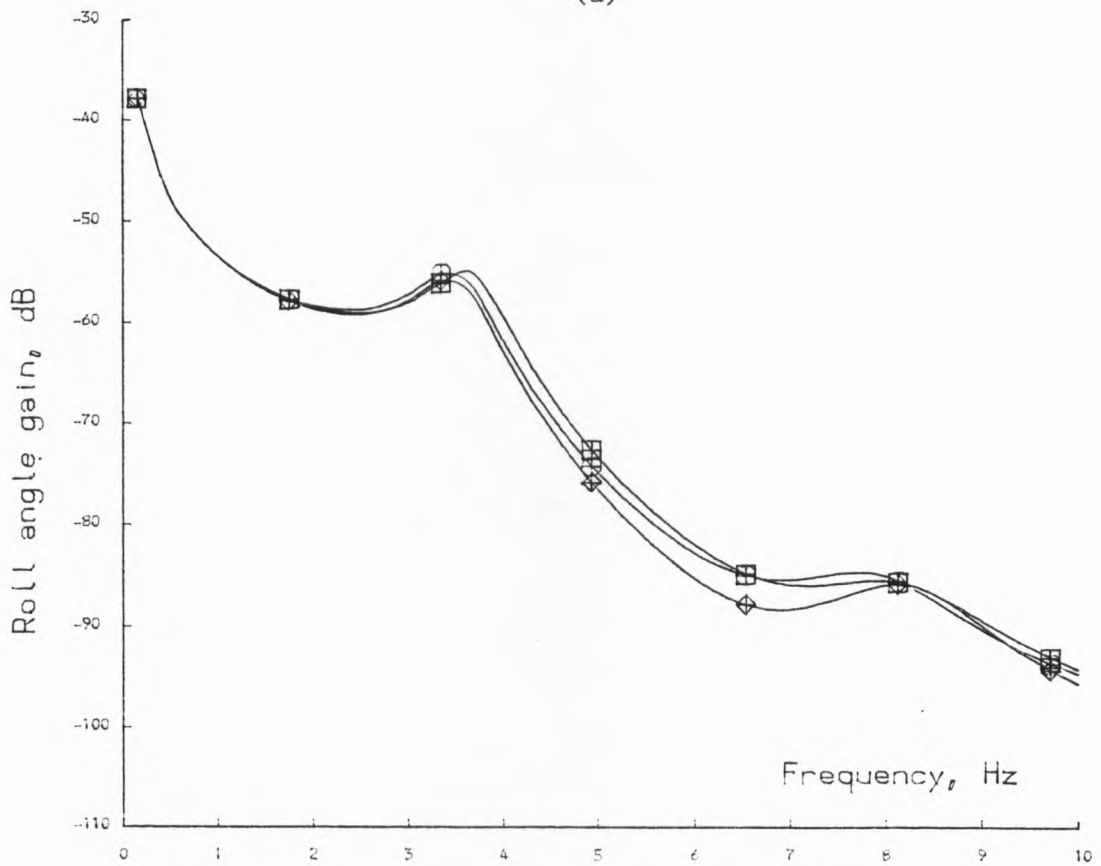


(d)

Figure 5.6 (cont.)



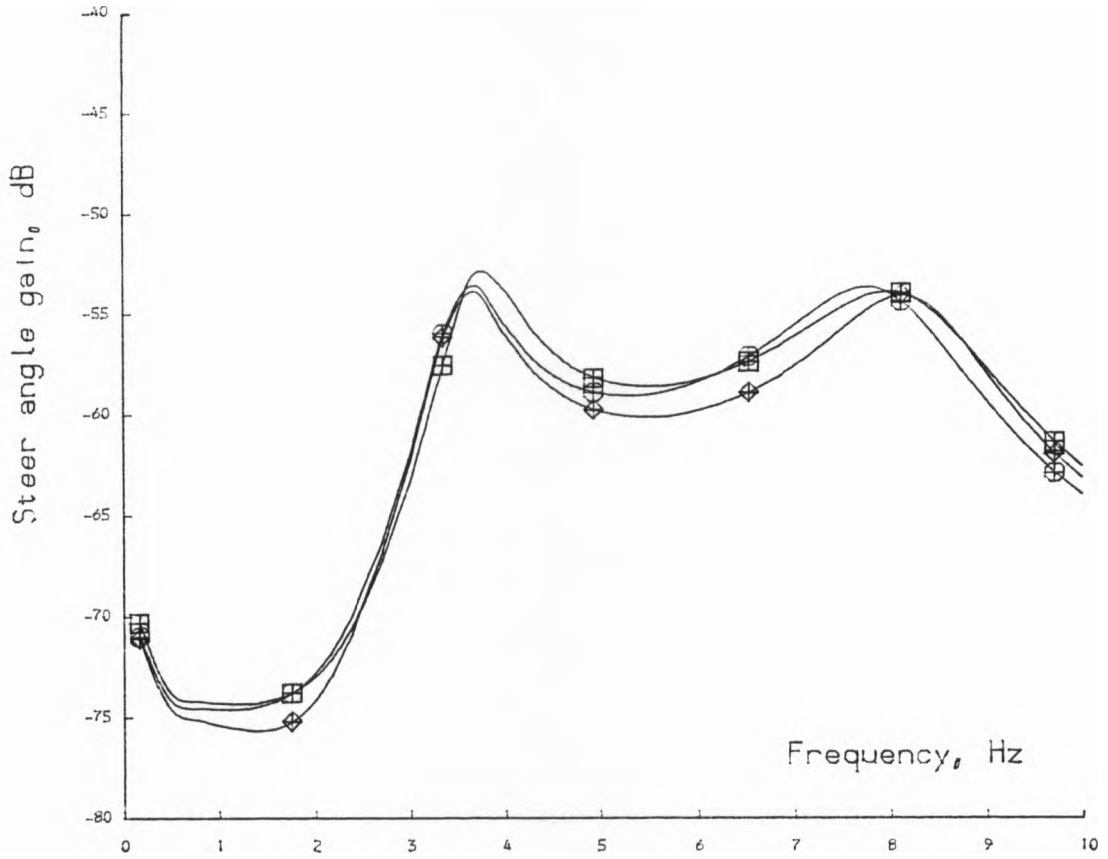
(a)



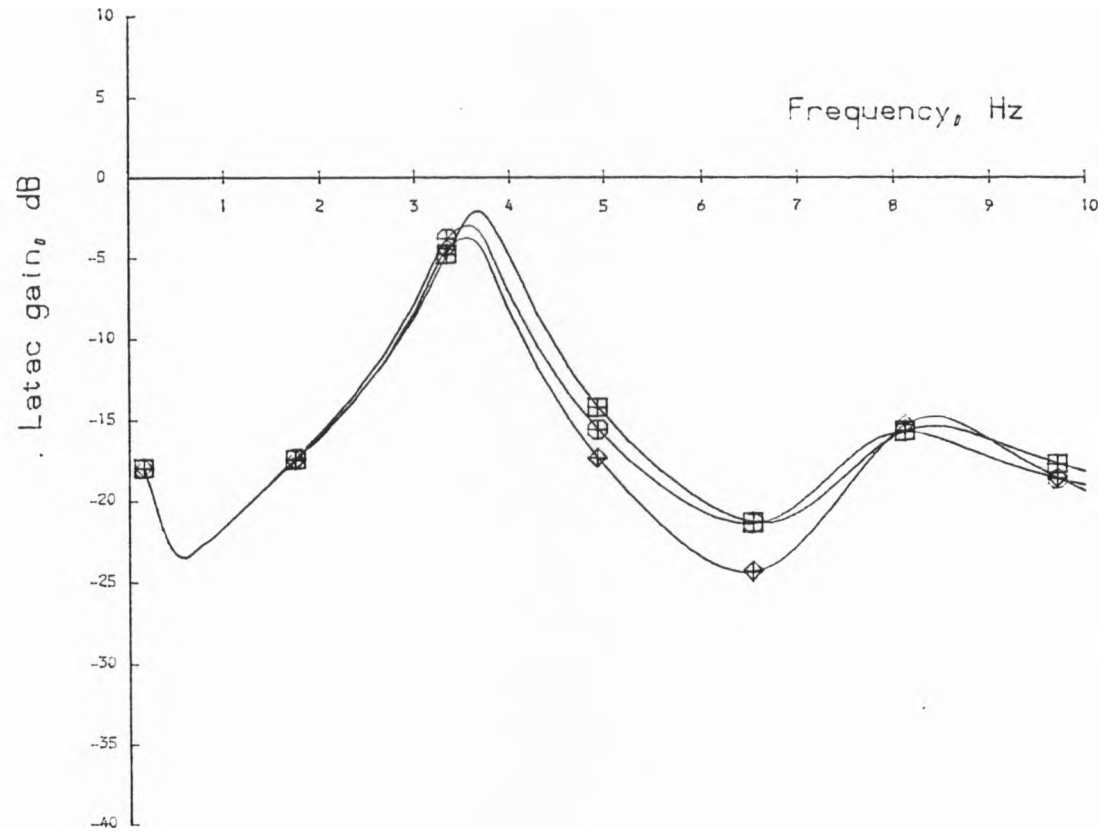
(b)

Figure 5.7

Selected frequency response gains for changes in frame masses and inertias.

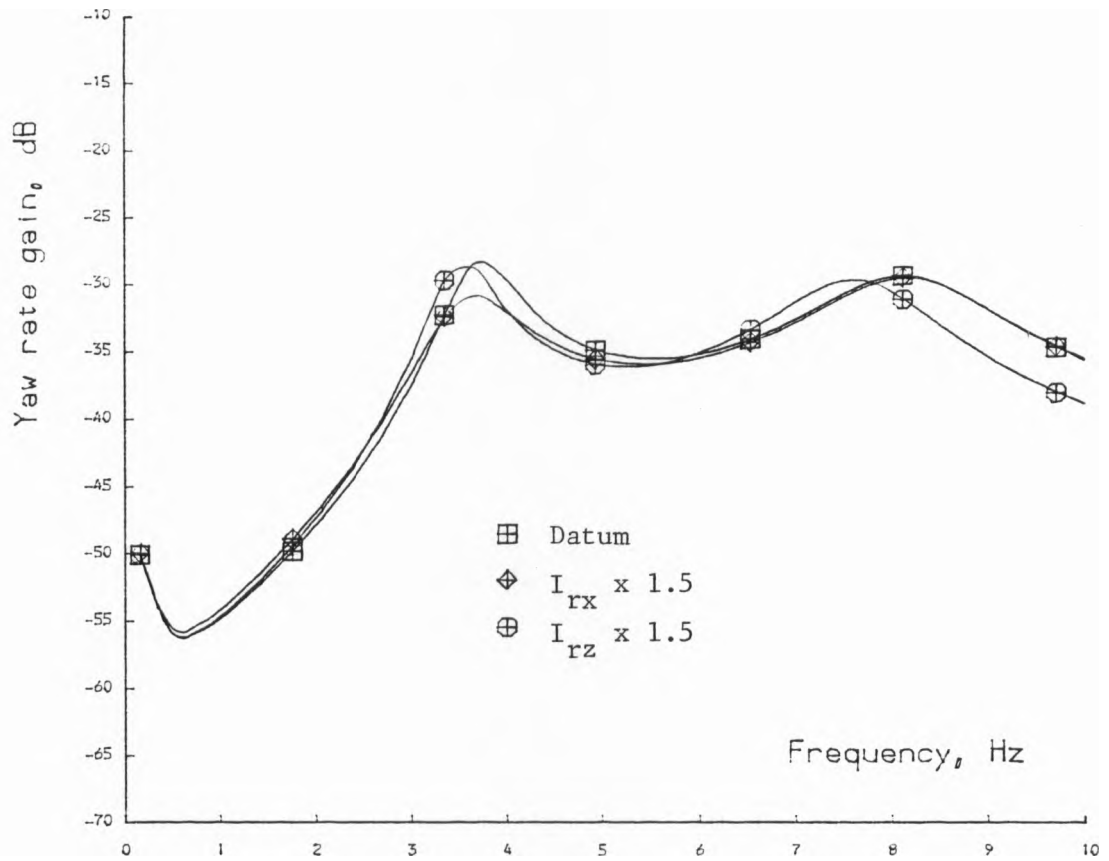


(c)

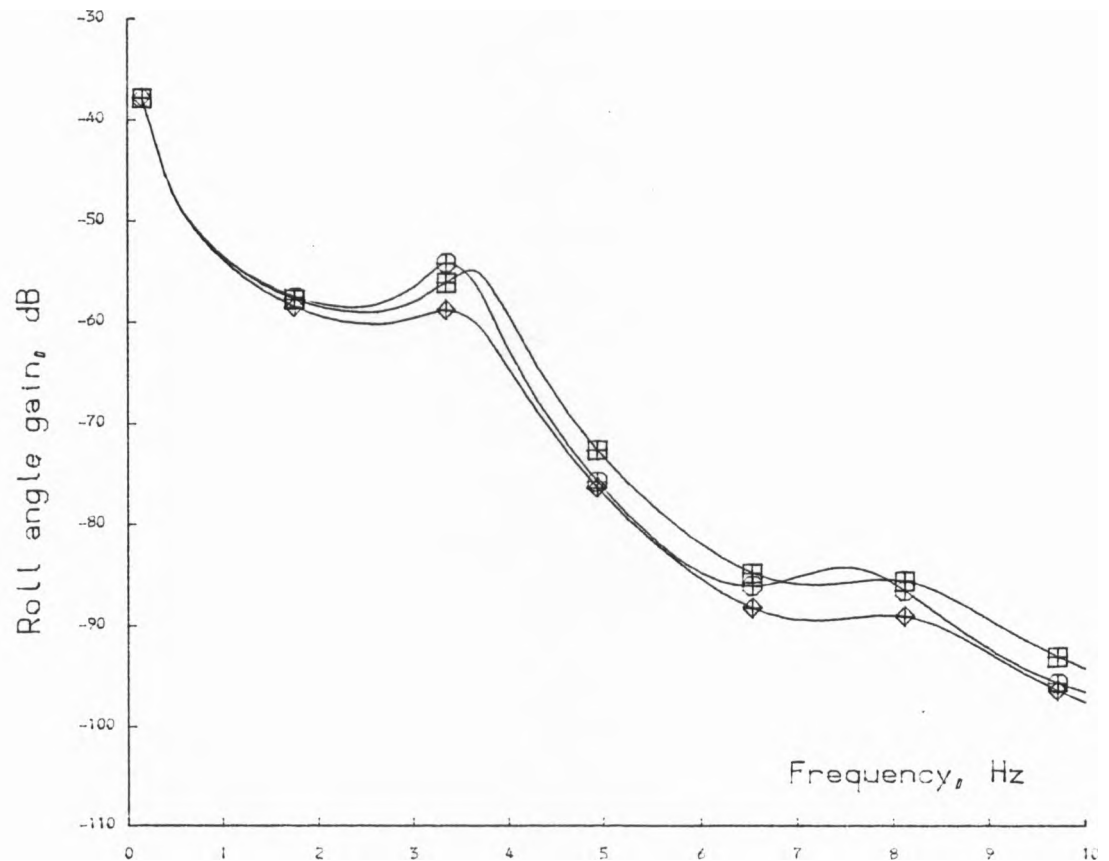


(d)

Figure 5.7 (cont.)



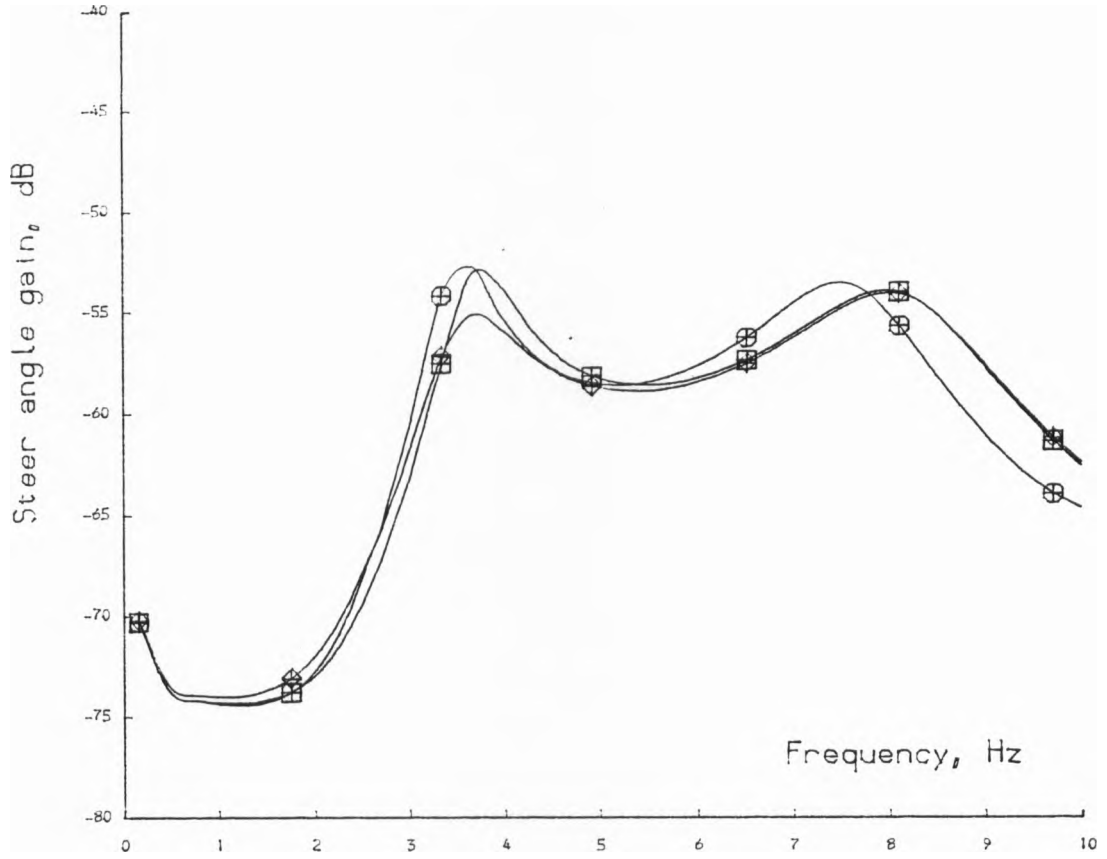
(a)



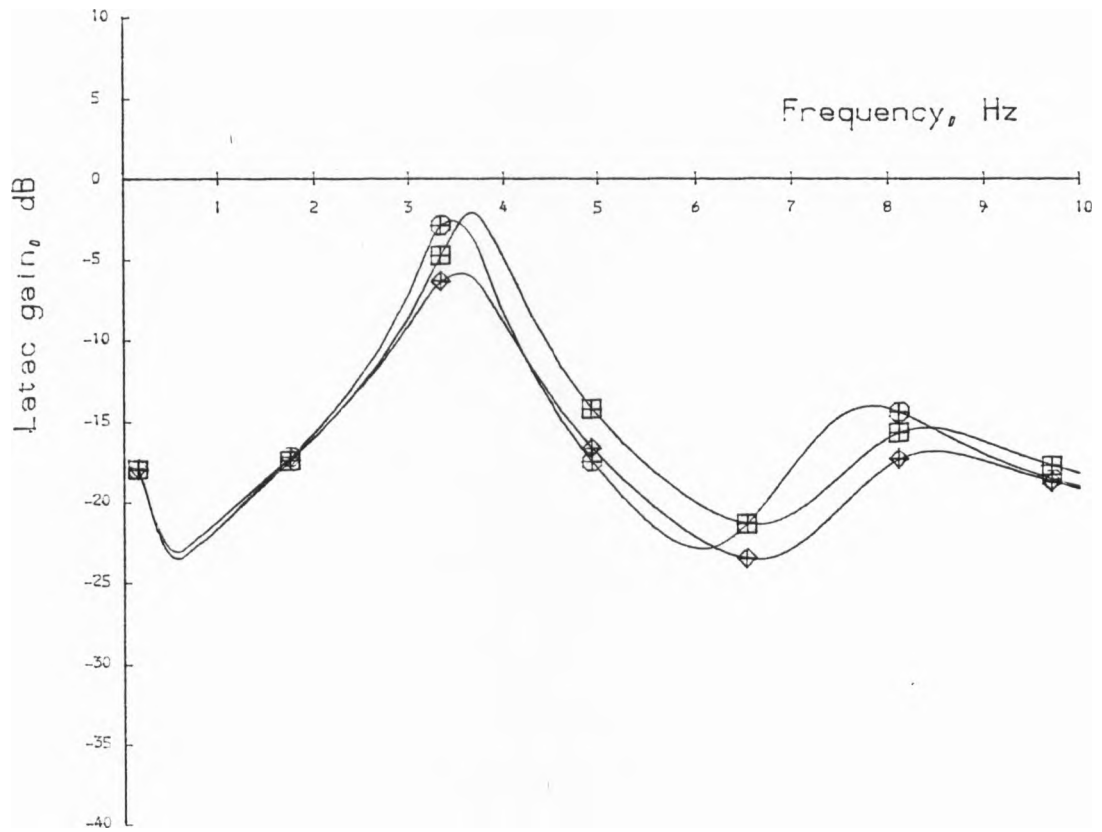
(b)

Figure 5.8

Selected frequency response gains for changes in the rear frame inertias.

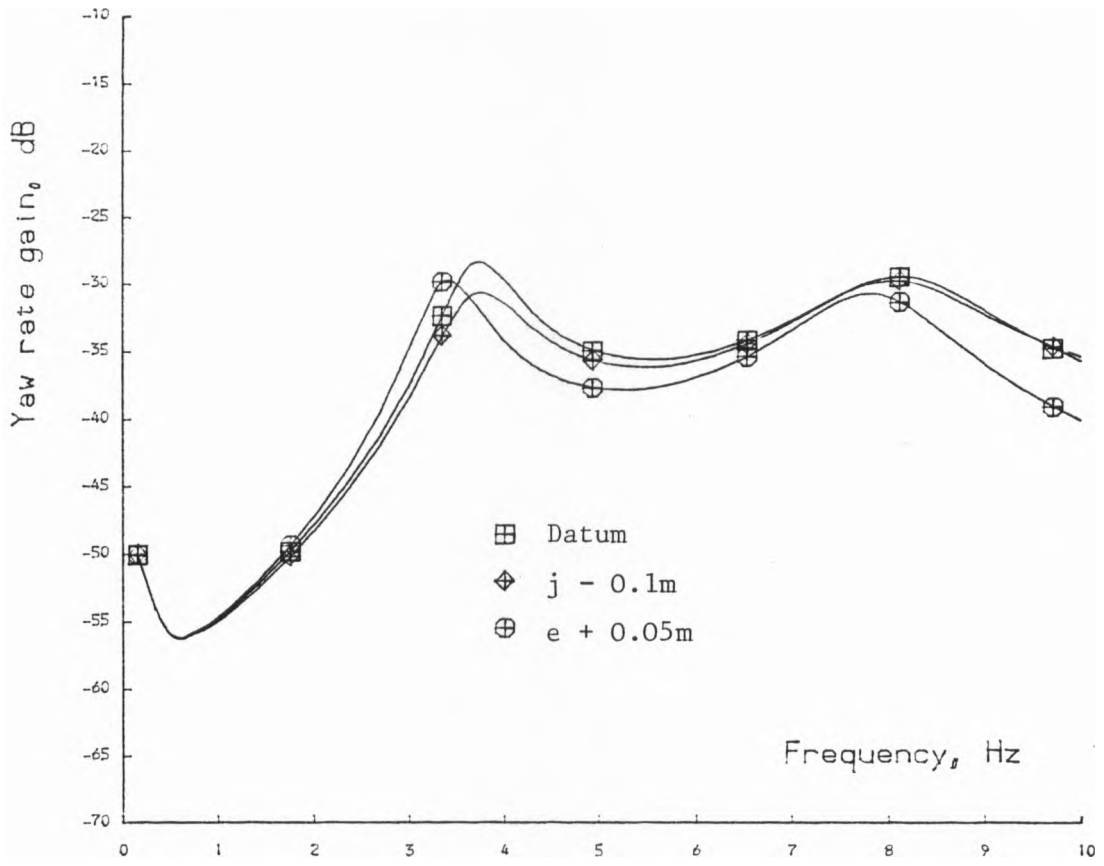


(c)

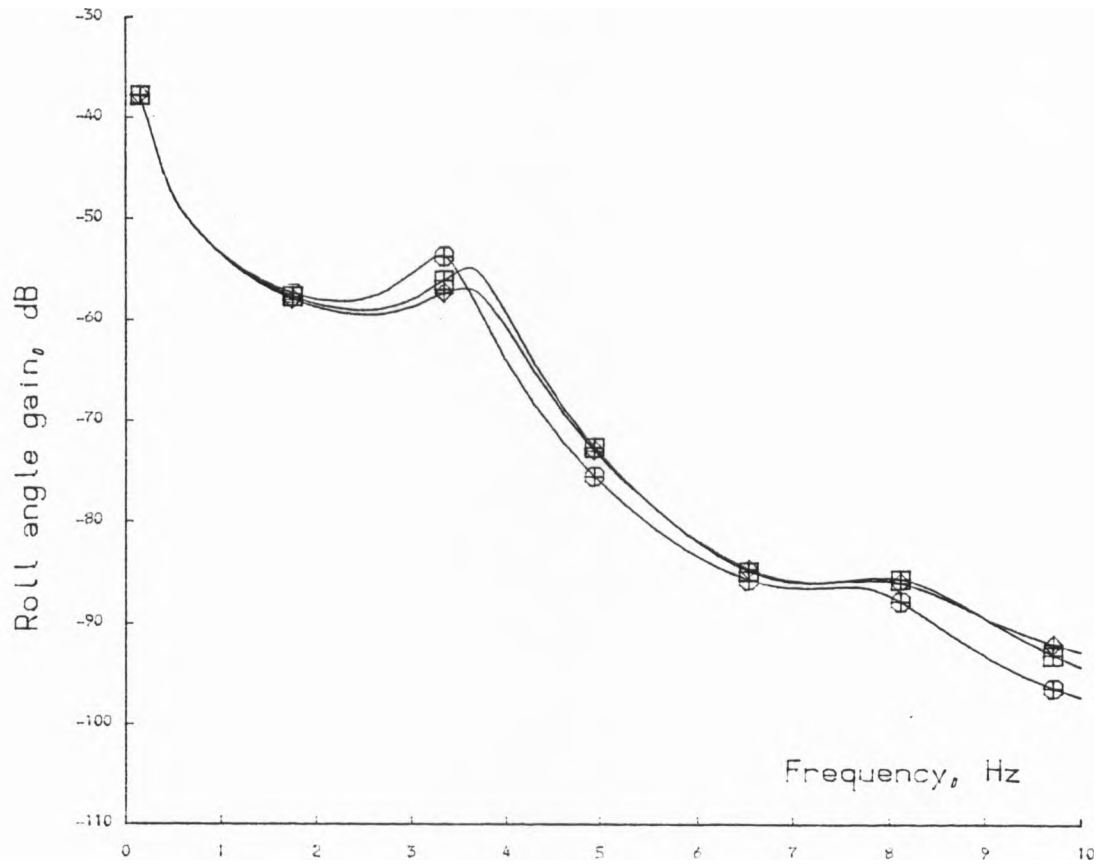


(d)

Figure 5.8 (cont.)

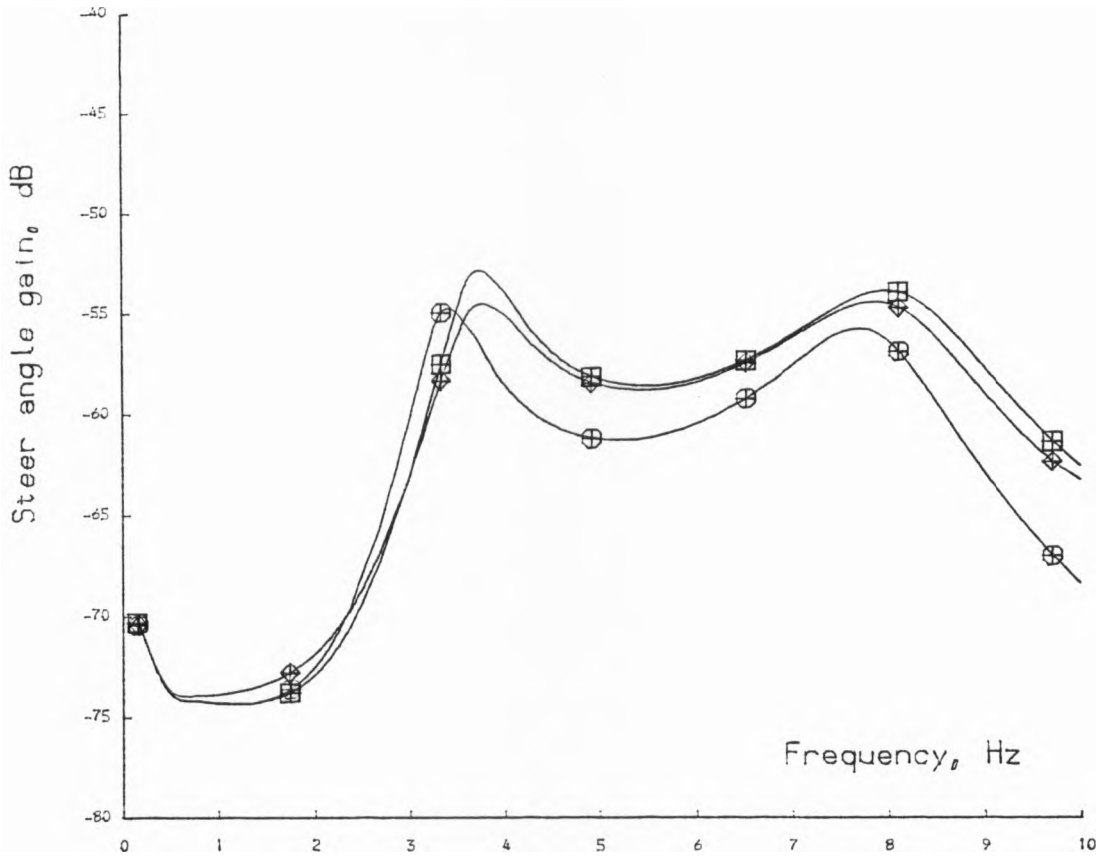


(a)

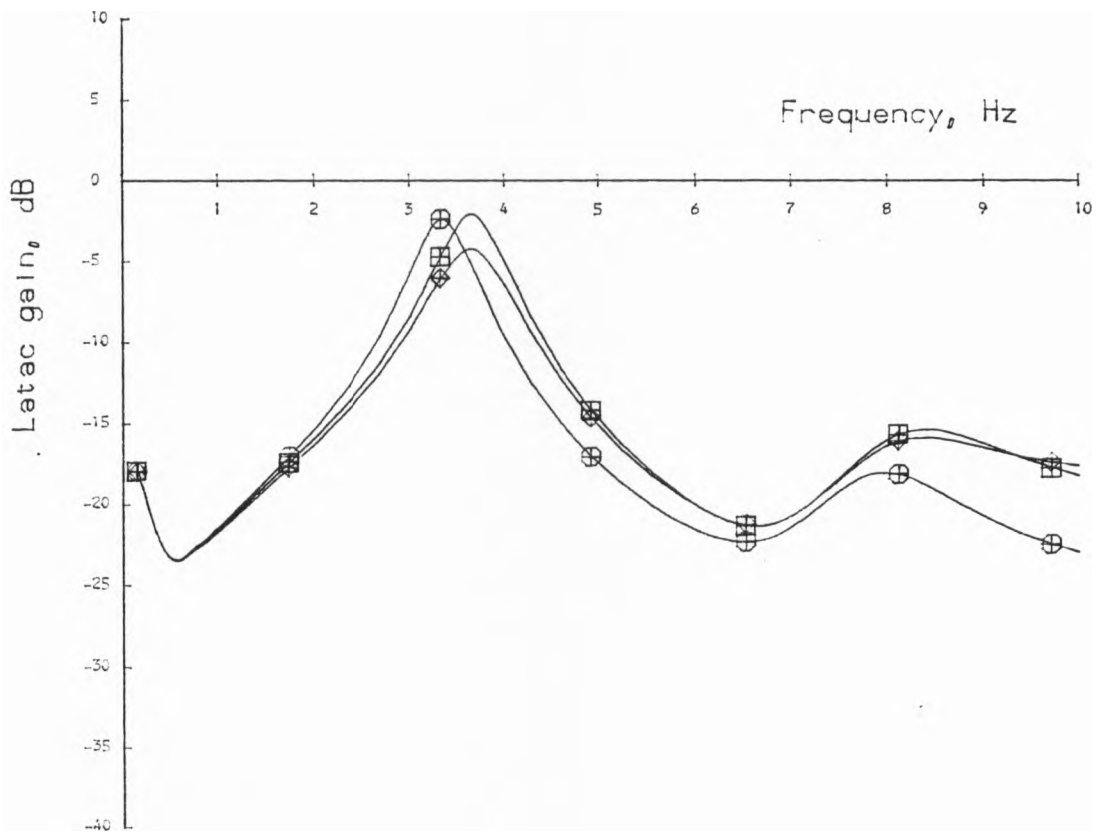


(b)

Figure 5.9  
Selected frequency response gains for changes in the position of the front frame c.g.

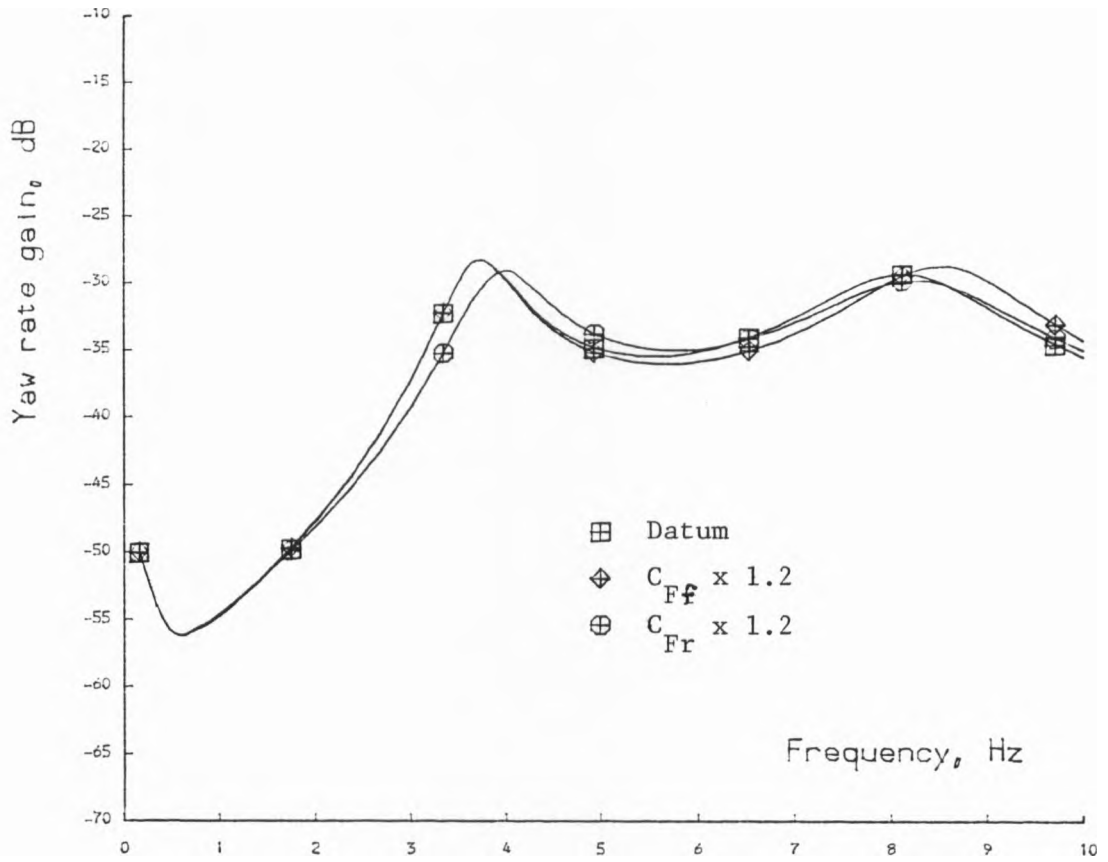


(c)

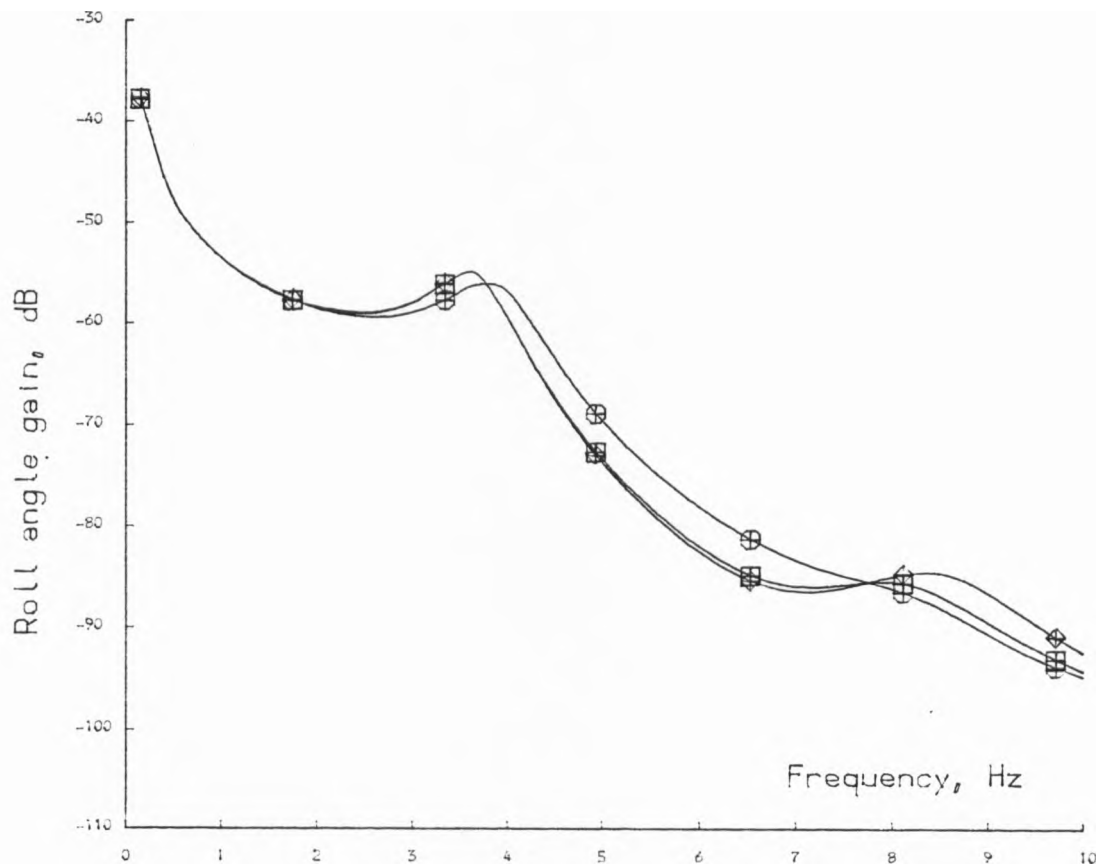


(d)

Figure 5.9 (cont.)



(a)



(b)

Figure 5.10

Selected frequency response gains for changes in tyre cornering stiffness.

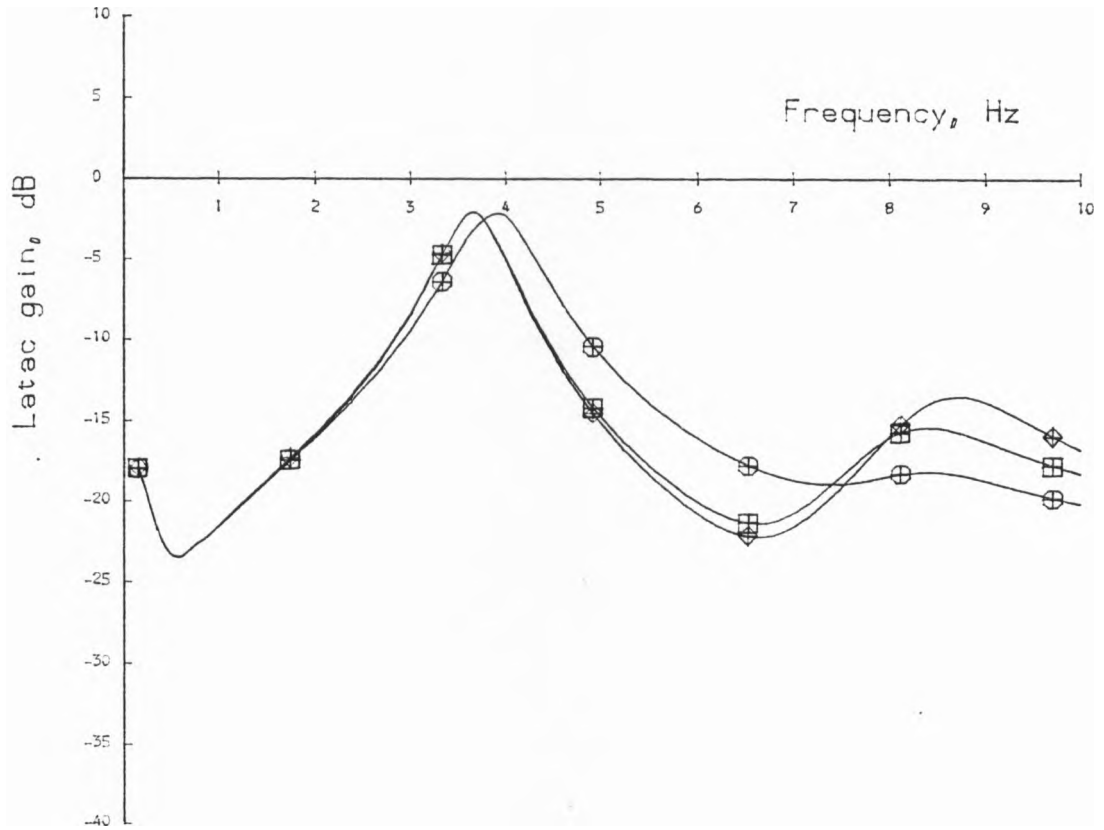
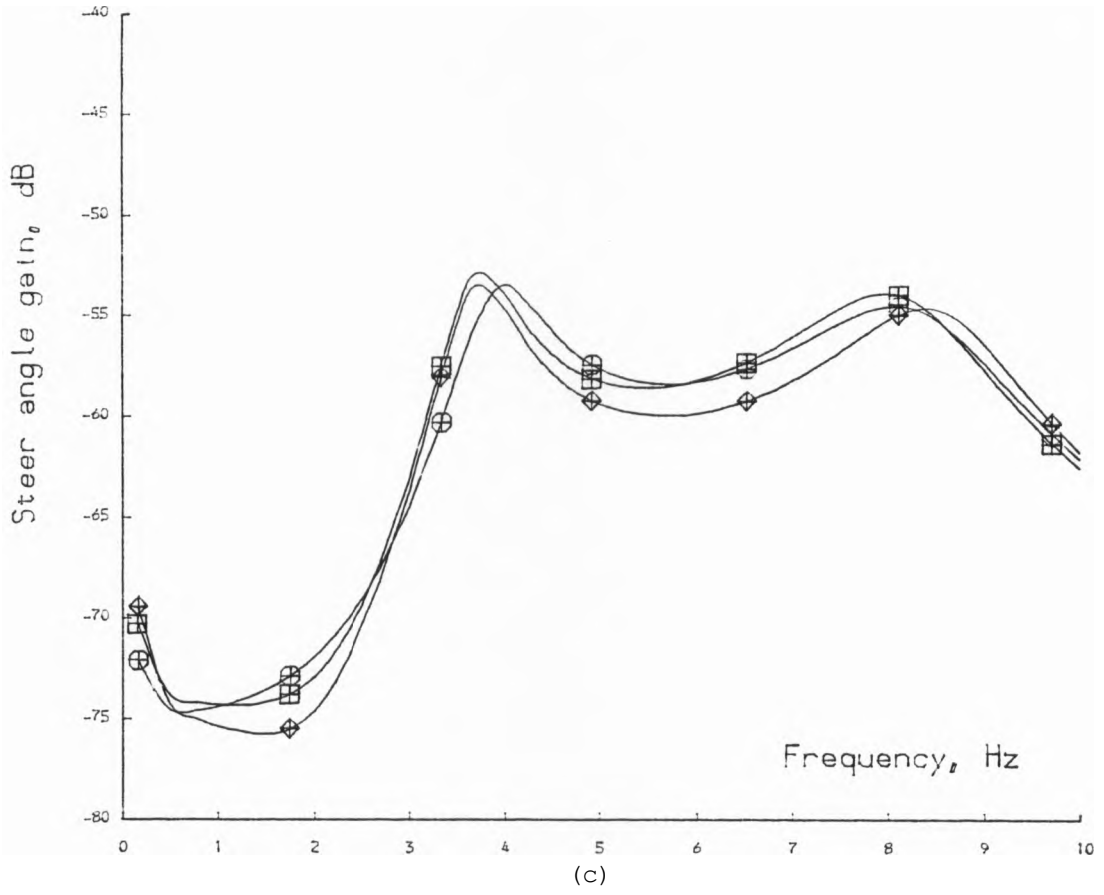


Figure 5.10 (cont.)

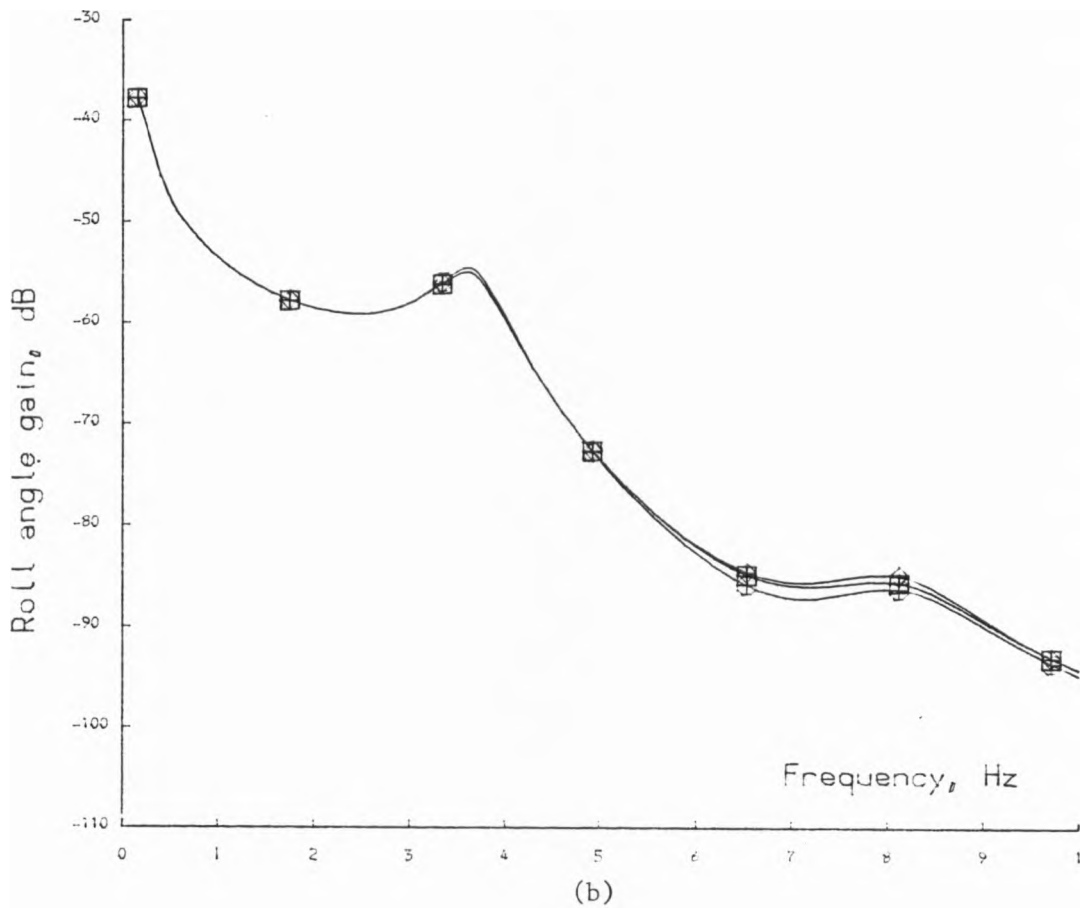
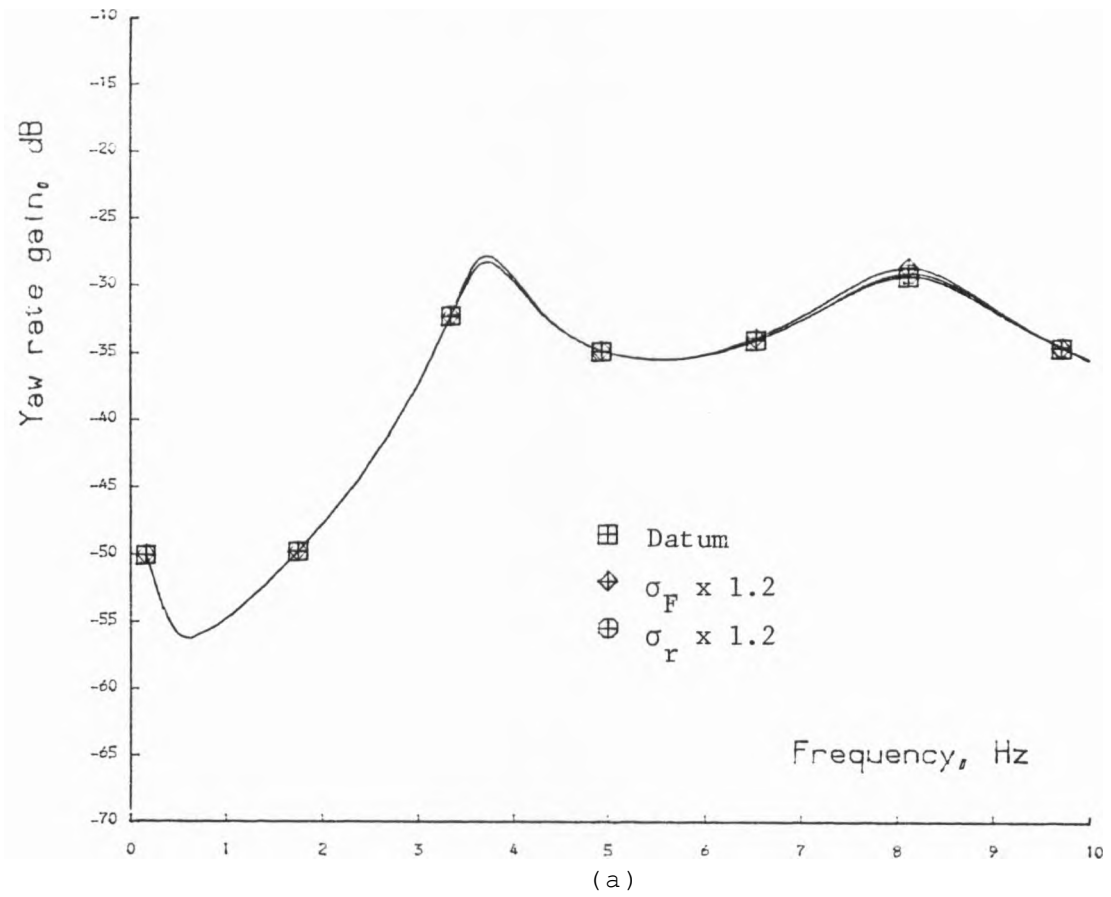
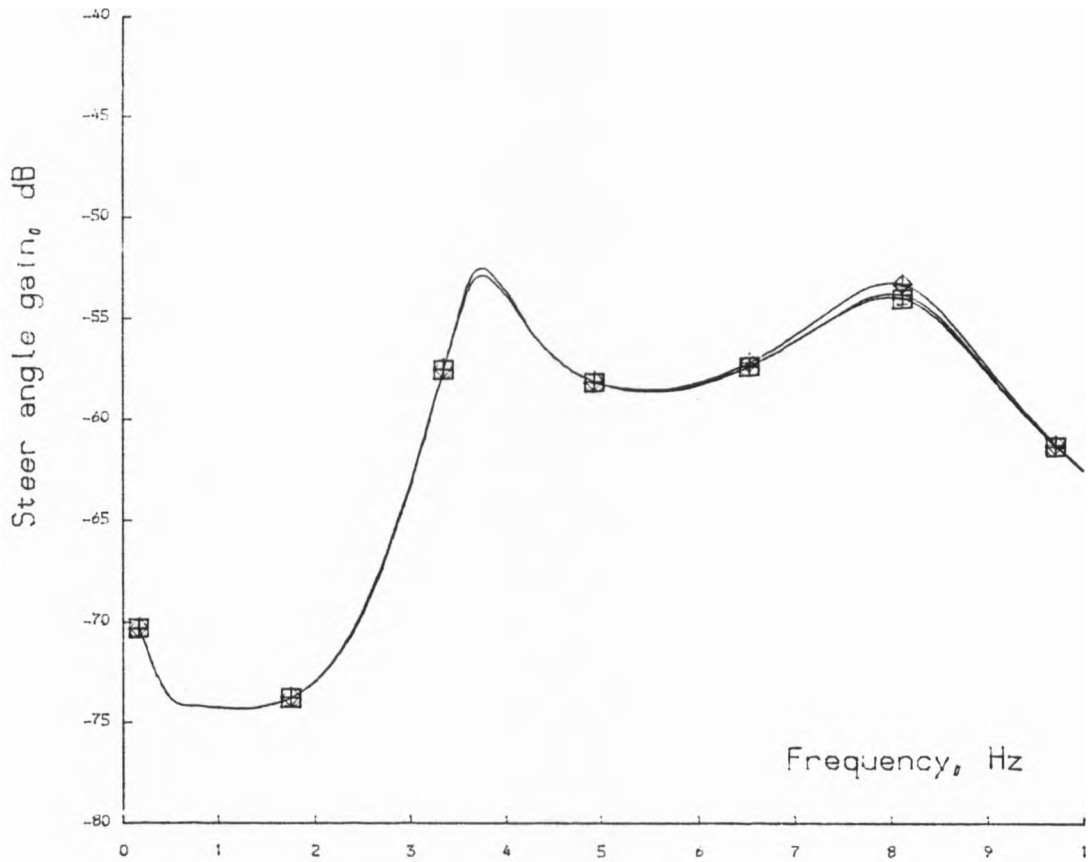
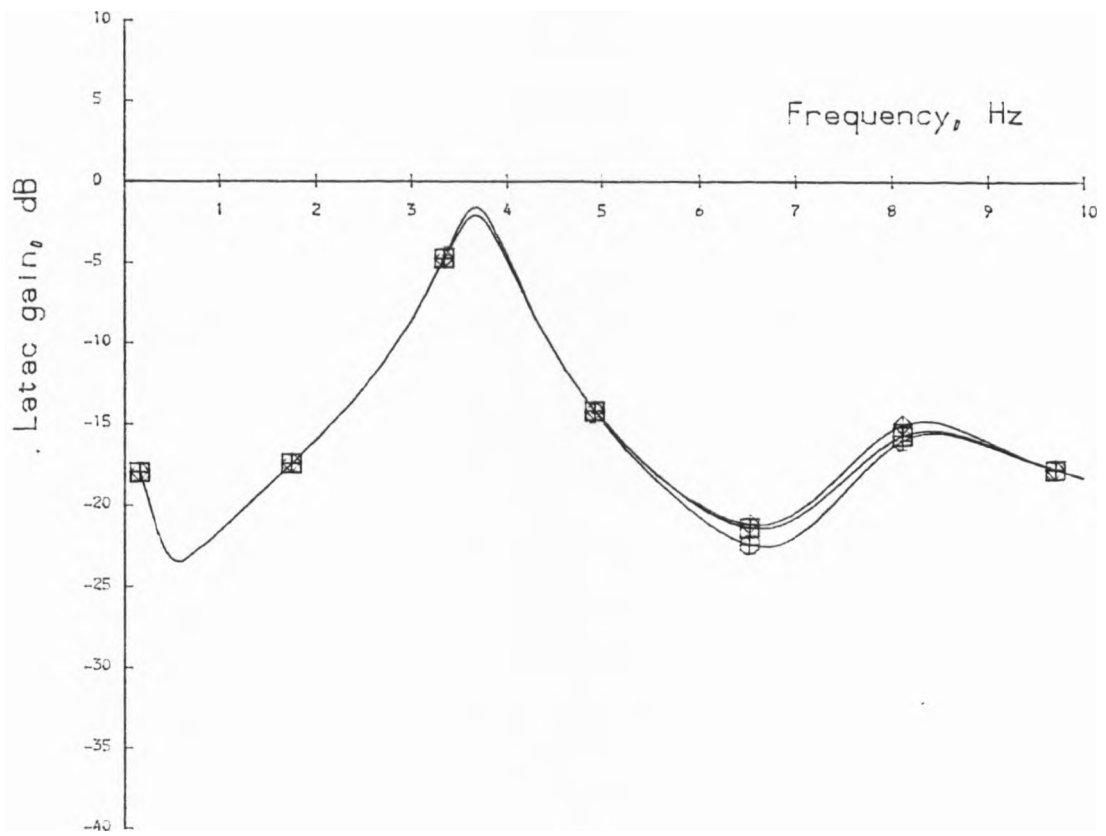


Figure 5.11

Selected frequency response gains for changes in tyre relaxation lengths.



(c)



(d)

Figure 5.11 (cont.)

#### 5.4. DISCUSSION

In parts of this discussion I will be comparing the frequency response results with the free vibration results. All of the effects on stability of parameter changes are taken from Sharp (1984b), except where otherwise indicated.

The responses for the datum parameter values can be seen in Fig.5.1, and all of them show peaks in the gains at the natural frequencies of the weave and wobble modes, 3.5 Hz and 8 Hz respectively. The responses are very similar in shape, apart from the roll angle gain, Fig.5.1(b), which tends to fall off rapidly with increasing frequency. This could be indicative of a responsiveness problem with this motorcycle, or it might merely reflect the small contribution of roll to the wobble mode, compared with the other variables.

Figure 5.2 illustrates the changes in the responses with speed. The general shapes of the curves and the manner in which they change with speed agree very well with the experimental results for the pulse response test by Aoki (1979). At 10 m/s the weave mode resonant frequency is below 1 Hz, and it rises with speed up to a maximum of 4 Hz, which is rather higher than the equivalent eigenvalue results indicate in Fig.3.2. This difference is caused by the fact that the frequency responses contain extra information concerning the forcing of the system, and the results are not necessarily inconsistent. The curves show that the weave mode is less easily excited at medium speeds compared with the lowest and highest speeds, mirroring the high medium speed stability of the weave mode that is indicated by the free vibration results. The wobble mode resonant frequency is not so variable with speed, the responses showing maximum gains around 15 to 25 m/s, and little excitation at high speeds, again in agreement with the free vibration results. One might note that it is substantially harder to excite roll angle and lateral acceleration (Fig.5.2(b)&(d)) than yaw rate and steer angle responses ((a)&(c)) around the wobble mode frequency at high speed. This reflects the dominance in the corresponding wobble mode eigenvector of steering and yawing motions.

The parameters most commonly identified as having large effects on the steering behaviour of a motorcycle are the mechanical trail

and the steering rake angle. Lengthening the trail of a machine is said to make the steering heavy and the machine less responsive. This claim seems to make sense in engineering terms, since any side forces at the tyre contact centre will consequently exert larger moments about the steer axis. Figure 5.3 shows that lengthening the trail decreases the gains of all the responses up to around 9 Hz, particularly between the weave and wobble mode resonant frequencies where the attenuation is typically around 5 dB. One might expect the 50 per cent increase in trail to lead to an attenuation of 3.5 dB purely by virtue of the change in the mechanical advantage. However, it is clear that there are other factors coming into play because the changes in the gains are much smaller than 3.5 dB at low frequencies. Nevertheless, the results presented here would tend to confirm the conventional wisdom about the effects of changes in trail. The stability results show that an increase in trail doesn't lead to any major changes in the stability properties of the same machine, apart from causing an increase in the wobble mode frequency. These results also show that increase.

An increase in the rake angle is thought to lead to light steering, and this also seems to be borne out by the results in Fig.5.3. The increase in gain is largest between the resonant frequencies of the two significant oscillatory modes, and is very small below 3.5 Hz.

In the motorcycling press, much is said about the virtues of constant steering geometry, e.g. Willoughby (1981). Indeed, one of the major criticisms of the telescopic front fork design is that as the machine pitches, the rake and trail alter. Why this is so undesirable is never fully explained. Under heavy braking, I estimate that one might get anything up to 10 degrees of pitch, and hence a 10 degree decrease in the rake angle and a consequent shortening of the trail. From my results one might expect the last two changes largely to cancel each other out as regards their effects on the responsiveness, and it is difficult to explain the poor reputation of telescopic forks in this respect. There are other steering designs which offer nearly constant steering geometry, but the vast majority of racing machines still use telescopic forks. If there were major handling advantages inherent in the other designs, then I think that the various problems involved in adopting them would have

been overcome, especially for racing. It is clear however, that designs which result in the changes in rake and trail having an additive effect on the responses, may well cause control problems under heavy braking, for example.

Lengthening the wheelbase of the machine by moving the rear wheel back has differing effects on the various frequency responses. The gains in respect of the yaw rate and steer angle, Fig.5.4(a)&(c), are slightly decreased up to the wobble mode frequency, but increased at higher frequencies. The roll angle and latic gains are reduced below the weave mode frequency, but are increased over the rest of the frequency range, Fig.5.4(b)&(d). It can be seen that it is significantly harder to excite the wobble mode compared with the datum case, and this agrees with the stability results. In fact, there is almost bound to be a conflict between stability and responsiveness at modal frequencies, because improved stability will generally be accompanied by lower response gains at those frequencies. It doesn't look as though moderate increases in wheelbase have a drastic effect on the responsiveness over the frequency range of interest, and the slight deterioration at low frequencies could easily be negated by other parameter modifications.

The effects on the responses of increasing the steer damping, Fig.5.4, agree well with the corresponding stability results. Large reductions in the gains at the wobble mode frequency are accompanied by rather smaller increases in gains at the weave mode frequency. This modification is unlikely to lead to responsiveness problems within the rider input bandwidth.

Figure 5.5 shows the effects of altering the position of the centre of gravity (c.g.) of the rear frame. Moving it downwards leads to a decrease in the roll angle and latic gains at frequencies above about 3.5 Hz, but has negligible effects on the other two responses. This is quite surprising, because one might expect the consequent reduction in the roll inertia about the tyre/ground contact line to increase the machine's roll response gain. Motorcycle riders are known to dislike machines that are top heavy, although the problem may be to do with the capsize mode behaviour or low speed manoeuvrability. Moving the c.g. forwards tends to make the curves flatter and significantly increases the roll angle and latic gains at frequencies above 4 Hz, Fig.5.5(b)&(d). Such a

modification is also very beneficial to the high speed stability properties, and the results agree well with common design practice. They also illustrate the well known fact that it is beneficial for riders to move their c.g.'s forwards (generally accomplished by bending right over the fuel tank) upon encountering a high speed weave oscillation, because the responses consequently become substantially attenuated at the appropriate frequency, and the stability properties improve.

Doubling the rear wheel polar moment of inertia has negligible effects on the responses, whereas doubling the front wheel polar moment of inertia causes very large changes, Fig.5.6. All of the gains are substantially reduced at most frequencies, except from 4 to 6 Hz, and the weave mode resonant frequency is increased. According to Sharp (1985), the effects on the stability properties of such modifications would be small, apart from a decrease in capsize mode stability. So, it would appear that significant increases in responsiveness, without penalising the stability behaviour, can be obtained by reducing the front wheel polar moment of inertia. This could well explain the recent popularity of smaller front wheels on racing machines, which have reduced in diameter from 0.48m (19 inches) to 0.41m (16 inches) over the last few years. Indeed, I have the impression that the limiting factors that prevent the use of even smaller front wheels concern tyre overheating and wear problems and the necessity for large disc brakes. Previously, drum brakes had to be fitted as part of the central hub and this was probably the main limitation in the past.

Changes made to the masses and inertias of the front and rear frames don't strongly affect the frequency responses, although increasing the mass of the rear frame does appear to decrease the overall responsiveness between the weave and wobble mode resonant frequencies, Fig.5.7. These effects are much smaller than I expected from my knowledge of real motorcycles.

Figure 5.8 shows the effects of separately altering the rear frame inertias about the x and z axes. The roll angle and latic gains are more strongly affected by these changes than are the yaw rate and steer angle gains, the former pair showing some attenuation at most frequencies above 3.5 Hz due to increased inertias. Hence, keeping the inertias as small as possible should lead to small

improvements in responsiveness, particularly during rapid manoeuvres.

The frequency response function gains are generally insensitive to the vertical position of the front frame e.g., Fig.5.9. Moving  $G_f$  further forward of the steer axis however, leads to reduced gains above around 3.5 Hz. The stability results show that such a change would deteriorate the weave and wobble modes at this speed, but would improve the wobble mode at its critical speed. Nevertheless, it might be worthwhile keeping the mass centre as near the steer axis as possible (and thus minimising the steer inertia) to obtain the response advantages at high frequencies, whilst stabilising the medium speed wobble by adding a little steer damping. This may partly explain why racing machines, having low steer inertias compared with road machines, invariably have a steer damper fitted.

The effects of altering the tyre cornering stiffnesses can be seen in Fig.5.10. The frequency responses are fairly insensitive up to the wobble mode frequency to changes in front tyre cornering stiffness, apart from the steer angle response which shows reduced gains as a result of increased stiffness. Such a change made to the rear tyre brings about markedly increased gains between 4 and 8 Hz in the roll and latic responses, although it is difficult to say anything general about the effects upon the other two variables. Comparisons made with the corresponding stability results indicate that it is probably worthwhile trying to increase the rear tyre cornering stiffness, as much as other constraints allow, in order to obtain improved responsiveness, because the effects on stability would be small. Reducing the stiffness of the front tyre would not appreciably harm the high speed responses and would lead to improvement in the medium speed wobble mode.

Changes made to the relaxation lengths of the tyres, Fig.5.11, had little effect on the responses below 6 Hz.

All of the responses were found to be insensitive to changes in the tyres' aligning moment stiffnesses.

### 5.5. CONCLUSIONS

Comparison of the theoretical frequency response gains of a large motorcycle with the only suitable experimental data available, has shown that the two are in broad general agreement.

I have compared the effects of various parameter changes on the straight running frequency responses, with the changes in handling properties predicted by the conventional knowledge of the motorcycling fraternity. This has led to tentative explanations of the significance of various design features, including steering geometry, inertia properties and some tyre parameters, although the effects of other features are yet to be clearly identified.

It is clear that there is some interplay between stability and responsiveness, but the relationship is not a simple one. I conclude that the frequency response results are a very useful supplement to the free vibration results, since the effects of parameter changes on the former cannot be directly predicted from the latter.

CHAPTER 6

THE STRAIGHT LINE STABILITY CHARACTERISTICS OF MOTORCYCLE AND  
TRAILER COMBINATIONS

Two new models, each representing a motorcycle towing a type of trailer, are described. The effects of trailer parameter variations are illustrated and discussed, and recommendations are made regarding the designs most likely to ensure stability.

### 6.1. INTRODUCTION

In April of 1984 it became legal for British motorcyclists to tow trailers with machines exceeding an engine capacity of 125cc. The speed limit for these combinations is 22 m/s (50 mph), but I expect that many trailer towing motorcyclists will grossly exceed this limit, having read a few reports of trailers being towed in a straight line at over 45 m/s (100 mph). Up to the time of writing I haven't read any reports in the motorcycling press of straight line stability problems, apart from one journalist who complained of a minor trailer weave at over 40 m/s (90 mph) on a bumpy country road! The lack of reports of instability may be due to the present scarcity of these combinations on British roads, although trailers have been used in the USA and on the Continent for many years without arousing any previous theoretical examination. Nevertheless, knowing of the work done by Hales (1963) on automobile and trailer combinations, which has adequately represented their real life behaviour, I felt that it was worthwhile modelling the motorcycle and trailer system in a similar manner.

The addition of a heavy trailer is reported to worsen the handling of motorcycles while cornering, particularly on bumpy roads, and it has been observed by one constructor that a long drawbar is better than a short one in this respect. Although I won't be examining the cornering behaviour here, it is clearly desirable to ascertain the influences of various parameters on straight line stability, such as forward speed, trailer mass and inertias, drawbar length, hitch position and trailer tyre properties. This theoretical knowledge may help trailer owners and manufacturers to employ safer designs and avoid dangerous loading conditions.

There are two types of motorcycle trailer currently for sale in Britain. The first is a conventional, twin wheel, single axle type similar to that commonly towed by cars, and the other is a single wheel unit which rolls with the motorcycle. I have consequently developed theoretical models for both of these designs.

## 6.2. THE MODELS

The motorcycle model is the same as that developed in Chapter 3. The twin wheel trailer is modelled as a lumped mass attached to the rear frame of the motorcycle (i.e. that part comprising the engine, rigidly attached rider etc.) by a Hooke's joint (Fig 6.1). The trailer has a single freedom to yaw about a vertical axis passing through the joint. The assumptions applying to the complete system include those given in section 3.2, with the following additions:

- (a). Small vertical movements of the trailer due to motorcycle roll are ignored.
- (b). Changes in trailer tyre vertical load due to aerodynamic drag are not considered, although the effect of trailer attachment on the motorcycle tyres' vertical loads has been accounted for.
- (c). Trailer tyre rolling resistance is ignored.

The single wheel trailer is modelled in a nearly identical way, except that it has a roll freedom as well as a yaw freedom, and assumption (a) doesn't apply. Figure 6.1 suffices to give the dimensions relevant to both models.

In each case, the responses of the trailer tyre forces and moments to side slip are modelled using first order lags. Side force responses to camber are considered instantaneous. Trailer tyre moment responses to camber are not included, since they are likely to make negligible difference to the results, as explained by Jones (1982).

## 6.3. THE EQUATIONS OF MOTION

For each model, these consist of the equations given in section 3.3, plus additional terms describing the inertia forces and tyre forces and moments due to the trailer. In addition, there is one extra equation describing the motion of the trailer and two equations for the trailer tyre side force and aligning moment. For brevity, only the extra terms and equations will be given here. The derivation of both sets of equations is described in Appendix 2.

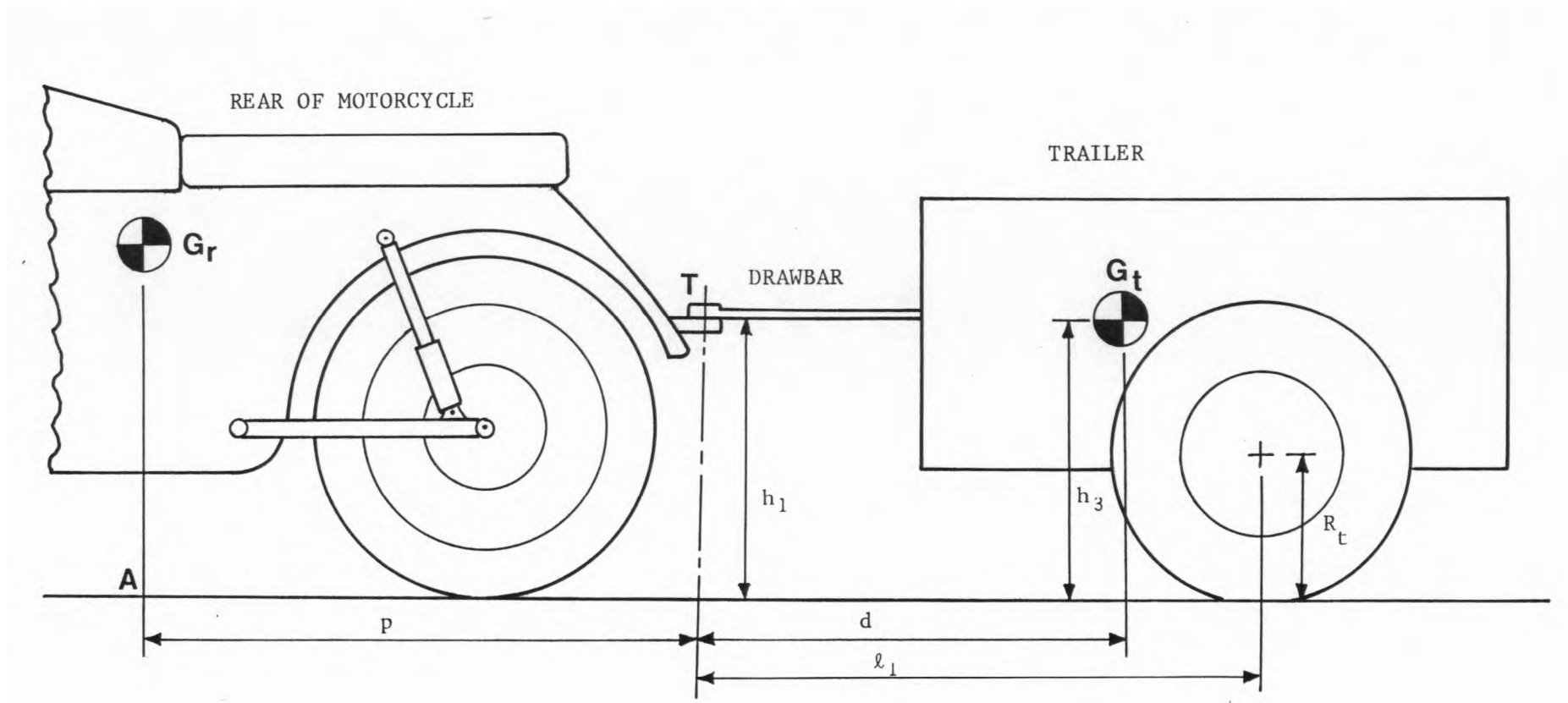


Figure 6.1

Dimensions of trailer.

The equations are linearised for small perturbations from a straight-running condition, and may be reduced to first order by the same method as described in Chapter 3, resulting in a total of 18 equations with constant coefficients, for each model. The equations have been solved to give eigenvalues and eigenvectors for the free vibration behaviour of the system.

### 6.3.1. Equations for the Twin Wheel Trailer

The extra terms are added as follows:

To equation 3.1 on the left hand side (l.h.s.),

$$M_{tr} \{\dot{v} + Ur - (p + d)\dot{r} + h_1\ddot{\phi} - d\ddot{\alpha}\}$$

and on the right hand side (r.h.s.),  $2Y_t$

To equation 3.2 on the l.h.s.,

$$- M_{tr}(p + d)\{\dot{v} + Ur - (p + d)\dot{r} + h_1\ddot{\phi} - d\ddot{\alpha}\} + I_{tz}(\dot{r} + \dot{\alpha})$$

and on the r.h.s.,  $- 2(p + l_1)Y_t + 2M_{zt}$

To equation 3.3 on the l.h.s.,

$$M_{tr}h_1\{\dot{v} + Ur - (p + d)\dot{r} + h_1\ddot{\phi} - d\ddot{\alpha}\}$$

and on the r.h.s.,  $2h_1Y_t$

The equation of motion for the trailer is:

$$\begin{aligned} & - M_{tr}d\{\dot{v} + Ur - (p + d)\dot{r} + h_1\ddot{\phi} - d\ddot{\alpha}\} + I_{tz}(\dot{r} + \dot{\alpha}) + D_t\dot{\alpha} \\ & = - 2l_1Y_t + 2M_{zt} \end{aligned}$$

The trailer tyre side force equation is:

$$\sigma_t \dot{Y}_t + U Y_t = - C_{Ft} \{v - (p + l_1)r + h_1\dot{\phi} - l_1\dot{\alpha} - U\alpha\} - C_{Mt}(r + \dot{\alpha})$$

The trailer tyre moment equation is:

$$\sigma_t \dot{M}_{zt} + U M_{zt} = C_{Mt} \{v - (p + l_1)r + h_1\dot{\phi} - l_1\dot{\alpha} - U\alpha\}$$

### 6.3.2. Equations for the Single Wheel Trailer

The extra terms are added as follows:

To equation 3.1 on the l.h.s.,

$$M_{tr} \{\dot{v} + Ur - (p + d)\dot{r} + h_3\ddot{\phi} - d\ddot{\alpha}\}$$

and on the r.h.s.,  $Y_t + C_{1t}\phi$

To equation 3.2 on the l.h.s.,

$$\begin{aligned} & - M_{tr}(p + d)\{\dot{v} + Ur - (p + d)\dot{r} + h_3\ddot{\phi} - d\ddot{\alpha}\} + I_{tz}(\dot{r} + \ddot{\alpha}) \\ & - I_{txz}\ddot{\phi} - i_{twy}\dot{\phi}U/R_t \end{aligned}$$

and on the r.h.s.,  $-(p + \ell_1)(Y_t + C_{1t}\phi) + M_{zt}$

To equation 3.3 on the l.h.s.,

$$\begin{aligned} & M_{tr}h_3\{\dot{v} + Ur - (p + d)\dot{r} + h_3\ddot{\phi} - d\ddot{\alpha}\} + I_{tx}\ddot{\phi} - I_{txz}(\dot{r} + \ddot{\alpha}) \\ & + i_{twy}(\dot{r} + \ddot{\alpha})U/R_t - M_{tr}h_3g\phi \end{aligned}$$

The equation of motion for the trailer is:

$$\begin{aligned} & - M_{tr}d\{\dot{v} + Ur - (p + d)\dot{r} + h_3\ddot{\phi} - d\ddot{\alpha}\} + I_{tz}(\dot{r} + \ddot{\alpha}) + D_t\dot{\alpha} - I_{txz}\ddot{\phi} \\ & - i_{twy}\dot{\phi}U/R_t = -\ell_1(Y_t + C_{1t}\phi) + M_{zt} \end{aligned}$$

The trailer tyre side force equation is:

$$\sigma_t \dot{Y}_t + U Y_t = -C_{Ft} \{v - (p + \ell_1)r - \ell_1\ddot{\alpha} - U\alpha\} - C_{Mt}(r + \dot{\alpha})$$

The trailer tyre moment equation is:

$$\sigma_t \dot{M}_{zt} + U M_{zt} = C_{Mt} \{v - (p + \ell_1)r - \ell_1\ddot{\alpha} - U\alpha\}$$

#### 6.4. RESULTS

Figures 6.2, 6.7-11, 6.13-14 and 6.19-25 show the most significant free vibration eigenvalues for the models, plotted on the real/imaginary plane. The plot symbol size is related to forward speed which increases from 5 m/s to 45 m/s in a geometric series with ratio 1.2.

Selected eigenvectors for the least damped oscillatory modes can be seen in Figs.6.4-6 and 6.15-18.

The datum parameter values are listed in Appendix 1. Those for the trailers are intended to represent the properties of the heaviest trailers that the construction and use regulations permit, and may be thought of as being worst cases, although some motorcyclists may load their trailers more heavily than is permitted.

#### 6.5. DISCUSSION

##### 6.5.1. The Twin Wheel Trailer

From Fig.6.2 it can clearly be seen that the stability of the motorcycle is substantially deteriorated by the attachment of the trailer. Both the wobble and weave modes have become unstable, the wobble mode in the speed range from 5 m/s up to around 25 m/s, and the weave mode above 40 m/s. A third significant oscillatory mode has been introduced by the attachment of the trailer. It has a characteristic frequency of around 1.5 Hz and becomes less stable as speed increases. The associated eigenvectors show that the mode is dominated by trailer yaw, which is around 100 times larger than any of the other motion variables, and which lags the motorcycle yaw motion by about 15 degrees. Consequently, I will call this the trailer swing mode. The capsize mode eigenvalues, Fig.6.3, are only slightly affected by the addition of the trailer, indicating marginally better damping than for the motorcycle alone throughout the speed range. Parameter variations relating to the trailer had no appreciable effects on the capsize mode, and no further results are given for it.

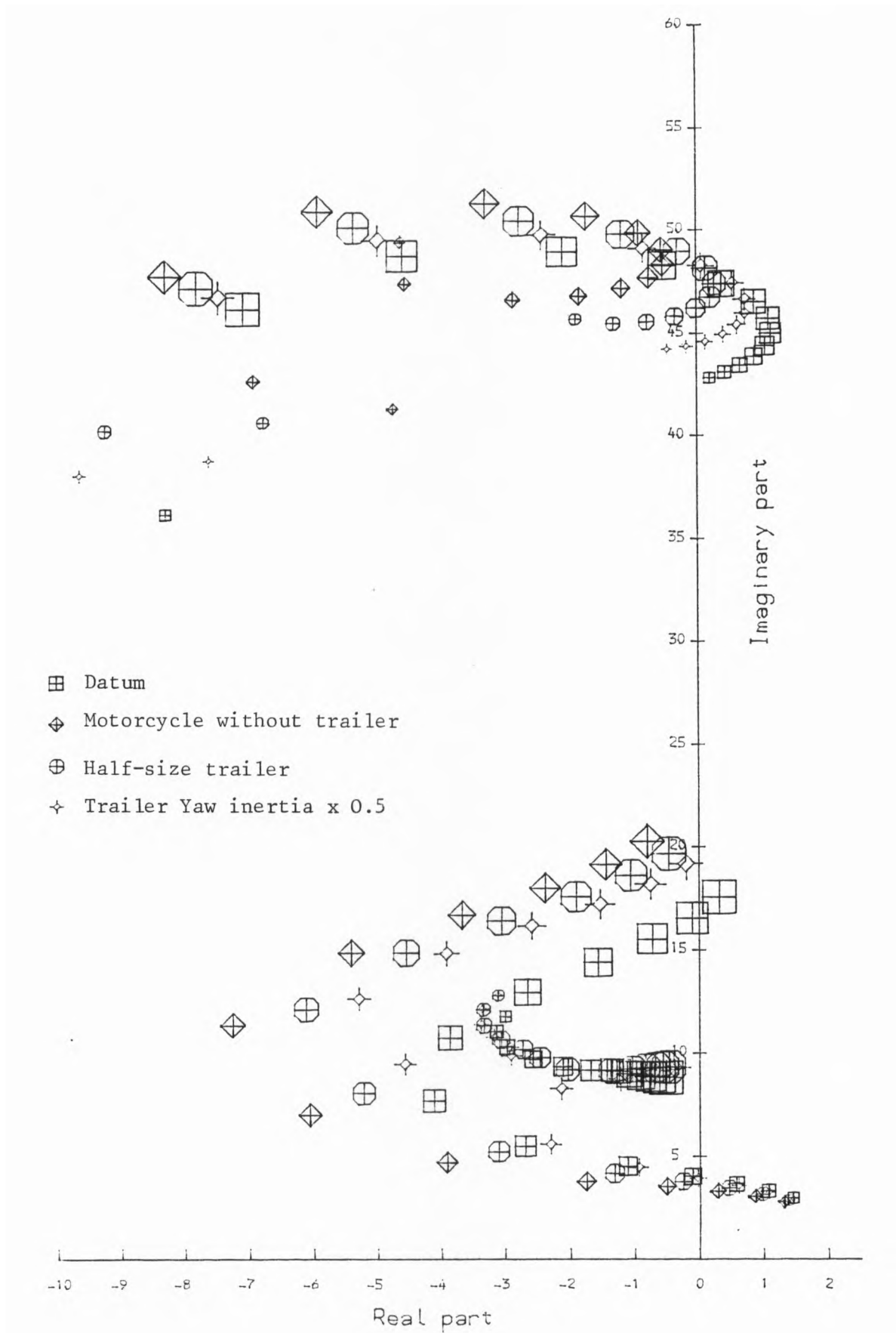


Figure 6.2

Oscillatory mode eigenvalues for changes in trailer size, twin wheel trailer.

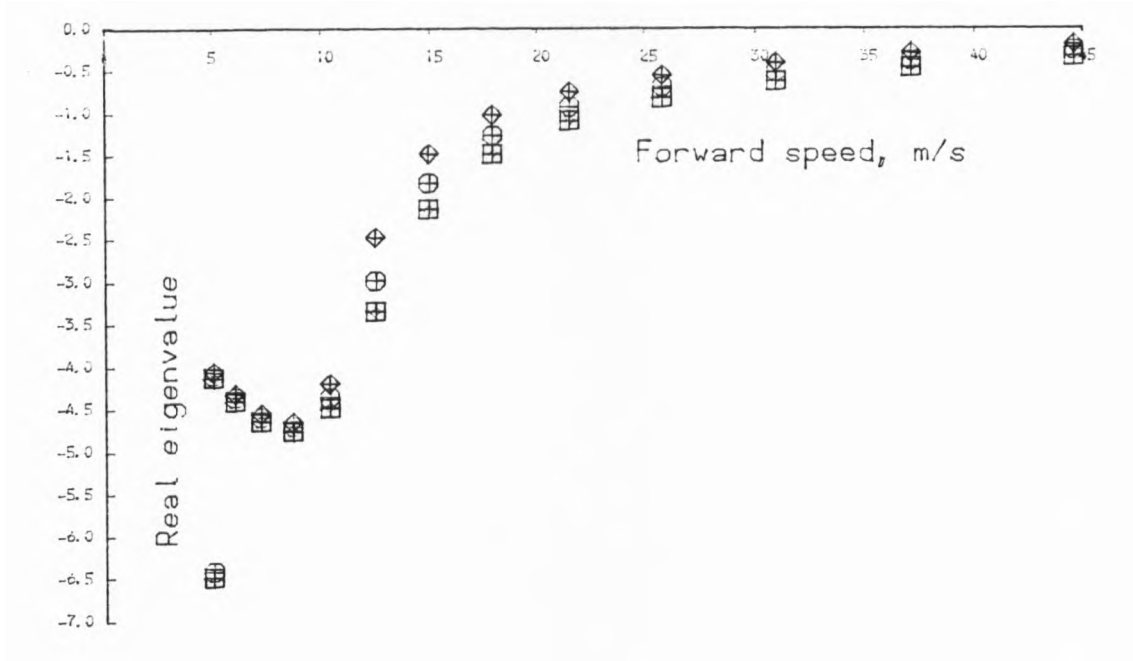


Figure 6.3

Capsize mode results corresponding to Fig.6.2.

Eigenvectors for the datum case wobble mode at 15 m/s can be seen in Fig.6.4. The size and phase relationships are the same as those for the motorcycle alone, given in Fig.3.5, except for the addition of the trailer yaw rate which is in antiphase with the motorcycle yaw rate, and approximately 1.3 times larger. Fig.6.5 shows the eigenvectors for the motorcycle weave mode at the same speed. Again, these are similar to those for the motorcycle alone as given by Sharp (1984b), with the addition of the trailer yaw rate which is approximately 4 times larger than, and nearly in phase with, the front frame steer rate. Eigenvectors for the motorcycle weave mode at the highest speed can be seen in Fig.6.6. The trailer yaw rate is still nearly in phase with the steer rate, and is now the largest motion variable, the roll rate having reduced relatively in size compared with Fig.6.5. The eigenvectors are otherwise similar to those presented in Fig.3.6 for the motorcycle alone.

The effects of altering the trailer mass and inertia so as to simulate a trailer of half the datum size, are also illustrated in Fig.6.2. It is clear that the wobble and weave modes become much more stable compared with the datum case, although the effect on the trailer swing mode is small. Hence it is desirable that any trailer attached to a motorcycle should be as small as possible for maximum

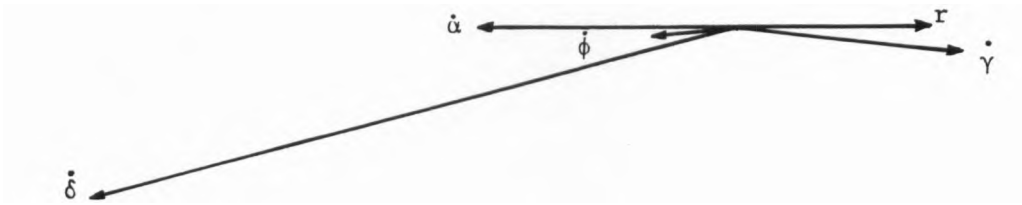


Figure 6.4

Wobble mode eigenvectors, 15m/s, datum case, twin wheel trailer.

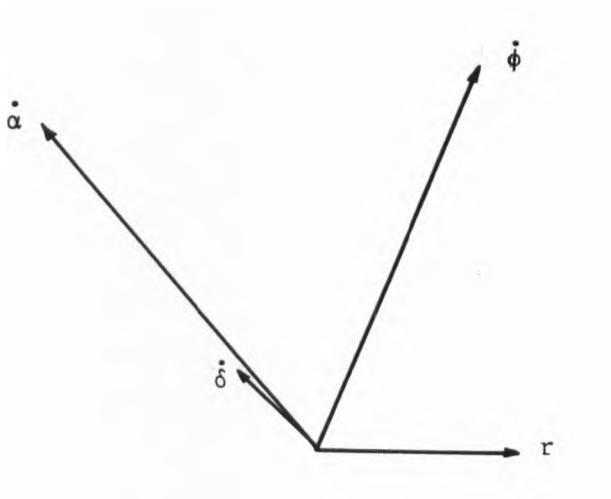


Figure 6.5

Weave mode eigenvectors, 15m/s, datum case, twin wheel trailer.

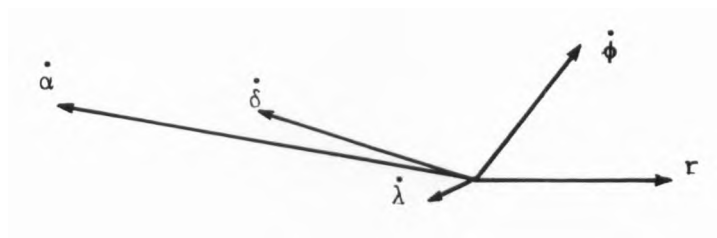


Figure 6.6

Weave mode eigenvectors, 45m/s, datum case, twin wheel trailer.

safety. The legal trailer mass limit is 150 kg, or three quarters of the kerbside mass of the motorcycle, whichever is the lesser. Since the motorcycle modelled here is fairly large, the trailer mass of 150 kg is only around half that of the motorcycle. Consequently, I would argue that the effects on the stability properties of smaller motorcycles are likely to be more dramatic than those shown here, since the trailers may represent larger proportions of the total masses of the vehicles whilst still being within the legal limit.

Reducing the yaw inertia of the trailer while keeping the mass constant is beneficial to the weave and wobble modes, but leads to a slight deterioration of the trailer swing mode, Fig.6.2. This implies that reductions in trailer dimensions such as length and width are likely to be beneficial to overall straight line stability, for a given trailer mass.

The effects of altering the hitch height are illustrated in Fig.6.7. The results show that lowering the hitch improves both of the motorcycle oscillatory modes, and has negligible effect on the trailer swing mode. There are practical limitations to this modification, of course, and the datum value for the hitch height was chosen to be near to that likely to be used on most machines.

Figure 6.8 shows the effects of varying the trailer tyre parameters. Neither of the variations appreciably affected the motorcycle weave or wobble modes, as one might expect. However, increasing the trailer tyre cornering stiffness improves the stability of the trailer swing mode, whereas increasing the relaxation length makes it worse. Putting more air in the tyres would increase their cornering stiffness, but would reduce the contact length and also the adhesion on bumpy surfaces due to reduced vertical compliance. Hence, the overall benefits of pumping up the tyres may not be very large.

From Fig.6.9 it can be seen that moving the hitch rearwards on the motorcycle appreciably deteriorates the stability of the weave and wobble modes throughout the speed range, but has no effect on the trailer swing mode. Conversely, increasing the length of the trailer drawbar improves the weave and wobble modes, whilst leaving the trailer swing mode with much the same damping, but a slightly

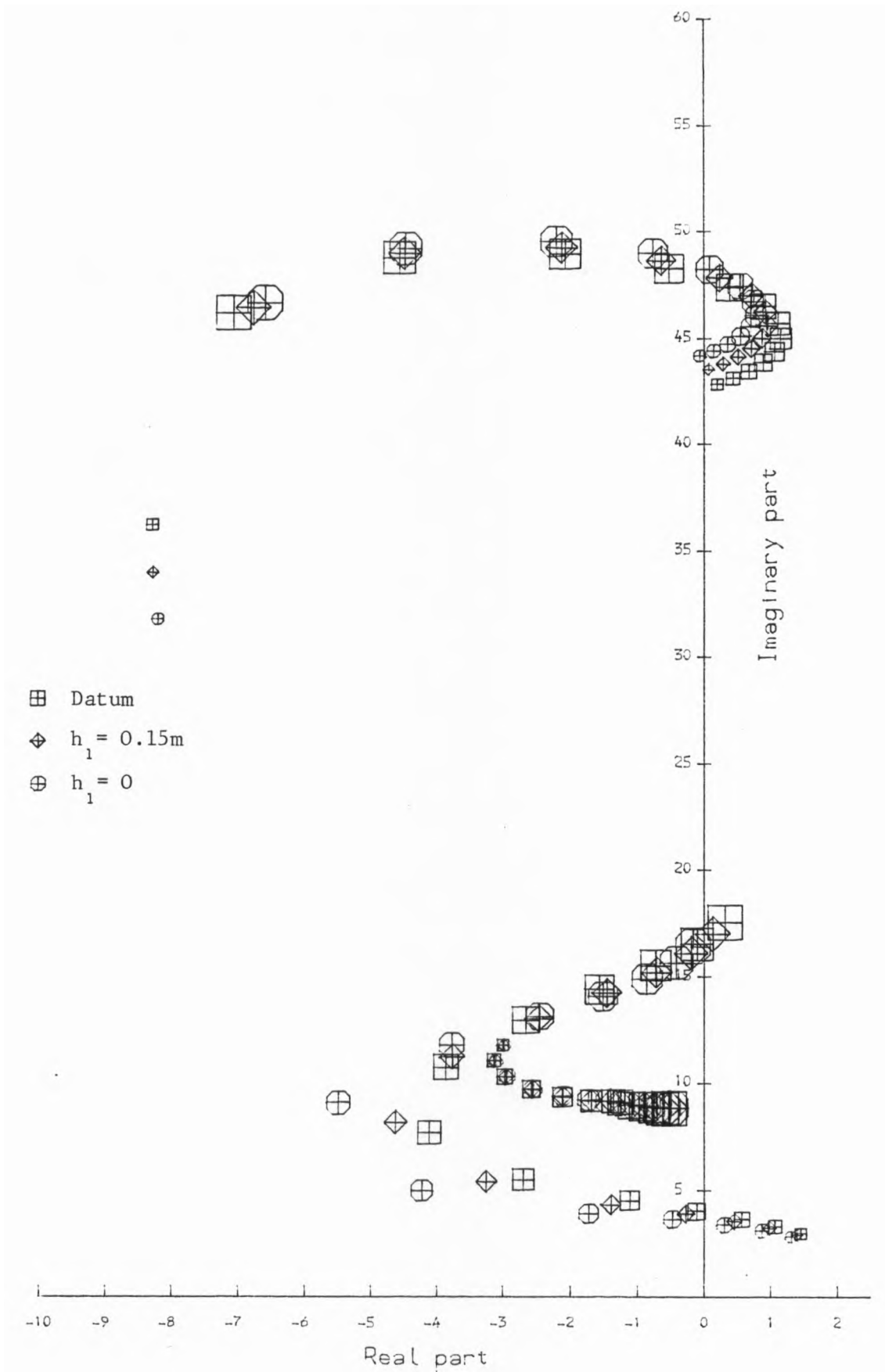


Figure 6.7

Oscillatory mode eigenvalues for changes in hitch height, twin wheel trailer.

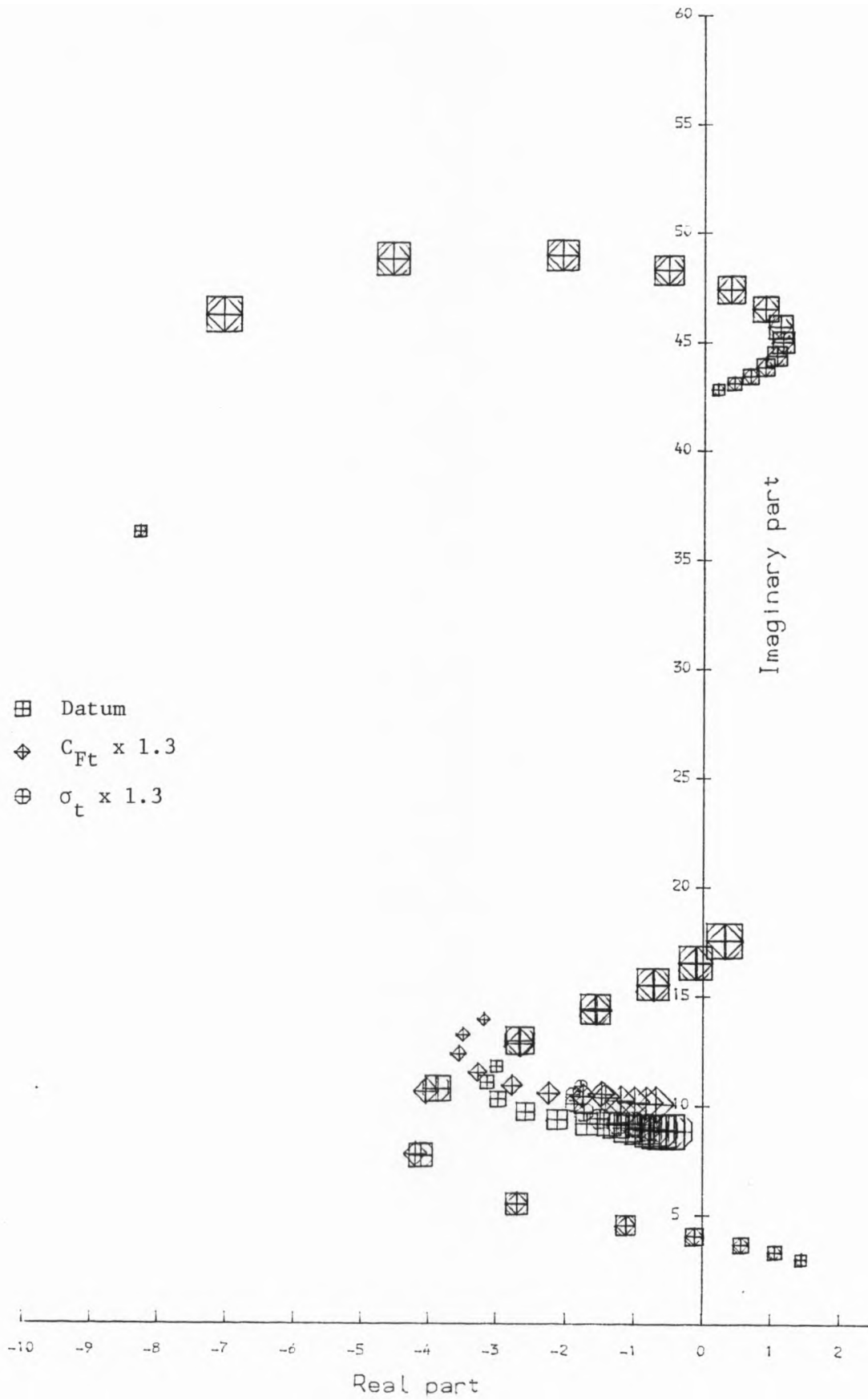


Figure 6.8

Oscillatory mode eigenvalues for changes in tyre parameters, twin wheel trailer.

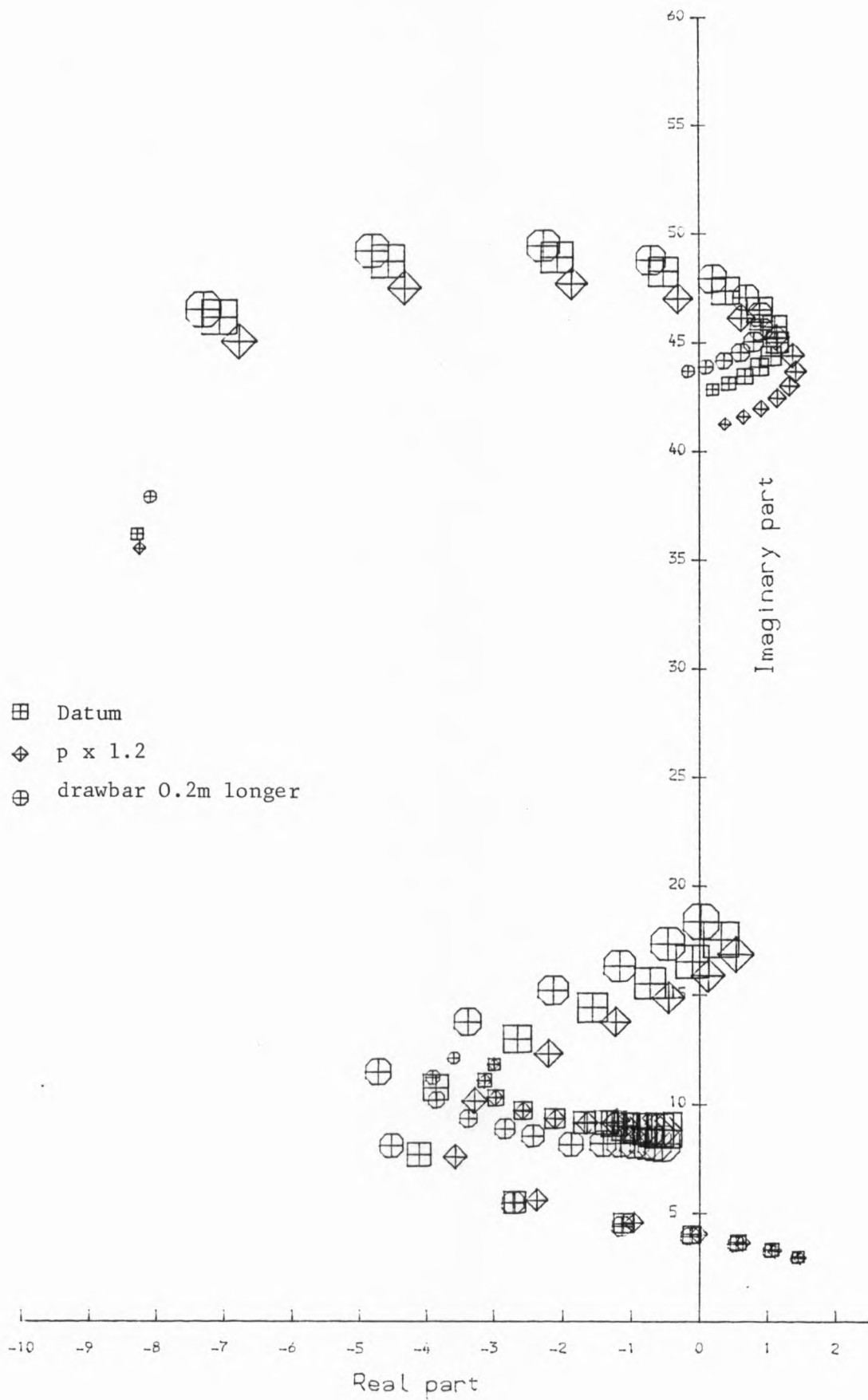


Figure 6.9

Oscillatory mode eigenvalues for changes in hitch position and drawbar length, twin wheel trailer

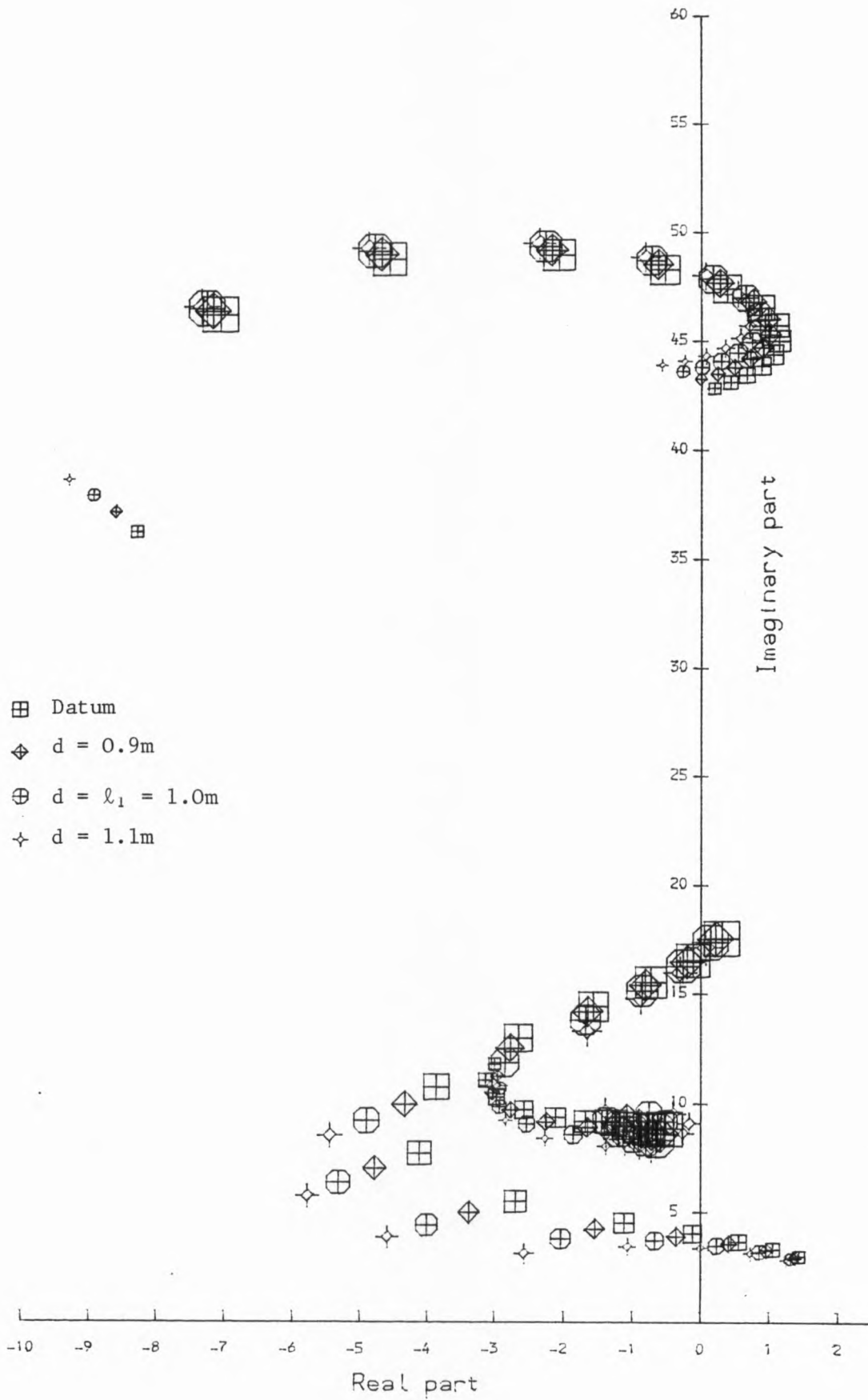


Figure 6.10

Oscillatory mode eigenvalues for changes in trailer c.g. position, twin wheel trailer.

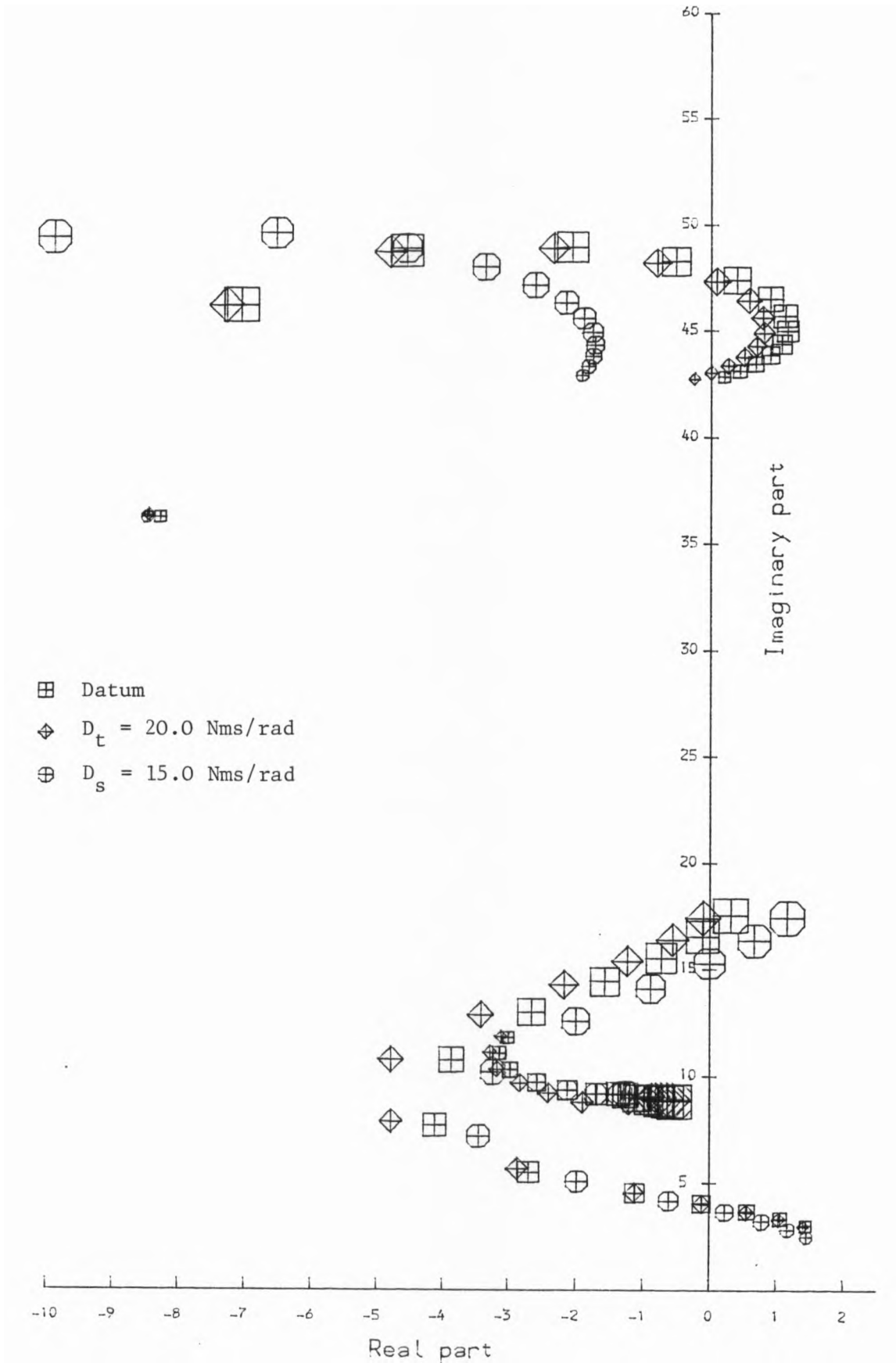


Figure 6.11

Oscillatory mode eigenvalues for changes in damping, twin wheel trailer.

lower frequency at high speeds. This parameter effect appears to be in general agreement with the real life observations mentioned earlier.

Figure 6.10 shows that moving the centre of gravity of the trailer to the rear has a beneficial effect on the weave and wobble modes. However, moving it to the rear of the trailer axle destabilises the trailer swing mode at moderately high speeds, and a satisfactory compromise will probably be achieved by having the trailer centre of gravity over, or a little forward of, the axle.

Introducing a linear viscous damper between the motorcycle and the trailer, Fig.6.11, increases the stability of the motorcycle wobble and weave modes at all speeds, but has little effect on the trailer swing mode. A moderate value for the steer damping, such as would easily be obtainable from a proprietary steer damper, has a large beneficial effect on the wobble mode, but appreciably decreases the weave mode stability at high speed. These results are in agreement with the corresponding results for a motorcycle alone, given by Sharp (1984b). The trailer swing mode is negligibly affected at the highest (most critical) speed by this modification.

Since, for the datum set of parameter values, the motorcycle weave and wobble modes are the most problematic, I decided to try using a combination of parameter values aimed at stabilising these modes whilst not deteriorating the trailer swing mode, and retaining the same trailer mass and inertia properties. Although the highly unstable wobble mode could be dramatically improved by the use of steer damping, it is necessary to observe that these results represent a "hands off" condition, and in real life the rider may provide a significant amount of steer damping by means of his hands and arms. Hence, I regard the results for the wobble mode as rather pessimistic, and have not added any steer damping to improve it, thus avoiding the destabilising effects on the weave mode at high speeds.

From my previous results it is clearly desirable to move the hitch forward on the motorcycle, although there is a practical limit to this set by the layout of the machine. Also, the trailer drawbar is best made longer, but there is a legal limit to the length of the trailer specified in the construction and use regulations, and I

think practical considerations imply a drawbar length of little more than was used for the datum case, anyway. One method of solving both of these problems might be to use a double drawbar, as shown in Fig.6.12. This moves the effective hitch point much further forward than would be possible with a single drawbar, and also makes the effective drawbar length much larger, whilst keeping the overall vehicle length the same. The disadvantages are that the hitch joint assembly has to be more complicated than before, and the hinges at the body of the trailer have to provide it with pitch restraint as well as enabling yawing motion. During low speed vehicle turning, substantial trailer off-tracking could occur, but since the motorcyclist already has to accept a large deterioration in manoeuvrability upon attaching any trailer, I think this is likely to be a small consideration. Such a hitch arrangement was suggested for use on trucks towing trailers by Crolla and Sharp (1983). They indicated that the off-tracking problem could be minimised by careful attention to the design of the hitch, the geometry of which has been analysed by Paul (1979).

The results for the motorcycle and trailer with this modification, a moderate amount of hitch damping, and the trailer centre of gravity over the axle, can be seen in Fig.6.13. All of the oscillatory modes are now stable throughout the speed range (apart from the low speed weave, which the rider would easily be able to control), although the effects on the trailer swing mode were small.

#### 6.5.2. The Single Wheel Trailer

The addition of the trailer to the motorcycle substantially deteriorates the wobble mode throughout the speed range, Fig.6.14. The eigenvectors for this mode at 15 m/s can be seen in Fig.6.15, and are similar to those for the motorcycle alone. The trailer and motorcycle yaw rates are almost exactly in antiphase, the former being approximately 1.4 times larger than the latter. This mode shape is very similar to that for the twin wheel trailer case. There are two other significant oscillatory modes, both of which generally increase in frequency as road speed increases. Figures 6.16 and 17 show the eigenvectors for the higher frequency mode at 15 m/s and 45 m/s respectively. In terms of the amplitude and phase relationships of the motion variables excluding the trailer yaw

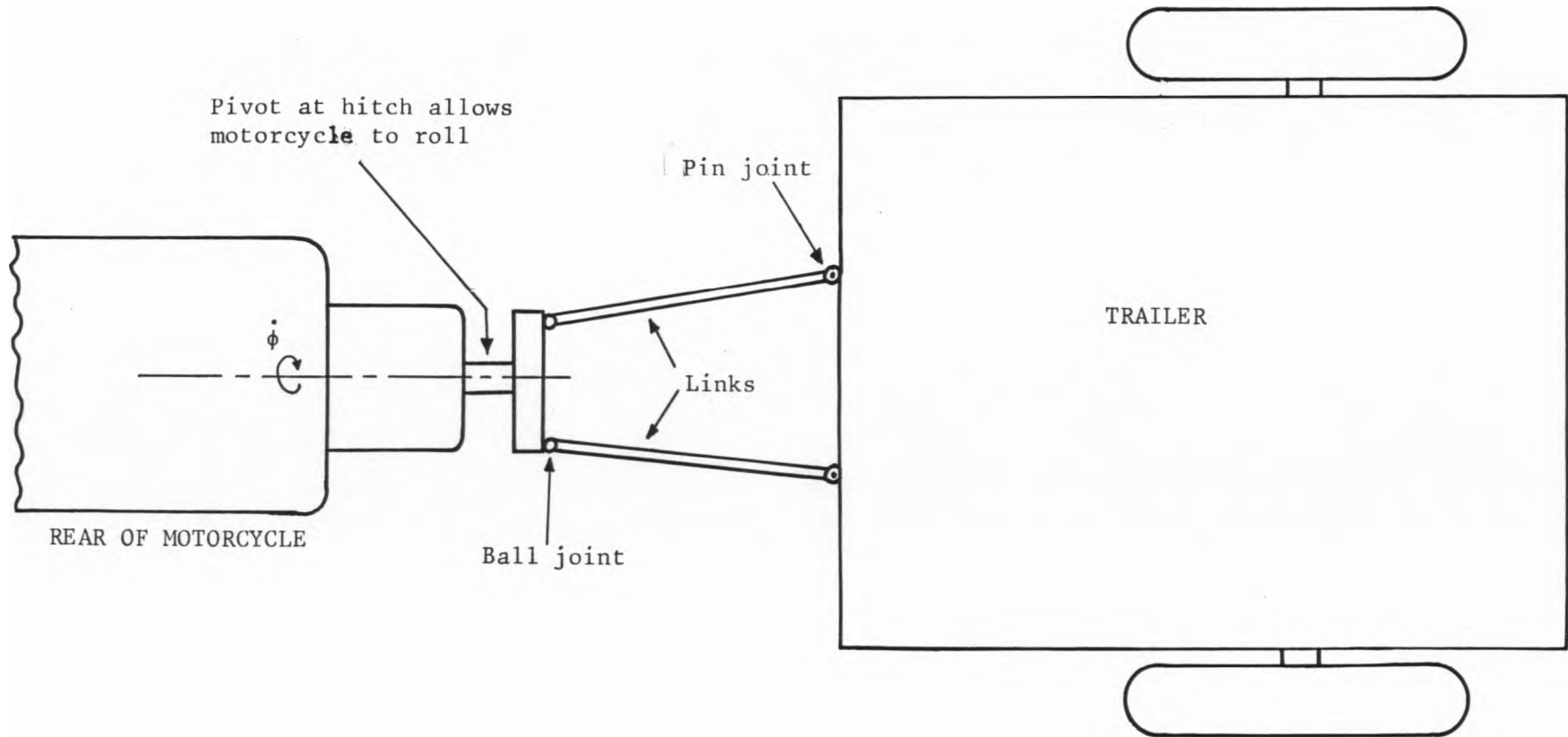


Figure 6.12  
Double drawbar configuration for twin wheel trailer.

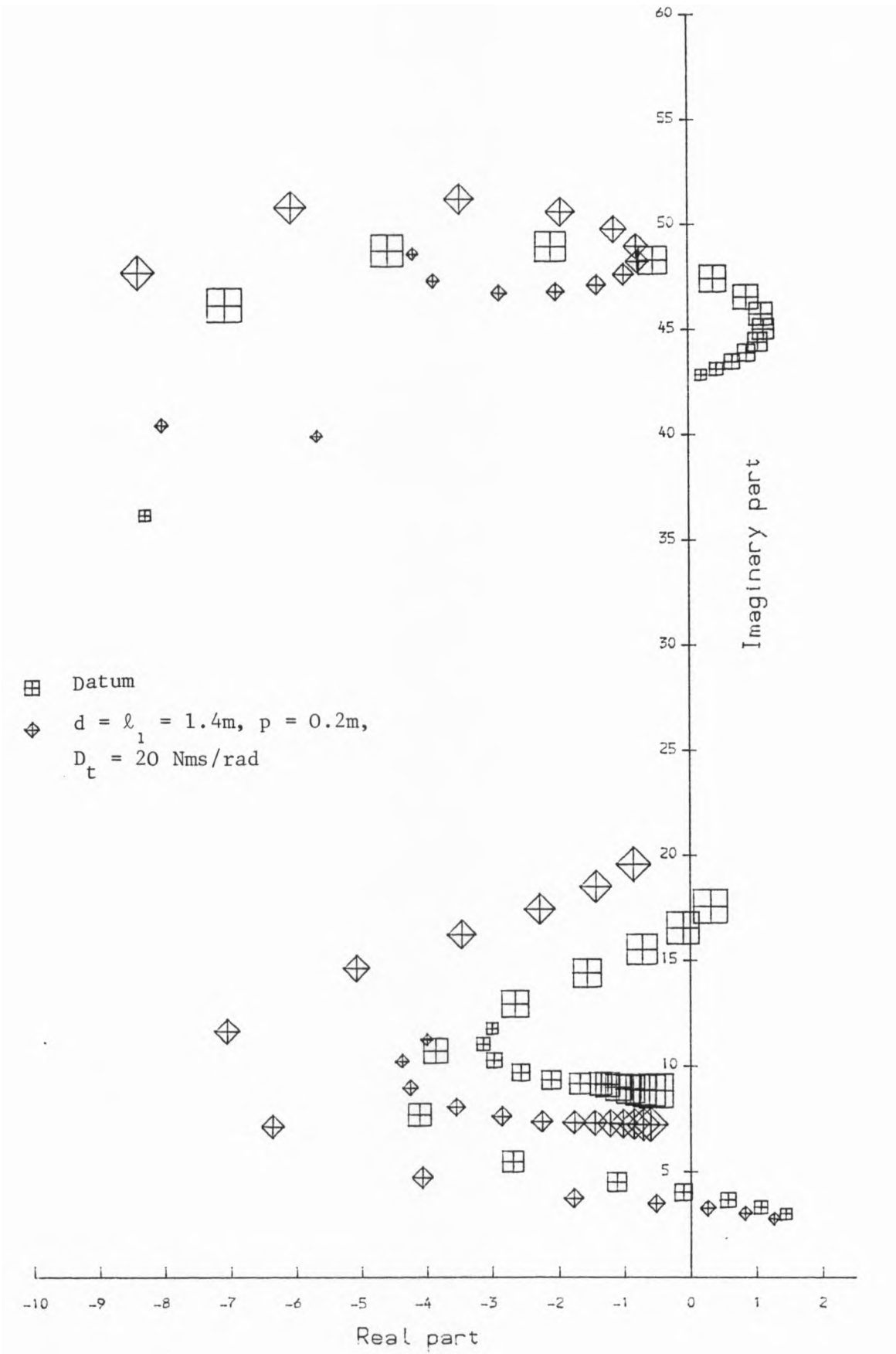
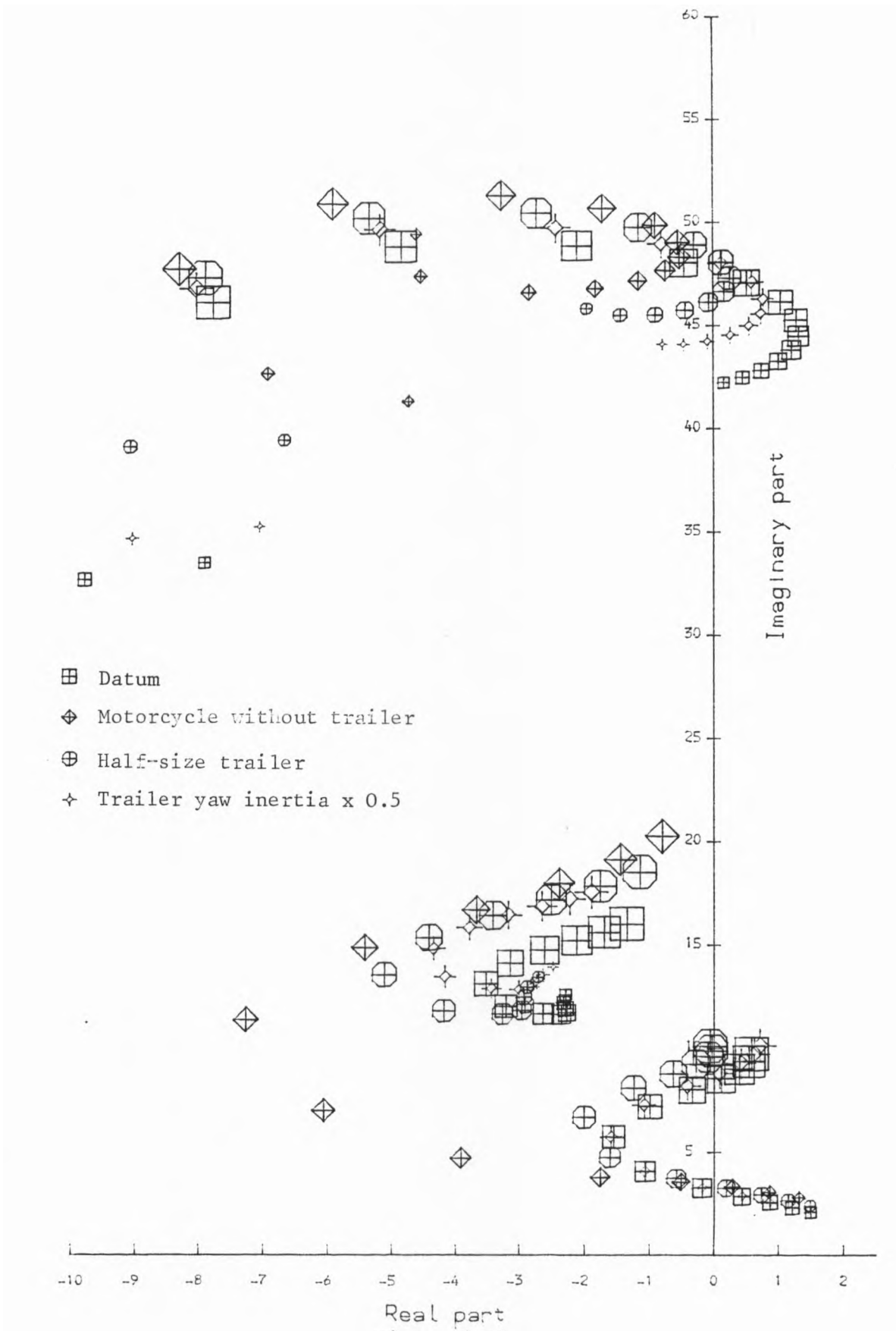


Figure 6.13

Oscillatory mode eigenvalues for datum case and modified twin wheel trailer.



Oscillatory mode eigenvalues for changes in trailer size, single wheel trailer.

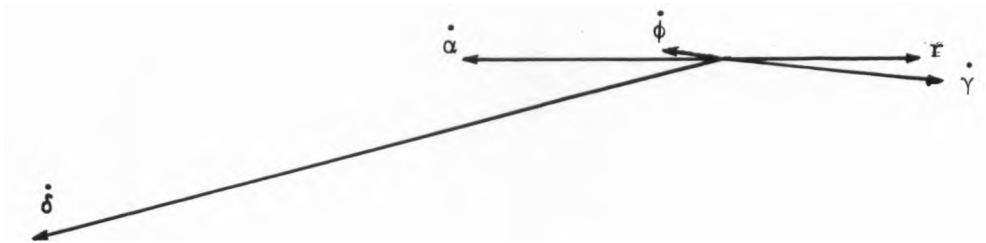


Figure 6.15

Wobble mode eigenvectors, 15m/s, datum case, single wheel trailer.

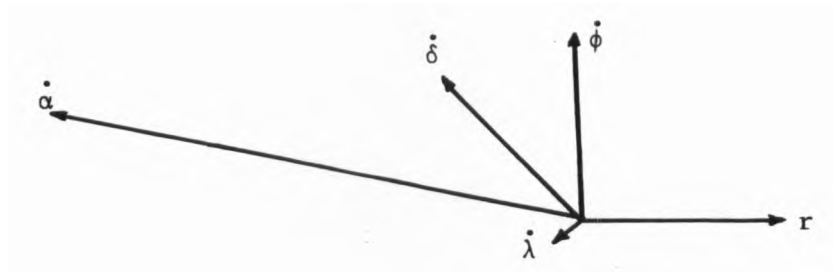


Figure 6.16

Weave mode eigenvectors, 15m/s, datum case, single wheel trailer.

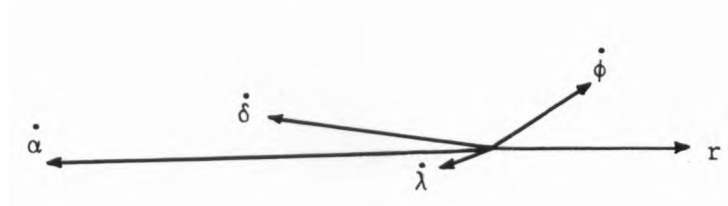


Figure 6.17

Weave mode eigenvectors, 45m/s, datum case, single wheel trailer.

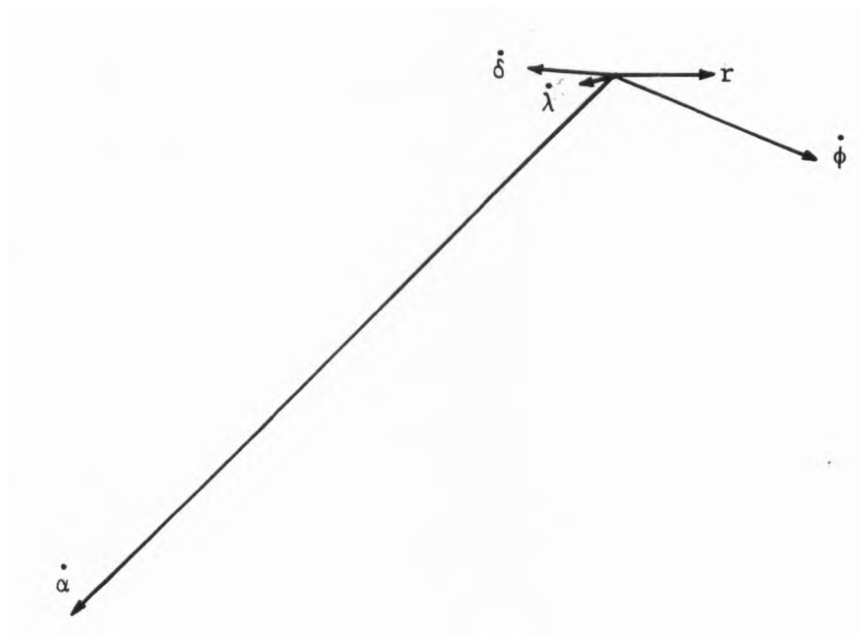


Figure 6.18

Trailer weave mode eigenvectors, 45m/s, datum case, single wheel trailer.

rate, these closely resemble the eigenvectors of the motorcycle weave mode as given by Sharp (1984b). In this case however, the trailer yaw rate has become the largest motion variable, by a factor of approximately two, and is roughly in antiphase with the motorcycle yaw rate. Nevertheless, I will refer to this as the weave mode. It is stable throughout the speed range, and the addition of the trailer appears to have improved the stability at low and high speeds compared with the motorcycle alone. Figure 6.18 shows the eigenvectors for the lowest frequency oscillatory mode at 45 m/s. This mode is clearly dominated by the trailer yaw rate, which lags the motorcycle yaw rate by about 135 degrees and is approximately 3.5 times bigger than the next largest motion variable, the roll rate. Consequently, I will call this the trailer weave mode. It is very unstable at low and high speeds, and appears to be the most problematical of the oscillatory modes, although the rider would probably be able to control it at low speed. Comparison with the results for the twin wheel trailer show that the single wheel trailer has worse effects on the straight line stability, for a given trailer size.

The capsize mode results were negligibly affected by the addition of the trailer, and they won't be discussed here.

From Fig.6.14 it can be seen that reducing the size of the trailer improves the wobble and trailer weave modes substantially at their most critical speeds, whilst making the weave mode slightly less stable at high speeds. Halving the yaw inertia appreciably improves the wobble and weave modes, but marginally worsens the trailer weave mode.

Increasing the height of the trailer mass centre slightly deteriorates the wobble and trailer weave modes, but improves the weave mode at high speeds, Fig.6.19. Increasing the trailer wheel polar moment of inertia has negligible effects on all of the modes.

Altering the tyre properties, Fig.6.20, doesn't affect the wobble mode at all. Increasing the cornering stiffness and aligning moment coefficients decreased the trailer weave mode damping, but increased the weave mode damping, at high speeds. Alterations to the tyre side force/camber coefficient had little effect on either mode. An increased trailer tyre relaxation length led to slightly

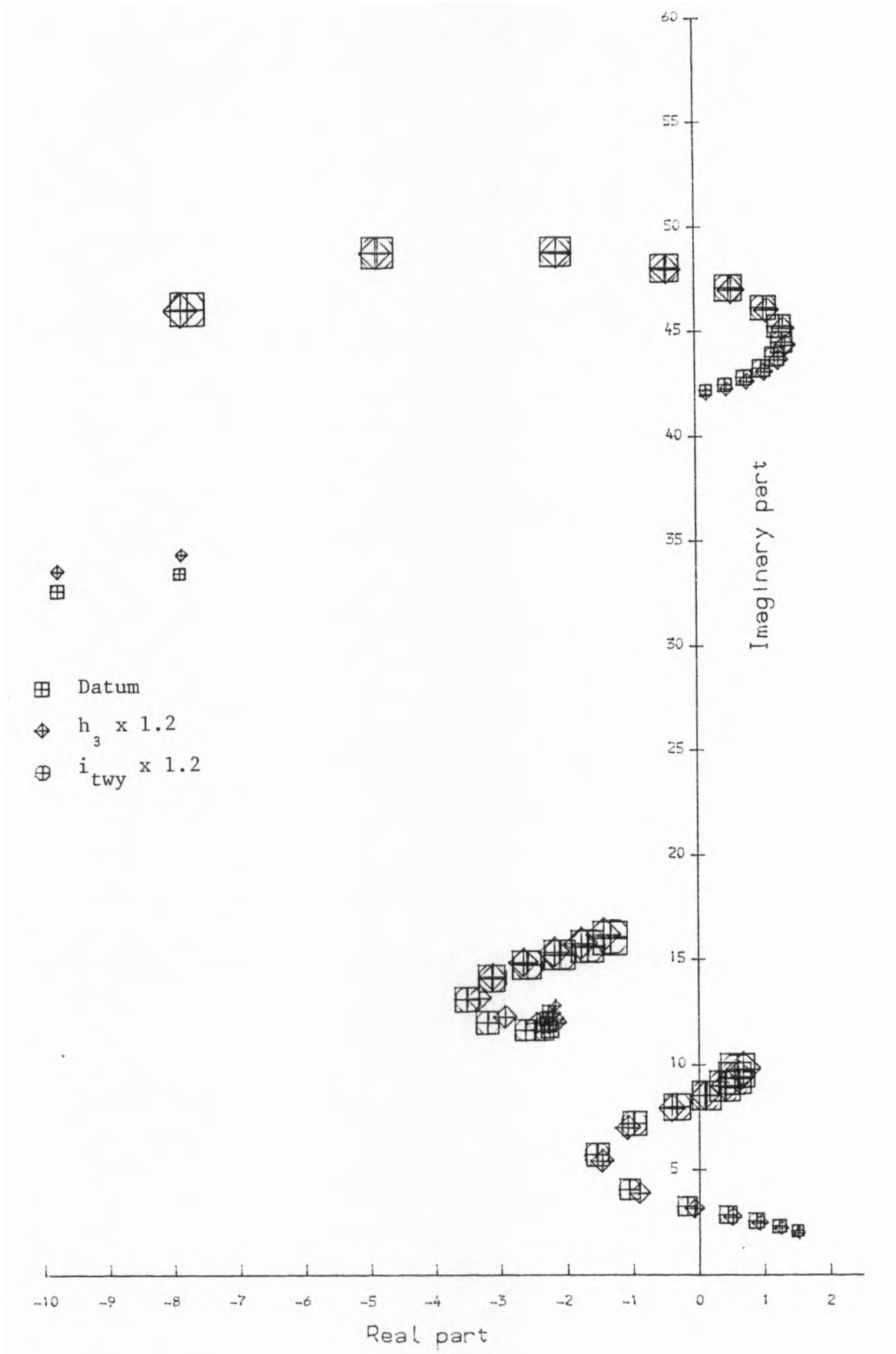


Figure 6.19

Oscillatory mode eigenvalues for changes in trailer c.g. height and wheel inertia, single wheel trailer.

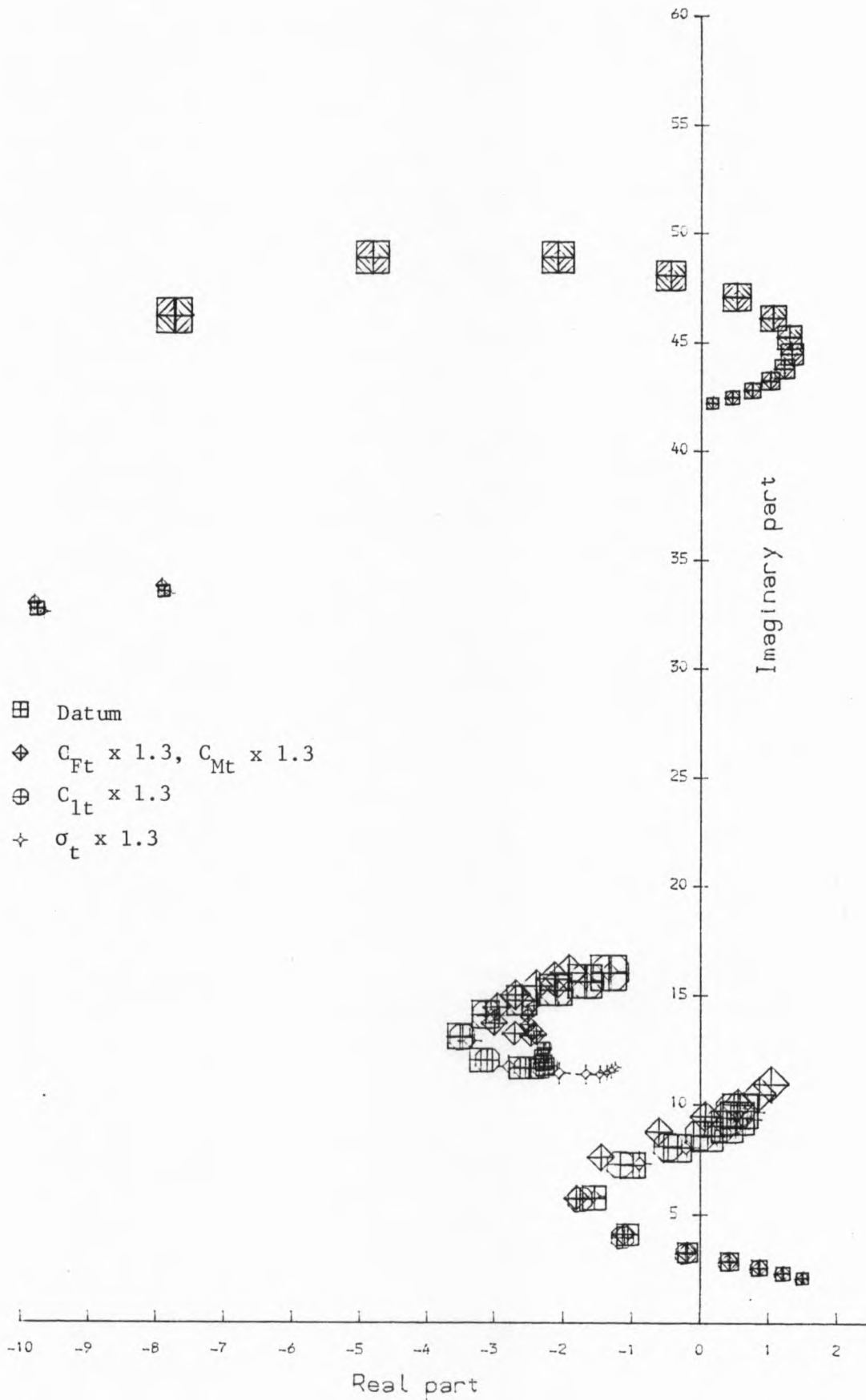


Figure 6.20

Oscillatory mode eigenvalues for changes in tyre parameters, single wheel trailer.

decreased trailer weave mode stability at high speeds.

Figure 6.21 illustrates the effects of varying the hitch position and drawbar length. Moving the hitch to the rear had a destabilising effect on all three of the oscillatory modes, whereas increasing the drawbar length improved the stability of the modes, in general agreement with the results for the twin wheel trailer.

The effects of altering the position of the trailer centre of gravity can be seen in Fig.6.22. The stabilities of the wobble and weave modes were improved at their most critical speeds by moving the centre of gravity to the rear. This change, however, caused the trailer weave mode to become less stable, and since this mode is likely to be the most problematical, a good compromise will probably be reached by positioning the centre of gravity just in front of, or over, the wheel spindle.

Introducing a damper between the motorcycle and trailer stabilises the wobble and weave modes throughout the speed range, but slightly destabilises the trailer weave mode at moderately high speeds, around the legal limit, Fig.6.23. Increasing the steer damping improves the wobble mode substantially, but reduces the weave mode damping, as mentioned previously, and has little effect on the trailer weave mode at high speeds.

Alterations made to the roll inertia and non-zero product of inertia of the trailer, had very little effect on the results, as shown in Fig.6.24.

As with the twin wheel trailer, I have simulated the effect of a combination of parameter changes, in an attempt to stabilise all of the modes throughout the speed range whilst retaining the datum mass and inertia properties, Fig.6.25. Unfortunately, it isn't possible to use a double drawbar with the single wheel trailer because it would simply fall on its side. The results show that, although it is relatively easy to stabilise the wobble mode, the trailer weave mode is much harder to improve, and is still very slightly unstable at high speeds. Also, the trailer is now much longer than it was for the datum case.

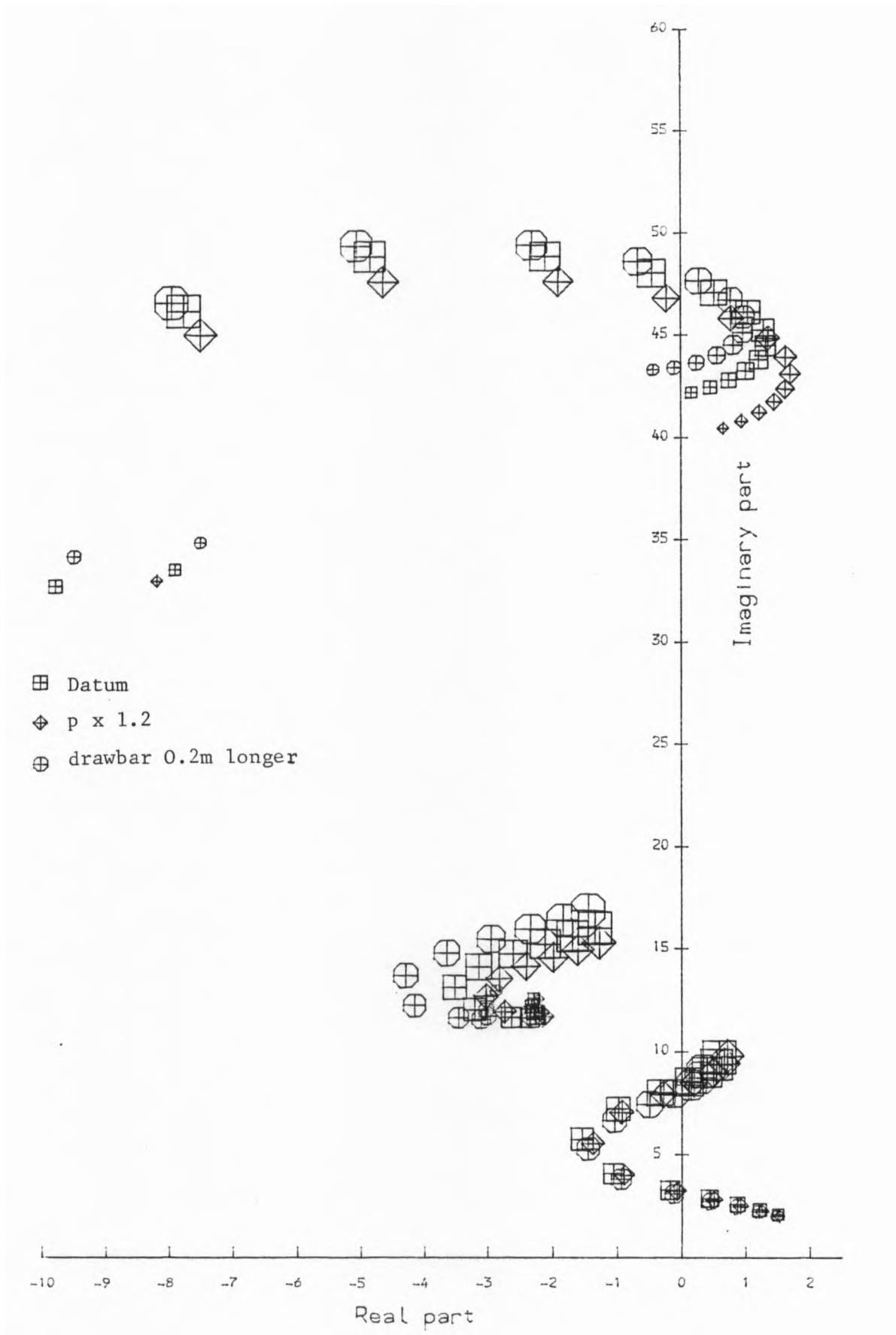


Figure 6.21

Oscillatory mode eigenvalues for changes in hitch position and drawbar length, single wheel trailer.

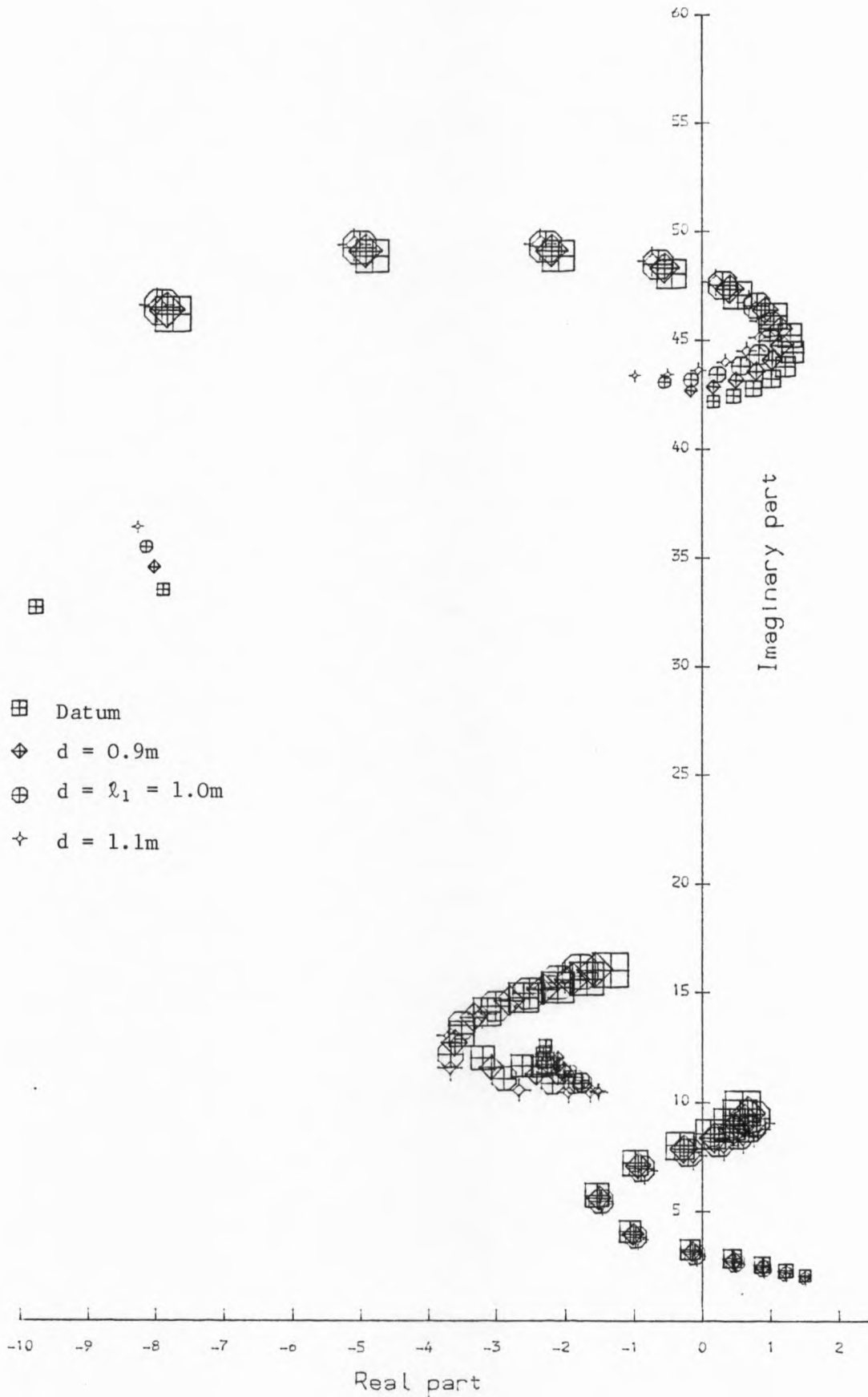
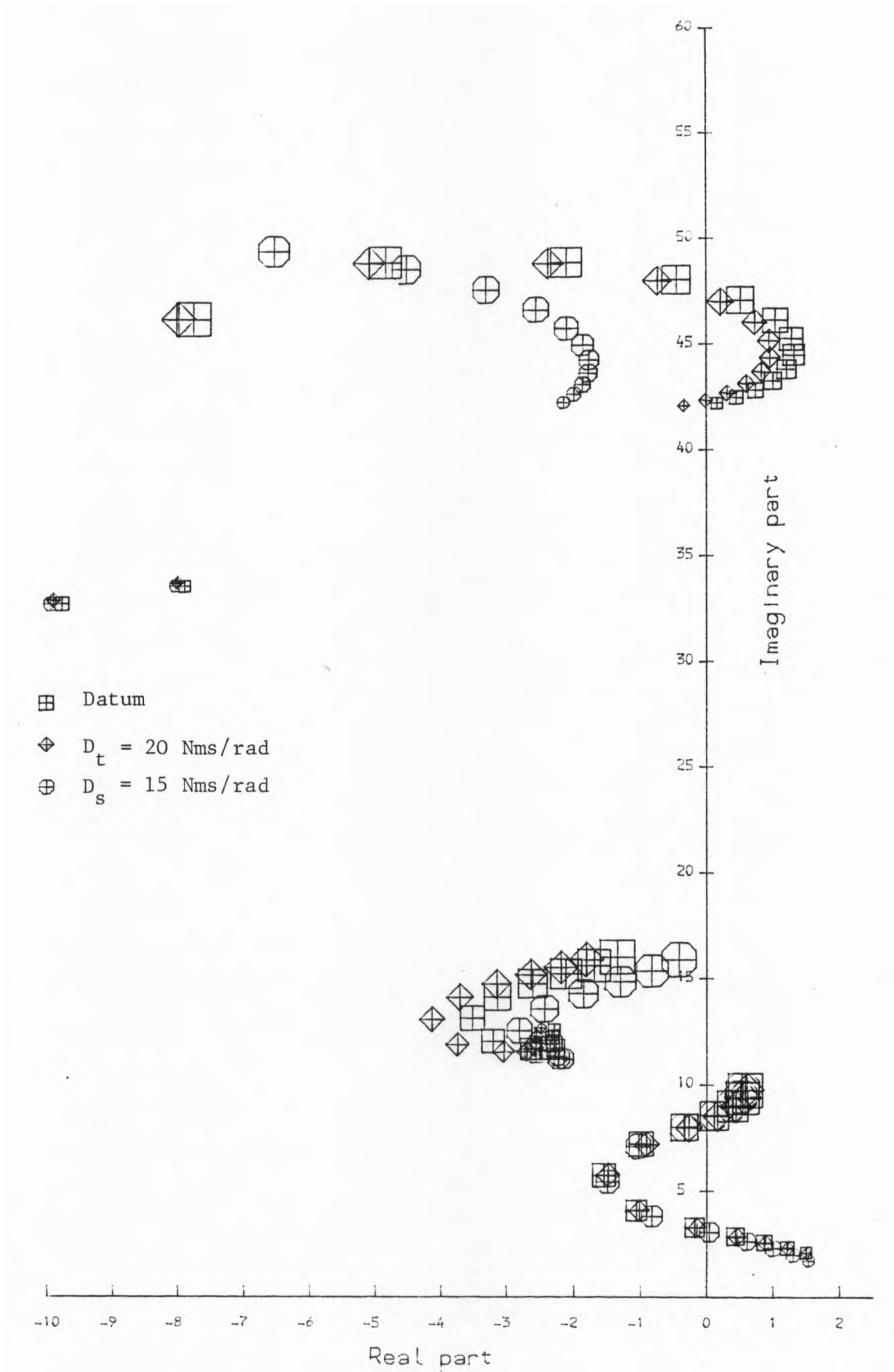


Figure 6.22

Oscillatory mode eigenvalues for changes in trailer c.g. position, single wheel trailer.



Oscillatory mode eigenvalues for changes in damping, single wheel trailer.

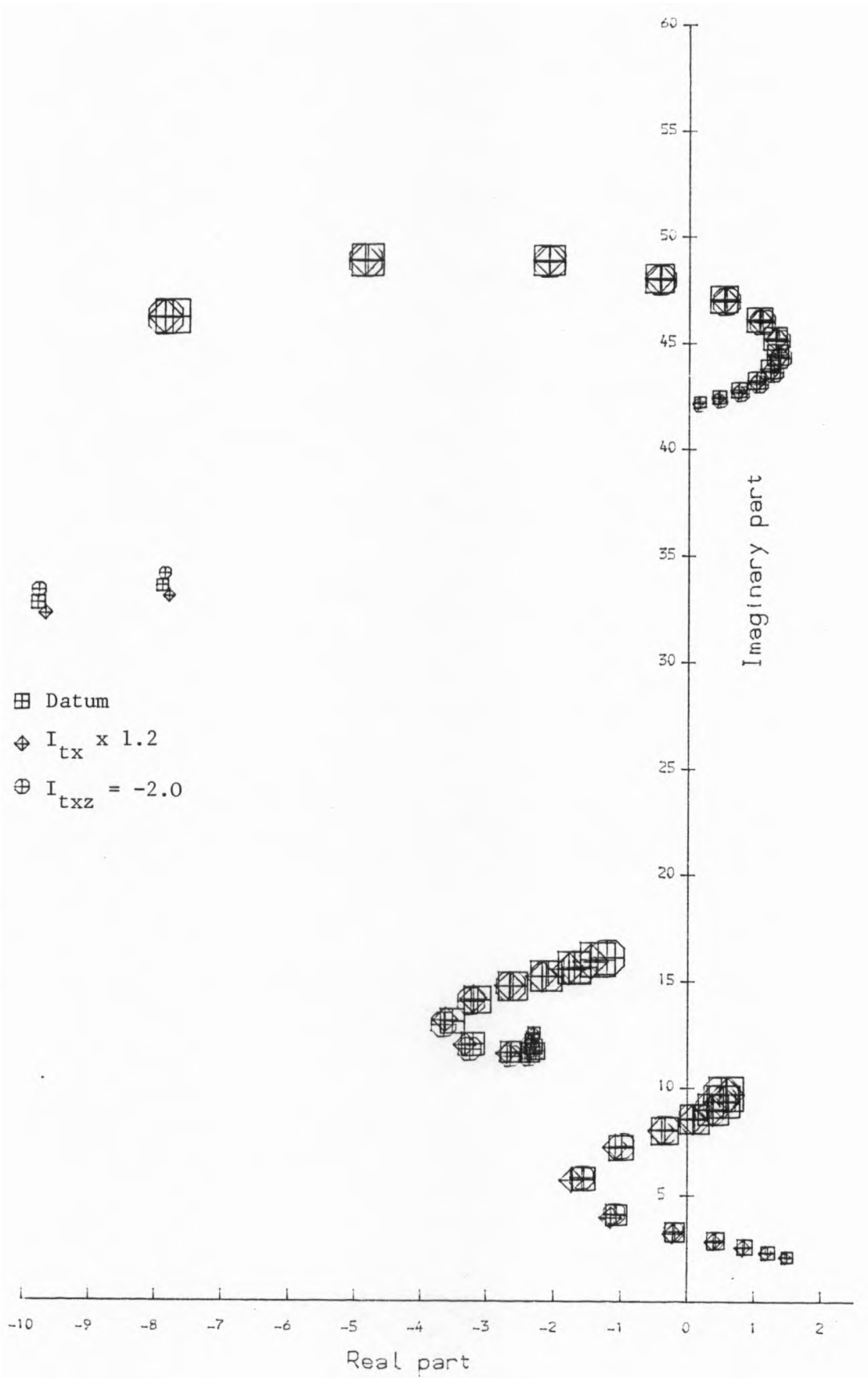


Figure 6.24

Oscillatory mode eigenvalues for changes in trailer inertias, single wheel trailer.

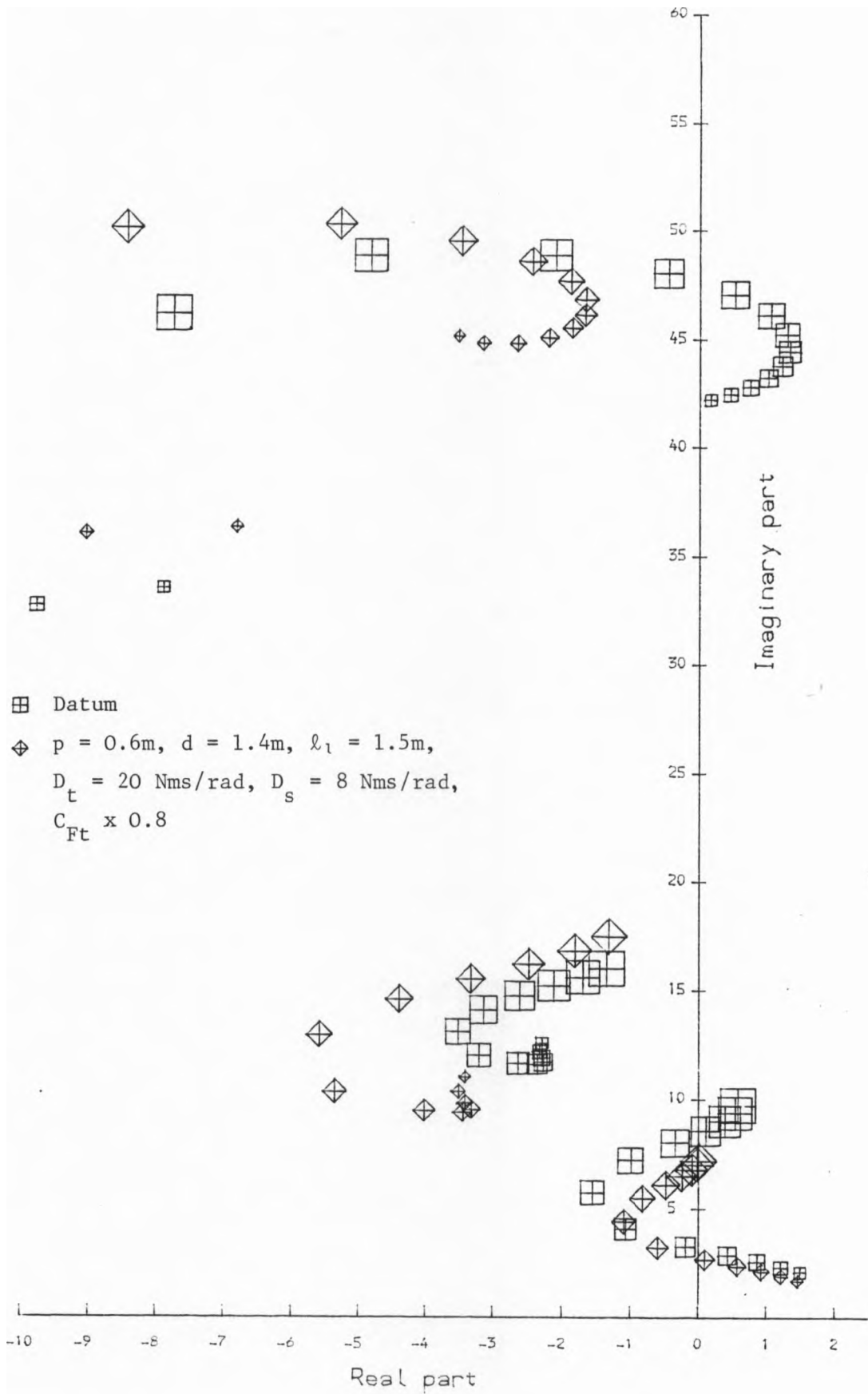


Figure 6.25

Oscillatory mode eigenvalues for datum case and modified single wheel trailer.

## 6.6. CONCLUSIONS

I have shown that, in theory, attaching a trailer to a motorcycle is likely to bring about a marked deterioration in straight line stability, and that such performance is likely to be worse with a single wheel, rather than with a twin wheel, trailer of a given size. The lack of reports of real life stability problems with such combinations may be partially accounted for by their scarcity and the apparent pessimism of the theoretical results in respect of the wobble mode due to the "hands off" nature of the free vibration behaviour. In addition, all of the test reports that I have read have concerned very large motorcycles (often over 1000cc) and comparatively small trailers, and the predicted instabilities may be more apparent for smaller motorcycles towing relatively large trailers.

It is clear that the most effective way to ensure stability is to stay below the prescribed speed limit, and keep the trailer mass as small as possible.

The most beneficial design modification that can be made is to use a double drawbar (not suitable for a single wheel trailer), or other means of lengthening the drawbar and keeping the hitch well forward on the motorcycle. Alterations to the mass distributions of the trailers and the introduction of steer and hitch damping, have varying effects on the different modes, and it is difficult to say anything general about them. It is likely that the attainment of good stability properties will be aided by positioning the centres of mass of the trailers over, or just in front of, the wheel(s).

CHAPTER 7

DESIGN OF A MODAL MOTION SIMULATOR

The design of a modal motion simulator, using a scale model of a motorcycle driven by stepper motors controlled by a microcomputer, is described. Details of the hardware and software are given, and suggestions for refinements are made.

### 7.1. INTRODUCTION

Once the eigenvectors for the principal modes of motion of a motorcycle have been calculated, they can be plotted on the real/imaginary plane to give an illustration of the magnitude and phase relationships of the various outputs such as yaw rate, roll angle etc., as shown in Fig.3.5. However, such diagrams can be difficult to interpret, and picturing the overall movement of the motorcycle can present problems even to those familiar with motorcycle dynamics, let alone an audience unversed in the characteristics of a medium speed wobble oscillation, for example.

One method aimed at making the task of imagination easier involves creating moving stick diagrams of the motorcycle for display on a computer terminal. The generation of this type of display requires the use of a large amount of relatively complex software and a mini-computer. The resultant display suffers from a lack of portability, in that it can't be moved from the computer installation to a conference elsewhere, say. The best that can be done to overcome this is to make a film or video recording of the display as it appears on the visual display unit, which clearly detracts from the flexibility of the demonstration. Stick diagrams are also lacking in realism, and can still require a lot of imagination on the part of the viewer.

The alternative described here employs a microcomputer and digital linear actuators (stepper motors incorporating an internally threaded rotor driving a leadscrew shaft), to drive a one-sixth scale model of a motorcycle. The whole display unit is easily portable and can be used wherever a suitable 240V mains supply is available, or it can be powered from a 12V d.c. supply such as a car battery.

### 7.2. METHOD OF OPERATION

The scale model of the motorcycle is a proprietary item, purchased in kit form from a hobby shop.

In order to adequately demonstrate the oscillatory modes of a motorcycle, any model must have the freedom to yaw, roll, steer and move laterally, usually all at the same time. This is accomplished

here by suspending the motorcycle at two points from a cradle so that the tyres just clear the surface of the display platform, Fig.7.1. The motorcycle is restrained longitudinally by a hinged rod attached to the rear lamp. Three digital linear actuators, with their shaft axes horizontal and perpendicular to the plane of symmetry of the model, are used to move the rear frame of the motorcycle via hinged rods. Since their points of attachment to the model form the three corners of a triangular plane, it is evident that the required rolling, yawing and lateral motions can be produced by driving the three actuator shafts so that they perform sinusoidal oscillations with the necessary amplitude and phase relationships. A fourth actuator coupled to the front wheel gives the required steering motion of the front frame about the rear frame.

### 7.3. DERIVATION OF THE ACTUATOR MOTIONS

As was explained in Chapter 3, point A in Fig.7.1 is used as a reference point for the various axis systems used in the derivation of the equations of motion. There, its motion is described by its longitudinal and lateral velocities, but, for the purposes of this simulation, we are interested only in the lateral velocity of A along the  $AY_1$  axis,  $v$  (see Fig.A2.3). The rear frame has a yaw velocity  $r$  about axis  $AZ_1$  and a roll angle of  $\phi$  about  $AX_1$ , which then defines the axis system  $AX_2Y_2Z_2$ . Thus the motion of the rear frame can be described by the parameters  $v$ ,  $r$  and  $\dot{\phi}$ . A rotation of  $\epsilon$  about  $AY_2$  accounts for the steering head angle and defines the  $AX_3Y_3Z_3$  axis system, and the front frame has a steer angle of  $\delta$  degrees about the  $AZ_3$  axis. The frame flex angles,  $\gamma$  and  $\lambda$ , as modelled in Chapter 3, are too difficult to simulate easily here, and too small to make a noticeable difference to the observed motion of the model. Hence they have been left out of the calculations, and the motion of the front frame is described by the parameters  $v$ ,  $r$ ,  $\dot{\phi}$  and  $\dot{\delta}$ .

Once the stability analysis has yielded the real and imaginary parts of the motion variable eigenvectors, the amplitude and phase of the lateral motion of any point on the rear frame is given by (see Fig.7.1):

$$\text{Amplitude} = \sqrt{D_i^2 + D_r^2}$$

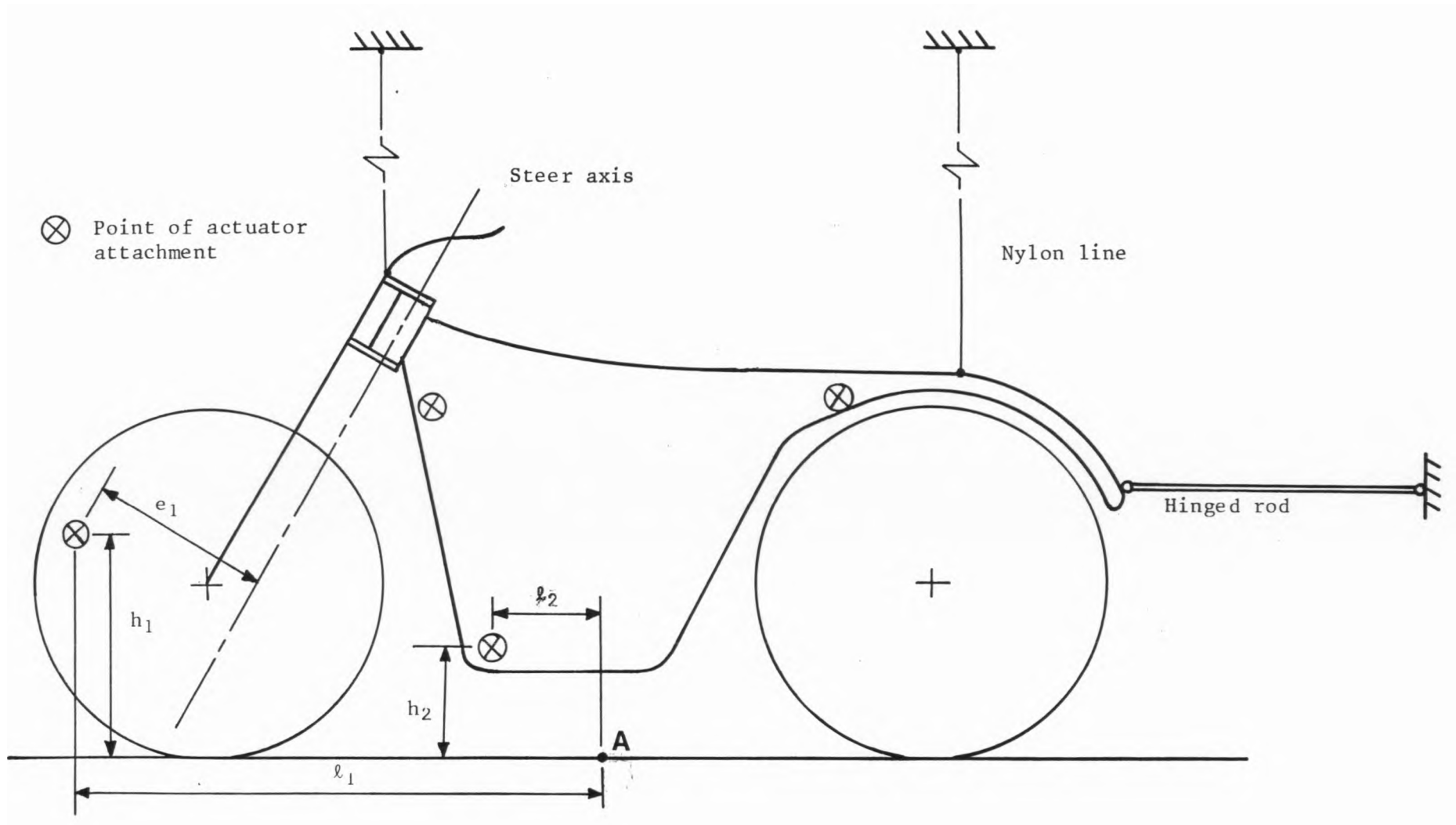


Figure 7.1

Model restraints and actuator attachment points.

and 
$$\text{Phase} = \tan^{-1} \left[ \frac{D_i}{D_r} \right]$$

where 
$$D_r = v_r + l_2 r_r + h_2 \dot{\phi}_r$$

and 
$$D_i = v_i + l_2 r_i + h_2 \dot{\phi}_i$$

For the front frame,

$$D_r = v_r + l_1 r_r + h_1 \dot{\phi}_r + e_1 \dot{\delta}_r$$

$$D_i = v_i + l_1 r_i + h_1 \dot{\phi}_i + e_1 \dot{\delta}_i$$

Hence, the required motions of the actuators can be calculated for any set of eigenvectors, knowing the locations of the actuator rods on the model relative to where point A is estimated to be.

#### 7.4. DEVELOPMENT OF THE SIMULATION MODEL

Stepper motors were chosen in preference to other types of actuators, such as servo motors, because of their cheapness, simplicity and the ease with which they can be interfaced to the microcomputer. Also, one of the most important factors was that they don't need any form of positional feedback, since the computer can keep track of their position by counting the number of steps taken in each direction, provided the starting position is known and no steps have been missed.

The stepper motors used for this application can produce a maximum linear force of over 5 N, quite adequate to drive the model provided that resistance to lateral movement of the motorcycle is low, which is why it is suspended. The linear shaft movement is 51  $\mu\text{m}$  per motor step, and the maximum speed is around 400 steps/sec, depending on the linear force. This gives a maximum shaft speed of around 20 mm/sec.

Each motor is powered from a 12V d.c. supply via an integrated circuit (IC) driver chip, type SAA1027, Fig.7.2. This simplifies the task of making the actuator shaft move by combining the phasing logic for a reversible drive together with the output drive stages in a single chip. Pin 15 of the IC is the trigger input, which accepts logic level pulses, the repetition rate and number of which control the velocity and position of the

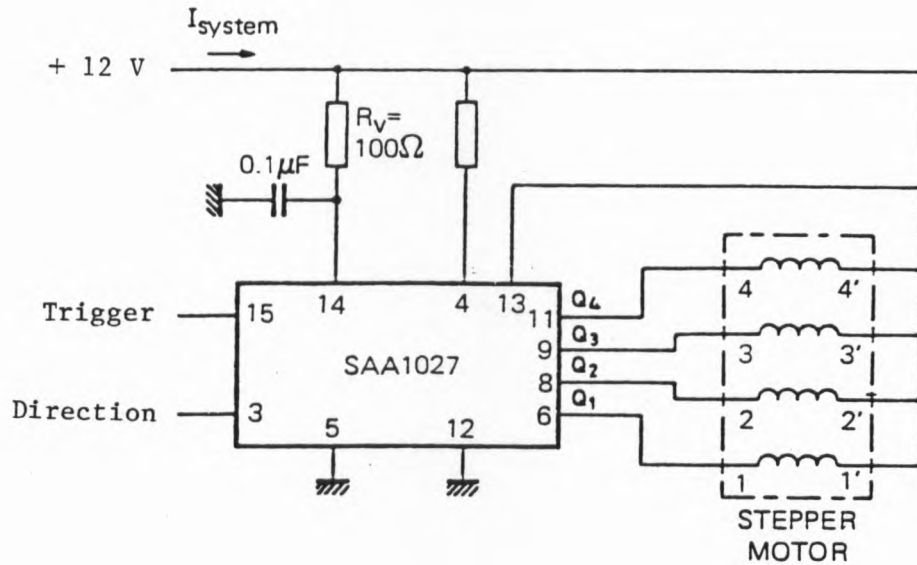


Figure 7.2

Actuator driver circuit.

actuator shaft. The direction of rotation of the stepper rotor is controlled by the logic level applied to pin 3, high for anticlockwise, and low for clockwise rotation. Thus, the motors can each be controlled by two bits of a binary word coming from the parallel output port of a computer. Since these ports can typically output eight bits at a time, we saw that it would be possible to control the four stepper motors with a stream of eight bit words, either generated in real time or taken from a "look up table" of sine waves in computer memory.

The microcomputer used, primarily because it had already been purchased for the experimental programme detailed in Chapter 2, is a Z80 based Nascom 2, which has adequate memory and the required parallel output port, as well as other necessary interfaces for a monitor/TV and cassette recorder. The Nascom has its own Basic language interpreter program, which allowed much of the required software to be written in the high level language whilst still providing the facility for manipulation of individual bits of memory. We soon realised that the production of sine wave motion of the desired frequency in real time is an unrealistic proposition using Basic on an eight bit microcomputer, although it may just be possible using complex assembly language routines.

This meant that we had to formulate a two stage program, the first part using the eigenvector information to calculate and store in memory the binary data bytes required to give the sinusoidal motion, and the second part outputting the data from memory to the stepper motor drivers at the appropriate rate. I will now describe these two procedures.

In order for a stepper motor to produce sinusoidal motion, it is desirable to split one period of the motion into a number of equal time increments, depending on the frequency and amplitude required. This was done as follows:

If we take a sinusoid described by

$$x = A \sin(\omega t)$$

then the maximum rate of change is

$$\dot{x} = A\omega$$

I knew that for the actuator shafts, this is 20 mm/sec, and thus the maximum possible amplitude,  $A$ , is constrained by the required frequency, which I chose to be 0.25 Hz, giving an amplitude of 12.7 mm. Choosing a significantly higher frequency would have reduced the amplitude of the oscillation too much and might have impaired an observer's ability to ascertain what was happening to the model.

If the maximum stepper motor speed is 400 steps/sec, then the time required for each step is at least 2.5 milliseconds. Since the period of the sine wave is four seconds, then a total of 1600 individual time increments per cycle is necessary. In the event, I reduced the maximum amplitude a little to ensure that the stepper motors were within their capabilities.

Having decided upon the number of time increments, I wrote a program in Basic which calculates, for each stepper motor, whether it is necessary to output a trigger pulse to pin 15 of the driver chip, and if so, in which direction the rotor should move, during each time increment.

The program does this by taking the yaw rate, roll rate, lateral velocity and steer rate eigenvectors for the relevant mode, and calculating the relative amplitudes and phases of the actuator

shafts as described earlier. The largest actuator shaft amplitude is found and changed so that it is equal to the maximum possible amplitude found above, and the other actuator's amplitudes are scaled accordingly. The phase of one of the actuators is subtracted from those of the other three, and the direction and number of steps needed for each of the three actuators to reach its correct start position relative to the first, are calculated and stored in memory.

The program then enters a loop which calculates the required position of each actuator shaft (in terms of steps away from the start position) for each successive time increment. This position is compared with that for the previous increment, and if a step in either direction is necessary then the relevant bit in the binary word is set to logical one, and the direction control bit is set to logical one or zero, as required. The eight bit binary word is formed by assigning the two most significant bits (MSB's) to actuator one, the next two MSB's to actuator two, and so on until the word is complete and can be stored in memory. This loop is executed a total of 800 times, not 1600, because the second half period of a sine wave is a mirror image of the first. Hence, the data bytes for the first half period of the sinusoids can be used to produce the second half by inverting their direction bits as they are output to the driver chips. This is easily accomplished in the actuator driver routine.

Despite this economy of calculation, the program takes approximately two minutes to produce the required data, primarily due to the slowness of the interpreted Basic language on the Nascom. Although this may not seem an unduly long time to wait, we felt that this could be a handicap when displaying the model to an audience because of the necessary delay between the demonstrations of different modes of oscillation.

A partial solution to this problem is to select a number of interesting modes beforehand, and calculate and store the sets of data in memory, to be output when necessary. It is possible to store up to around thirty selectable blocks of 800 data bytes in the Nascom's fast access memory, far more than are ever likely to be needed. However, these would take a long time to calculate before each demonstration session, and a better solution is to calculate them once and store the relevant block of data on cassette tape. A

rather faster program can then be used just for the display, as follows.

At the start of each demonstration session, the model is set up to be in its datum position, that is straight and level. The data for the various modes is read into memory from cassette, along with the Basic and assembly language programs which control the model. The Basic program displays a menu of the modes that can be simulated, and asks the operator to select one. Then it moves the model to the start position determined by the phases of the actuators, and asks the operator to select one of three possible frequencies for the oscillations. The frequency is varied by altering the size of a number in a software delay loop that is entered between the output of each data byte. Unfortunately, the Nascom Basic is too slow to output the data bytes fast enough in order to produce the maximum model oscillation frequency of 0.25 Hz, so the program calls an assembly language subroutine to do this.

The delay is passed as an argument to the subroutine, along with the start address in memory of the required block of sine wave data. The subroutine waits for a keyboard stroke to tell it to start, and then outputs the 800 data bytes for the first half period of the oscillation. These are followed by the same data bytes with their direction bits reversed, and then the original data again, and so on until the operator decides to stop the motion with another keystroke. Control is returned to the main program, and the operator can select another frequency for the same mode, or another mode entirely. In the latter case, the model moves back to the datum position, ready to assume the initial attitude required by the next mode. This allows the operator to check whether or not the actuators have missed a noticeable number of steps, and carry out adjustments to the shaft positions if necessary.

A photograph of the microcomputer and simulation model can be seen in Fig.7.3.

#### 7.5. LIMITATIONS AND POSSIBLE REFINEMENTS

The simulation model has been working satisfactorily for a number of months, but there are limitations and room for improvement.

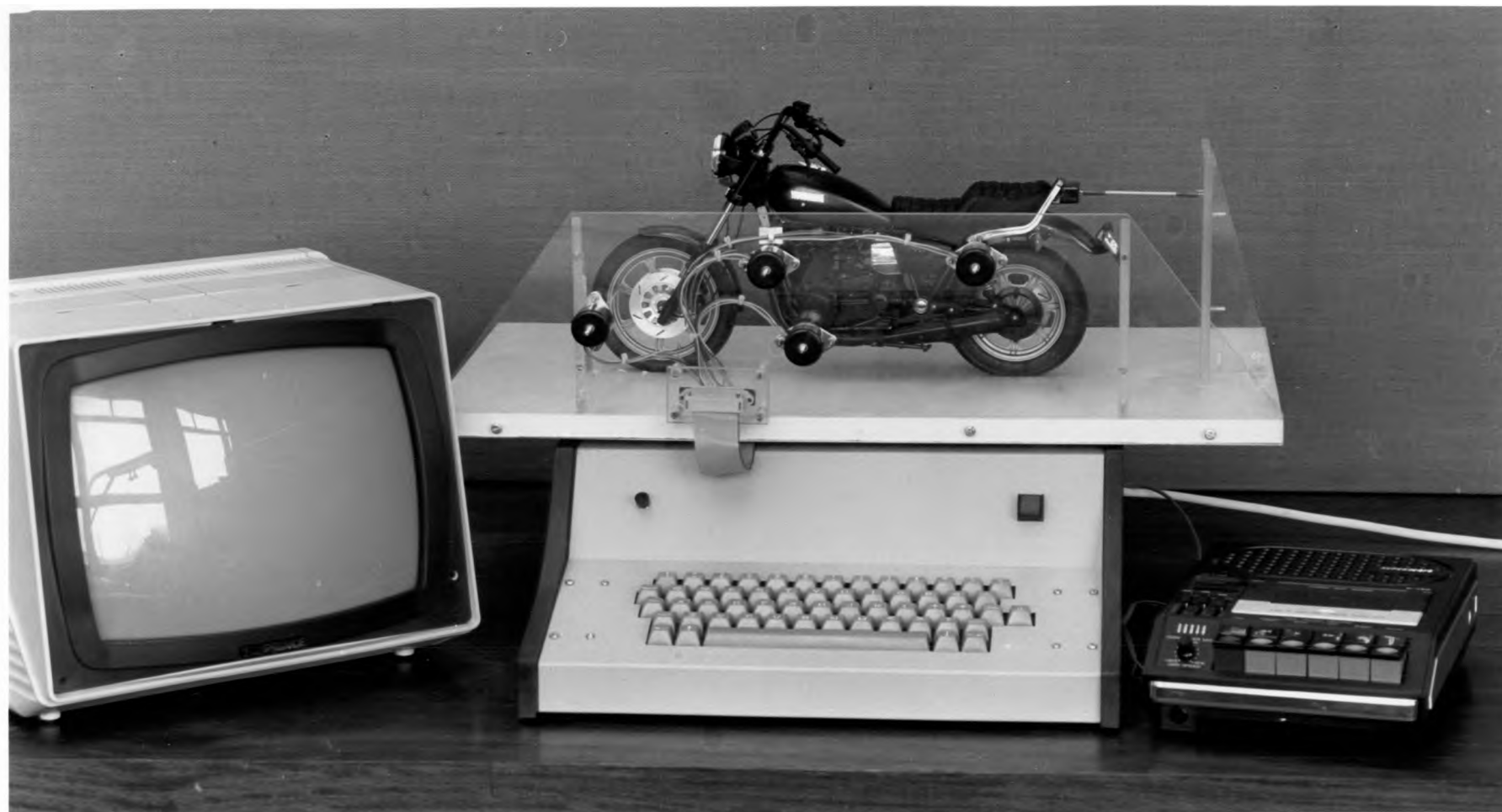


Figure 7.3

Nascom microcomputer and modal motion simulator.

I think the major limitation of this model is that it cannot illustrate the various frame flexibilities being investigated. It would also be interesting to see a simulation of the oscillations exhibited by motorcycles and trailers, as examined in Chapter 6. However, to do these things would require a substantial re-design of both the hardware and software, and it can be seen that computer generated stick diagrams are likely to be more versatile in this respect.

An increase in the maximum frequency of oscillation might lead to a more realistic appearance, but this would necessitate using larger stepper motors.

It would add a lot to the visual impact and educational value of the model if the oscillations could be made to grow or decrease in amplitude, depending on the sign and magnitude of the real part of the corresponding eigenvalue. However, I can't think of an easy way to add this feature without substantial complication of the simulation strategy, given that real time generation of the data is discounted.

Some marginal gains in ease of operation might be made by switching to a compiled computer language, such as Pascal or C, which would obviate the need for a separate assembly language subroutine, and cut down the calculation time for the sine wave data.

At present the model is suitable for use only by a skilled operator who can load the data and programs from tape, and link them together to run the display. It would not be difficult, however, to modify the simulator so that it is suitable for public exhibition, where anyone could select a mode from a menu and start the simulation themselves.

CHAPTER 8

CONCLUSIONS

A discussion of the conclusions from Chapters 2-7 is presented.

The microcomputer based data acquisition system has reached an advanced stage of development. The data collection and processing software has been tested in the laboratory using simulated test signals, and the system performed as required. All that remains to be done is to mount the system on the motorcycle and carry out the appropriate test programme. This will allow rigorous comparison of theoretical and experimental frequency responses, resulting in possible validation of the theory, new information on rider behaviour, and possible indications of deficiencies in the theory which could lead to improvements. The measuring system should be suitable for application to other problems, particularly concerning vehicles, where small size, light weight, low cost, high accuracy, and the requirement for a 12V d.c. supply voltage are notable features.

A new frame flexibility, involving rotation of the rear wheel assembly about an inclined axis, has been incorporated in the theoretical model. The stability results have been shown to be comparatively insensitive to the corresponding stiffness value, although the weave mode is slightly improved at high speeds by increasing the stiffness to well above that normally obtaining. Very low stiffness values that may simulate the effects of worn swinging arm bearings lead to marked deteriorations in both medium and high speed stability.

The measurement of frame stiffnesses and deflection modes by static and dynamic methods has shown large discrepancies in the results for the front wheel assembly. This is thought to be due to the presence of a significant lateral, translational flexibility and the effects of inertia forces when conducting tests near to the resonant frequency. Consequently, a fundamental reconsideration of the method of representing this flexibility has been undertaken, leading to the development of a new theoretical model and further stiffness measurements, the results of which will soon be available. The stiffness value measured for the rear wheel assembly is approaching the region of diminishing returns in respect of the theoretical stability results.

Examination of the theoretical frequency responses of a large motorcycle has shown that they agree fairly well with the small amount of experimental data available. The effects of various

parameter changes on responsiveness to steer torque inputs have been studied, and in many cases the results broadly agree with the expectations arising from motorcyclists' subjective opinions. Design features of particular importance appear to be steering geometry, steer inertia, front wheel inertia and rear tyre cornering stiffness. There does appear to be some relationship between stability and frequency response results, but I conclude that it is necessary to obtain both in order to gain an adequate understanding of the effects of various parameters on the dynamics of a motorcycle. However, the problem of how to interpret the frequency response results has not greatly diminished, and much further work needs to be done, possibly including the measurement of riders' subjective ratings of the effects on responsiveness of design changes.

According to the theoretical results presented here, attaching a trailer to a motorcycle results in a large deterioration in straight line stability, which is worse for single wheel, rather than twin wheel, trailers. As well as reducing the damping of the motorcycle modes, each of the trailers has associated with it a new, significant oscillatory mode. The twin wheel trailer swing mode is dominated by trailer yaw and has a frequency of around 1.5 Hz, stability decreasing with increasing speed. The single wheel trailer weave mode involves mainly trailer yaw and roll, and is very unstable at low and high speeds, the characteristic frequency increasing with speed. For best stability, the trailers should be kept as small and light as possible and high speeds should be avoided. Lengthening the drawbar and positioning the hitch further forwards on the motorcycle lead to dramatic improvements in stability, and a novel hitch design has been suggested for the twin wheel trailer for this purpose.

A modal motion simulator has been developed which will adequately demonstrate the weave and wobble modes in slow motion. However, the simulator is rather limited in that it can't demonstrate the role of important frame flexibilities and can't easily be adapted to simulate the motorcycle with a trailer, say. Suggestions for improvements have been made, but even when these are taken into account it is evident that computer animated stick diagrams provide a more versatile solution, despite being less life-like and not easily portable.

NOMENCLATURE

<u>Symbol</u>	<u>Description</u>
$a_1, a_2, a_3, a_4,$ $a_5, b, b_1, b_2, d,$ $e, h, h_1, h_3, j,$ $l, l_1, p, s$	dimensions, Figs.3.1, 6.1 and A2.1
A	amplitude, Chapter 7
c.g.	centre of gravity
C	static stiffness, Chapter 4
$C_F$	tyre cornering stiffness
$C_M$	tyre aligning moment constant
$C_l$	tyre side force/camber constant
D	stepper motor motion vector, Chapter 7
$D_c$	aerodynamic drag constant
$D_f, D_r$	front and rear frame twist damping constants
$D_s$	steer damping constant
$D_t$	hitch damping constant
f	$(j - s - e \sin \epsilon) / \cos \epsilon$ or frequency, Chapter 4
$f_n$	resonant frequency
F	Rayleigh dissipative function
$\underline{F}$	tyre force vector
g	acceleration due to gravity
G	mass centre
$h_{cp}$	height above ground of aerodynamic centre of pressure
$i_{fy}, i_{ry}, i_{rwy},$ $i_{twy}$	spin inertias of front wheel, engine parts (referred to rear wheel), rear wheel, and trailer wheel.
$I_{fx}, I_{fz}, I_{rx},$ $I_{rz}, I_{rxz}, I_{rwx},$ $I_{rwz}, I_{rwxz}, I_{tx},$ $I_{tz}, I_{txz}$	moments and products of inertia of front, rear, rear wheel, and trailer assemblies referred to appropriate mass centres and reference axes shown in Figs.A2.2 and 8.
k	$l + (e + t - j \sin \epsilon) / \cos \epsilon$
m	moment arm
$\underline{M}$	tyre moment vector

<u>Symbol</u>	<u>Description</u>
$M_b, M_f, M_r, M_{tr}$	masses
$M_x, M_z$	tyre overturning and aligning moments
$Q_i$	generalised force
$q_i$	generalised coordinate
$r$	yaw rate, or frequency ratio (Chapter 4)
$r_{tw}, r_{wr}$	trailer and rear wheel yaw velocities
$R$	wheel radius
$R_\alpha, R_{\epsilon_1}, R_\lambda, R_\phi$	rotation matrices
$s_l$	$(s - t \sin \epsilon) / \cos \epsilon$
$S_f, S_r$	front and rear frame torsional stiffnesses
$t$	time or linear dimension, Fig 3.1
$T$	kinetic energy (transpose when superscript)
$U$	forward velocity of reference point A, Fig.A2.3.
$v$	lateral velocity of reference point A
$\underline{v}$	velocity of mass centre
$v_{tw}, v_{wr}$	trailer and rear wheel contact centre lateral velocities.
$V$	potential energy
$x$	displacement
$X$	longitudinal tyre force
$y_l$	lateral position of reference point A
$Y$	lateral tyre force
$Z$	vertical tyre force
$\alpha$	trailer yaw angle relative to motorcycle
$\gamma$	front frame twist angle
$\delta$	front frame steer angle
$\delta q_i$	virtual displacement
$\epsilon$	steering rake angle, Fig.3.1
$\epsilon_1$	rear twist axis inclination angle, Fig.3.1
$\zeta$	damping as a proportion of critical
$\dot{\theta}$	wheel spin velocity
$\lambda$	rear frame twist angle
$\sigma$	tyre relaxation length

<u>Symbol</u>	<u>Description</u>
$\phi$	roll angle
$\phi_r, \psi_r$	effective rear wheel camber and steer angles
$\psi$	yaw angle of rear frame
$\omega$	circular frequency
 <u>Suffices:</u>	
b	rear wheel
f	front
fl	flywheel
i	general term or imaginary part (Chapter 4)
r	rear or real part (Chapter 4)
t, tr	trailer
w	wheel
x, y, z	directions

REFERENCES

- ALSTEAD C.J. (1982) "Motorcycle Steering Behaviour." Doctoral Thesis, University of Leeds.
- AOKI A. (1979) "Experimental Study on Motorcycle Steering Performance." S.A.E. 790265.
- BRORSSON B. (1983) "Wobble and Weave in Motorcycles." Trafiksaekerhetsverket, Borlaenge, Sweden.
- CROLLA D.A. and SHARP R.S. (1983) "Stability and Steering Response Problems of Trucks Towing Trailers." Proc. I.Mech.E. Conference on Road Vehicle Handling, MEP, London.
- EATON D.J. (1973) "Man-Machine Dynamics in the Stabilisation of Single Track Vehicles." Doctoral Dissertation, University of Michigan, Ann Arbor.
- HALES F.D. (1963) "The Lateral Stability of a Simplified Articulated Vehicle." Proc. I.Mech.E. Symposium on Control of Vehicles, paper 7, 3-14.
- JOHANSEN S. (1982) "The Effect of Frame Flexibility on the Stability of Motorcycles." Short summary of M.Sc. Dissertation, University of Aalborg, Denmark.
- JONES C.J. (1982) "Tyre Behaviour and Vehicle Dynamics Problems." Doctoral Thesis, University of Leeds.
- KANE T.R. (1978) "The Effects of Frame Flexibility on High Speed Weave of Motorcycles." S.A.E. 780306.
- KOENEN C. (1983) "The Dynamic Behaviour of a Motorcycle when running straight ahead and when cornering." Delft University Press.
- N.P.S.R.I. (1976) (National Public Services Research Institute) "The Photographic Analysis of Motorcycle Operator Control Responses." Motorcycle Safety Foundation Inc., Linthicum, Maryland.
- PACEJKA H.B. (1971) "The Tyre as a Vehicle Component." Chapter 7 of Mechanics of Pneumatic Tyres (Ed. S.K. Clark), Washington D.C., N.B.S. Monograph 122.
- PACEJKA H.B. (1972) "Analysis of the Dynamic Response of a Rolling String-type Tyre Model to Lateral Wheel Plane Vibrations." Vehicle System Dynamics, 1, Swets and Zeitlinger, Lisse, 37-66.
- PACEJKA H.B. (1975) "Principles of Plane Motions of Automobiles." Proc. I.U.T.A.M. Symposium on the Dynamics of Vehicles, Delft, Swets and Zeitlinger, Lisse, 33-59.
- PAUL B. (1979) "Kinematics and Dynamics of Planar Machinery." Prentice Hall, Englewood Cliffs, N.J.
- PEARSALL R.H. (1922) "The Stability of a Bicycle." Proc. Instn. Auto. Engrs., 17, 395-403.

- RICE R.S. (1978) "Rider Skill Influences on Motorcycle Maneuvring." S.A.E. 780312.
- ROE G.E. and THORPE T.E. (1976) "A Solution of the Low-speed Wheel Flutter Instability in Motorcycles." J. Mech. Engng. Sci., 18 (no.2) , 57-65.
- ROLAND R.D. (1973) "Simulation Study of Motorcycle Stability at High Speed." Proc. 2nd Int. Conf. on Automotive Safety, San Fransisco.
- SHARP R.S. (1971) "The Stability and Control of Motorcycles." J. Mech. Engng. Sci., 13 (no.5), 316-329.
- SHARP R.S. (1974) "The Influence of Frame Flexibility on the Lateral Stability of Motorcycles." J. Mech. Engng. Sci., 16 (no.2), 117-120.
- SHARP R.S. and ALSTEAD C.J. (1980) "The Influence of Structural Flexibilities on the Straight-running Stability of Motorcycles." Vehicle System Dynamics, 9, Swets and Zeitlinger, Lisse, 327-357.
- SHARP R.S. (1982) "Motorcycle Stability and Responses to Steering Control." Proc. 1st Course on Advanced Vehicle System Dynamics, I.C.T.S.-P.F.T. Proceedings Series, Vol.IV, 237-262.
- SHARP R.S. and ALSTEAD C.J. (1983) "Frequency Responses of Motorcycles to Steering Torque Inputs and to Front Wheel and Tyre Imperfections." Proc. I.Mech.E. Conference on Road Vehicle Handling, MEP, London, 193-200.
- SHARP R.S. (1984) Private communication.
- SHARP R.S. (1984b) "The Stability and Control of Motorcycles." Proc. 2nd Course on Advanced Vehicle System Dynamics, I.C.T.S.-P.F.T.
- SHARP R.S. (1985) Private communication.
- SPIERINGS P.T.J. (1981) "The Effects of Lateral Front Fork Flexibility on the Vibrational Modes of Straight-running Single Track Vehicles." Vehicle System Dynamics, 10, Swets and Zeitlinger, Lisse, 21-35.
- VERMA M.K. (1978) "Theoretical and Experimental Investigations of Motorcycle Dynamics." Doctoral Dissertation, University of Michigan, Ann Arbor.
- VERMA M.K. (1981) "Transient Response Test Procedures for Measuring Vehicle Directional Control." Vehicle System Dynamics, 10, Swets and Zeitlinger, Lisse, 333-356.
- WEIR D.H. and ZELLNER J.W. (1979) "Experimental Investigation of the Transient Behaviour of Motorcycles." S.A.E. 790266.
- WILLOUGHBY V. (1981) "Back to Basics." Haynes, Yeovil, England.
- WILSON-JONES R.A. (1951) "Steering and Stability of Single Track Vehicles." Proc. Auto. Div. Instn. Mech. Engrs., 191-213.

APPENDIX 1

DATUM PARAMETER VALUES

For the motorcycle (Yamaha XS650B) plus rider:

<u>Parameter</u>	<u>Value</u>	<u>Units</u>
$M_f$	40.59	kg
$M_r$	220.3	kg
$M_b$	25.0	kg
$I_{fx}$	3.97	$\text{kgm}^2$
$I_{fz}$	0.71	$\text{kgm}^2$
$I_{rx}$	32.07	$\text{kgm}^2$
$I_{rz}$	15.17	$\text{kgm}^2$
$I_{rxz}$	0.57	$\text{kgm}^2$
$I_{rwx}$	0.4	$\text{kgm}^2$
$I_{rwz}$	0.4	$\text{kgm}^2$
$I_{rwxz}$	0.0	$\text{kgm}^2$
$i_{fy}$	0.58	$\text{kgm}^2$
$i_{ry}$	0.41	$\text{kgm}^2$
$i_{rwy}$	0.65	$\text{kgm}^2$
$a_4$	0.527	m
$b$	0.565	m
$b_1$	0.33	m
$b_2$	0.557	m
$e$	0.049	m
$h$	0.607	m
$h_{cp}$	0.66	m
$j$	0.572	m
$l$	0.87	m
$R_f$	0.336	m
$R_r$	0.321	m
$s$	1.2	m
$t$	0.094	m
$\epsilon$	0.47	rad
$\epsilon_1$	1.435	rad
$S_f$	50000	Nm/rad
$S_r$	46000	Nm/rad
$D_c$	0.377	kg/m
$D_f$	79.1	Nms/rad
$D_r$	17.7	Nms/rad
$D_s$	2.0	Nms/rad

For the twin wheel trailer:

<u>Parameter</u>	<u>Value</u>	<u>Units</u>
$M_{tr}$	150.0	kg
$I_{tz}$	30.0	$\text{kgm}^2$
$d$	0.8	m
$h_1$	0.3	m
$l_1$	1.0	m
$p$	0.6	m
$D_t$	0.0	Nms/rad
$C_{Ft}$	$8.0 \times Z_t$	N/rad
$C_{Mt}$	$0.03 \times C_{Ft}$	Nm/rad
$\sigma_t$	0.4	m

The datum parameter values for the single wheel trailer are the same as above, with the following additions:

<u>Parameter</u>	<u>Value</u>	<u>Units</u>
$I_{tx}$	15.0	$\text{kgm}^2$
$I_{txz}$	0.0	$\text{kgm}^2$
$i_{twy}$	0.2	$\text{kgm}^2$
$h_3$	0.3	m
$R_t$	0.15	m
$C_{1t}$	$1.5 \times Z_t$	N/rad

APPENDIX 2

DERIVATION OF THE EQUATIONS OF MOTION

A2.1 THE REAR WHEEL YAW/CAMBER MODEL

A2.2 THE TWIN WHEEL TRAILER MODEL

A2.3 THE SINGLE WHEEL TRAILER MODEL

A2.1 THE REAR WHEEL YAW/CAMBER MODEL

A diagram of the model can be seen in Fig.A2.1. Some of the dimensions that define the position of the rear wheel assembly mass centre,  $G_b$ , differ from those given in Fig.3.1. This is because the dimensions used here are more convenient for the immediate purposes of the analysis, but it will be found that they can be expressed in terms of those used in Fig.3.1 at a later stage.

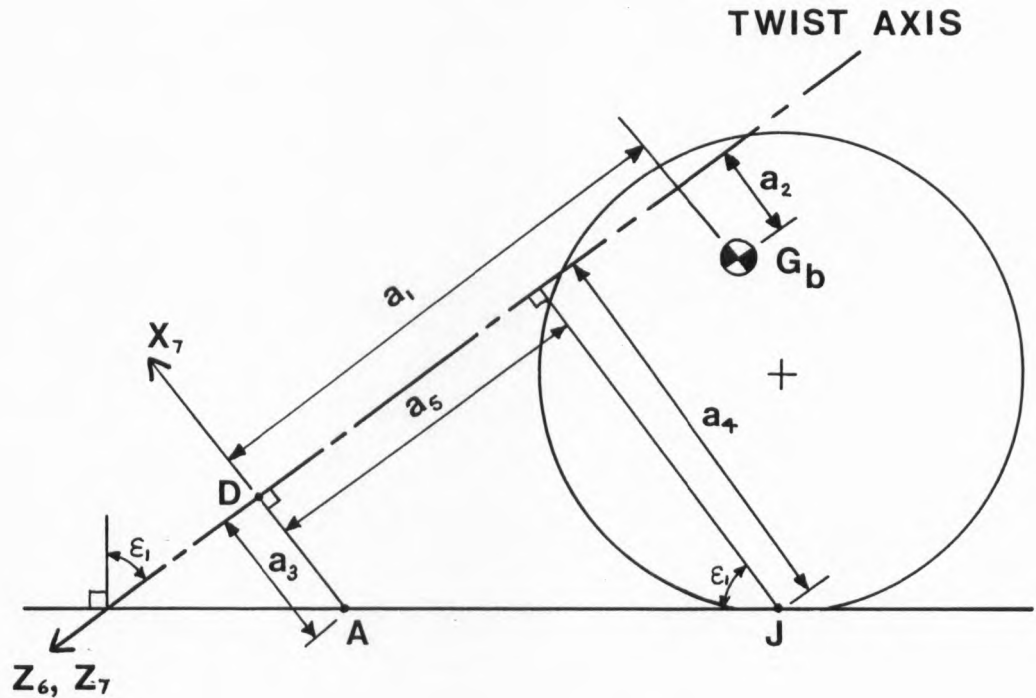


Figure A2.1

Rear wheel yaw/camber model dimensions.

Point A lies directly below the centre of mass of the rear frame when the motorcycle is upright, and is the origin of a right-handed axis system  $AX_1Y_1Z_1$  which yaws with the rear frame. The relative orientations of the other axis systems,  $AX_2Y_2Z_2$  to  $AX_7Y_7Z_7$ , are illustrated in Fig.A2.2.

A vector expressed in one axis system can be transformed to another axis system by multiplication by appropriate rotation matrices,  $R_i$  (where  $i$  is the relevant coordinate).

For a roll angle  $\phi$ , about an axis parallel to  $AX_1$ ,

$$R_{\phi} = \begin{bmatrix} 1 & 0 & 0 \\ 0 & \cos\phi & \sin\phi \\ 0 & -\sin\phi & \cos\phi \end{bmatrix}$$

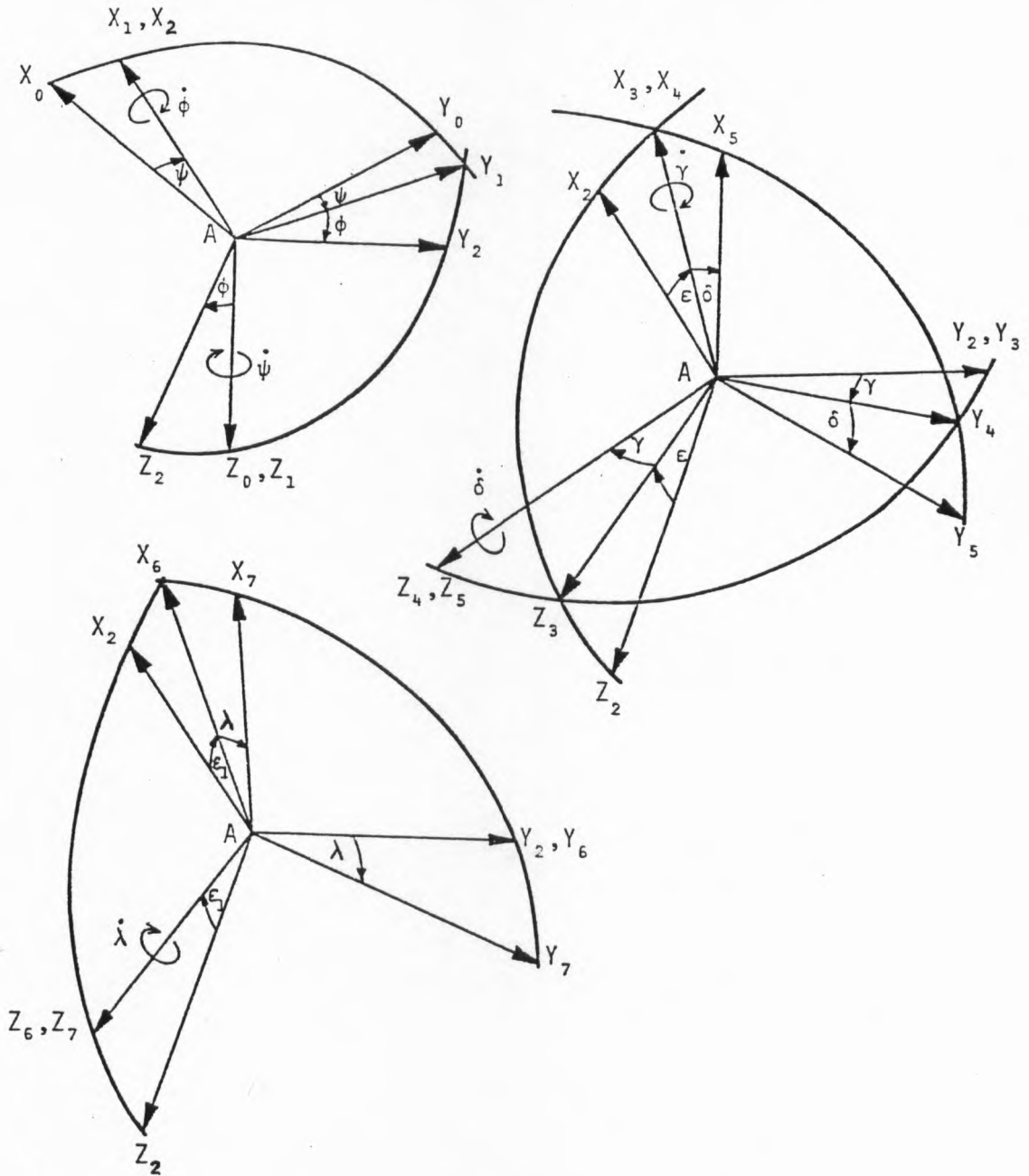


Figure A2.2  
Axis system definitions.

For the twist axis inclination angle  $\epsilon_1$ , about an axis parallel to  $AY_2$ ,

$$R_{\epsilon_1} = \begin{bmatrix} \cos\epsilon_1 & 0 & -\sin\epsilon_1 \\ 0 & 1 & 0 \\ \sin\epsilon_1 & 0 & \cos\epsilon_1 \end{bmatrix}$$

For a twist angle  $\lambda$ , about an axis parallel to  $AZ_6$ ,

$$R_\lambda = \begin{bmatrix} \cos\lambda & \sin\lambda & 0 \\ -\sin\lambda & \cos\lambda & 0 \\ 0 & 0 & 1 \end{bmatrix}$$

All rotations are defined to be positive when made in the clockwise direction. Rotations in the other direction may be applied by multiplying the relevant vector by  $R_i^T$ .

The motorcycle has no longitudinal or lateral displacement dependent forces acting upon it, and it is convenient to describe the motion of A by its longitudinal and lateral velocities,  $U$  and  $v$ , Fig.A2.3. The yawing motion can also be described by its velocity,  $\dot{\psi} = r$ , and these modifications result in the order of the system being reduced by two. Since coordinates expressing the position of A with reference to a set of fixed axes, such as  $x_0$  and  $y_0$ , no longer exist, the conventional equations of Lagrange must be adapted to apply to the quasi-coordinates  $U$ ,  $v$  and  $\psi$ . This has been done by Pacejka (1975) and yields the following equations:

For the lateral motion,

$$\frac{d}{dt} \left[ \frac{\partial T}{\partial v} \right] + r \frac{\partial T}{\partial U} = Q_{y_1} \quad (A2.1)$$

and for the yawing motion,

$$\frac{d}{dt} \left[ \frac{\partial T}{\partial r} \right] + U \frac{\partial T}{\partial v} - v \frac{\partial T}{\partial U} = Q_\psi \quad (A2.2)$$

The longitudinal velocity is assumed to be constant, so the relevant equation is not presented here.

The Lagrange equation for the  $i$ th generalised coordinate,  $q_i$ , is:

$$\frac{d}{dt} \left[ \frac{\partial T}{\partial \dot{q}_i} \right] - \frac{\partial T}{\partial q_i} + \frac{\partial V}{\partial q_i} + \frac{\partial F}{\partial \dot{q}_i} = Q_i \quad (A2.3)$$

$T$  is the kinetic energy of the system,  $V$  is the potential energy,  $F$  is the dissipative energy and  $Q_i$  is the generalised force relating to  $q_i$ , derived from the virtual work done by the tyre forces and moments for a virtual displacement  $\delta q_i$ . For this model the generalised true coordinates are  $\delta$ ,  $\phi$ ,  $\gamma$  and  $\lambda$ .

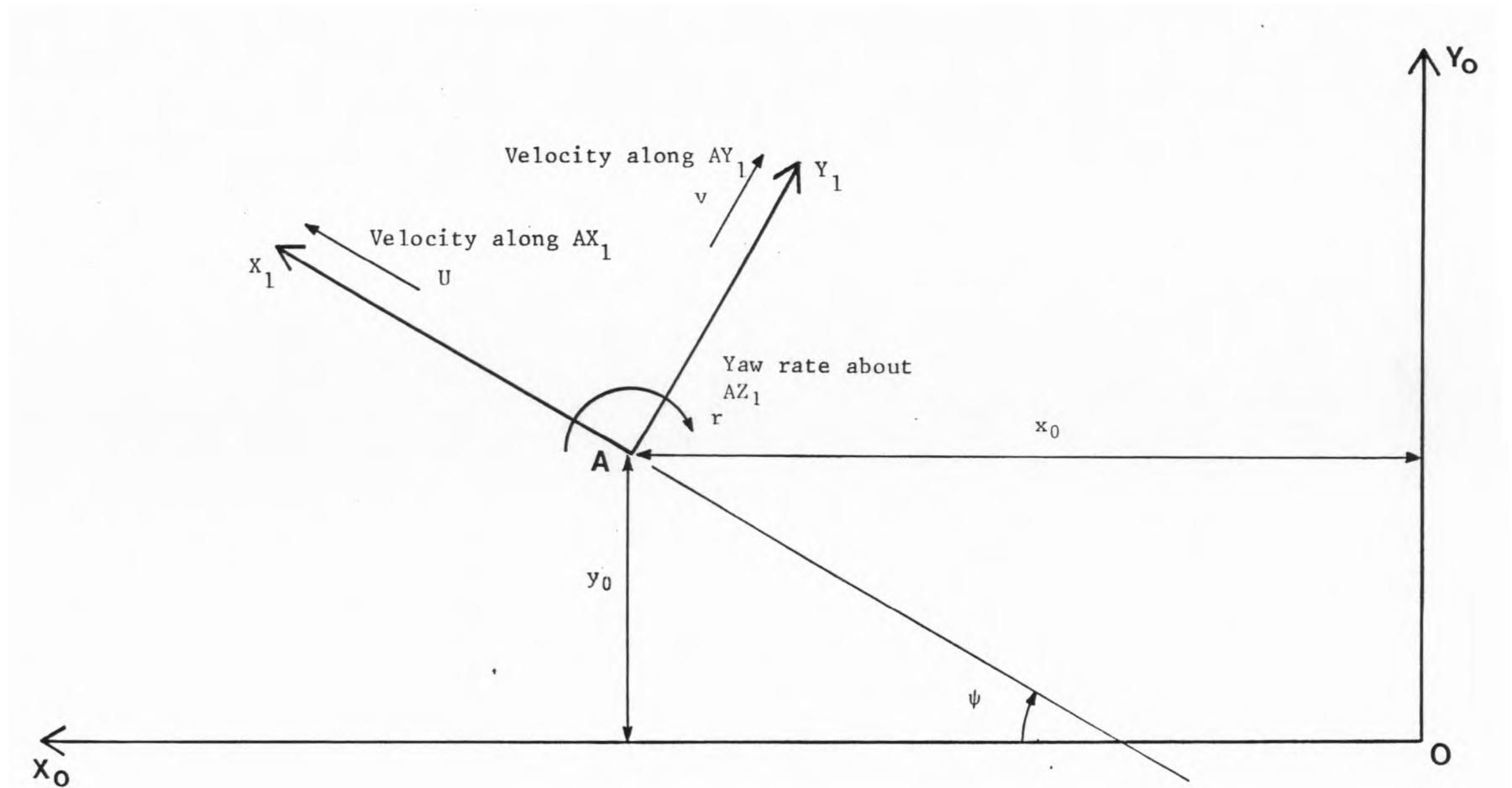


Figure A2.3

Relationship between fixed and moving axes.

THE KINETIC ENERGY, T

This may be expressed as the sum of the following kinetic energies:

(a).  $T_f$ , for the front frame assembly, as given by Sharp and Alstead (1980) for model C.

(b).  $T_r$ , for the rear frame excluding the rear wheel assembly, as given by Sharp (1971).

(c).  $T_{fl}$ , for the engine flywheel, appearing as the second term in the equation for  $T_w$  in the above paper.

(d).  $T_b$ , for the rear wheel assembly, including terms accounting for the rotational energy of the rear wheel.

In order to find the translational component of  $T_b$ , we had to find the absolute velocity of  $G_b$  as follows:

$$\underline{DG}_b \text{ in axis system 7 is } \begin{bmatrix} -a_2 \\ 0 \\ -a_1 \end{bmatrix}$$

$$\text{and transformed to axis system 6 is } R_\lambda^T \begin{bmatrix} -a_2 \\ 0 \\ -a_1 \end{bmatrix} = \begin{bmatrix} -a_2 \cos \lambda \\ -a_2 \sin \lambda \\ -a_1 \end{bmatrix}$$

$$\underline{AD} \text{ in axis system 6 is } \begin{bmatrix} a_3 \\ 0 \\ 0 \end{bmatrix}$$

$$\text{and therefore } \underline{AG}_b \text{ is } R_\phi^T R_{\epsilon_1}^T \begin{bmatrix} a_3 - a_2 \cos \lambda \\ a_2 \sin \lambda \\ -a_1 \end{bmatrix} \text{ in } AX_1 Y_1 Z_1$$

$$= \begin{bmatrix} -b_2 \\ -a_2 \sin \lambda \cos \phi + b_1 \sin \phi \\ -b_1 \cos \phi - a_2 \sin \lambda \sin \phi \end{bmatrix} \tag{A2.4}$$

where, for convenience,

$$b_1 = (a_3 - a_2 \cos \lambda) \sin \epsilon_1 + a_1 \cos \epsilon_1 \tag{A2.5}$$

$$b_2 = (a_3 - a_2 \cos \lambda) \cos \epsilon_1 - a_1 \sin \epsilon_1 \quad (\text{A2.6})$$

Since the rotational velocity of axis system 1 is  $\begin{bmatrix} 0 \\ 0 \\ r \end{bmatrix}$

and the velocity of point A is  $\begin{bmatrix} U \\ v \\ 0 \end{bmatrix}$

then the absolute velocity of  $G_b$ ,  $\underline{v}_b$ , is:

$$\begin{aligned} \begin{bmatrix} U \\ v \\ 0 \end{bmatrix} + \frac{d}{dt}(\underline{AG}_b) &= \frac{\partial}{\partial t}(\underline{AG}_b) + \begin{bmatrix} 0 \\ 0 \\ r \end{bmatrix} \wedge \underline{AG}_b + \begin{bmatrix} U \\ v \\ 0 \end{bmatrix} \\ &= \begin{bmatrix} U - (b_1 \dot{\phi} - a_2 \dot{\lambda})r + a_2 \cos \epsilon_1 \lambda \dot{\lambda} \\ -a_2 \dot{\lambda} + b_1 \dot{\phi} + b_2 r + v \\ -a_2 \dot{\lambda} \dot{\phi} - a_2 \lambda \dot{\phi} + b_1 \phi \dot{\phi} - a_2 \sin \epsilon_1 \lambda \dot{\lambda} \end{bmatrix} \end{aligned} \quad (\text{A2.7})$$

where terms of third order and above have been eliminated. For small values of  $\lambda$ ,  $b_1$  and  $b_2$  become the dimensions denoted as such in Fig.3.1.

The translational kinetic energy for the rear wheel assembly is thus given by:

$$\begin{aligned} \frac{1}{2} M_b \underline{v}_b^2 &= \frac{1}{2} M_b \{ (U - (b_1 \dot{\phi} - a_2 \dot{\lambda})r + a_2 \cos \epsilon_1 \lambda \dot{\lambda})^2 \\ &\quad + (v - a_2 \dot{\lambda} + b_1 \dot{\phi} + b_2 r)^2 \\ &\quad + ((b_1 \dot{\phi} - a_2 \dot{\lambda}) \dot{\phi} - a_2 (\sin \epsilon_1 \lambda + \phi) \dot{\lambda})^2 \} \end{aligned} \quad (\text{A2.8})$$

In order to find the rotational kinetic energy, it is necessary to find the velocity vector for axis system 7, which is:

$$\begin{aligned} R_{\epsilon_1} R_\lambda \left[ R_\phi \begin{bmatrix} 0 \\ 0 \\ r \end{bmatrix} + \begin{bmatrix} \dot{\phi} \\ 0 \\ 0 \end{bmatrix} \right] + \begin{bmatrix} 0 \\ 0 \\ \dot{\lambda} \end{bmatrix} \\ = \begin{bmatrix} \cos \epsilon_1 \dot{\phi} - \sin \epsilon_1 r \\ \lambda (\sin \epsilon_1 r - \cos \epsilon_1 \dot{\phi}) + \phi r \\ \sin \epsilon_1 \dot{\phi} + \cos \epsilon_1 r + \dot{\lambda} \end{bmatrix} = \begin{bmatrix} \omega_x \\ \omega_y \\ \omega_z \end{bmatrix} \end{aligned} \quad (\text{A2.9})$$

And the rotational kinetic energy is given by:

$$\frac{1}{2}I_{rwx}\omega_x^2 + \frac{1}{2}I_{rwy}\omega_y^2 + \frac{1}{2}I_{rwz}\omega_z^2 - I_{rwxz}\omega_x\omega_z$$

which accounts for everything except the spin energy of the rear wheel:

$$\frac{1}{2}i_{rwy}(2\omega_y\dot{\theta}_r + \dot{\theta}_r^2)$$

Thus the total rotational kinetic energy is:

$$\begin{aligned} & \frac{1}{2}I_{rwx}(\cos\epsilon_1\dot{\phi} - \sin\epsilon_1r)^2 + \frac{1}{2}I_{rwz}(\sin\epsilon_1\dot{\phi} + \cos\epsilon_1r + \dot{\lambda})^2 \\ & - I_{rwxz}(\cos\epsilon_1\dot{\phi} - \sin\epsilon_1r)((\sin\epsilon_1r - \cos\epsilon_1\dot{\phi})\lambda + \phi r) \\ & + \frac{1}{2}i_{rwy}[2(\lambda(\sin\epsilon_1r - \cos\epsilon_1\dot{\phi}) + \phi r)\dot{\theta}_r + \dot{\theta}_r^2] \end{aligned} \quad (A2.10)$$

since  $\omega_y^2$  is negligible when  $\lambda$ ,  $r$ ,  $\phi$ , and  $\dot{\phi}$  are small.

The total kinetic energy of the system is thus:

$$\begin{aligned} T = & \frac{1}{2}M_f\{(U - j\phi r - e\delta r - f\gamma r)^2 + (v + kr + j\dot{\phi} + f\dot{\gamma} + e\dot{\delta})^2\} \\ & + \frac{1}{2}I_{fx}(-\sin\epsilon r + \cos\epsilon\dot{\phi} + \dot{\gamma})^2 + \frac{1}{2}I_{fz}(\cos\epsilon r + \sin\epsilon\dot{\phi} + \dot{\delta})^2 \\ & + i_{fy}[\{(\sin\epsilon\delta + \phi + \cos\epsilon\gamma)r + (-\cos\epsilon\delta + \sin\epsilon\gamma)\dot{\phi} - \delta\dot{\gamma}\}\dot{\theta}_f + \frac{1}{2}\dot{\theta}_f^2] \\ & + \frac{1}{2}M_r\{(U - h\phi r)^2 + (v + h\dot{\phi})^2 + (h\phi\dot{\phi})^2\} \\ & + \frac{1}{2}I_{rx}\dot{\phi}^2 + \frac{1}{2}I_{ry}(\phi r)^2 + \frac{1}{2}I_{rz}r^2 - I_{rxz}\dot{\phi}r \\ & + \frac{1}{2}M_b\{U - (b_1\phi - a_2\lambda)r + a_2\cos\epsilon_1\lambda\dot{\lambda}\}^2 \\ & + (v - a_2\dot{\lambda} + b_1\phi + b_2r)^2 \\ & + \{(b_1\phi - a_2\lambda)\dot{\phi} - a_2(\sin\epsilon_1\lambda + \phi)\dot{\lambda}\}^2 \\ & + \frac{1}{2}I_{rwx}(\cos\epsilon_1\dot{\phi} - \sin\epsilon_1r)^2 + \frac{1}{2}I_{rwz}(\sin\epsilon_1\dot{\phi} + \cos\epsilon_1r + \dot{\lambda})^2 \\ & - I_{rwxz}(\cos\epsilon_1\dot{\phi} - \sin\epsilon_1r)((\sin\epsilon_1r - \cos\epsilon_1\dot{\phi})\lambda + \phi r) \\ & + \frac{1}{2}i_{rwy}[2(\lambda(\sin\epsilon_1r - \cos\epsilon_1\dot{\phi}) + \phi r)\dot{\theta}_r + \dot{\theta}_r^2] \end{aligned} \quad (A2.11)$$

THE WHEEL SPIN CONSTRAINT EQUATIONS

It is necessary to find the longitudinal velocity of point J in order to eliminate  $\dot{\theta}_r$  from the equations of motion. However, the substitution for  $\dot{\theta}_r$  must not be made until after the differentiation of the energy expressions has been performed, to avoid introducing erroneous terms into the equations of motion.

Vector  $\underline{AJ}$  in  $AX_1Y_1Z_1$  is found in a similar fashion to  $\underline{AG}_b$ , and

$$\underline{AJ} = \begin{bmatrix} -b \\ -a_4\lambda \\ 0 \end{bmatrix} \quad (A2.12)$$

for small  $\lambda, \phi$ .

$$\frac{d}{dt}(\underline{AJ}) = \frac{\partial}{\partial t}(\underline{AJ}) + \begin{bmatrix} 0 \\ 0 \\ r \end{bmatrix} \wedge (\underline{AJ})$$

and the total longitudinal velocity of J is  $U + a_4\lambda r$ , which reduces to U for small  $\lambda, r$ , and the angular velocity for the rear wheel is thus given by:

$$\dot{\theta}_r = -U/R_r \quad (A2.13)$$

Similarly, for the front wheel,

$$\dot{\theta}_f = -U/R_f \quad (A2.14)$$

assuming no longitudinal slip in both cases.

THE POTENTIAL ENERGY, V

The potential energy for the front frame is given by the expressions for  $V_f$  and  $V_\gamma$  by Sharp and Alstead (1980), model C.

The potential energy of the rear frame is as given in equation (5), Sharp (1971).

The potential energy of the rear wheel assembly was obtained by finding the absolute value of the z component of  $\underline{AG}_b$  in axis system 1, and multiplying it by  $M_b g$ :

$$V_b = M_b g(a_2\lambda\phi + b_1\cos\phi)$$

To this must be added the strain energy associated with the rear

frame flexibility:

$$V_{\lambda} = \frac{1}{2} S_r \lambda^2$$

Hence the total potential energy of the system is:

$$\begin{aligned} V = & M_f g (s \cos \phi - e \phi \delta - f \phi \gamma + e \sin \epsilon \cos \phi \cos \delta - e \cos \epsilon \delta \gamma \\ & + f \cos \epsilon \cos \phi \cos \gamma) + M_r g h \cos \phi + M_b g (a_2 \lambda \phi + b_1 \cos \phi) \\ & + \frac{1}{2} S_f \gamma^2 + \frac{1}{2} S_r \lambda^2 \end{aligned} \quad (\text{A2.15})$$

THE DISSIPATIVE ENERGY, F

The energy dissipated due to structural damping in the front and rear frames and by the steering damper, is given by:

$$F = \frac{1}{2} D_f \dot{\gamma}^2 + \frac{1}{2} D_r \dot{\lambda}^2 + \frac{1}{2} D_s \dot{\delta}^2 \quad (\text{A2.16})$$

THE EFFECTIVE REAR WHEEL CAMBER AND STEER ANGLES,  $\phi_r$  AND  $\psi_r$

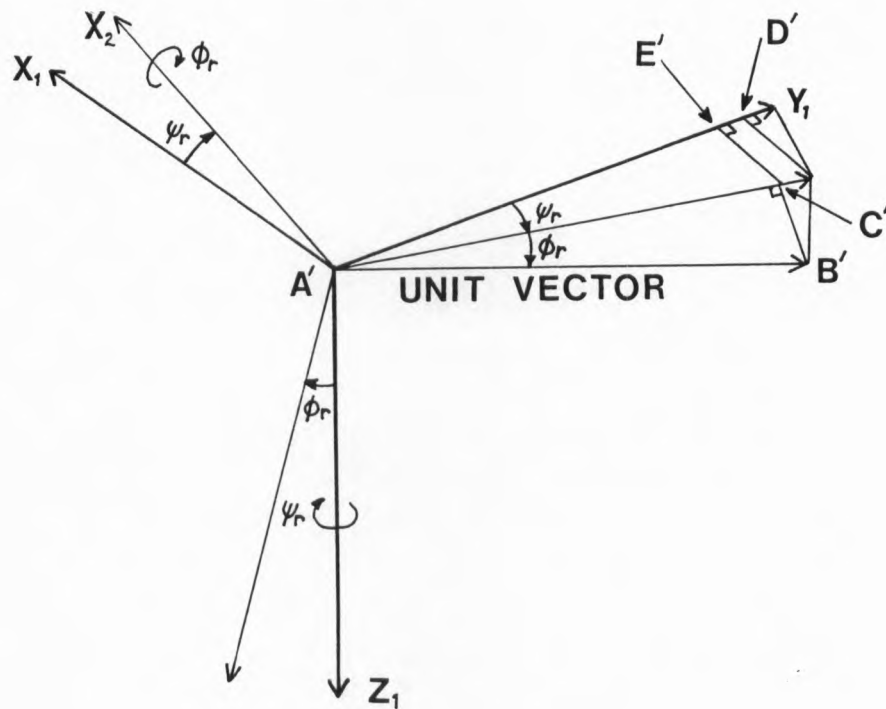


Figure A2.4

Steered and cambered unit vector.

If one considers a unit vector perpendicular to the wheel plane, steered  $\psi_r$  about  $A'Z_1$  and then cambered  $\phi_r$  about  $A'X_2$  (see Fig.A2.4), one can see that:

$$A'B' = 1$$

$$A'C' = \cos\phi_r$$

$$A'D' = \cos\psi_r$$

$$A'E' = \cos\phi_r \cos\psi_r$$

$$B'C' = -\sin\phi_r$$

$$C'E' = \cos\phi_r \sin\psi_r$$

A unit vector perpendicular to the wheel plane can be written as

$$\begin{bmatrix} 0 \\ 1 \\ 0 \end{bmatrix}$$

in axis system 7. Expressed in axis system 1 this becomes:

$$R_\phi^T R_{\epsilon_1}^T R_\lambda^T \begin{bmatrix} 0 \\ 1 \\ 0 \end{bmatrix} = \begin{bmatrix} -\sin\lambda \cos\epsilon_1 \\ \cos\phi \cos\lambda - \sin\phi \sin\lambda \sin\epsilon_1 \\ \sin\phi \cos\lambda + \cos\phi \sin\lambda \sin\epsilon_1 \end{bmatrix}$$

Then the components along axes parallel to  $AY_1$  and  $AZ_1$  can be equated to  $C'E'$  and  $B'C'$  respectively. Thus for small angles,

$$\phi_r = \phi + \lambda \sin\epsilon_1$$

This expression was inserted into the equations relating to the camber responses of the rear tyre.

$\psi_r$  will be a small angle so that:

$$\cos\psi_r \approx 1 \tag{A2.17}$$

Equating the component of the unit vector parallel to  $AX_1$  to  $C'E'$ , yields:

$$\sin\psi_r \approx \psi_r \approx \lambda \cos\epsilon_1 \tag{A2.18}$$

THE GENERALISED FORCES,  $Q_i$

The generalised forces due to the front tyre are the same as those given for model C by Sharp and Alstead (1980). The contributions from the rear tyre are calculated as follows (in all cases, ignoring second order terms in motion variables):

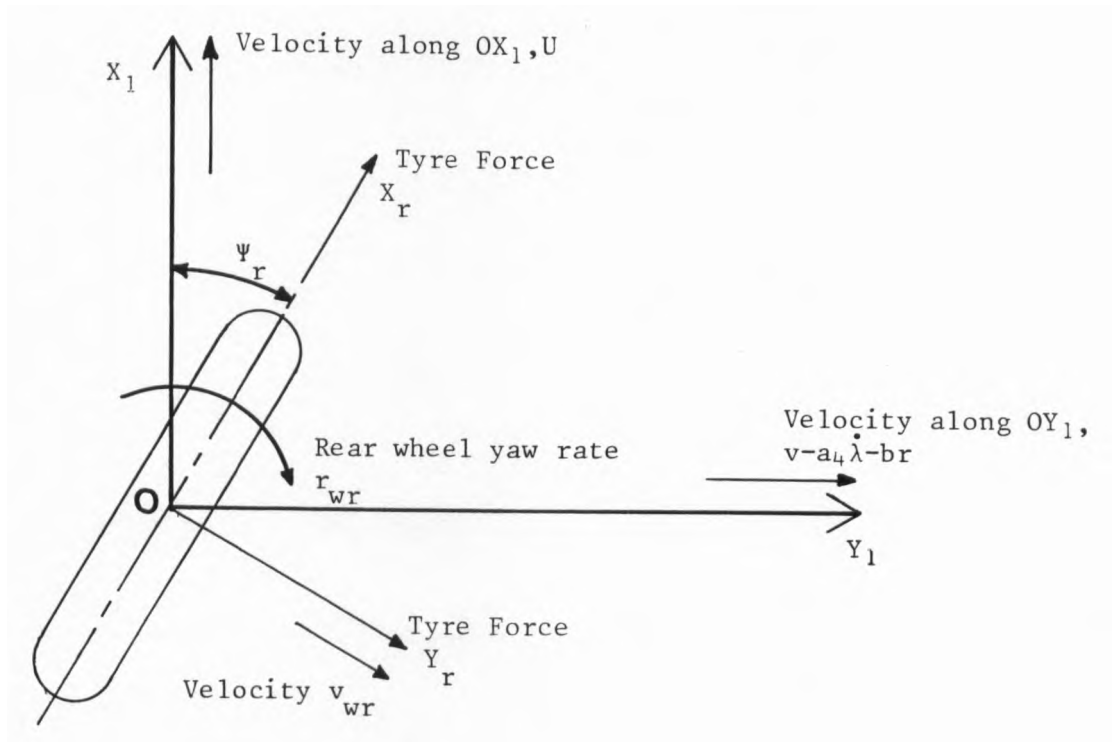


Figure A2.5

Rear tyre forces and velocities.

From Fig.A2.5 it can be seen that the rear tyre force vector  $\underline{F}_r$ , in axis system 1, is:

$$\begin{bmatrix} X_r \cos \psi_r - Y_r \sin \psi_r \\ X_r \sin \psi_r + Y_r \cos \psi_r \\ Z_r \end{bmatrix}$$

and the tyre moment vector  $\underline{M}_r$ , is:

$$\begin{bmatrix} M_{xr} \cos \psi_r \\ M_{xr} \sin \psi_r \\ M_{zr} \end{bmatrix}$$

(the component about the y axis due to the rolling resistance of the rear tyre is negligible and does not appear).

(i). For the yawing motion,  $\psi$

The contribution of the rear tyre forces to  $Q_\psi$  is given by the component about the  $AZ_1$  axis of

$$\begin{aligned} \underline{AJ} \wedge \underline{F}_r + \underline{M}_r \\ = X_r \lambda (a_4 - b \cos \epsilon_1) - b Y_r + M_{zr} \end{aligned} \quad (A2.19)$$

(ii). For the rolling motion,  $\phi$

The vectors  $\underline{AJ}$ ,  $\underline{F}_r$ , and  $\underline{M}_r$  must be expressed in axis system 2, in which case:

$$\begin{aligned} \underline{AJ} &= \begin{bmatrix} -b \\ -a_4 \lambda \\ 0 \end{bmatrix} \\ \underline{F}_r &= \begin{bmatrix} X_r - Y_r \lambda \cos \epsilon_1 \\ X_r \lambda \cos \epsilon_1 + Y_r + Z_r \phi \\ -Y_r \phi + Z_r \end{bmatrix} \\ \underline{M}_r &= \begin{bmatrix} M_{xr} \\ M_{xr} \lambda \cos \epsilon_1 + M_{zr} \phi \\ M_{zr} \end{bmatrix} \end{aligned}$$

and the contribution to  $Q_\phi$  is given by the component about the  $AX_2$  axis of

$$\begin{aligned} \underline{AJ} \wedge \underline{F}_r + \underline{M}_r \\ = M_{xr} - a_4 Z_r \lambda \end{aligned} \quad (A2.20)$$

(iii). For the rear yaw/camber,  $\lambda$

The vectors  $\underline{DJ}$ ,  $\underline{F}_r$  and  $\underline{M}_r$  must be expressed in axis system 7, in which case:

$$\underline{DJ} = \begin{bmatrix} -a_4 \\ 0 \\ -a_5 \end{bmatrix}$$

$$\underline{F}_r = \begin{bmatrix} (X_r - Y_r \lambda \cos \epsilon_1) \cos \epsilon_1 + (Y_r \phi - Z_r) \sin \epsilon_1 + Y_r \lambda \\ - Z_r \sin \epsilon_1 \lambda + Y_r + Z_r \phi \\ (X_r - Y_r \lambda \cos \epsilon_1) \sin \epsilon_1 + (Z_r - Y_r \phi) \cos \epsilon_1 \end{bmatrix}$$

$$\underline{M}_r = \begin{bmatrix} M_{xr} \cos \epsilon_1 - M_{zr} \sin \epsilon_1 \\ M_{zr} (\lambda \sin \epsilon_1 + \phi) \\ M_{xr} \sin \epsilon_1 + M_{zr} \cos \epsilon_1 \end{bmatrix}$$

and  $Q_\lambda$  is given by the component about the  $AZ_7$  axis of:

$$\begin{aligned} \underline{DJ} \wedge \underline{F}_r + \underline{M}_r \\ = a_4 \lambda Z_r \sin \epsilon_1 - a_4 Z_r \phi - a_4 Y_r + M_{xr} \sin \epsilon_1 + M_{zr} \cos \epsilon_1 \end{aligned} \quad (A2.21)$$

(iv). For the lateral motion, v

The contribution to  $Q_{y_1}$  is given by the component of  $\underline{F}_r$  along an axis parallel to  $AY_1$ ,

$$= X_r \cos \epsilon_1 \lambda + Y_r \quad (A2.22)$$

The rear tyre forces and moments don't contribute to  $Q_\gamma$  or  $Q_\delta$ .

$X_r$  is constant for a given speed, and is calculated from the drive thrust necessary to overcome aerodynamic drag and the rolling resistance of the front tyre.  $Y_r$  is the independent variable for one of the tyre equations.

#### THE AERODYNAMIC YAW MOMENT

When the motorcycle rolls, the aerodynamic drag force  $D_c U^2$ , which is considered as acting at the location of the centre of pressure, height  $h_{cp}$ , produces a yaw moment given by:

$$\begin{bmatrix} 0 \\ -h_{cp} \sin \phi \\ h_{cp} \cos \phi \end{bmatrix} \wedge \begin{bmatrix} -D_c U^2 \\ 0 \\ 0 \end{bmatrix} = D_c U^2 h_{cp} \phi \quad (A2.23)$$

This term appears on the right hand side of the equation for the yaw

motion.

THE LATERAL AND YAW VELOCITIES OF THE REAR WHEEL

It was necessary to find the lateral velocity of point J as follows:

In axis system 1,

$$\begin{aligned} \underline{AJ} &= \begin{bmatrix} -b \\ -a_4\lambda \\ 0 \end{bmatrix} \\ \frac{d}{dt}(\underline{AJ}) &= \frac{\partial}{\partial t}(\underline{AJ}) + \begin{bmatrix} 0 \\ 0 \\ r \end{bmatrix} \wedge \underline{AJ} \\ &= \begin{bmatrix} 0 \\ -a_4\dot{\lambda} - br \\ 0 \end{bmatrix} \end{aligned}$$

and the absolute velocity of point J is thus:

$$\begin{bmatrix} U \\ v - a_4\dot{\lambda} - br \\ 0 \end{bmatrix}$$

From Fig.A2.5 it can be seen that the lateral velocity of the rear wheel contact centre is given by:

$$v_{wr} = (v - a_4\dot{\lambda} - br)\cos\psi_r - U\sin\psi_r$$

and using equations A2.17 and A2.18 this becomes:

$$v_{wr} = v - a_4\dot{\lambda} - br - U\cos\epsilon_1\lambda \quad (A2.24)$$

The yaw velocity of the rear wheel is given by:

$$r_{wr} = r + \dot{\psi}_r$$

which becomes

$$r_{wr} = r + \cos\epsilon_1\dot{\lambda} \quad (A2.25)$$

#### THE EQUATIONS OF MOTION

The expressions for  $T$ ,  $V$  and  $F$  (equations A2.11, 15, 16) were then differentiated and the resultant terms were substituted into the appropriate Lagrangian equations, A2.1 to A2.3. The equations of motion were linearised for small perturbations from a straight running condition by eliminating second order terms and using the following approximations:

$$\sin\lambda \approx \lambda, \cos\lambda \approx 1, \sin\phi \approx \phi, \cos\phi \approx 1, \sin\gamma \approx \gamma, \cos\gamma \approx 1$$

The wheel spin terms were eliminated using A2.13, 14, and the generalised forces and moments arising from the rear tyre (equations A2.19 to A2.22) were added to those due to the front tyre. The expressions for the lateral and yaw velocities of the rear tyre contact patch (equations A2.24, 25) were inserted into the equations for the rear tyre forces and moments, along with the expression for the camber angle. The resultant equations of motion for the system are as given in Chapter 3.

A2.2 THE TWIN WHEEL TRAILER MODEL

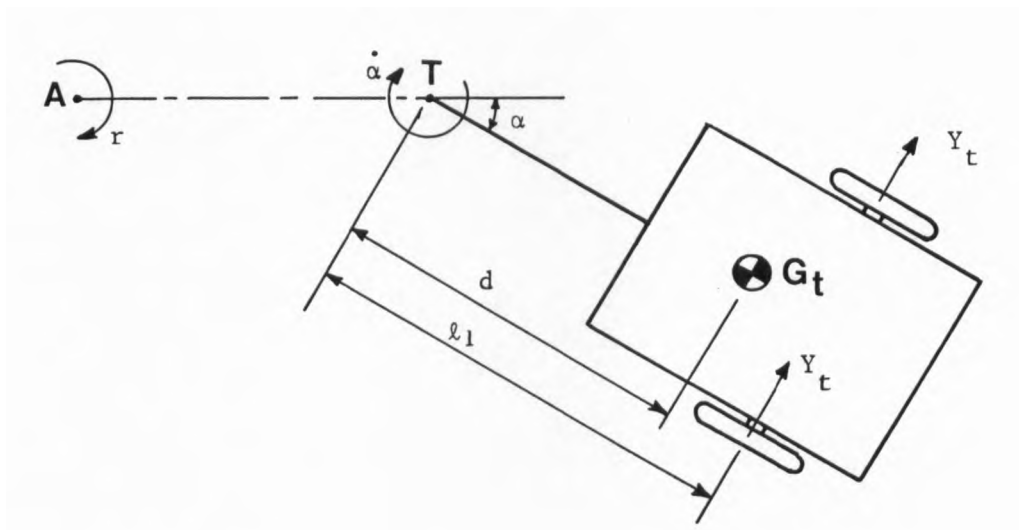


Figure A2.6

View of trailer from above.

The relevant dimensions of the motorcycle and trailer can be seen in Fig.6.1. The trailer is modelled as a lumped mass that yaws about an axis parallel to  $AZ_2$ , passing through the hitch point T, which is a part of the rear frame of the motorcycle. The position of the trailer relative to the motorcycle is conveniently described by the angle  $\alpha$ , Fig.A2.6, which is used as a generalised coordinate. The equation of motion of the trailer can thus be derived using the corresponding Lagrangian equation:

$$\frac{d}{dt} \frac{\partial T}{\partial \dot{\alpha}} - \frac{\partial T}{\partial \alpha} + \frac{\partial V}{\partial \alpha} + \frac{\partial F}{\partial \alpha} = Q_{\alpha} \quad (A2.26)$$

The additional terms arising in the other equations of motion for the system can be obtained by differentiating the expressions for the various trailer energies, making the appropriate substitutions in equations A2.1, 2 and 3, and adding the trailer tyre contributions to the generalised forces,  $Q_i$ .

THE TRAILER KINETIC ENERGY,  $T_{tr}$

In order to find the translational kinetic energy, it was necessary to find the absolute velocity of the trailer c.g.,  $G_t$ .

Vector  $\underline{AT}$  (Fig.6.1) in axis system 1 is  $\begin{bmatrix} -p \\ 0 \\ -h_1 \end{bmatrix}$ .

To resolve this in axis system 2, multiply by the rotation matrix,  $R_\phi$ :

$$R_\phi \begin{bmatrix} -p \\ 0 \\ -h_1 \end{bmatrix} = \begin{bmatrix} -p \\ h_1 \sin\phi \\ -h_1 \cos\phi \end{bmatrix}$$

Then the velocity of point T relative to A is given by:

$$\begin{aligned} \frac{d}{dt} (\underline{AT}) &= \frac{\partial}{\partial t} (\underline{AT}) + \begin{bmatrix} 0 \\ 0 \\ r \end{bmatrix} \wedge \underline{AT} \\ &= \begin{bmatrix} -h_1 \sin\phi r \\ h_1 \cos\phi \dot{\phi} - pr \\ h_1 \sin\phi \dot{\phi} \end{bmatrix} \end{aligned}$$

and the absolute velocity of the hitch point T, is:

$$\frac{d}{dt} (\underline{AT}) + \begin{bmatrix} U \\ v \\ 0 \end{bmatrix} = \begin{bmatrix} U - h_1 \sin\phi r \\ v + h_1 \cos\phi \dot{\phi} - pr \\ h_1 \sin\phi \dot{\phi} \end{bmatrix} \quad (\text{A2.27})$$

From Fig.A2.6, it can be seen that the velocity of  $G_t$  relative to T is

$$\begin{bmatrix} d \sin\alpha(\dot{\alpha} + r) \\ -d \cos\alpha(\dot{\alpha} + r) \\ 0 \end{bmatrix}$$

and thus the absolute velocity of  $G_t$  is:

$$\underline{v}_{tr} = \begin{bmatrix} U - h_1 \sin\phi r + d \sin\alpha(\dot{\alpha} + r) \\ v + h_1 \cos\phi \dot{\phi} - pr - d \cos\alpha(\dot{\alpha} + r) \\ 0 \end{bmatrix} \quad (\text{A2.28})$$

(ignoring small vertical movements of  $G_t$  caused by motorcycle roll).

In order to obtain the rotational kinetic energy, it was necessary to find the angular velocity of the trailer. The angular velocity of axis system 2 is:

$$R_\phi \begin{bmatrix} 0 \\ 0 \\ r \end{bmatrix} + \begin{bmatrix} \dot{\phi} \\ 0 \\ 0 \end{bmatrix} = \begin{bmatrix} \dot{\phi} \\ \sin\phi r \\ \cos\phi r \end{bmatrix}$$

and thus the angular velocity of the trailer about the  $AZ_2$  axis is  $\dot{\alpha} + r$ , for small  $\phi$ , and the rotational kinetic energy is:

$$\frac{1}{2}I_{tz}(\dot{\alpha} + r)^2$$

The angular velocity components about  $AX_2$  and  $AY_2$  are zero because the trailer has neither pitch nor roll freedoms.

Hence the total kinetic energy of the trailer is given by (neglecting terms that won't give rise to first order terms in the equations of motion):

$$\begin{aligned} T_{tr} = & \frac{1}{2}M_{tr}\{(U - h_1\dot{\phi}r + d\alpha(\dot{\alpha} + r))^2 \\ & + (v + h_1\dot{\phi} - pr - d(\dot{\alpha} + r))^2\} \\ & + \frac{1}{2}I_{tz}(\dot{\alpha} + r)^2 \end{aligned} \quad (A2.29)$$

THE POTENTIAL ENERGY,  $V_{tr}$

This is considered to be constant and thus has no derivatives that contribute to the equations of motion.

THE DISSIPATIVE ENERGY,  $F_{tr}$

The energy dissipated by a damper connected between the trailer and the rear frame of the motorcycle is given by:

$$F_{tr} = \frac{1}{2}D_t\dot{\alpha}^2 \quad (A2.30)$$

THE GENERALISED FORCES,  $Q_i$

(i). For the trailer yawing motion,  $\alpha$ .

Considering a virtual displacement  $\delta\alpha$ , the total work done by the tyre forces and moments is  $(-2Y_t\ell_1 + 2M_{zt})\delta\alpha$ , and thus the generalised force is:

$$-2Y_t\ell_1 + 2M_{zt} \quad (A2.31)$$

(ii). For the motorcycle yawing motion,  $\psi$ .

Considering a virtual displacement  $\delta\psi$ , the work done by the trailer tyre forces and moments is  $(-2(p + \ell_1)Y_t + 2M_{zt})\delta\psi$ , and thus the contribution of the trailer tyres to  $Q_\psi$  is:

$$-2(p + \ell_1)Y_t + 2M_{zt} \quad (A2.32)$$

(iii). For the lateral motion of the vehicle,  $v$ .

The trailer tyre forces do work  $2Y_t\delta y_1$  during a virtual displacement  $\delta y_1$ , and so their contribution to  $Q_{y_1}$  is:

$$2Y_t \quad (A2.33)$$

(iv). For the rolling motion,  $\phi$ .

The trailer tyre forces do work  $2h_1Y_t\delta\phi$  during a virtual displacement  $\delta\phi$ , and thus their contribution to  $Q_\phi$  is:

$$2h_1Y_t \quad (A2.34)$$

The trailer tyre forces and moments do no work for virtual displacements of the other motion variables.

#### THE LATERAL AND YAW VELOCITIES OF THE TRAILER TYRES

The absolute velocities of the trailer tyre contact patches in axis system 1 are given by (from equation A2.28, substituting  $\ell_1$  for  $d$  and ignoring second order quantities):

$$\begin{bmatrix} U \\ v + h_1\dot{\phi} - pr - \ell_1(r + \dot{\alpha}) \\ 0 \end{bmatrix}$$

Hence, the lateral velocity of the trailer tyre is (from Fig.A2.7):

$$\begin{aligned} & (v + h_1\dot{\phi} - pr - \ell_1(r + \dot{\alpha}))\cos\alpha - U\sin\alpha \\ \therefore v_{tw} &= v + h_1\dot{\phi} - (p + \ell_1)r - \ell_1\dot{\alpha} - U\alpha \end{aligned} \quad (A2.35)$$

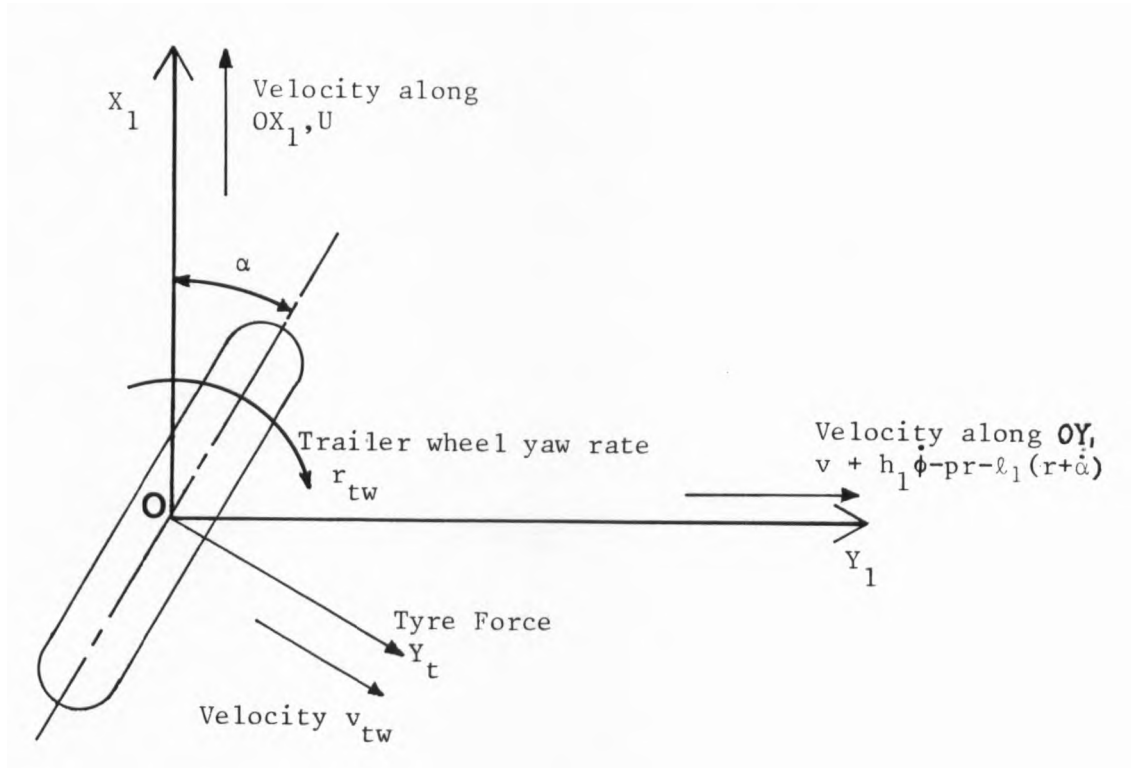


Figure A2.7

Trailer tyre velocities.

The yaw velocity of the trailer tyres is clearly:

$$r_{tw} = r + \dot{\alpha} \quad (A2.36)$$

THE TYRE FORCES AND MOMENTS,  $Y_t$  and  $M_{zt}$

For a first order lag, the trailer tyre force equation is:

$$\sigma_t \dot{Y}_t + U Y_t = -C_{Ft} v_{tw} - C_{Mt} r_{tw} \quad (A2.37)$$

and the moment equation is:

$$\sigma_t \dot{M}_{zt} + U M_{zt} = C_{Mt} v_{tw} \quad (A2.38)$$

where  $\sigma_t$ ,  $C_{Ft}$  and  $C_{Mt}$  are the trailer tyre relaxation length, cornering stiffness and aligning moment constant respectively.

#### THE VERTICAL TYRE LOADS

The changes in the motorcycle tyres' vertical loads due to the addition of the trailer, given by simple statics, are, for the front wheel:

$$- M_{tr}(\ell_1 - d)(p - b)g/\ell_1(b + \ell)$$

and for the rear wheel:

$$M_{tr}(\ell_1 - d)(\ell + p)g/\ell_1(b + \ell)$$

The total vertical load on the trailer tyres is:

$$M_{tr}dg/\ell_1$$

#### THE EQUATIONS OF MOTION

To obtain the equation of motion of the trailer, equations A2.29 and 30 were differentiated and the resultant terms were substituted into equation A2.26 along with the expression for the generalised force, A2.31.

The additional terms in the other equations of motion were derived using the expressions for  $T_{tr}$ ,  $F_{tr}$  and the trailer tyres' contributions to the generalised forces.

The trailer tyre force and moment equations were obtained by substituting the expressions for  $v_{tw}$  and  $r_{tw}$  (A2.35 and 36) into equations A2.37 and 38.

The above terms and equations consequently appear as given in section 6.3.1.

A2.3 THE SINGLE WHEEL TRAILER MODEL

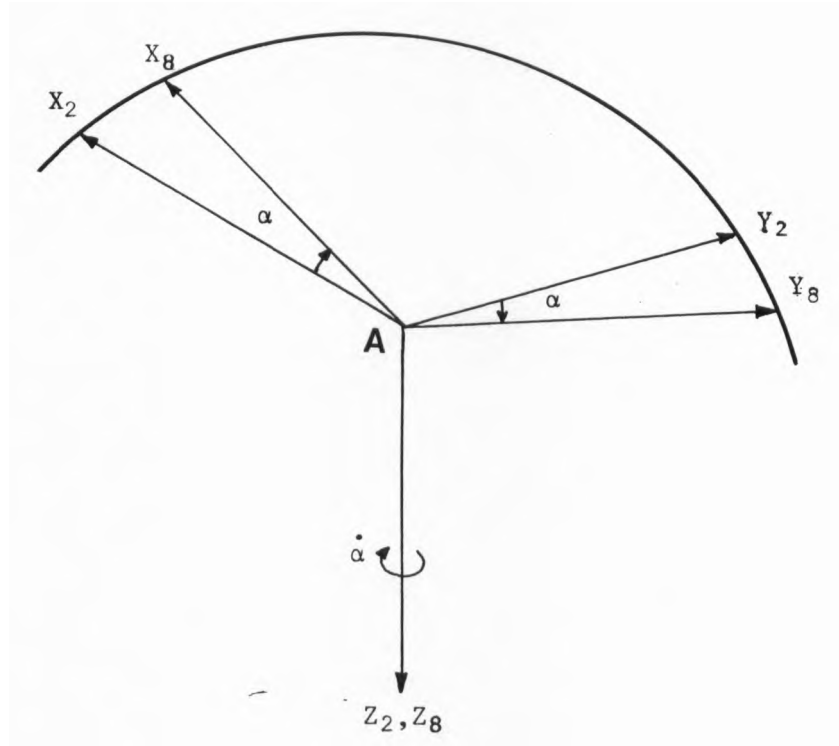


Figure A2.8

Definition of axis system 8.

This is modelled very similarly to the twin wheel trailer, except that it has the freedom to roll about the  $AX_2$  axis with the motorcycle. A new axis system  $AX_8Y_8Z_8$  is defined as depicted in Fig.A2.8, and the corresponding rotation matrix relating vectors in  $AX_2Y_2Z_2$  to those in  $AX_8Y_8Z_8$  is

$$R_{\alpha} = \begin{bmatrix} \cos\alpha & \sin\alpha & 0 \\ -\sin\alpha & \cos\alpha & 0 \\ 0 & 0 & 1 \end{bmatrix}$$

THE KINETIC ENERGY,  $T_{tr}$

The vector  $\underline{TG}_t$  expressed in axis system 8 is  $\begin{bmatrix} -d \\ 0 \\ h_1 - h_3 \end{bmatrix}$

and transformed into axis system 1 this becomes:

$$R_{\phi}^T R_{\alpha}^T \begin{bmatrix} -d \\ 0 \\ h_1 - h_3 \end{bmatrix} = \begin{bmatrix} -d \cos\alpha \\ -d \sin\alpha \cos\phi - (h_1 - h_3)\sin\phi \\ -d \sin\alpha \sin\phi + (h_1 - h_3)\cos\phi \end{bmatrix} \quad (A2.39)$$

The velocity of  $G_t$  relative to T is given by:

$$\begin{aligned} \frac{d}{dt} (\underline{TG}_t) &= \frac{\partial}{\partial t} (\underline{TG}_t) + \begin{bmatrix} 0 \\ 0 \\ r \end{bmatrix} \wedge \underline{TG}_t \\ &= \begin{bmatrix} d\alpha(\dot{\alpha} + r) + (h_1 - h_3)r\dot{\phi} \\ -d(\dot{\alpha} + r) - (h_1 - h_3)\dot{\phi} \\ -d\dot{\phi}\dot{\alpha} - d\alpha\dot{\phi} - (h_1 - h_3)\dot{\phi}\dot{\phi} \end{bmatrix} \end{aligned}$$

ignoring terms that won't contribute first order terms to the equations of motion.

The absolute velocity of the hitch is the same as that given by the two wheel trailer analysis, equation A2.27, and thus the absolute velocity of the centre of mass of the trailer is:

$$\underline{v}_{tr} = \begin{bmatrix} U + d\alpha(\dot{\alpha} + r) - h_3r\dot{\phi} \\ v - d(\dot{\alpha} + r) + h_3\dot{\phi} - pr \\ -d\dot{\phi}\dot{\alpha} - d\alpha\dot{\phi} + h_3\dot{\phi}\dot{\phi} \end{bmatrix} \quad (A2.40)$$

The translational kinetic energy of the trailer was then given by  $\frac{1}{2}M_{tr} \underline{v}_{tr}^2$ .

The angular velocity of axis system 8 is given by:

$$\begin{aligned} R_\alpha &\left[ R_\phi \begin{bmatrix} 0 \\ 0 \\ r \end{bmatrix} + \begin{bmatrix} \dot{\phi} \\ 0 \\ 0 \end{bmatrix} \right] + \begin{bmatrix} 0 \\ 0 \\ \dot{\alpha} \end{bmatrix} \\ &= \begin{bmatrix} \dot{\phi} \\ -\dot{\phi}\alpha + r\dot{\phi} \\ r + \dot{\alpha} \end{bmatrix} = \begin{bmatrix} \omega_x \\ \omega_y \\ \omega_z \end{bmatrix} \end{aligned}$$

and the rotational kinetic energy is given by:

$$\frac{1}{2}I_{tx}\omega_x^2 + \frac{1}{2}I_{tz}\omega_z^2 - I_{txz}\omega_x\omega_z + \frac{1}{2}i_{twy}(2\omega_y\dot{\theta}_t + \dot{\theta}_t^2)$$

because  $\omega_y^2$  is negligible.

Hence, the total kinetic energy of the trailer is:

$$\begin{aligned} T_{tr} &= \frac{1}{2}\{(U + d\alpha(\dot{\alpha} + r) - h_3r\dot{\phi})^2 \\ &\quad + (v - d(\dot{\alpha} + r) + h_3\dot{\phi} - pr)^2\} \\ &\quad + \frac{1}{2}I_{tx}\dot{\phi}^2 + \frac{1}{2}I_{tz}(\dot{\alpha} + r)^2 - I_{txz}\dot{\phi}(\dot{\alpha} + r) \\ &\quad + \frac{1}{2}i_{twy}\{2(r\dot{\phi} - \dot{\phi}\alpha)\dot{\theta}_t + \dot{\theta}_t^2\} \end{aligned} \quad (A2.41)$$

The velocity component of the centre of mass in the  $AZ_1$  direction has been left out because it becomes of fourth order when squared.

After differentiation of the energy expressions,  $\dot{\theta}_t$  was eliminated using the equation:

$$\dot{\theta}_t = -U/R_t$$

THE POTENTIAL ENERGY,  $V_{tr}$

It was necessary to find the component of  $\underline{AG}_t$  in the  $AZ_1$  direction.  $\underline{AT}$  expressed in axis system 2 is:

$$\begin{bmatrix} -p \\ 0 \\ -h_1 \end{bmatrix}$$

which is  $\begin{bmatrix} -p \\ h_1 \sin\phi \\ -h_1 \cos\phi \end{bmatrix}$  in axis system 1.

Therefore the  $AZ_1$  component of  $\underline{AG}_t$  is (using equation A2.39),  
 $-h_3 \cos\phi - d \sin\alpha \sin\phi$

Hence, the potential energy is:

$$V_{tr} = M_{tr}g(h_3 \cos\phi + d \sin\alpha \sin\phi)$$

THE DISSIPATIVE ENERGY,  $F_{tr}$

This is as given for the twin wheel trailer.

THE GENERALISED FORCES,  $Q_i$

These were obtained by the same method as used for the twin wheel trailer, except that the trailer tyre side force response to wheel camber was added to  $Y_t$ .

(i). For the trailer yawing motion,  $\alpha$ .

$$Q_\alpha = -\ell_1(Y_t + C_{1t}\phi) + M_{zt} - \ell_1\phi Z_t \quad (A2.42)$$

where  $Z_t$  is the vertical load on the trailer tyre (positive downwards).

(ii). For the motorcycle yawing motion,  $\psi$ .

The contribution to  $Q_\psi$  from the trailer tyre is

$$- (p + l_1)(Y_t + C_{1t}\phi) + M_{zt} \quad (A2.43)$$

(iii). For the lateral motion of the vehicle,  $v$ .

The contribution to  $Q_{y_1}$  from the trailer tyre is

$$Y_t + C_{1t}\phi \quad (A2.44)$$

The trailer tyre forces and moments don't contribute to any of the other generalised forces.

#### THE LATERAL AND YAW VELOCITIES OF THE TRAILER TYRE

The absolute velocity of the trailer tyre contact patch in axis system 1 is given by (using equation A2.40, substituting  $l_1$  for  $d$ , ignoring  $h_3$  and disregarding second order quantities):

$$\begin{bmatrix} U \\ v - l_1(\dot{\alpha} + r) - pr \\ 0 \end{bmatrix}$$

and the velocity of the tyre contact centre in a direction perpendicular to the wheel plane is:

$$(v - (p + l_1)r - l_1\dot{\alpha})\cos\alpha - U\sin\alpha$$

$$\therefore v_{tw} = v - (p + l_1)r - l_1\dot{\alpha} - U\alpha \quad (A2.45)$$

when linearised for small perturbations.

Also,

$$r_{tw} = r + \dot{\alpha} \quad (A2.46)$$

#### THE EQUATIONS OF MOTION

These were obtained using the same method as for the twin wheel trailer, and appear in section 6.3.2. The expressions for  $v_{tw}$  and  $r_{tw}$  were substituted into equations A2.37 and 38 to give the trailer tyre side force and moment equations. The vertical tyre loads are as given for the twin wheel trailer.